THE UNIVERSITY OF HULL

WETTING PROPERTIES OF PROTECTIVE COATINGS BASED ON STRUCTURED SURFACES

being a Thesis submitted for the Degree of Doctor of Philosophy

in the University of Hull

by

Emmanuel Etim Ubuo

BSc (Uyo, Nigeria), MSc (Port Harcourt, Nigeria)

May 2016

DEDICATION

This Thesis is dedicated to the memory of my dear sister, Theresa Ubuo. I left her residence in Lagos, Nigeria for this programme in United Kingdom but she passed away during the course of this PhD. I miss her every day.

ACKNOWLEDGEMENTS

My sincere gratitude goes to my two supervisors, Dr Tommy Horozov and Prof Vesselin Paunov for the excellent guidance throughout the duration of the PhD programme. I am very grateful to Nigerian Tertiary Education Trust Fund (TETFund) and Akwa Ibom State University, Nigeria for funding this work to completion.

Inspirations and financial assistance from Christopher Ente (London), Moses David (Canada), Prof Bernie Binks (Hull) and Hamza Alshehri (Soudi Arabia) will ever remain fresh in my mind. I am also grateful to Prof Paul Fletcher and other lecturers in the former Surfactant and Colloid Group of the University of Hull who contributed immensely to give me effective grooming during the research training.

I am as well grateful to all my colleagues and friends in Dr Tommy Horozov's and Prof Vesselin Paunov's Research Groups, Prof Gilian Greenway, Prof Dave Evans and the entire staff of Chemistry Department, University of Hull, UK. I am particularly grateful to some technical staff of the Department including, Tony Sinclair who assisted me in providing additional scanning electron microscope (SEM) images; Nigel Parkin for the repairs of the spin coater instrument; and Julia Malle for timely fabrication of various in-house made glass apparatus.

Finally, my sincere gratitude and love go to my wife, Florence and our children, Edidiong, Unwana and Idara. My success became a reality as a result of all your patience and sacrifices through the duration of this PhD work. Also, appreciated are my parents, brothers and sisters including, Okon Ubuo, Martina, Edwin, Emilia, Etim Jnr, Boniface and Mary Ubuo. I would not have succeeded without your helps and earnest supports, thank you all.

Declaration

Except where stated, this thesis is a result of my own work. No part of this thesis has already been or is being concurrently submitted for any degree or other certificates at any other university or institution.

Some of the results in this project have given rise to the following conferences and presentations:

Oral presentations:

Wetting and bio-fouling of porous coatings impregnated with oil, Formula VII Conference, Barcelona, Spain, July 4^{th}-7^{th}, 2016.

Fabrications of silica coatings with tunable wettability, University of Hull Research Colloquia, Chemistry Department, University of Hull, May 15, 2015.

Fabrication and characterisation of slippery surfaces using oil-impregnated nano-porous silica coatings, 37 Annual International Conference of Chemical Society of Nigeria, Uyo, Nigeria, 7^{th} – 12^{th} September, 2014.

Superhydrophobic, Sticky and Slippery surfaces, Surfactant and Colloid Group Seminar, Faculty of Science and Engineering, May 7, 2014. University of Hull, UK

Poster Presentations

Gradual impregnation and wetting properties of porous coatings in bio-fouling environment, Juliot-Curie Conference 2015, September 16 and 17, 2015, Cambridge, UK.

Fabrication of superhydrophobic and slippery surfaces using silica particles, PhD Experience Conference, University of Hull, April, 2014, Hull, UK.

Abstract

Extreme water repellency observed on the surface of lotus leaf and the mechanism behind it is well studied and used for the fabrication of self-cleaning materials. Recently, the slippery mechanism of the rim of Nepenthes pitcher plant was revealed and mimicked in the so called Slippery Liquid-Infused Porous Surfaces (SLIPS). Here, we have fabricated silica nano-porous coatings using hydrophobic fumed silica. The partial impregnations of the coatings with different amounts of non-volatile oil (squalane) allows us to gradually tune its wetting behaviour from a superhydrophobic state in the absence of oil, through various intermediate wetting states, to slippery surfaces at high loading of oil. Superhydrophobic and slippery surfaces produced were found to possess low retention of water drops and good anti-biofouling characteristics towards algae cells. The intermediate coatings between the superhydrophobic and to slippery surfaces were found to exhibit different degrees of water and algae cells adhesions in similar trends. A simplified one-step deposition for large scale production of the coatings has been developed from a single formulated dispersion. In order to understand the wetting mechanism of the squalane-impregnated surfaces, the coatings were duplicated into solid states by similar partial impregnation using curable polydimethylsiloxane, PDMS (Sylgard 184). In these forms, the SEM images have clearly revealed the morphology of these gradual oil-impregnated coatings to spans from hierarchical nano/micro-structured coatings through larger scales of roughness to smoother coatings. Studies with curable Sylgard have led to the development of a simple and environmentally friendly method to grow ultra-thin polymeric films on solid surfaces for the fabrication of a more stable coatings and the modification of structured materials such as silica/aluminium oxide coatings as well as different metals and paper materials. In-depth characterisation of the fabricated substrates including, the porosity and thickness of the coating as well as the distribution and mass of the impregnated oil have been determined using capillary-driven impregnation, Dektak profiling system, fluorescence microscopy, and gravimetric analysis, respectively. Wetting properties of the coatings such as contact angles, sliding angles, sliding forces, contact angle hysteresis and adhesion of algae cells have been investigated and are discussed in term of the resulted changes in the surface architectural structures and surface chemistry following the gradual oil impregnation.

Table of Contents

List of Figures

List of abbreviation

V_P	Pore volume
V_S	Volume of the solid (silica particles)
γ_{LA}	Surface tension of liquid in air
γ_{SA}	Surface energy of solid in air,
γ_{SL}	Liquid-solid interfacial energy
θ_A	Advancing contact angle
θ_C	Cassie-Baxter (apparent) contact angle
θ_E	Young's equilibrium contact angle
θ_R	Receding contact angle
θ_W	Wenzel (apparent) contact angle
φ_S	Solid fraction of the wetted
µm	micrometre
CAH	Contact angle hysteresis
DCDMS	Dichlorodimethylsilane
deg	Degree
DSA	Drop shape analyser
h	Hour
HMDS	Hexamethyldisilazane
M	Molar concentration
M_C	Mass of the microscope slides after coating
M_I	Mass of the impregnated coating
M_O	Mass of the microscope slides before coating
PDMS	Polydimethylsiloxane
PFDTS	Perfluorodecyltrichlorosilane

rpm	Revolutions per minute
SEM	Scanning electron microscope
SiO_2	Silicon dioxide
SLIPS	Slippery liquid infused porous substrates
TLC	Thin layer chromatographic
UV	Ultraviolet
Vol.%	Volume percent
W_a	Work of adhesion
W_c	Work of cohesion
Wt.%	Weight percent
FR	Flow rate
S	Spreading parameter
nm	Nanometre
r	Roughness factor
s	Second
v	Velocity
θ	Contact angle

CHAPTER 1

INTRODUCTION

1.1 Wetting of solid surfaces

Wetting can be described as the relative ability of a liquid (or fluid) to adhere to another surface due to the intermolecular interactions when they are brought in contact. The degree of wetting is a result of the balance between the cohesive and adhesive forces which determines whether the liquid will spread of the surface or will form a drop of finite contact angle. Wetting phenomena occur in many processes in adhesive, coatings/painting, dyeing printing, cleaning as well as, biofouling and corrosion [1].

The way a particular liquid phase (e.g. water) wets solid surfaces differs from one solid material to another. In some (e.g. clean glass), it may either spread to form a wetting film, in others (e.g. aluminium plate), it may partially form a drop of finite contact angle, and in some cases (e.g. lotus leaf), the water phase may form nearly spherical drops and roll off the surface. In the same manner, different liquids will wet a particular solid differently. For instance, if water, oil and mercury are dropped on a clean glass substrate, water will definitely show the highest wettability, followed by oil, and then, mercury (glass wettability: water $>$ oil $>$ mercury). Studies have revealed that wetting (complete wetting, partial wetting or non-wetting) of liquid droplet on solid surfaces is dependent largely on two major factors, the surface chemistry and the topography (smoothness or roughness) of solid material [2].

In a liquid, the molecule in the bulk is attracted by the neighbouring molecules in all directions equally. Molecules at the surface are attracted inward because the surface molecules lack nearby molecules above them. This pull develops a tension on the surface of a liquid (surface tension) which can only by overcome by a force higher than

the pull. In a solid, molecules are closely packed so as to achieve maximum attraction and minimum repulsion [3]. The surface molecules possess excess energy that can attract external molecules to achieve the minimum energy [4]. Thus, the surfaces of both the solid and the liquid are governed by the tensions generated by the excess interactions of the surface molecules, which give rise to attraction or adhesion in solid and cohesion in liquid (Figure 1.1).

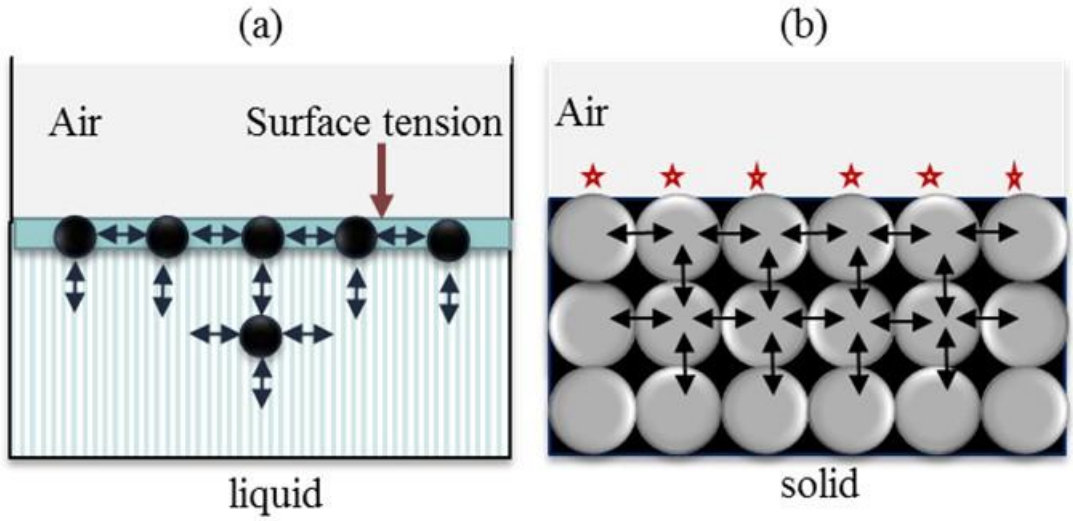

Figure 1.1 Intermolecular interactions that cause cohesion/surface tension in liquid and adhesion/surface energy in solid. In a liquid (a), molecules in the bulk have balance interactions in all direction and therefore remain in equilibrium whereas surface molecules bounded to air lack such balance attractions but are pulled inward by other molecules. This effect generates tension at the liquid surface. In the case of solid (b) molecules are closely packed so as to achieve maximum attraction and minimum repulsion. However, the unbalanced interactions of the surface molecules render them active and therefore possess excess free energy (shown by the stars) that can be minimised by external interactions including the adhesion of liquid.

The configuration of a liquid droplet on solid surface is therefore controlled by the strengths of this adhesion between the liquid and force of the solid surface and the

cohesive force of the liquid. Strong adhesion between the solid and the liquid normally cause marked wetting whereas high cohesive force within the liquid usually leads to non-wetting**.** These opposing characteristics are always dictated by the spreading parameter, S, which, in general, is the difference between the work of adhesion, W_a, and the work of cohesion, W_c, as shown in Eq. 1.1 [5, 6].

$$S = W_a - W_c \qquad 1.1$$

In the above equation, if S > 0, the liquid drop spreads completely in order to lower the surface free energy; if S < 0, the drop does not spread but form an equilibrium dome shape on solid with a finite contact angle, θ.

The three-phase contact angle, θ of a liquid at the solid-liquid interface is a useful parameter for measuring the degree of wetting. The contact angle of a liquid droplet on the solid surface is the angle a droplet make between the solid-liquid interface and a tangent to a liquid drawn to the three-phase boundary where the liquid, gas and solid meet (Figure 1.2a). Conventionally, when the contact angle of water is less than 90° (θ < 90°), the solid material is said to be hydrophilic. It is hydrophobic when θ > 90°. Wetting at the extremes of these two cases are termed super-hydrophilic (θ < 10°) and super-hydrophobic (θ ≥ 150°), respectively.

Wetting of water droplet on different solid surfaces are also illustrated in Figure 1.2 (a-c). In the figure, when θ is large the liquid-solid contact area becomes small but when it is small, the wetted portion is large. The later happens when the molecular attraction between the liquid and the solid is greater than the one within the liquid. As a result, the liquid-liquid interaction is disrupted in favour of the liquid-solid.

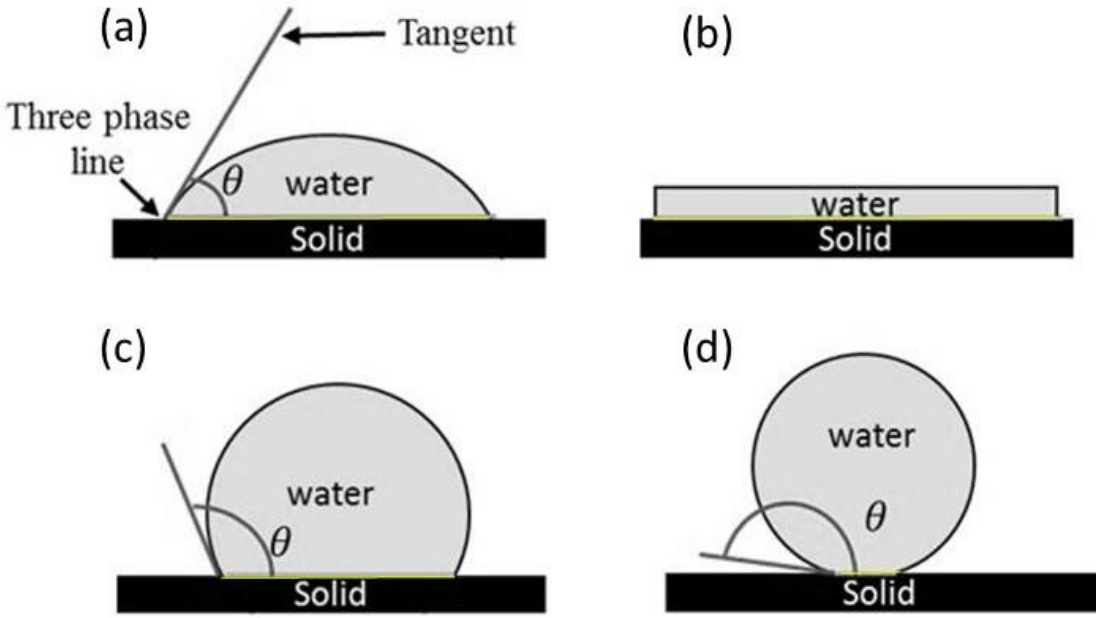

Figure 1.2 Wetting behaviour of a water droplet on different solid surfaces. The yellow lines show contact area of solid-liquid interface. Contact area varies inversely with contact angle of droplet. (a) Hydrophilic surface, (b) super-hydrophilic surface, (c) hydrophobic surface and (d) superhydrophobic surface. Larger contact angle of the droplet means a decrease in contact area between the droplet and solid surfaces.

1.2 Wetting of smooth solid surfaces

The physics of the wetting of a flat surface was first considered by Thomas Young in 1805 [7]. He observed the so called contact angle of a liquid on a dry solid surface and related it to a force (the surface energy of solid, liquid and the interfacial tension between the solid and liquid) acting on the droplet to obtain the equilibrium contact of the droplet with the surface (Figure 1.3).

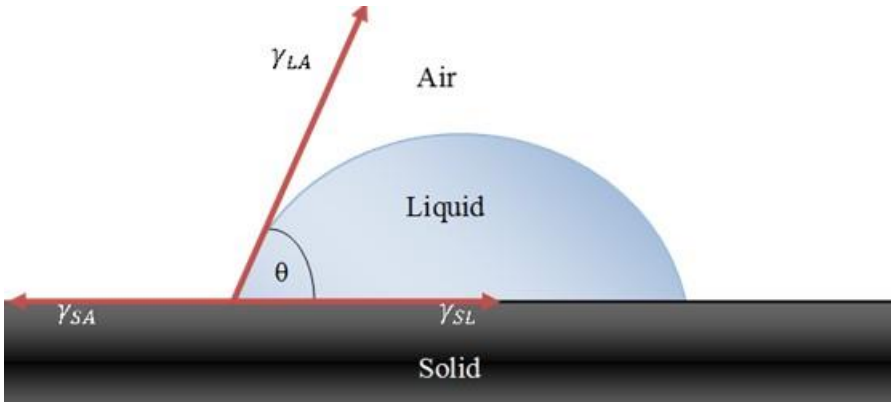

Figure 1.3 Diagram showing the tensions acting on the three phase contact line of a liquid drop on a smooth solid surface in air.

$$cos\theta_E = \frac{\gamma_{SA} - \gamma_{SL}}{\gamma_{LA}} \qquad 1.2$$

In Figure 1.3, θ (given in Eq.1.2 as θ_E) is the Young's contact angle on a flat solid, γ_{SA} is the surface energy of solid in air, γ_{SL} is the liquid-solid interfacial energy and γ_{LA} is the surface tension of liquid in air.

1.3 Wetting of rough surfaces

Wetting of rough surfaces is described by the homogeneous model propounded by Wenzel in 1936 [8] and heterogeneous wetting discovered by Cassie and Baxter in 1944 [9].

1.3.1 Wenzel model

This model considers homogeneous wetting in which the liquid wets a rough surface and maintains intimate contact with the top and the hollow portions of the solid material

[8]. The Wenzel mode of wetting on hydrophobic solid substrate is illustrated in Figure 1.4. The actual contact angle of such wetting was given by Wenzel as shown in Eq. 1. 3.

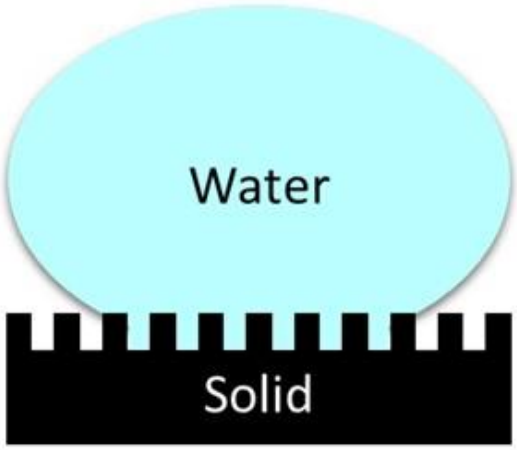

Figure 1.4 Wetting of a liquid on a rough surface using the Wenzel model. The liquid wets solid surface fully and through the contour of the rough substrate.

$$cos\theta_W = rcos\theta_E = r\frac{\gamma_{SV}-\gamma_{SL}}{\gamma_{LV}} \qquad 1.3$$

θ_W is the Wenzel (apparent) contact angle at equilibrium, θ_E is the Young contact angle, and r $>$ 1 is the ratio of the true surface area of the solid to its horizontal projection. Simple mathematical interpretation of Eqn. 3 is that, for hydrophilic flat surface where θ is less than 90 °, contact angle of a rough surface, θ_W becomes smaller than contact angle of a flat surface, θ_E. For hydrophobic flat surface with θ greater than 90 °, contact angle of a rough surface, θ_W becomes bigger than contact angle of the flat surface, θ_E. Thus, increasing of the surface roughness amplifies the hydrophilicity or the hydrophobicity depending on the surface chemistry of the original material.

1.3.2 **Cassie-Baxter model**

In the Wenzel mode of wetting, the entire contour of a rough solid surface is in contact with the liquid, but Cassie-Baxter focused on another possibility in which the liquid droplet could bridge across the top structural features of the rough surface so that the droplet rests on top while the grooves are occupied by other materials (e.g. air). A sketch in Figure 1.5 shows a water droplet sitting on a solid-air composite. Because the droplet is resting on both the air and the solid material, the cosine of the contact angle of liquid droplet was given by Cassie-Baxter as the average of the cosines of the contact angles of the participating surfaces multiplied by the respective fractions of their contact area with the droplet (Eq. 1.4).

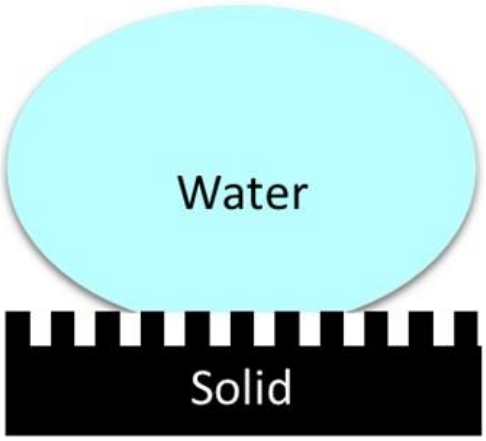

Figure 1.5 Wetting of a liquid on a rough surface using the Cassie-Baxter model. Here droplet sits on solid-air composites without penetrating the grooves.

$$cos\theta_C = \varphi_S cos\theta_E + (1 - \varphi_S) cos\theta_a \qquad 1.4$$

In the above, φ_S is the fraction of the solid surface present at the top (i.e. solid – liquid contact), $(1 - \varphi_S)$ is the fraction occupied by air, θ_E is the Young contact angle and θ_a is the contact angle of the air portion (180 ^{o}). Hence, the above equation can be rewritten as shown in Eq. 1.4b.

$$cos\theta_C = \varphi_S cos\theta_Y + \varphi_S - 1 \qquad 1.4b$$

1.4 Contact angle hysteresis

In the Young model, the liquid drop forms an equilibrium contact angle on the solid surface. The implication of the theory is that the contact line can move freely on such a perfectly smooth surface and even if the volume of the droplet is changed the contact angle will remain the same and equal to the equilibrium contact angle [10, 11]. Further investigations have demonstrated that the above equation can best be applied to an ideal surface which is rigid, insoluble, nonreactive, chemically homogeneous and with a perfectly smooth topography, which is rare to find [10, 12]. On real surfaces (observed to be smooth), liquid droplets are commonly observed to get stuck when tilted (e.g. windscreen). Such droplets usually show different contact angles across its contact line perimeter ranging between a minimum (upper) and maximum (downward) value. A similar process is also observed experimentally during injection and withdrawal of liquid from a sessile liquid drop. When liquid is pumped into the droplet, the three-phase contact line is usually pinned to the substrate while the droplet increases in volume to a certain value of contact angle before the three phase contact line jumps or increases. The maximum contact angle formed before the jump in liquid-solid interfacial area is termed an advancing contact angle, θ_A. When a liquid is removed from the sessile droplet at stationary three-phase contact line, the minimum contact angle reached before the three-phase contact line decreases is called a receding contact angle, θ_R. The difference between θ_A and θ_R is known as contact angle hysteresis (CAH) [2, 13]. Illustrations of advancing and receding contact angles and contact angle hysteresis are shown in Figure 1.6.

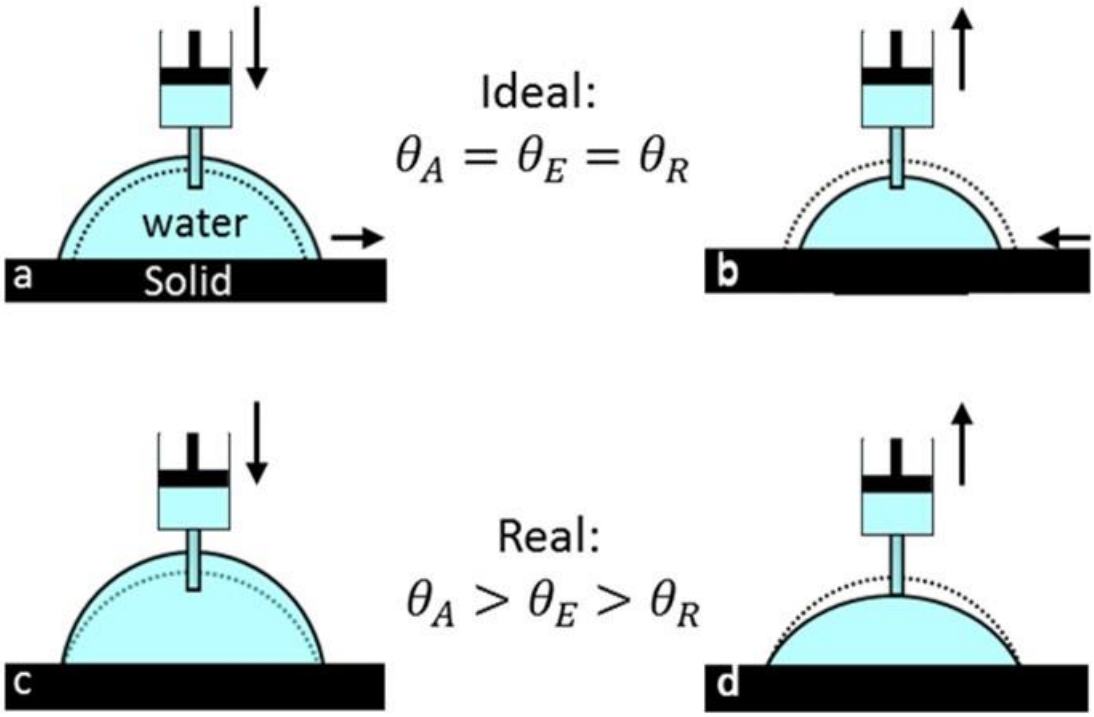

Figure 1.6 Behaviour of water droplets on an ideal solid surface (a, b) and real solid surface (c, d). Arrows indicate movement of the water phase. The broken lines indicate the configuration of initial (or equilibrium) droplet before addition (advancing) or removal (receding) of liquid. On an ideal (molecularly smooth) solid surface (a, b), addition or removal of liquid leads to a free movement of contact line on the surface without pinning, and no difference between advancing and receding contact angles occurs, in spite of change in the volume of droplet. On a real solid surface (c, d), addition or removal of liquid leads to pinning of the contact line, resulting an in the increase in advancing angle and a decrease in the receding angle. The displayed inequalities show the comparison of the advancing, equilibrium and the receding contact angles.

Hysteresis on rough surfaces can be explained using the two models describing the wetting of a rough solid surface. In addition to amplification of contact angle, another possible consequence of the Wenzel wetting regime of wetting is that as the liquid wets through the contours of the microstructures, the structures between the grooves have the tendency to pin the three phase contact line and thus prevent the free movement the droplet [14]. When this occurs, the liquid droplet becomes stuck and this gives rise to a

contact angle hysteresis. The Cassie-Baxter model drop shows much less hysteresis compared to a Wenzel model drop and is therefore preferred in applications involving moving droplets [15]. Earlier experimental investigation to study the effect of surface roughness, as cited by Quere [16], was reported by Johnson and Dettre. Data obtained in the work showing variation of advancing and receding contact angles with the surface roughness are presented in Figure 1.7. "As the roughness (defined here only qualitatively) increases, a significant increase of the hysteresis can be observed. Then, both angles suddenly increase while the hysteresis nearly vanishes. It can be observed that the value of contact angle decreases sharply at a point at where the Wenzel mode switched over to the Cassie-Baxter regime."

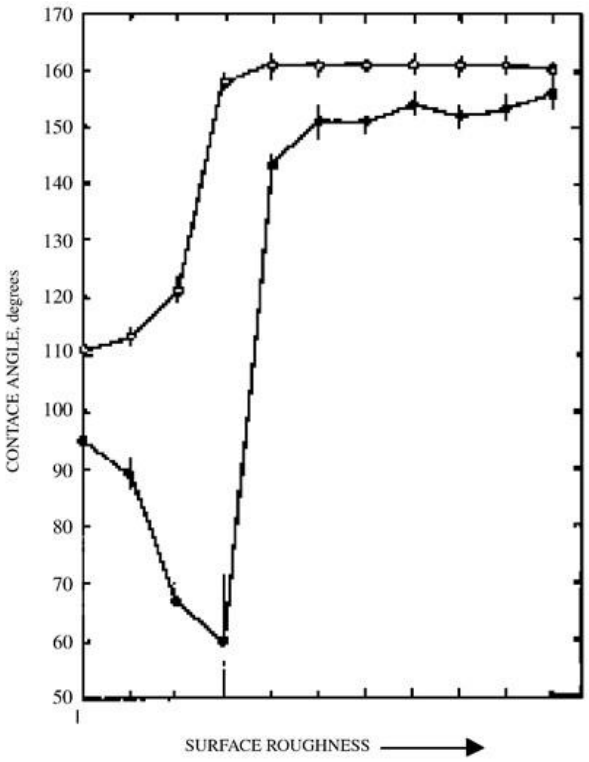

Figure 1.7 Static contact angle of water on wax substrates, as a function of the substrate roughness. Both the advancing angle (open symbols) and the receding ones (full symbols) are displayed (from Johnson and Dettre). The plot taken from ref. [16].

In addition to solid surface, Lam *et al.* [17] investigated a low-rate dynamic advancing and receding contact angles of 21 liquids from two homologous series (i.e. n-alkanes and 1-alcohols) and octamethylcyclotetrasiloxane (OMCTS) on FC-732-coated silicon wafer surfaces and reported that the receding contact angles do not reflect only properties of the solid, but also of the liquid as well. According to their findings, the receding contact angles of inert and hydrophobic surfaces were found to decrease with time, and therefore the process was affected by liquid retention, penetration, sorption or swelling. A related report by Lam *et al.* [18] also suggested that the contact angle hysteresis decreases with the chain length of a non-polar liquid (alkane) and stated that the receding contact angle became equal to the advancing contact angle when the alkane molecules become very long. They reported the chain length and size of the liquid molecule as contributing factor to contact angle hysteresis.

1.4.1 Limitations of Cassie-Baxter and Wenzel models

These two models have received very wide investigations and modifications to suit different conditions. As earlier mentioned, the traditional Cassie-Baxter model assumes a zero pressure gradient and the shape of the liquid interface between the grooves of solid is assumed to be flat [19]. On hydrophobic solid-air, Cassie-Baxter surface is characterised with a high contact angle and water repellency due to the additional hydrophobicity offered by the air pockets [19]. Wenzel model describes a homogeneous wetting which allows liquid to penetrate the trough of textured surfaces or the pores of the porous substrates. In this case, the liquid has the tendency to be hindered or become stuck between the surface bumps thereby reducing or prevent self-cleaning effect. However, the assumptions of Wenzel and Cassie-Baxter do not always hold perfectly in

certain conditions of the surface. Parameters, such as the randomness of the structures over different length scales, including protrusion heights, sizes/separations, condition of pressured, impacted or vibrated drops and the use of different materials and techniques have been reported as reasons for the instability or the transition between the Cassie-Baxter state and the Wenzel state [19-27].

Latthe *et al.* [22] reported that solid/liquid contact mode will change from the Cassie-Baxter to the Wenzel state under the condition of pressured, impacted or vibrated drop. Investigation on the penetration resistance effect arising from such compressibility of the entrapped air by droplets carried by Kim and Hidrovo [19] indicated that micro-cavities can maintain the Cassie state of a liquid meniscus, resting on top of the surface, in larger pressure ranges than open spaced micro-pillars arrays. Erbil and Cansoy [23], as well as Lee *et al.* [24], in their separate reports, made known that increase in heights and spacing of microstructures on rough surfaces enhances transition from Cassie-Baxter state to Wenzel model. Bormashenko *et al.* studied wetting of pigeon feathers and reported that the transition from Cassie-Baxter to Wenzel state under drop evaporation when drop radius became small enough for capillarity-induced water penetration into the troughs, formed by barbs/barbules network [20] Patankar [28] agreed with their earlier findings [15] which reported that there can be two contact angles, corresponding to Wenzel's and Cassie's theories on the same rough surface; that one has a lower energy than the other, and that one that offers minimum energy depends on the geometric parameters of the surface. He however argues that it is not guaranteed that a drop will always exist in the lower energy state. He cited the example of a drop formed by depositing it gently on the rough surface. Such a drop, according to him may remain in this state without transition. He therefore claims that the state at which a drop will settle depends typically on how the drop is formed and that work (such as

depositing the drop from some height, pushing the drop, or using a heavy drop) has to be done for transition from the Cassie-Baxter state to the Wenzel state to occur.

Nevertheless, transition from one mode to the other may not necessarily be perfectly achieved as the state of thermodynamic equilibrium may not be reached but an intermediate zone, or metastable equilibrium where partial wetting of the air-trapped Cassie-Baxter surface are observed. In such situations, a combination of both the Wenzel and the Cassie-Baxter models apply [23, 29] and can as well be described by Eq. 1.4b (see Figure 1.8).

Quere review on rough wetting is of the opinion that the evaluation of φ_S shown in Figure 1.8, and characterisation of such wettability is a bit difficult even on a well-designed patterns and more complex on irregular or disordered surfaces [16].

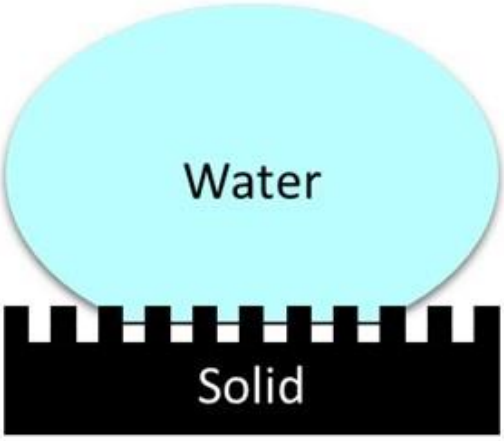

Figure 1.8 Cassie-Baxter model of wetting of a rough surface. Liquid partially displaces air and impregnates into the of the microstructure, but still rest on both the solid and the air.

1.5 Super-hydrophobic surfaces

1.5.1 Natural superhydrophobic surfaces

Super-hydrophobic materials are highly hydrophobic and wetting is almost totally impaired. Such materials are characterised with water contact angle of at least 150º. However, it has been observed that the highest contact angle of a water droplet on smooth hydrophobic solid surface falls within 110 ± 10º [30, 31]. Remarkably, the surface of some naturally occurring plant leaves are found to be super-hydrophobic. Extensive investigations on numerous plants showing this characteristics are listed in the work of Neinhuis and Barthlott [32]. Similar surfaces are found in animals such as the wings of some birds and insect legs [20, 33]. The common features on the surfaces of these organisms are the roughened, or structured, coverage at the micro-to the nanoscales [20, 32-35]. Scanning electron microscope images of some of the superhydrophobic plants studied by Neinhuis and Barthlott are shown in Figure 1.9.

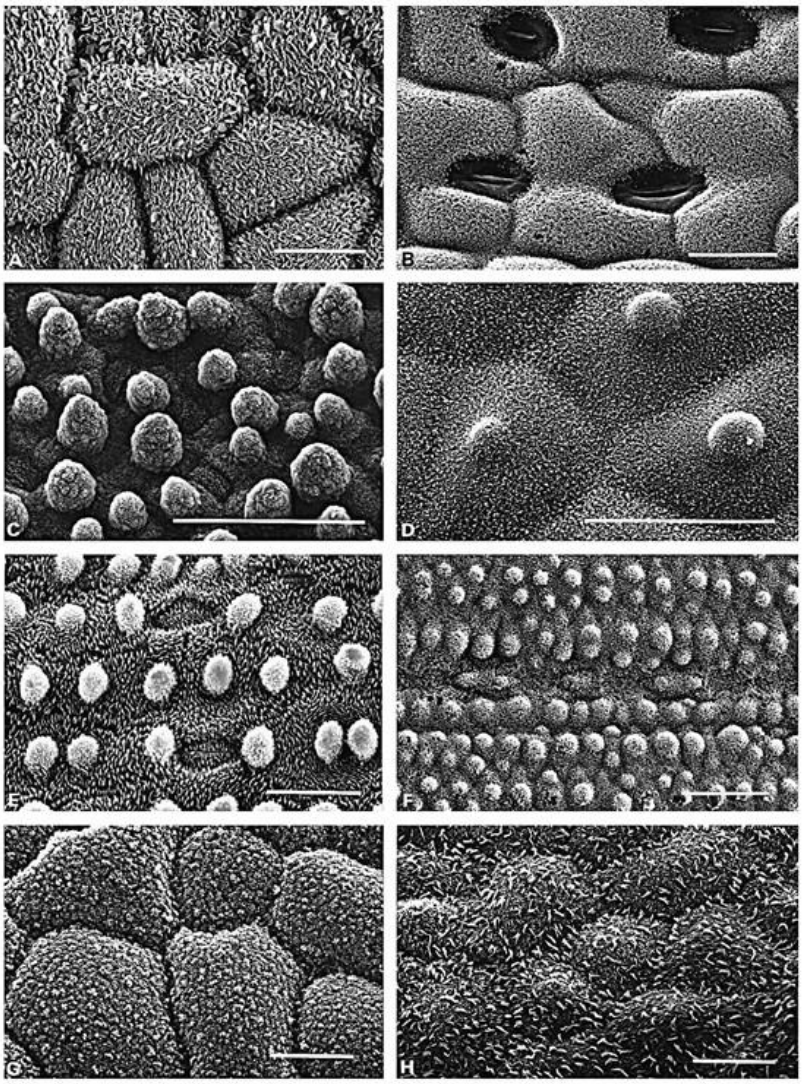

Figure 1.9 Micromorphological characteristics of water-repellent leaf surfaces. Water repellent leaf surfaces of *Hypericum aegypticum* (A) and *Marsilea mutica* (B) are due to convex epidermal cells and a dense layer of epicuticular waxes. Scale bars are 20 µm. C, *Nelumbo nucifera*; D, *Lupinus polyphyllos*. Every epidermal cell forms a papilla and is superimposed by a dense layer of epicuticular waxes. Scale bbar is 50 µm. E, *Gladiolus watsonioides*; F; *Sinarundinaria nitida*. The epidermal cells are subdivided into several papillae and covered by epicuticular waxes. Scale bars 20 µm. Increased roughness due to a differentiation within the wax layer: on the leaf surfaces of *Tropaeolum majus* (G) wax tubules aggregate to form larger clusters, while in *Melaleuca hypericifolia* (H) the wax layer is characterized by larger single platelets. Scale bar is 20 µm. Images obtained from [32].

One of the useful applications emanating from these natural architectural designed surfaces is the popular “Lotus effect” which signify the natural ability of the Lotus leaves to undergo self-cleaning even when it grows in muddy water [36]. Studies have shown that the Lotus effect is caused by the chemical composition of its surface, mainly made of hydrophobic epicuticular wax nano-crystalloids, and the bumpy micro topography. The roughness allows the surface to trap air within the pores, and the synergy created by the hydrophobic surface and the entrapped air pockets is responsible for the high contact angle and repellency of the leaf. In the process of rolling away, water droplets sweep off adhered debris and other foreign bodies from the leaf to maintain a clean surface. It has been established that the Lotus effect does not only clean the surface of the leaf but plays an important role in the defense against pathogenic organism, using its water repellency as a measure to deprive such organisms (e.g. spores) of water necessary for their growth [32, 36].

It is worth nothing that predicting the Lotus effect based on high contact angle alone could be misleading. The surface of a rose petal also possesses micro scale roughness and exhibit contact angle as high as up to 150º. However, unlike the lotus leaf with self-cleaning properties, it is characterized with high adhesiveness of the water drop and is referred to as “the petal effect”. Feng *et al.* and Wang *et al*. who investigated the wettability of the plant attributed the so called petal effect to dual scales of micro and nano roughness found on the plant surface. They believed, the larger scale allow Wenzel wetting regime to occur and is responsible for adhesion or large hysteresis, while the nanofold roughness entrapped air and exhibit high repulsion to the droplet and that this give rise to the observed high contact angle [37, 38].

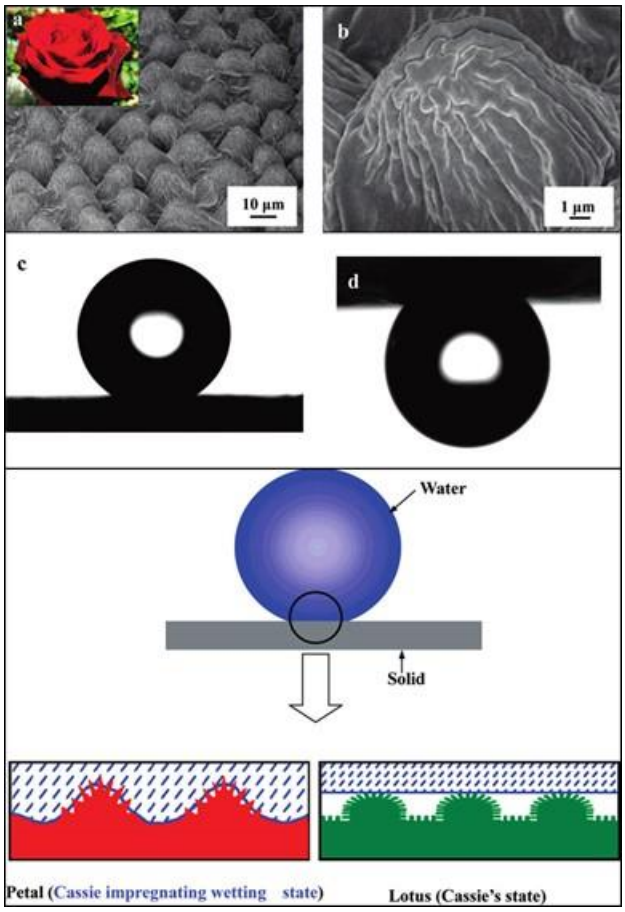

Figure 1.10 (a, b) SEM images of the surfaces of a red rose petal showing a periodic array of micropapillae and nanofolds on each papillae top. (c) Shape of a water droplet on the petal's surface, indicating its superhydrophobicity with a contact angle of 152.4°. (d) Shape of water on the petal's surface when it is turned upside down. (d) Schematic illustrations of a drop of water in contact with the petal of a red rose and a Lotus leaf (the Cassie-Baxter state). All obtained from ref. [37].

In a related investigation, Chang *et al*. investigated the wettability of scallion and garlic and reported advancing angles of the surfaces exceeding 150º but with very high contact angle hysteresis similar to the petal effect mentioned above. They attributed the super-hydrophobic nature of the leaves to epicuticular wax on microstructures surfaces of the leaves. However, they differ somehow from the earlier description of hysteresis on the

leaves. According to their report “Although impregnation may result in a certain extent of CA hysteresis, it may not be the only factor.” They believed the adhesion was likely caused by unusual chemical defects associated with organosulfur compounds (e.g. diallyl disulphide, DADS) found in the leaves. In their experiments, it was reported that DADS which is insoluble in water, was observed to spread spontaneously on water to form thin yellow film, instead of forming an oil lens. Subsequent spreading of superhydrophobic surface with DADS, the surface became highly adhesive to water, which was attributed to relatively low surface energy between water and DADS blemishes [39].

Bhushan and Her studied the wetting properties of two different rose petals (*Rosa, cv. Bairage* and *Rosa cv. Showtime*) and reported super-hydrophobic wetting with high adhesion on *Rosa, cv. Bairage* and super-hydrophobic wetting with low adhesion similar to lotus leaf on Rosa, *cv.* Showtime. Their finding indicated that Rosa *cv.* Showtime, with higher density and height of the bumps on the petals prevented penetration of water between the micro-bumps and exhibited low adhesion compared to *Rosa cv. Bairage* which has a large spacing of the microstructures and reduced height of the structures, enabling water penetration and decrease in the static contact angle, as well as an increase in contact angle hysteresis [40]. Figure 1.11 shows schematic illustrations of shape, heights and spacing of the microstructures on the two rose petals studied.

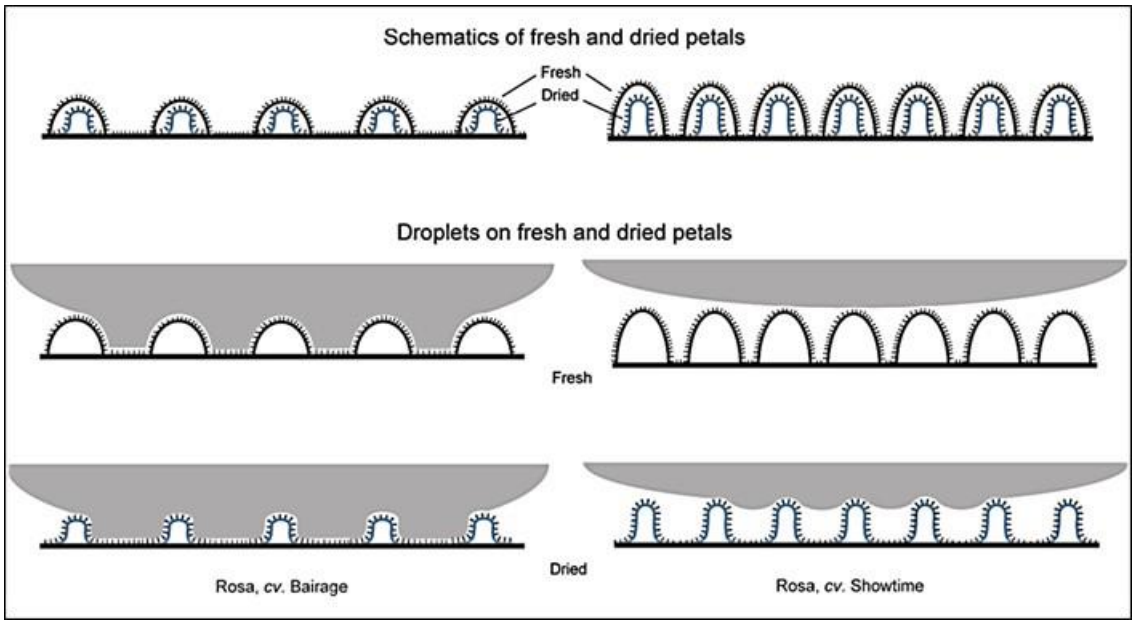

Figure 1.11 Schematic illustrations of shape changes between fresh and dried petals' hierarchical structure and schematics of a water droplet contacting fresh and dried rose petal surfaces. Left column shows the schematic for Rosa, cv. Bairage, with a super-hydrophobic and high adhesion surface, and right column shows Rosa, cv. Showtime, with a super-hydrophobic and low adhesion. Schematics taken from ref. [40].

1.5.2 **Artificial super-hydrophobic surfaces**

Serious effort dedicated in studying natural super-hydrophobic surfaces is aimed at replication and manipulation of the surface and reasonable achievements have been recorded in this direction. Several techniques for the fabrication of super-hydrophobic surfaces have been employed. In spite of the varieties, the basic guiding principle in making a super-hydrophobic surfaces involves the creation of pattern or roughness on the solid material of interest followed by surface modification of the substrate with a low surface energy materials.

1.5.2.1 Creation of micro/nanostructured surfaces

Rough surfaces can be produced by many techniques. The general idea involves either sculpturing of a smooth surface, or by depositing a rough layer on a smooth surface.

Techniques involving sculpturing of the smooth surface

- *Lithography*: Lithography involves creation and transferring of micro or nanoscale imprints on a material of choice. This may involve the use of light/electron beams (photo/electron lithography), or the use of stamps bearing the required microscopic pattern (soft lithography). In light or electron beam lithography for instance, light or electron beam is shined or directed through a designed mask onto a light or electron sensitive surface (resist). The effect of the light activates the area based on the designs of the mask thereby transferring the geometrical shapes of a mask to the surface. Soft lithography involves the physical contact of the master imprint with the surface. In this case, an imprint from the master can be pressed onto the substrate, or a patterned master can used as a mould [41, 42].
- *Etching*: In the case of etching, acids or reactive ions are used to attack exposed or unprotected portion of the material to create roughness on the surface [43, 44]. Choi *et al*. fabricated hierarchical aluminium surfaces using three different kinds of alkaline-based chemical etchants, The solutions were prepared by adding sodium hydroxide and zinc nitrate hexahydrate and nickel nitrate hexahydrate (as metal precursors) in deionized water at 70 °C. Initial etching with sodium hydroxide and the nickel containing solution produced needle-like microstructures. Nanoscale flakes on microscale porous structured were formed after etching with zinc containing solutions. A Super-hydrophobic aluminium

surface with 159º water contact angle were obtained after surface fluorination [43]. Micro-structured surfaces were also obtained by Qi *et al*. using a similar method in acidic media, assisted copper, silver and chromium ions (1 M HCl and 0.1 M metal nitrate) [44].

- *Plasma treatment*: Plasma treatment is another form of etching but uses ions with more energy to impact on the selected area of the sample. When such a substance is accelerated and impacted on low molecular weight material hollows or roughness are inscribed on them. A two-step plasma process involving oxygen, O_2 and tetrafluoromethane, CF_4 was used by Fresnais *et al*. to modify low density polyethylene. Oxygen plasma actually roughened the surface while CF_4 plasma blended the surface with a non-polar layer. Wettability studies on the sample gave super-hydrophobic surfaces with a water contact angle exceeding 170° [45]. A similar process was used by Han and Moon to fabricate super-hydrophobic surface on a glass by helium based CH_4 and C_4F_8 atmospheric pressure plasmas [46].

Techniques involving deposition of rough layers on smooth surfaces

- *Layer-by-layer Deposition*: A thin film fabrication technique involving deposition of oppositely charged material. In such processes, thin nanocomposite films are assembled on a surface by alternately depositing mutually attractive molecules or particles. In the process, a bilayer film is formed by depositing a cationic polymer onto an anionic polymer bound to the surface. Subsequent alternating additions of more cationic and anionic polymers produce additional bilayers. This process is performed again and again until the grafted thin film so formed reaches the desired thickness, or properties [47].

Zhao *et al* [48] fabricated a branchlike structure of silver, aggregates on the matrix of a layer-by-layer polyelectrolyte multilayer by an electrodeposition technique to form a self-assembled monolayer of *n*-dodecanethiol with contact angle of 154° and a tilt angle lower than 3°.

- *Electro-spinning*: Electro-spinning method makes it possible to produce fibers with diameters in the micro or nanometers scale on the surface. Arrangements of these fibers can be made to enhance directional roughness that can clear liquid off the surface easily. The fibers can as well be roughened for the surface to attain a higher super-hydrophobic state. Super-hydrophobic pullulan membranes were prepared by electrospinning of hydrophobised pullulan [49].
- *Chemical vapour deposition (CVD)***:** In chemical vapour deposition, thin micro/nano films are deposited on a required surface exposed to vaporised reaction. Micro-roughened coating has been reported by Daly and Horn by simply by placing stainless steel plate above a burner (Figure 1.12). [50].
- *Electrodeposition*: This method allows the desired surface to be electroplated with dissolved metal ions in an electrolytic cell [51-54]. Liu *et al*. has reported super-hydrophobic surface coated on copper cathodic substrate with an electrolyte solution. The surface adhesion of the coating was controlled by the reaction time [51].
- *Use of nanorods, carbon nanotubes and nanoparticles***:** Superhydrophobic surfaces have been realised by systematic assemblies of metallic or semiconductor nanorods [55-61], nanowires [62-66], nanotubes [67, 68] nanoparticles (including silica, silver gold, aluminium, titanium and Zinc oxides [69-76]. The aim of this technique is basically to transfer the nanoroughness offered by the minute nature of these materials to the surface.

- *Templating*: Most of the methods used to fabricate super-hydrophobic surfaces are either complicated or involves the use of special apparatus. The use of a template is a facile and inexpensive approach to obtain a super-hydrophobic surface from common hydrophobic materials for commercial and scientific needs. In the methods, micro-roughened surfaces, including natural surfaces and already designed surfaces are used as a master piece to reproduce the same surface without going through the rigorous process of designing a new one. Templates of different shapes and designs have been reported [77-79]. Templates of Lotus leaf have been used to fabricate an artificial lotus leaf on PDMS by Sun *et al* [79], while Yuan *et al*. used taro leaf on polystyrene [77] respectively. Park *et al*. reported fabrication of thin anodized aluminum oxide (AAO) templates on a substrate with highly-ordered nanopores through soft lithography. Dry etching process in combination with the imprinted polymer film enabled the control of the thickness of the thin hexagonally or tetragonally ordered nanoporous template [80].

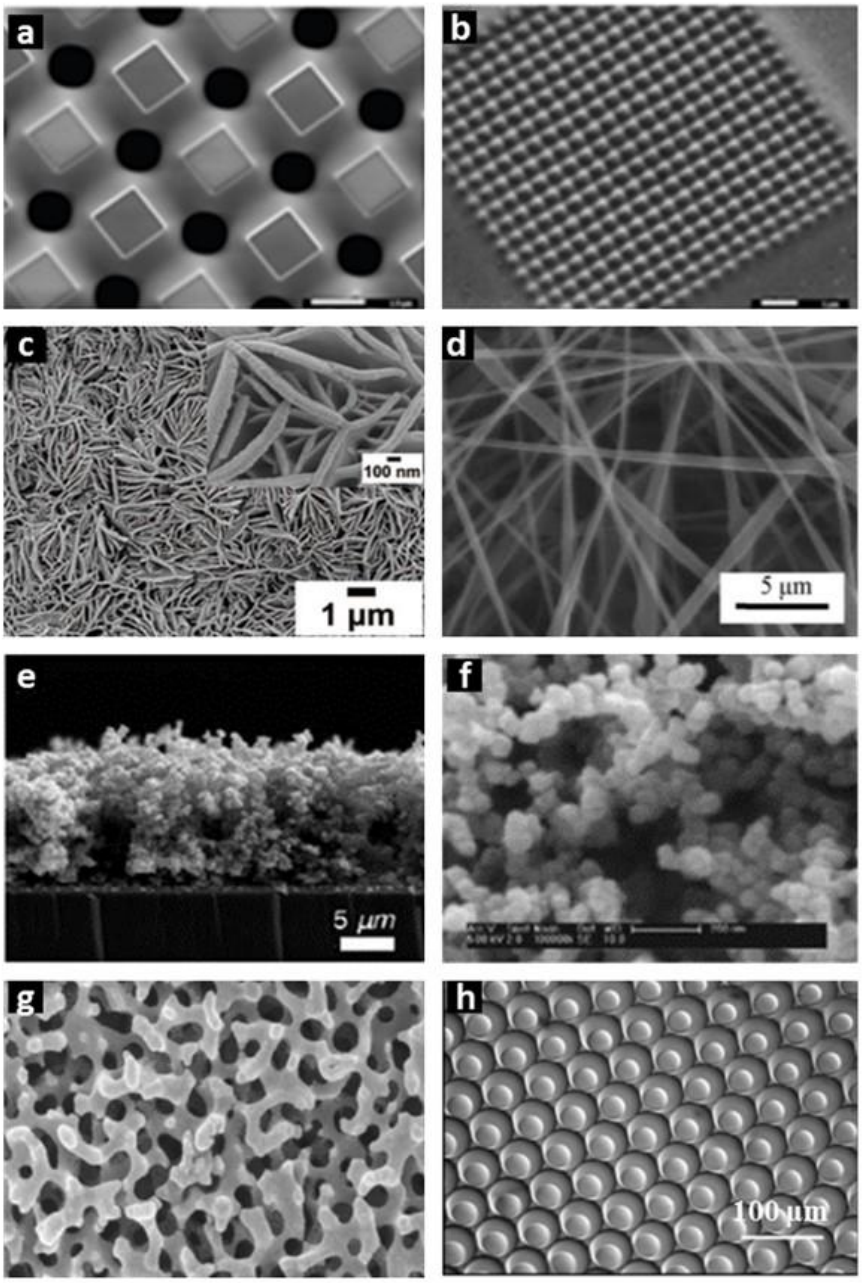

Figure 1.12 SEM images of different micro/nanostructured surfaces. (a, b) Dual-scale electron-beam-lithography with secondary nanostructures shown in (b), both taken from ref. [41] (c) Electrochemical deposition on metals, from ref. [81] (d) Electrospinning of fluorinated silane functionalized pullulan, from ref. [49] (e) Electrodeposited and annealed TiO_2 film, prepared from $TiCl_4$, taken from ref. [82] (f) Kerosene soot sample, from ref. [50] (g) Glass surface after treatment to induce thermal spinodal phase separation, followed by preferential removal by etching, taken from ref. [83] (h) O/W/O double emulsion drops produced in a PDMS device with spatially patterned wettability. [84].

1.5.3 Chemical modification with low surface energy materials

Chemical modification is a process aimed at altering the surface chemistry of non-hydrophobic material to hydrophobic state in order to enhance the functionality of such materials to super-hydrophobic states. Organofunctional silanes and fluorinated compounds are widely used for modification of hydrophilic materials to hydrophobic states. The choice of these coupling agents depends on availability of the hydrolysable group in the compounds. Trichloro(trifluorooctyl) silane is composed of both hydrophobic and hydrophilic ends, thus, cannot bond directly to the substrate. To change the compound to reactive specie; the hydrophilic end the silane is hydrolyzed for effecting bonding to silicone; the organic part is exposed against water attack [85].

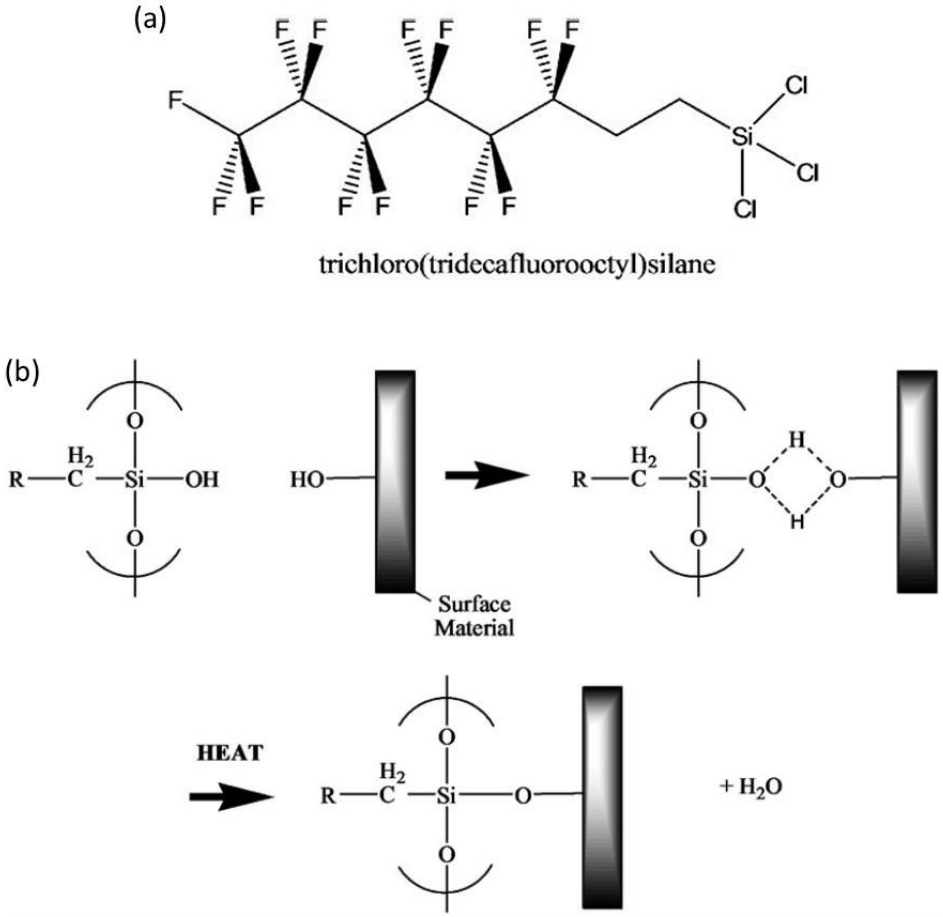

Figure 1.13 (a) An example of a fluoroalkylsilane (FAS) molecule. (b) Proposed condensation reaction at a surface (hydroxyl groups) by using an altered FAS; R=hydrophobic chain of the FAS molecule (obtained from ref. [85]).

However, apart from using polar solvents (e.g. water, methanol, ethanol), modification of this nature can as well be carried out in organic solvents (anhydrous medium such as. acetone, toluene) and dehydrated surface [86, 87].

Vapour phase hydrophobisation of a substrate using silane compounds has also been used. Surface modification of alumina by hexamethyldisilazane, HMDS to hydrophobic surface in vapour phase has been reported by Tasaltin *et al*. In order to increase the density of the surface hydroxyl groups before the actual surface modification, the

samples were first submerged in deionized water at 100°C for 1 min. The samples were then dried at 50°C and then put in a sealed vessel and liquid HMDS introduced for its vapour to react with the exposed substrate. The reaction was carried out at 100 °C for 4 to 9 h. Boiled water submersion and hydrophobisation was repeated trice to obtain maximum hydrophobicity. Schematic illustrating the modification process is shown in Figure 1.14 [88]

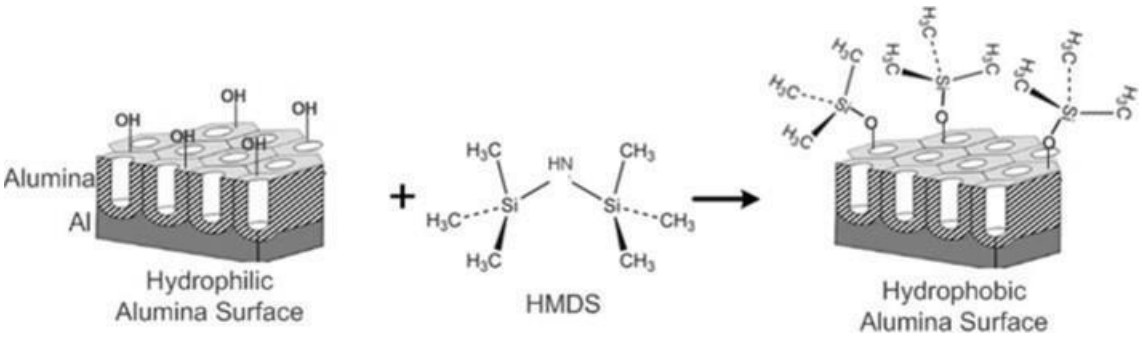

Figure 1.14 Schematic illustration of HMDS modification process on a nanoporous alumina surface. Scheme adapted from ref [88].

Other organic compounds have also been reported for solid substrate modification [89-93]. Chen *et al*. used electrochemical method in an electrolytic solution containing nickel chloride ($NiCl_2.6H_2O$), myristic acid and ethanol to make a super-hydrophobic copper cathode plate [89], while Zhang *et al.* have produced stable aluminum alloy by simply immersing of the substrate in a solution of hydrochloric acid and fatty acid molecules [92].

1.5.4 **Smart and switchable surfaces**

Some fabricated surfaces are referred to as smart because they are structured to respond to certain needs that ordinary mono-functional surfaces cannot act against. In nature, the

Namib desert-beetle, for instance, uses the wettability on its patterned back to collect drinking water from fog-laden wind. The back of this beetle is made of alternating hydrophilic hills, and wax coated hydrophobic channels. The hydrophilic bumps helps the beetle to collect water from the atmosphere while the super-hydrophobic channels roll the water away toward the beetle's mouth [94].

Zhai *et al*. replicated Namib Desert beetle back by creating hydrophilic pattern on hydrophobic surface with water harvesting characteristic. Super-hydrophobic coatings with contact angle angle of 172° was first fabricated. Hydrophilic patterns on super-hydrophobic surfaces were then created with water/2-propanol solutions of a polyelectrolyte to produce surfaces with extreme hydrophobic contrast. Selective deposition of multilayer films onto the hydrophilic patterns introduces different properties to the area including hydrophilic surfaces with contact angle less 20°. They suggested possible applications of the materials in water harvesting surfaces, controlled drug release coatings, open-air microchannel devices, and lab-on-chip devices [95].

A two-level structured self-adaptive surface with reversible tunable properties has also been reported by Minko *et al.* to create an ultrahydrophobic and hydrophobic tunable surfaces used to control adhesion [96]. Also reported are wavelength-selective caged surfaces, reported by Miguel *et al.* [97], photo sensitive surface [98] and humidity responsive surfaces by Shen *et al*. and shown in Figure 1.15 [99].

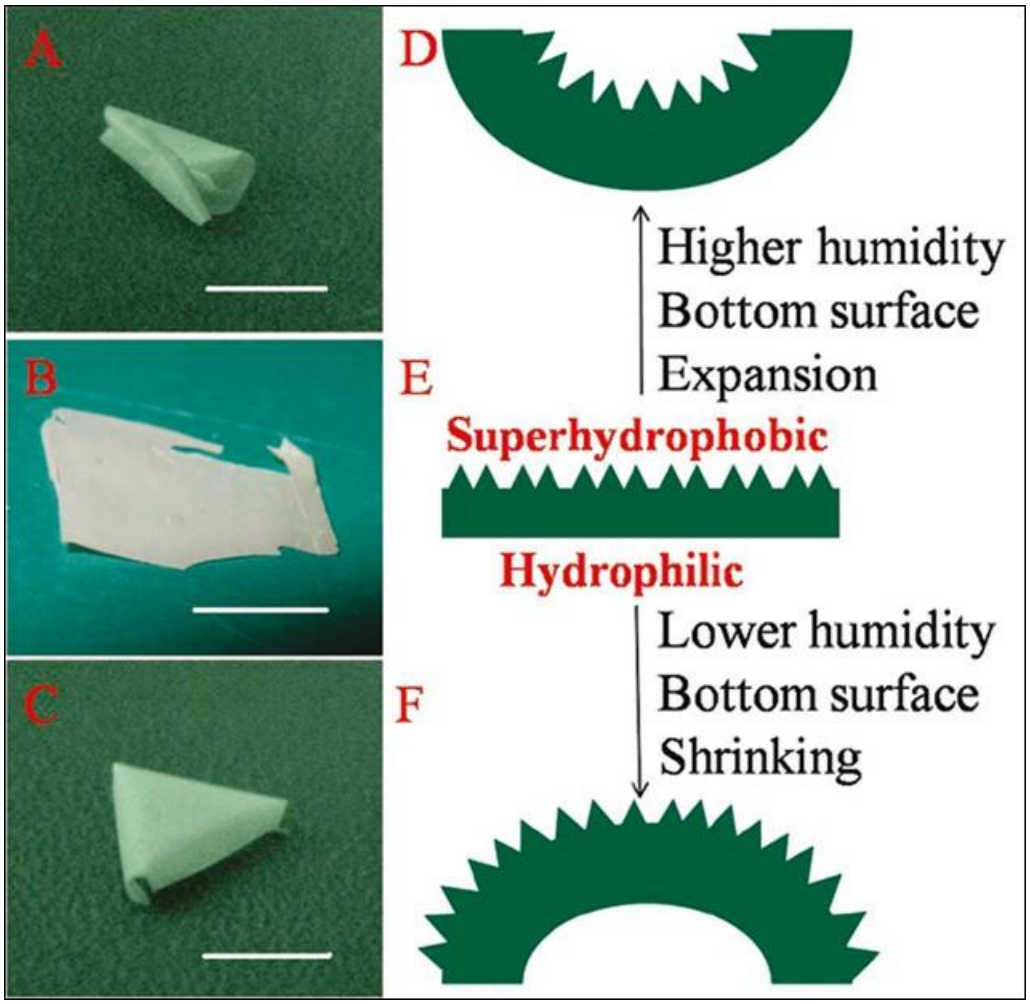

Figure 1.15 Left: Images of the steady-state shapes of a (PEI/PAA) 20 free-standing film under different RH (T = 20 ^{o}C). (A) At 95% RH, the upper surface is rolled inside. (B) At 85% RH, the film is almost flat. (C) At 75% RH, the bottom surface is rolled inside. Right: Schematic illustration of shape transitions of an asymmetric free-standing film toward humidity changes. The upper surface is super-hydrophobic, and the bottom surface is hydrophilic (E). The bottom surface can either shrink (F) or expand (D), leading to different shape transitions. Scale bars show 1 cm. Images obtained from ref. [99].

1.5.5 **Application of silica micro/nano-particles**

Silica is a stable oxide of silicon (silicon dioxide), SiO_2. It is abundant as native sandstone, silica and quartzite and volcanic ash. It can also be found in synthetic form as fumed silica, monodisperse silica, colloidal silica and silica gel.

Silica particles are usually applied to the surface as a dispersion. Uniform spreading of the particles over the surface can be achieved by spin coating, involving centripetal acceleration to spread a drop of dispersion, drainage (or spilt off), solvent evaporation, film thinning and solidification. Dip coating where the substrate is wetted by dipping into the dispersion and then withdrawn at a constant speed. During the withdrawal process some of the coated film is drained by gravity to produce a thin film on the substrate. This is followed by evaporation of solvent drying of the coated film.

Silica plays significant roles in surface enhancement and material technology due its unique physical and chemical properties. Most studies focus on silica coating with specific surface characteristics with a view toward improving the physical properties of the film [100]. Application of silica as a filler in composite materials are known to improve mechanical properties of the materials [101]. Due to the porosity and high surface area of silica nanoparticles, it has the ability to absorb many other substances, and this enhances its application as a catalyst, adsorbent or porous separation media [102, 103]. As a result of the excellent insulation properties of silica, thermal and chemical stability of various compounds and composites have been achieved by the use of silica [104]. The role of silica (e.g. fumed silica) in coatings as additives has been very remarkable. Industrial preparation of silica in various sizes has further contributed to making it one of the most widely used materials in the world. Fumed silica is composed of primary particles of silica (10 nm) irreversibly fused together to form an

open branched chain of particles, formed by continuous flame hydrolysis of silica tetrachloride [105]. The fineness of fumed silica particles, for instance, brings out additional properties such as surface smoothness, rheology, anti-settling agent, good adhesion promoter, and are also used as anti-corrosion agent on metal surfaces [106].

Furthermore, the outstanding feature of silica surface which allows it to be used in controlling surface wettability is the availability of hydroxyl functional groups on its surface, and the subsequent possibility to chemically modify its hydrophilic surface to hydrophobic surface with various organofunctional silane. This characteristic has widened the use of silica as multifunctional material across many fields [107, 108].

Stability of silica particle-stabilised emulsions depends largely on the particle wettability [109, 110]. Horozov *et al*. have reported that the structure and stability of silica particle monolayers at the water-octane interface strongly depend on the particle hydrophobicity. In their investigation, it was found that very hydrophobic particles give well-ordered and stable (both toward aggregation and sedimentation) horizontal and vertical monolayers. The stability was attributed to the presence of uncompensated electric charges at the particle-octane interface, which resulted in strong long-range Coulomb repulsion between particles through the octane (Figure 1.16). The repulsion in less hydrophobic particles was found to be smaller and insufficient to prevent the particle aggregation [111].

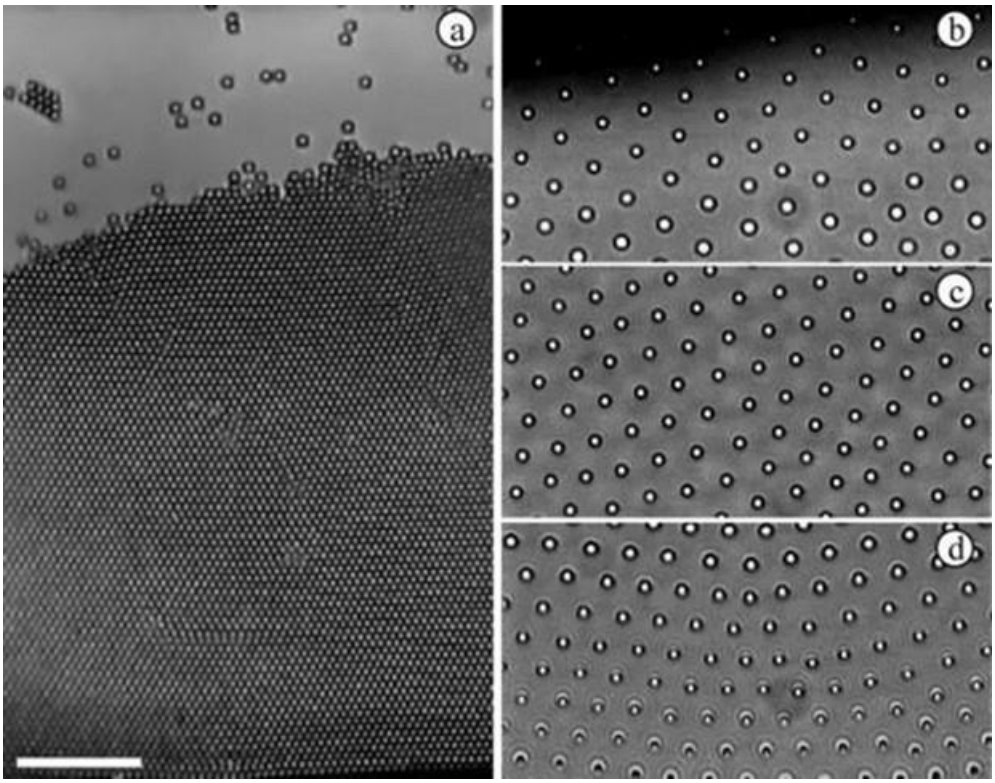

Figure 1.16 Vertical silica particle monolayers at the octane-water interface 1 h after their formation in a circular frame with diameter 6.2 mm. The images are taken at the bottom (a, d), top (b), and middle (c) of the frame. Particle contact angles measured through the water are 65° (a) and 152° (b-d). The scale bar is equal to 50 μm. Image obtained from ref. [111]

1.6 Biofouling and slippery surfaces

Among various implications of wetting, biofouling seems to post serious threats to life and property. It involves the preliminary attachment of microbial cells to a surface and subsequent accumulation of other cells embedded in a matrix of polysaccharide on wetted solid or fluid interfaces [112]. The negative impacts of biofouling include contamination of water and food [113], destruction of medical equipment [114], cosmetic degradation [115, 116], difficulty in domestic and industrial cleaning [117],

microbiologically influenced corrosions (MIC)/biodegradation of process equipment [118, 119] and increasing the drag on ships due to the attachment and growth of marine biomass on the submerged part of the ship hull. In addition to these tremendous side effects associated with chemical controls of biofouling, biofilms are known to exhibit effective resistance toward all forms of chemicals intended to kill or control their growth, including antibiotics, biocides and disinfectants [118, 120]. The difficulty to prevent the adhesion of biofilms on affected materials has been attributed to the broad mechanisms employed by these organisms to stick to most solid materials, including both hydrophobic and hydrophilic surfaces [118, 121]. It has also been found that surface roughness can even create a hiding place for biofilms to thrive and be protected from applied shear forces of cleaning fluids [122]. However, findings by Graham and Cady [123] noted that those early investigations were carried out at macro-scale. He claimed that most micro-organisms are found at micrometre range with nanometre appendages and are therefore able to establish adhesion and accumulate between the grooves larger enough protect them. They then suggested that controlling the surface wettability at micro- to nano-scale would achieve more.

However, another feature of interest found in plants is the presence of directional micro-roughness on the rim of Nepenthes pitcher plant. The rim of this plant is slippery and helps to slide prey into the cone-shaped leaves for its nutrients. However, in spite of the early knowledge about the pitcher rim, a clear mechanism for its slippery nature was not well understood for a long period of research [124-127]. In 2004, Bohn and Federle [128] reported that the wettability of the peristome (rim), activated by nectar secreted at the inner margin of the peristome and by rain water, was the prerequisite for the sliding tendency of the carnivorous pitcher plant. According to their investigation, insects stepping on the wet peristome were observed to fall prey, whereas virtually no insect

was captured on dry peristome. In a related work, Baurer and Federle [129] pointed out that “the stability of water films on the peristome is probably the key factor that prevents insect adhesion” and finally proposed mimicry of the peristome by micro/ nanofabrication techniques for variety of applications.

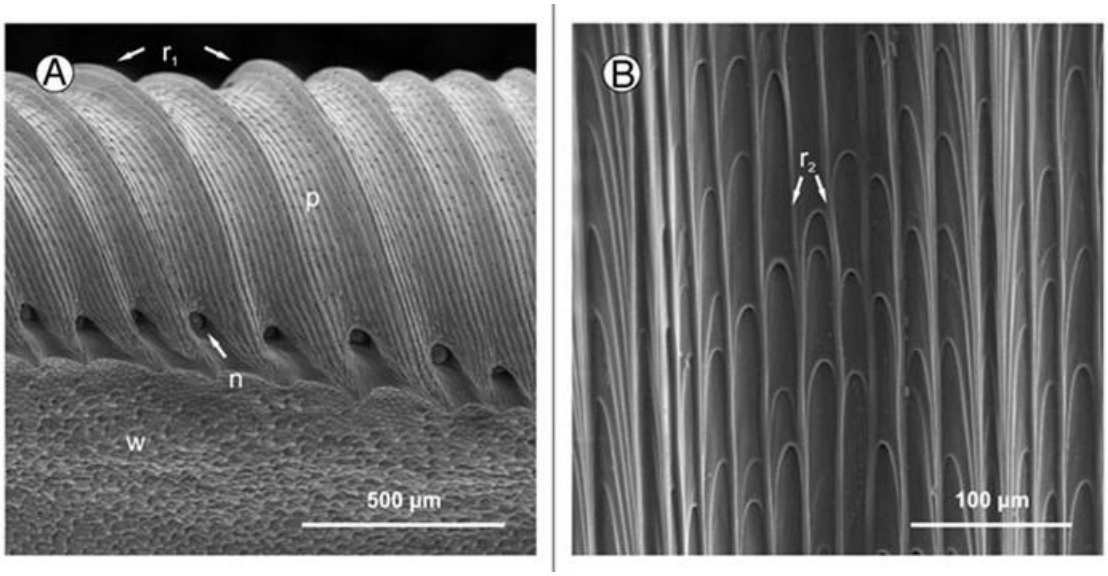

Figure 1.17 (A) Peristome surface (p) of *Nepenthes alata*, structured by first (r_1) and second order radial ridges. In between the tooth-like projections at the inner edge of the peristome the pores of large extrafloral nectaries (n) can be seen. Below the peristome is the wax-covered inner wall surface (w). (B) The second order ridges (r_2) are formed by straight rows of overlapping epidermal cells. Image taken from ref. [129].

Recently, the slippery mechanism of the rim of Nepenthes pitcher plant was better revealed and mimicked in the so called Slippery Liquid-Infused Porous Surfaces (SLIPS). SLIPS, reported as an omniphobic surface capable of repelling both oil and water [130], can generally be made by infusing an immiscible lubricant (to the ambient fluid) onto a structured solid that has a higher chemical affinity to the lubricant than the

ambient fluid [131]. The inventors of SLIPS have also reported the successful application of the material for the prevention of biofilms adhesion.

The premise for the SLIPS design is that a liquid surface is intrinsically smooth and defect-free down to the molecular scale. Such a surface provides immediate self-repair by wicking into damaged sites in the underlying substrate. SLIPS surface can be chosen to repel immiscible liquids of virtually any surface tension if it is designed based on the following three criteria:

1. The lubricating liquid must wick into, wet and stably adhere within the substrate.
2. The solid must be preferentially wetted by the lubricating liquid rather than by the liquid one wants to repel.
3. The lubricating and impinging test liquids must be immiscible.

The first requirement is satisfied by using micro/nano-textured, rough substrates whose large surface area, combined with chemical affinity for the liquid, facilitates complete wetting by, and adhesion of, the lubricating fluid. To satisfy the second and third criteria - the formation of a stable lubricating film that is not displaced by the test liquid, one must determine the chemical and physical properties required for working combinations of substrates and lubricants.

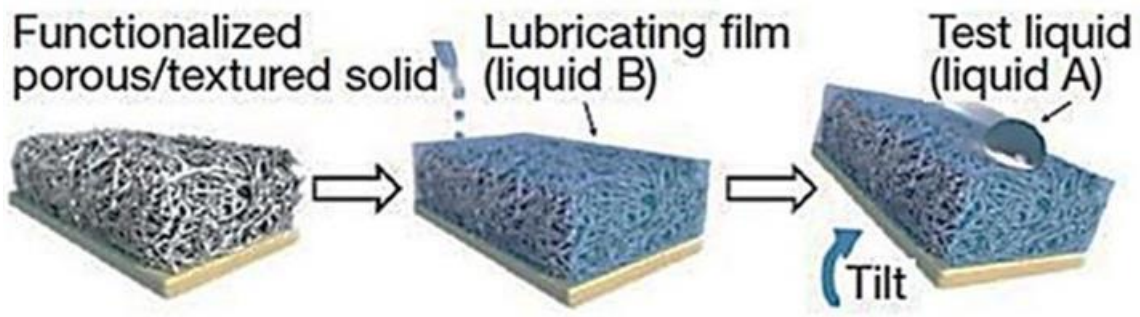

Figure 1.18 Schematics showing the fabrication of a SLIPS by infiltrating a functionalized porous/textured solid with a low-surface energy, chemically inert liquid to form a physically smooth and chemically homogeneous lubricating film on the surface of the substrate. Image taken from ref. [131].

1.7 Wetting and Corrosion of metal surfaces

Metals are crucial to all aspects of modern life. However, metal surfaces, like other solid materials suffer from the negative consequences of wetting. The worst effect seems to be the electrochemical degradation or corrosion of refined metals. Corrosion is a natural phenomenon. Ores are quite stable in ordinary water but metals extracted from ores are prone to corrosion. To change the ores to purer and more useful metal requires energy addition. Thus, refined metals are at higher energy levels which are not natural states and this makes them unstable. Corrosion is a process which tends to return metals to thermodynamic equilibrium with the ambient environment [132].

One can therefore consider corrosion as the reverse process of metal extraction which allows metals to undergo degradation into its constituents by chemical or electrochemical interaction with its environment. Chemical corrosion (or dry corrosion) can takes place by direct attack of metal by corrosive gases like oxygen and chlorine gas

in a dry environment and usually leads to the formation of metallic oxide on metal surface. Such films may remain protective on the surface of metal against further attack (e.g. oxide of aluminium), but some also may as well be unstable (e.g. oxides of silver, Ag and platinum, Pt). Electrochemical corrosion or wet corrosion occurs due to electrochemical action of moisture and oxygen on a metal surface. In most cases, the aqueous phase in contact with the metal is not usually pure, they may either carry dust, microbes, dissolved salts and gases or get mixed with adhered contaminants on metal surfaces [133]. Settlement of a water droplet on a metal surface has the tendency to cause differential aeration between the central bottom and the edge of the droplet and thus, initiate a corrosion cell on the metal surface. Metal dissolves at the less noble part (anode, central bottom) as ions into water (or electrolyte) leaving electrons behind on the metal which are then consumed by the secondary process at the nobler end (cathode, edge of the droplet). While a typical anodic process is dissolution of metal, cathodic reactions are basically the consumption of the electrons generated by anodic reaction and may occur in a number of ways, including hydrogen evolution reaction (HER), oxygen reduction and metal ion reduction [134-136]. Corrosion cell created by wetting of water phase and the likely anodic and cathodic reactions are illustrated in Figure 1.19.

Anodic reaction $M \rightarrow M^{n+} + ne^{-}$ 1.5

Cathodic reactions $2H^{+} + 2e^{-} \rightarrow H_2$ 1.6

$\frac{1}{2}O_2 + 2H^{+} + 2e^{-} \rightarrow H_2O$ 1.7

$M^{3+} + e^{-} \rightarrow M^{2+}$ 1.8

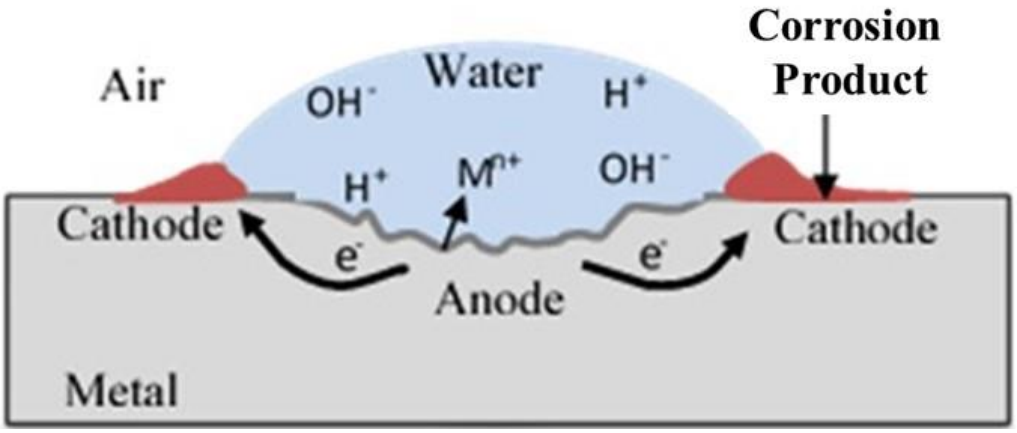

Figure 1.19 Typical example of corrosion of metal initiated by aerated water droplet on metallic surface. Low oxygen supply is eminent at the central bottom of the droplet. This differential aeration (oxygen concentration) between the central bottom and the edge of water drop leads to anodic and cathodic sites which in turn initiate electrochemical cell with metal surface serving as electronic conductors (electrodes) and water as ionic conductor (electrolyte).

Exposed metal surfaces are usually wetted by droplets or a thin water film emanating from rainfall, dew condensation and melting of snow. Chen *et al.* [137] observed that such metal surfaces experience wetting and drying cycles with different periods. Therefore, the changes of surface states such as the formation and spreading of micro-droplets, and formation of a water film are vital for the initial atmospheric corrosion. In order to understand the initial corrosion process for pure magnesium and its alloy, these authors investigated the process of the formation, spreading and transformation of micro-droplets into a thin water film and subsequent corrosion of pure magnesium and its alloy in an oversaturated water environment from wet condition to dry state (in a repeated nine different cycles) using an environmental scanning electron microscope (ESEM). It was observed that the number of the micro-droplets on the metal surface increased with the wetting time and began to connect with one another to form larger

drops. After the first wet cycle the fresh metal surface was covered by corrosion products (Figure 1.20). At the second and subsequent wet cycles, it took shorter time for the formation and spreading of the micro-droplets, which indicated that the corrosion products were more hydrophilic than the fresh metal surface and stimulated the formation and spreading of the micro-droplets.

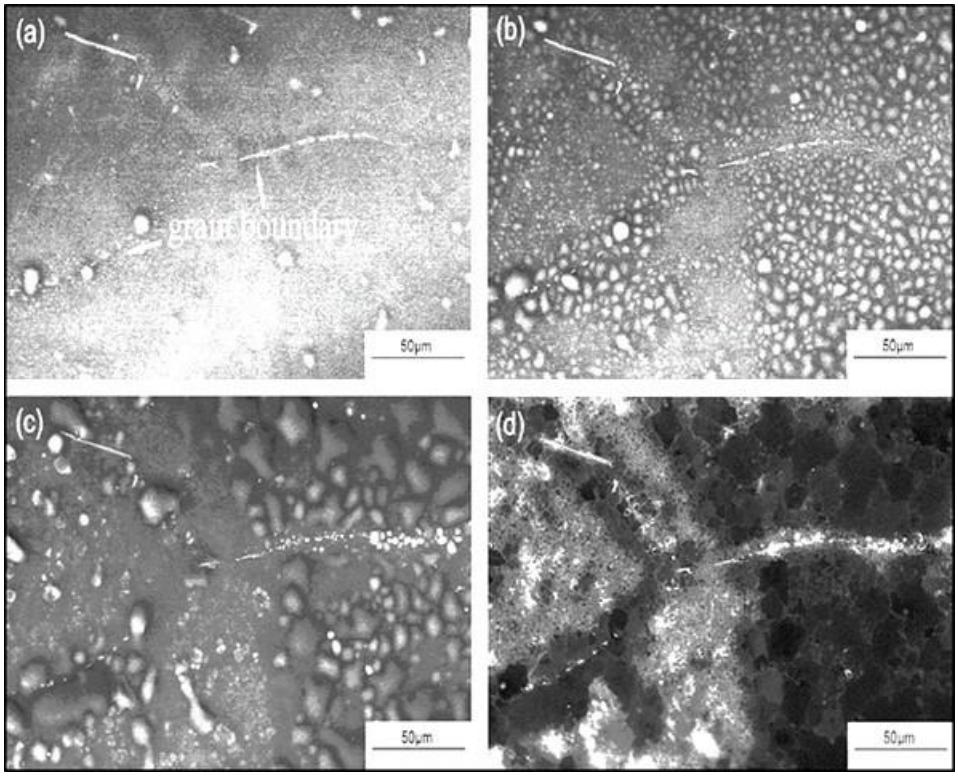

Figure 1.20 Evolution of the micro-droplets on the surface during the first cycle at 20 min per cycle (MPC) at the wetting time: (a) 1 min; (b) 10 min; (c) 20 min; and (d) the corrosion morphology at the end of the first cycle. Images obtained from ref. [137].

Besides various measures used for corrosion preventions [134, 138, 139], hydrophobisation process seems to be more involved in wetting investigations for the purpose of isolating moisture and its accompanying negative consequences from the metal surfaces. Moreover, with adequate characterisations, the possibility of achieving

durable metal surfaces against corrosion with the newly invented SLIPS seems very bright. However, super-hydrophobic coatings have been reported as anti-corrosion barriers against degradation of some metals [140, 141]. Two roughness methods have recently been used by Li *et al.* [140] to fabricate super-hydrophobic iron surfaces. The first one was chemical etching of the substrate by hydrochloric acid 8, M HCl for 30 min. The second approach was galvanic replacement of the iron surface by silver nitrate ($AgNO_3$) solution. In each case, hydrophobic modification of the substrates with ethanol solution containing 0.01 mol/L stearic acid at 40 °C for 30 min was carried out. Super-hydrophobic surfaces with 152 ° and 156° water contact angles were obtained for the two steps, respectively. The fabricated surfaces were found to exhibit excellent anti-icing properties in comparison with the untreated iron.

Xu *et al.* [141] have also created super-hydrophobic surfaces on copper and galvanized iron with contact angle larger than 150° and less than 5° sliding angle. The hydrophobisation process was simple immersion of the clean metal substrates into a methanol solution of hydrolyzed *1H,1H,2H,2H*-perfluorooctyltrichlorosilane for 3-4 days at room temperature, rinsing of the resulted substrate with distilled water and then heating at 130 °C in air for 1 h. Super-hydrophobic properties with flower-like sub-micron structures which composed of nanosheets on the iron surface were achieved (Figure1.21).

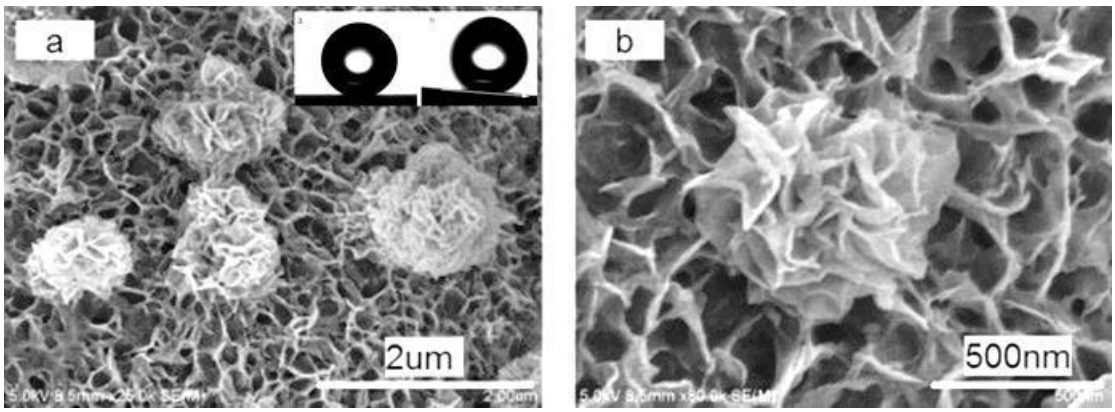

Figure 1.21 SEM images of the thin film on galvanized iron substrate: (a) overview of the film and (b) high-magnification image of the flowerlike sub-micron structure. The insert are the shape of a water droplet (2 µL) on the resulting surface of galvanized iron substrate and the sliding water droplet (3 µL) on a surface tilted at 4°. Images taken from ref. [141]. A similar procedure was used by Liu *et al*. to obtain super-hydrophobic film on zinc against corrosion [142].

He *et al*. used myristic acid to produce super-hydrophobic coatings on aluminium by anodizing annealed aluminium sheet under a constant current of 0.32 Ampere/cm^2 in 15 wt% sulphuric acid for 7 min. Chemical modification of the anodized surface was achieved by melting myristic acid for 30 min at 70 ^oC. Wettability tests carried out showed a static contact angle of 154° and effective corrosion resistant.

It is worth noting that hexavalent chromium (Cr^{6+}) corrosion inhibitors have been used for over a century as the most effective corrosion inhibitor for metal surfaces [143]. Unfortunately, restriction on chromates which are known to be carcinogenic is a serious setback on its applications [144]. Nevertheless, scientific investigation for the possible replacement of chromates is somehow focused on silica. In their investigation using nanoparticle-filled silane films as chromate replacements for corrosion protection of aluminium alloys, Palanivel *et al*. stated that ultra-thin silane films offer excellent

corrosion protection as well as paint adhesion to metal surfaces comparable to, and in some cases better than the layers of chromium. According to this investigation, it was noticed that cathodic reactions can be suppressed by a small amount of silica via reacting with cathodically generated OH^- ions, and later on forming passive Al-silicate compounds. The optimum silica amount in the corresponding silane solutions was observed to be between 5 and 15 ppm [145].

Lopez *et al*. has also reported the use of silica mono-and multilayered sol–gel coating systems for the improvement of the corrosion resistance of aluminium matrix composites reinforced with SiC particles beyond seven (7) days of immersion in 3.5 wt.% NaCl. The work further revealed that both thinner monolayered coating systems and multilayered coatings protected the substrate from the aggressive electrolyte attack in a similar protection behaviour at initial and final immersion time tests [146]. Comparable results have also been reported by Albert *et al.* [147] on the use of a silica based coating as an anti-corrosive agent for the protection of galvanized steel. In addition, the investigation found that rendering the coatings hydrophobic by any type of silylating agents was a good means to improve the corrosion resistance and protect the water-soluble inhibitor content.

Dalbin *et al.* [148] investigated silica-based coating procedure for the protection of electrogalvanized steel against corrosion to evaluate the viability of a simple and industrially easy-to-implement substitute to the widely employed chromate coatings that must be abandoned in the next few years. The silica-based layer was prepared from simple immersion of electrogalvanized sheets in a deposition bath composed of a nanometric silica particles/sodium metasilicate mixture at room temperature and found that the silica-based protective layer behaved almost as well as chromate coatings. They

suggested that further work should be carried on in order to better understand the presence of some localized attack which appeared after several days of salt spray tests without any spread-out or generalized corrosion, and to carry out similar investigation with other type materials and media.

1.8 Polydimethylsiloxane

Polydimethylsiloxane (PDMS) elastomers such as Sylgard 184, are useful materials employed for the modification of solid surfaces to achieve desired wettability and other properties. Polydimethylsiloxanes are formed from compounds that are largely available: sand and methanol, and the resultant polymers are easily cross-linked at room or elevated temperature to form elastomers. Various applications of polydimethylsiloxane are linked to their stability, inexpensive, low surface tension, non-toxicity, transparent appearance, toughness/tensile strength, elastic, bonding with other polymer and glass and unusual rheological (or flow) properties [149, 150]. Its curability from liquid through semisolid to solid is highly desirable in structural modifications and mimicry, especially in soft lithography [151]. The shortcoming of PDMS is its tendency to swell in organic solvents such as hydrocarbons, toluene, dichloromethane, and generally, it will render low performance when using with such liquids. [152]. However, the hydrophobic properties of the material are highly beneficial in many respects. In addition to being environmentally friendly and self-sealable, its stability in aqueous systems is essential to withstand adverse surface wettability in aqueous environments. Interestingly, considering the other attractive properties of PDMS different techniques, such as oxygen plasma treatment and UV treatments, have been used to modify PDMS from the hydrophobic to hydrophilic state [153, 154].

Taylor *et al*. generated micro-contact printing of lipid solutions on ITO glass slides using a stamp fabricated with Sylgard 184 (PDMS). The micro-patterns of square holes in glass were produced by laser ablation and the patterned glass substrates replicated with Sylgard 184. The PDMS stamps were made hydrophilic by surface oxidation with piranha solution (conc. H_2SO_4 and 30% H_2O_2 3:1 (v/v)) for 30 s at 40 °C. It was then rinsed several times with deionised water before treated with 10% APTES (3-aminopropyltriethoxysilane) in water for 2 hours at 50 °C. The modified PDMS stamps were stored in milli-Q water prior to use. The PDMS stamp was inked with the lipid solution for 30 s, wiped on dry paper and pressed. The pattern fabricated and for the preparation of monodispersed giant liposomes is shown in Figure 1.22 [155].

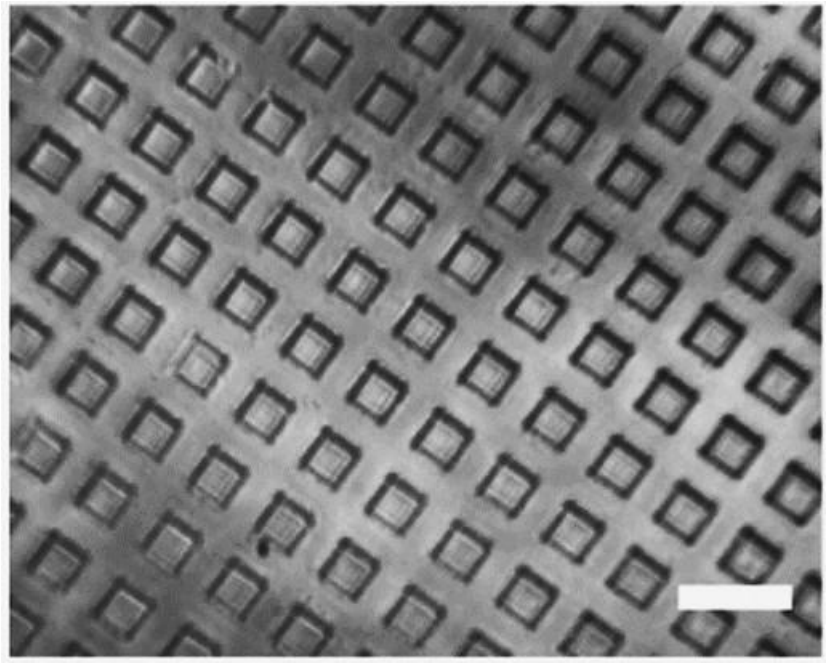

Figure 1.22 Optical micrograph of a PDMS stamp used for microcontact printing of lipid solution on ITO glass slides. Square size is 10 μm and square-to-square distance is 8 μm (bar is 20 μm). Image taken from ref. [155].

1.9 Research objectives and presentation

Findings to date have shown that wettability is governed by surface chemistry and geometry. Exciting combination of these two properties at the microscopic to nanoscopic scales of roughness have been employed to mimic super-hydrophobic surfaces found in natural organisms. Although these steps have yielded a variety of applications, control over some unwanted adhesions, such as biofilms is yet to be adequately realised. However, the recently introduced slippery liquid-infused porous surface SLIPS earlier mentioned in the preceding section of this work seems to be a promising discovery that may fill important gaps in biofouling, corrosion of metals and other areas endangered by wettability. Nevertheless, little is known about this hopeful invention. It should be noted that although manipulations at micro/nano-scale can lead to excellent results, little mistakes or poor knowledge over such manipulations can lead to grievous changes. For instance, both Lotus and petal effects described earlier are two opposing results that make use of micro/nano-scale roughness. Meanwhile, strong research argument on the lack of a clear understanding of the surface morphology of SLIPS as it affect the contact line of water droplet, and possible depletion or instability of the impregnated fluid has been raised [156]. Hence, better understanding of oil impregnated surfaces, investigations and characterisation to carefully trace the fabrication pathway of such structured surfaces before full scale applications is necessary. In addition, the possibility of using a particular technique, or material, to clearly achieve different modes of wettings will definitely widen applications and stipulate boundaries of such applications.

This work was directed to accomplish the following objectives.

1. Fabricated silica nano-porous coatings using modified and commercially available hydrophobic fumed silica.
2. Tuning the wetting behaviour of the porous substrate using non-volatile lubricants (e.g. squalane and silicone elastomers) from a superhydrophobic state in the absence of the oil, through various intermediate wetting states, to slippery surfaces at high loading of the oil**.**
3. Characterising various surfaces obtained and developing practical applications of the coatings.
4. Investigating the anti-biofouling properties of prepared coatings.

In order to achieve the above target, a series investigations were carried out and are divided into seven chapters. This Chapter gives an introduction, and reviews the wetting processes and fabrication solid surface for the control of unwanted wettings, as well as the research objectives. Chapter 2 describes a general description of the materials and methods used for the research. Chapter 3 gives brief investigations on wetting properties of different solid surfaces and modification of their surface chemistry. Fabrication of porous silica coatings toward stable super-hydrophobic properties achieved by altering the surface structural geometry using different sizes of silica particle are also investigated here. Central in this chapter is the gradual impregnation of a super-hydrophobic fumed silica coating with squalane solution in volatile solvent. Detailed characterisation of the coatings, including the thickness and porosity of the coatings, fluorescence microscopy to trace the distribution and relative amount of the impregnated squalane, contact and sliding angle measurements are described and discussed. Chapter 4 discusses *in situ* (one-step) preparation of squalane-impregnated silica coating for practical coating applications. Chapter 5 demonstrates useful combination of silica and liquid/polymerised silicone elastomer to reveals the

morphology of oil impregnated surfaces. Durability and protective roles the composites are also investigated. Chapter 6 investigates live algae cells adhesion on oil-impregnated silica coatings. Chapter 7 gives a summary of the main findings, conclusion and further work.

1.10 References

1. A. A. Tracton, *Coatings technology handbook*. 2005: CRC press.

2. E. Y. Bormashenko, *Wetting of real surfaces*. Vol. 19. 2013: Walter de Gruyter.

3. T. L. Brown, H. E. LeMay, and R. Wilson, *Chemistry: The central science*. 1988: Prentice Hall Englewood Cliffs, NJ.

4. P. Tasker, The stability of ionic crystal surfaces. *Journal of Physics C: Solid State Physics*, 1979. **12**(22): p. 4977.

5. E. Lugscheider and K. Bobzin, Wettability of PVD compound materials by lubricants. *Surface & Coatings Technology*, 2003. **165**(1): p. 51-57.

6. M. Kalin and M. Polajnar, The correlation between the surface energy, the contact angle and the spreading parameter, and their relevance for the wetting behaviour of DLC with lubricating oils. *Tribology International*, 2013. **66**: p. 225-233.

7. T. Young, An Essay on the Cohesion of Fluids. *Phil. Trans. R. Soc. Lond.*, 1805: p. 65-87.

8. R. N. Wenzel, Resistance of solid surfaces to wetting by water. *Industrial and Engineering Chemistry*, 1936. **28**: p. 988-994.

9. A. B. D. Cassie and S. Baxter, Wettability of porous surfaces. *Transactions of the Faraday Society*, 1944. **40**: p. 546.

10. K. Grundke, *et al*., *Wetting measurements on smooth, rough and porous solid surfaces*, in *Interfaces, Surfactants and Colloids in Engineering*. 1996, Springer. p. 58-68.

11. H. Kamusewitz and W. Possart, The static contact angle hysteresis and Young's equilibrium contact angle. *Contact Angle, Wettability and Adhesion*, 2006. **4**: p. 101-104.

12. A. Marmur, Equilibrium contact angles: theory and measurement. *Colloids Surfaces A: Physicochem. Eng. Aspects* 1996. **116** p. 55-61.

13. A. Sah, Precursor film: a key driver to determine wetting behavior in the vicinity of surface heterogeneity. *Soft Matter*, 2014. **10**(22): p. 3890-6.

14. A. J. Meuler, G. H. McKinley, and R. E. Cohen, Exploiting Topographical Texture To Impart Icephobicity. *Acs Nano*, 2010. **4**(12): p. 7048-7052.

15. B. He, J. Lee, and N. A. Patankar, Contact angle hysteresis on rough hydrophobic surfaces. *Colloids and Surfaces A: Physicochemical and Engineering Aspects*, 2004. **248**(1-3): p. 101-104.

16. D. Quere, Rough ideas on wetting. *Physica A*, 2002. **313**: p. 32–46.

17. C. N. C. Lam, *et al*., The effect of liquid properties to contact angle hysteresis. *Colloids and Surfaces a-Physicochemical and Engineering Aspects*, 2001. **189**(1-3): p. 265-278.

18. C. N. C. Lam, R. Wu, D. Li, M. L. Hair, and A. W. Neumann, Study of the advancing and receding contact angles: liquid sorption as a cause of contact angle hysteresis. *Advances in Colloid and Interface Science*, 2002. **96**(1-3): p. 169-191.

19. T. J. Kim and C. H. Hidrovo, Stability Analysis of Cassie-Baxter State under Pressure Driven Flow. *Proceedings of the 8th International Conference on Nanochannels, Microchannels and Minichannels, 2010, Pts a and B*, 2011: p. 1657-1662.

20. E. Bormashenko, Y. Bormashenko, T. Stein, G. Whyman, and E. Bormashenko, Why do pigeon feathers repel water? Hydrophobicity of pennae, Cassie-Baxter wetting hypothesis and Cassie-Wenzel capillarity-induced wetting transition. *J Colloid Interface Sci*, 2007. **311**(1): p. 212-6.

21. Y. J. Sheng, S. Jiang, and H. K. Tsao, Effects of geometrical characteristics of surface roughness on droplet wetting. *J Chem Phys*, 2007. **127**(23): p. 234704.

22. S. S. Latthe, A. B. Gurav, C. S. Maruti, and R. S. Vhatkar, Recent Progress in Preparation of Superhydrophobic Surfaces: A Review. *Journal of Surface Engineered Materials and Advanced Technology*, 2012. **02**(02): p. 76-94.

23. H. Y. Erbil and C. E. Cansoy, Range of applicability of the Wenzel and Cassie-Baxter equations for superhydrophobic surfaces. *Langmuir*, 2009. **25**(24): p. 14135-45.

24. J. B. Lee, H. R. Gwon, S. H. Lee, and M. Cho, Wetting Transition Characteristics on Microstructured Hydrophobic Surfaces. *Materials Transactions*, 2010. **51**(9): p. 1709-1711.

25. A. M. Peters, *et al*., Cassie-Baxter to Wenzel state wetting transition: Scaling of the front velocity. *European Physical Journal E*, 2009. **29**(4): p. 391-397.

26. D. M. Lopes, S. M. M. Ramos, L. R. de Oliveira, and J. C. M. Mombach, Cassie-Baxter to Wenzel state wetting transition: a 2D numerical simulation. *Rsc Advances*, 2013. **3**(46): p. 24530-24534.

27. R. J. Vrancken, *et al*., Fully Reversible Transition from Wenzel to Cassie-Baxter States on Corrugated Superhydrophobic Surfaces. *Langmuir*, 2010. **26**(5): p. 3335-3341.

28. N. A. Patankar, Transition between superhydrophobic states on rough surfaces. *Langmuir*, 2004. **20**(17): p. 7097-7102.

29. C. Dorrer and J. Ruhe, Condensation and wetting transitions on microstructured ultrahydrophobic surfaces. *Langmuir*, 2007. **23**(7): p. 3820-3824.

30. A. Lafuma and D. Quere, Superhydrophobic states. *Nat Mater*, 2003. **2**(7): p. 457-60.

31. D. Oner and T. J. McCarthy, Ultrahydrophobic surfaces. Effects of topography length scales on wettability. *Langmuir*, 2000. **16**(20): p. 7777-7782.

32. C. Neinhuis and W. Barthlott, Characterization and distribution of water-repellent, self-cleaning plant surfaces. *Annals of Botany*, 1997. **79**(6): p. 667-677.

33. G. Sun, Y. Fang, Q. Cong, and L.-q. Ren, Anisotropism of the Non-Smooth Surface of Butterfly Wing. *Journal of Bionic Engineering*, 2009. **6**(1): p. 71-76.

34. S. Selimovic, *Nanopatterning and Nanoscale Devices for Biological Applications*. 2014: CRC Press.

35. A. Otten and S. Herminghaus, How plants keep dry: A physicist's point of view. *Langmuir*, 2004. **20**(6): p. 2405-2408.

36. W. Barthlott and C. Neinhuis, Purity of the sacred lotus, or escape from contamination in biological surfaces. *Planta*, 1997. **202**(1): p. 1-8.

37. L. Feng, *et al*., Petal effect: A superhydrophobic state with high adhesive force. *Langmuir*, 2008. **24**(8): p. 4114-4119.

38. J. M. Wang, Q. L. Yang, M. C. Wang, C. Wang, and L. Jiang, Rose petals with a novel and steady air bubble pinning effect in aqueous media. *Soft Matter*, 2012. **8**(7): p. 2261-2266.

39. F.-M. Chang, S.-J. Hong, Y.-J. Sheng, and H.-K. Tsao, High contact angle hysteresis of superhydrophobic surfaces: Hydrophobic defects. *Applied Physics Letters*, 2009. **95**(6): p. 064102.

40. B. Bhushan and E. K. Her, Fabrication of superhydrophobic surfaces with high and low adhesion inspired from rose petal. *Langmuir*, 2010. **26**(11): p. 8207-17.

41. J. Feng, M. T. Tuominen, and J. P. Rothstein, Hierarchical Superhydrophobic Surfaces Fabricated by Dual-Scale Electron-Beam-Lithography with Well-Ordered Secondary Nanostructures. *Advanced Functional Materials*, 2011. **21**(19): p. 3715-3722.

42. D. Lipomi, R. Martinez, L. Cademartiri, and G. Whitesides, 7.11-Soft Lithographic Approaches to Nanofabrication. *Polymer Science: A Comprehensive Reference, Ed. K. Matyjaszewski and M. Möller, Elsevier, Amsterdam*, 2012.

43. H. J. Choi, *et al*., Fabrication of superhydrophobic and oleophobic Al surfaces by chemical etching and surface fluorination. *Thin Solid Films*, 2015. **585**: p. 76-80.

44. Y. Qi, Z. Cui, B. Liang, R. S. Parnas, and H. F. Lu, A fast method to fabricate superhydrophobic surfaces on zinc substrate with ion assisted chemical etching. *Applied Surface Science*, 2014. **305**: p. 716-724.

45. J. Fresnais, J. P. Chapel, L. Benyahia, and F. Poncin-Epaillard, Plasma-Treated Superhydrophobic Polyethylene Surfaces: Fabrication, Wetting and Dewetting Properties. *Journal of Adhesion Science and Technology*, 2009. **23**(3): p. 447-467.

46. D. Han and S. Y. Moon, Development of superhydrophobic surface on glass substrate by multi-step atmospheric pressure plasma treatment. *Thin Solid Films*, 2015. **587**: p. 34-38.

47. K. S. Liao, A. Wan, J. D. Batteas, and D. E. Bergbreiter, Superhydrophobic surfaces formed using layer-by-layer self-assembly with aminated multiwall carbon nanotubes. *Langmuir*, 2008. **24**(8): p. 4245-4253.

48. N. Higashi, T. Takagi, and T. Koga, Layer-by-layer fabrication of well-packed gold nanoparticle assemblies guided by a β-sheet peptide network. *Polymer Journal*, 2010. **42**(1): p. 95-99.

49. M. S. Islam, N. Akter, and M. R. Karim, Preparation of superhydrophobic membranes by electrospinning of fluorinated silane functionalized pullulan. *Colloids and Surfaces A: Physicochemical and Engineering Aspects*, 2010. **362**(1-3): p. 117-120.

50. H. M. Daly and A. B. Horn, Heterogeneous chemistry of toluene, kerosene and diesel soots. *Phys Chem Chem Phys*, 2009. **11**(7): p. 1069-76.

51. Y. Liu, *et al*., Fabrication of biomimetic superhydrophobic surface with controlled adhesion by electrodeposition. *Chemical Engineering Journal*, 2014. **248**: p. 440-447.

52. Q. Liu, D. X. Chen, and Z. X. Kang, One-Step Electrodeposition Process To Fabricate Corrosion-Resistant Superhydrophobic Surface on Magnesium Alloy. *Acs Applied Materials & Interfaces*, 2015. **7**(3): p. 1859-1867.

53. J. Zhang, M. D. Baro, E. Pellicer, and J. Sort, Electrodeposition of magnetic, superhydrophobic, non-stick, two-phase Cu-Ni foam films and their enhanced performance for hydrogen evolution reaction in alkaline water media. *Nanoscale*, 2014. **6**(21): p. 12490-12499.

54. Q. Y. Yu, *et al*., Fabrication of adhesive superhydrophobic Ni-Cu-P alloy coatings with high mechanical strength by one step electrodeposition. *Colloids and Surfaces a-Physicochemical and Engineering Aspects*, 2013. **427**: p. 1-6.

55. A. B. Gurav, *et al*., Superhydrophobic surface decorated with vertical ZnO nanorods modified by stearic acid. *Ceramics International*, 2014. **40**(5): p. 7151-7160.

56. S. Kumar, P. Goel, D. P. Singh, and J. P. Singh, Fabrication of Superhydrophobic Silver Nanorods Array Substrate Using Glancing Angle Deposition. *Solid State Physics: Proceedings of the 58th Dae Solid State Physics Symposium 2013, Pts a & B*, 2014. **1591**: p. 872-874.

57. G. K. Kannarpady, *et al*., Controlled Growth of Self-Organized Hexagonal Arrays of Metallic Nanorods Using Template-Assisted Glancing Angle

Deposition for Superhydrophobic Applications. *Acs Applied Materials & Interfaces*, 2011. **3**(7): p. 2332-2340.

58. M. Macias-Montero, *et al*., Plasma Deposition of Superhydrophobic Ag@ TiO2 Core@ shell Nanorods on Processable Substrates. *Plasma Processes and Polymers*, 2014. **11**(2): p. 164-174.

59. Y. L. Shi, W. Yang, X. J. Feng, Y. S. Wang, and G. R. Yue, Fabrication of superhydrophobic ZnO nanorods surface with corrosion resistance via combining thermal oxidation and surface modification. *Materials Letters*, 2015. **151**: p. 24-27.

60. Z. X. Jia, *et al*., Superhydrophobic surfaces with nanofibers or nanorods based on thiophene derivatives. *Applied Physics Letters*, 2010. **96**(4).

61. M. Macias-Montero, *et al*., Superhydrophobic supported Ag-NPs@ZnO-nanorods with photoactivity in the visible range. *Journal of Materials Chemistry*, 2012. **22**(4): p. 1341-1346.

62. Q. M. Pan, H. Z. Jin, and H. Wang, Fabrication of superhydrophobic surfaces on interconnected Cu(OH)(2) nanowires via solution-immersion. *Nanotechnology*, 2007. **18**(35).

63. Y. M. Shin, S. K. Lee, S. Jang, and J. H. Park, Superhydrophobic properties of a hierarchical structure using a silicon micro-tip array decorated with ZnO nanowires. *Current Applied Physics*, 2014. **14**(5): p. 665-671.

64. S. Peng, D. Tian, X. J. Yang, and W. L. Deng, Highly Efficient and Large-Scale Fabrication of Superhydrophobic Alumina Surface with Strong Stability Based on Self-Congregated Alumina Nanowires. *Acs Applied Materials & Interfaces*, 2014. **6**(7): p. 4831-4841.

65. K. Yadav, B. R. Mehta, K. V. Lakshmi, S. Bhattacharya, and J. P. Singh, Tuning the Wettability of Indium Oxide Nanowires from Superhydrophobic to Nearly Superhydrophilic: Effect of Oxygen-Related Defects. *Journal of Physical Chemistry C*, 2015. **119**(28): p. 16026-16032.

66. X. Zhang, Y. G. Guo, Z. J. Zhang, and P. Y. Zhang, Self-cleaning superhydrophobic surface based on titanium dioxide nanowires combined with polydimethylsiloxane. *Applied Surface Science*, 2013. **284**: p. 319-323.

67. L. Wermuth, M. Kolb, T. Mertens, T. Strobl, and D. Raps, Superhydrophobic surfaces based on self-organized TiO2-nanotubes. *Progress in Organic Coatings*, 2015. **87**: p. 242-249.

68. J. C. Gu, P. Xiao, Y. J. Huang, J. W. Zhang, and T. Chen, Controlled functionalization of carbon nanotubes as superhydrophobic material for adjustable oil/water separation. *Journal of Materials Chemistry A*, 2015. **3**(8): p. 4124-4128.

69. S. J. Bae, *et al*., A superhydrophobic layer formed by fluoro-derivative-treated gold sheets on grown-up zinc oxide nanoparticles for a spherical DNA hydrogel. *Colloids and Surfaces B-Biointerfaces*, 2013. **111**: p. 342-345.

70. F. Gentile, *et al*., Tailored Ag nanoparticles/nanoporous superhydrophobic surfaces hybrid devices for the detection of single molecule. *Microelectronic Engineering*, 2012. **97**: p. 349-352.

71. C. Guo, R. J. Liao, Y. Yuan, Z. P. Zuo, and A. Y. Zhuang, Glaze Icing on Superhydrophobic Coating Prepared by Nanoparticles Filling Combined with Etching Method for Insulators. *Journal of Nanomaterials*, 2015.

72. C. R. Crick, J. C. Bear, A. Kafizas, and I. P. Parkin, Superhydrophobic Photocatalytic Surfaces through Direct Incorporation of Titania Nanoparticles into a Polymer Matrix by Aerosol Assisted Chemical Vapor Deposition. *Advanced Materials*, 2012. **24**(26): p. 3505-3508.

73. S. Heinonen, *et al*., Bacterial growth on a superhydrophobic surface containing silver nanoparticles. *2nd International Conference on Competitive Materials and Technological Processes (Ic-Cmtp2)*, 2013. **47**.

74. R. V. Lakshmi, P. Bera, C. Anandan, and B. J. Basu, Effect of the size of silica nanoparticles on wettability and surface chemistry of sol-gel superhydrophobic

and oleophobic nanocomposite coatings. *Applied Surface Science*, 2014. **320**: p. 780-786.

75. Y. Zhang, *et al*., Functionalization of cotton fabrics with rutile TiO2 nanoparticles: Applications for superhydrophobic, UV-shielding and self-cleaning properties. *Russian Journal of Physical Chemistry A*, 2012. **86**(3): p. 413-417.

76. L. D. Zhang, *et al*., Synthesis and characterization of superhydrophobic and superparamagnetic film based on maghemite-polystyrene composite nanoparticles. *Applied Surface Science*, 2012. **259**: p. 719-725.

77. Z. Q. Yuan, *et al*., A novel preparation of polystyrene film with a superhydrophobic surface using a template method. *Journal of Physics D-Applied Physics*, 2007. **40**(11): p. 3485-3489.

78. W. B. Zhong, *et al*., Superhydrophobic polyaniline hollow bars: Constructed with nanorod-arrays based on self-removing metal-monomeric template. *Journal of Colloid and Interface Science*, 2012. **365**(1): p. 28-32.

79. M. H. Sun, *et al*., Artificial lotus leaf by nanocasting. *Langmuir*, 2005. **21**(19): p. 8978-8981.

80. M.-S. Park, G.-D. Yu, and K.-S. Shin, Alumina Templates on Silicon Wafers with Hexagonally or Tetragonally Ordered Nanopore Arrays via Soft Lithography. *Bulletin of the Korean Chemical Society*, 2012. **33**(1): p. 83-89.

81. H. Meng, S. Wang, J. Xi, Z. Tang, and L. Jiang, Facile means of preparing superamphiphobic surfaces on common engineering metals. *The Journal of Physical Chemistry C*, 2008. **112**(30): p. 11454-11458.

82. M. A. Malik, M. A. Hashim, F. Nabi, S. A. AL-Thabaiti, and Z. Khan, Anti-corrosion Ability of Surfactants: A Review. *International Journal of Electrochemical Science*, 2011. **6**(6): p. 1927-1948.

83. C. L. Riggs, T. Aytug, and J. T. Simpson, *Creating Optically Transparent, Durable Superhydrophobic Thin Film Coatings*, 2012, Oak Ridge National Laboratory Partnerships White Paper.

84. A. R. Abate, D. Lee, C. Holtze, A. Krummel, and W. D. Do T, Functionalized glass coating for PDMS microfluidic devices. *Lab-on-a-Chip Technology: Fabrication and Microfluidics, Caister Academic Press*, 2009.

85. C. R. Crick and I. P. Parkin, Preparation and characterisation of super-hydrophobic surfaces. *Chemistry*, 2010. **16**(12): p. 3568-88.

86. D. Ambrozewicz, *et al*., Fluoroalkylsilane versus alkylsilane as hydrophobic agents for silica and silicates. *Journal of Nanomaterials*, 2013. **2013**: p. 18.

87. M. E. McGovern, K. M. Kallury, and M. Thompson, Role of solvent on the silanization of glass with octadecyltrichlorosilane. *Langmuir*, 1994. **10**(10): p. 3607-3614.

88. N. Tasaltin, D. Sanli, A. Jonas, A. Kiraz, and C. Erkey, Preparation and characterization of superhydrophobic surfaces based on hexamethyldisilazane-modified nanoporous alumina. *Nanoscale Research Letters*, 2011. **6**.

89. Z. Chen, L. Hao, A. Chen, Q. Song, and C. Chen, A rapid one-step process for fabrication of superhydrophobic surface by electrodeposition method. *Electrochimica Acta*, 2012. **59**: p. 168-171.

90. H.-S. Jung, D.-S. Moon, and J.-K. Lee, Quantitative Analysis and Efficient Surface Modification of Silica Nanoparticles. *Journal of Nanomaterials*, 2012. **2012**: p. 1-8.

91. I. A. Rahman and V. Padavettan, Synthesis of Silica Nanoparticles by Sol-Gel: Size-Dependent Properties, Surface Modification, and Applications in Silica-Polymer Nanocomposites—A Review. *Journal of Nanomaterials*, 2012. **2012**: p. 1-15.

92. Y. Zhang, J. Wu, X. Yu, and H. Wu, Low-cost one-step fabrication of superhydrophobic surface on Al alloy. *Applied Surface Science*, 2011. **257**(18): p. 7928-7931.

93. L. C. de Smet, D. Ullien, E. J. Sudhölter, and M. Mescher, *Organic surface modification of silicon nanowire-based sensor devices*. 2011: INTECH Open Access Publisher.

94. X. Liu, Y. Liang, F. Zhou, and W. Liu, Extreme wettability and tunable adhesion: biomimicking beyond nature? *Soft Matter*, 2012. **8**(7): p. 2070-2086.

95. L. Zhai, *et al.*, Patterned superhydrophobic surfaces: toward a synthetic mimic of the Namib Desert beetle. *Nano Lett*, 2006. **6**(6): p. 1213-7.

96. S. Minko, *et al.*, Two-level structured self-adaptive surfaces with reversibly tunable properties. *Journal of the American Chemical Society*, 2003. **125**(13): p. 3896-3900.

97. V. San Miguel, C. G. Bochet, and A. del Campo, Wavelength-selective caged surfaces: how many functional levels are possible? *J Am Chem Soc*, 2011. **133**(14): p. 5380-8.

98. J. Erath, *et al.*, Phototunable surface interactions. *Langmuir*, 2013. **29**(39): p. 12138-44.

99. L. Shen, J. Fu, K. Fu, C. Picart, and J. Ji, Humidity responsive asymmetric free-standing multilayered film. *Langmuir*, 2010. **26**(22): p. 16634-7.

100. S. H. Moon, *et al.*, Rheological behavior and film characterization of fumed silica dispersion in carbodiimide based UV-curable coating material. *Macromolecular Research*, 2013. **21**(2): p. 146-152.

101. T. J. Kang, K. H. Hong, and M. R. Yoo, Preparation and properties of fumed silica/Kevlar composite fabrics for application of stab resistant material. *Fibers and Polymers*, 2010. **11**(5): p. 719-724.

102. M. A. Harmer, W. E. Farneth, and Q. Sun, High surface area nafion resin/silica nanocomposites: a new class of solid acid catalyst. *Journal of the American Chemical Society*, 1996. **118**(33): p. 7708-7715.

103. R. Leboda, Preparation and modification of complex pyrolytic carbon-silica adsorbents. *Chromatographia*, 1981. **14**(9): p. 524-528.

104. A. S. Eppler, G. Rupprechter, E. A. Anderson, and G. A. Somorjai, Thermal and chemical stability and adhesion strength of Pt nanoparticle arrays supported on silica studied by transmission electron microscopy and atomic force microscopy. *The Journal of Physical Chemistry B*, 2000. **104**(31): p. 7286-7292.

105. Q. Wan, C. Ramsey, and G. Baran, Thermal pretreatment of silica composite filler materials. *J Therm Anal Calorim*, 2010. **99**(1): p. 237-243.

106. N. M. Ahmed and H. T. M. Abdel-Fatah, *The role of silica fume pigments in corrosion protection of steel surfaces*. 2012: INTECH Open Access Publisher.

107. M. Vallet-Regi, M. Colilla, and B. Gonzalez, Medical applications of organic-inorganic hybrid materials within the field of silica-based bioceramics. *Chem Soc Rev*, 2011. **40**(2): p. 596-607.

108. A. Walcarius, Electrochemical applications of silica-based organic-inorganic hybrid materials. *Chemistry of Materials*, 2001. **13**(10): p. 3351-3372.

109. B. P. Binks and S. O. Lumsdon, Influence of particle wettability on the type and stability of surfactant-free emulsions. *Langmuir*, 2000. **16**(23): p. 8622-8631.

110. B. P. Binks and S. O. Lumsdon, Catastrophic phase inversion of water-in-oil emulsions stabilized by hydrophobic silica. *Langmuir*, 2000. **16**(6): p. 2539-2547.

111. T. S. Horozov, R. Aveyard, B. P. Binks, and J. H. Clint, Structure and stability of silica particle monolayers at horizontal and vertical octane-water interfaces. *Langmuir*, 2005. **21**(16): p. 7405-7412.

112. M. E. Cortés, J. Consuegra, R. Sinisterra, and A. Mendez-Vilas, Biofilm formation, control and novel strategies for eradication. *Science Against Microbial Pathogens: Communicating Current Research and Technological Advances*, 2011. **2**: p. 896-905.

113. C. G. Kumar and S. K. Anand, Significance of microbial biofilms in food industry: a review. *International Journal of Food Microbiology*, 1998. **42**(1-2): p. 9-27.

114. J. C. Darbord, Importance of cleaning for reprocessing endoscopes and thermolabile sterile medical devices: French use and regulations. *J Hosp Infect*, 2004. **56 Suppl 2**: p. S40-3.

115. F. Kawai, Microbial degradation of polyethers. *Applied Microbiology and Biotechnology*, 2002. **58**(1): p. 30-38.

116. J. Nemcova, I. Drobnicova, and M. Zemanova, Cosmetic Creams - Microbial-Degradation during Storage and Preservatives. *Folia Microbiologica*, 1984. **29**(5): p. 413-413.

117. N. Hoiby, T. Bjarnsholt, M. Givskov, S. Molin, and O. Ciofu, Antibiotic resistance of bacterial biofilms. *Int J Antimicrob Agents*, 2010. **35**(4): p. 322-32.

118. J. Gattlen, C. Amberg, M. Zinn, and L. Mauclaire, Biofilms isolated from washing machines from three continents and their tolerance to a standard detergent. *Biofouling*, 2010. **26**(8): p. 873-82.

119. H. A. Videla, Prevention and control of biocorrosion. *International Biodeterioration & Biodegradation*, 2002. **49**(4): p. 259-270.

120. G. D. Bixler and B. Bhushan, Biofouling: lessons from nature. *Philos Trans A Math Phys Eng Sci*, 2012. **370**(1967): p. 2381-417.

121. J. Genzer and K. Efimenko, Recent developments in superhydrophobic surfaces and their relevance to marine fouling: a review. *Biofouling*, 2006. **22**(5-6): p. 339-60.

122. W. Teughels, N. Van Assche, I. Sliepen, and M. Quirynen, Effect of material characteristics and/or surface topography on biofilm development. *Clinical oral implants research*, 2006. **17**(S2): p. 68-81.

123. M. Graham and N. Cady, Nano and Microscale Topographies for the Prevention of Bacterial Surface Fouling. *Coatings*, 2014. **4**(1): p. 37-59.

124. M. Riedel, A. Eichner, and R. Jetter, Slippery surfaces of carnivorous plants: composition of epicuticular wax crystals in Nepenthes alata Blanco pitchers. *Planta*, 2003. **218**(1): p. 87-97.

125. L. Gaume, *et al*., How do plant waxes cause flies to slide? Experimental tests of wax-based trapping mechanisms in three pitfall carnivorous plants. *Arthropod Struct Dev*, 2004. **33**(1): p. 103-11.

126. I. Scholz, *et al*., Slippery surfaces of pitcher plants: Nepenthes wax crystals minimize insect attachment via microscopic surface roughness. *J Exp Biol*, 2010. **213**(Pt 7): p. 1115-25.

127. E. V. Gorb, M. J. Baum, and S. N. Gorb, Development and regeneration ability of the wax coverage in Nepenthes alata pitchers: a cryo-SEM approach. *Sci Rep*, 2013. **3**: p. 3078.

128. H. F. Bohn and W. Federle, Insect aquaplaning: Nepenthes pitcher plants capture prey with the peristome, a fully wettable water-lubricated anisotropic surface. *Proc Natl Acad Sci U S A*, 2004. **101**(39): p. 14138-43.

129. U. Bauer and W. Federle, The insect-trapping rim of Nepenthes pitchers: surface structure and function. *Plant signaling & behavior*, 2009. **4**(11): p. 1019-1023.

130. T. S. Wong, *et al*., Bioinspired self-repairing slippery surfaces with pressure-stable omniphobicity. *Nature*, 2011. **477**(7365): p. 443-7.

131. P. Kim, *et al*., Liquid-Infused Nanostructured Surfaces with Extreme Anti-Ice and Anti-Frost Performance. *Acs Nano*, 2012. **6**(8): p. 6569-6577.

132. B. A. Shaw and R. G. Kelly, What is corrosion? *Interface-Electrochemical Society*, 2006. **15**(1): p. 24-27.

133. J. Chen, J. Q. Wang, E. H. Han, and W. Ke, Effects of dust and salt particles on the formation and spreading of micro-droplets on AZ91 magnesium alloy. *Corrosion Science*, 2008. **50**(5): p. 1449-1459.

134. D. A. Jones, Measurement and Prevention of Corrosion by Electrochemical Methods. *Industrial & Engineering Chemistry Product Research and Development*, 1972. **11**(1): p. 12.

135. L. Umoru, A. Afonja, and B. Ademodi, Corrosion Study of AISI 304, AISI 321 and AISI 430 Stainless Steels in a Tar Sand Digester. *Journal of Minerals & Materials Characterization & Engineering*, 2008. **7**(4): p. 291-299.

136. T. A. Vijey, Study of Corrosion Properties of AISI 430 Stainless steel by Non-electrochemical immersion Technique. *International Journal of Engineering Trends and Technology (IJETT)*, 2013. **4**(6): p. 2442-2446.

137. J. Chen, J. Q. Wang, E. Han, and W. Ke, In situ observation of formation and spreading of micro-droplets on magnesium and its alloy under cyclic wet-dry conditions. *Corrosion Science*, 2007. **49**(3): p. 1625-1634.

138. E. Ghali, V. S. Sastri, and M. Elboujdaini, *Corrosion prevention and protection: practical solutions*. 2007: John Wiley & Sons.

139. G. Grundmeier, W. Schmidt, and M. Stratmann, Corrosion protection by organic coatings: electrochemical mechanism and novel methods of investigation. *Electrochimica Acta*, 2000. **45**(15): p. 2515-2533.

140. K. Q. Li, X. R. Zeng, H. Q. Li, and X. J. Lai, study on the fabrication of superhydrophobic iron surfaces by chemical etching and galvanic replacement methods and their anti-icing properties. *Applied Surface Science*, 2015. **346**: p. 458-463.

141. W. G. Xu, H. Q. Liu, S. X. Lu, J. M. Xi, and Y. B. Wang, Fabrication of superhydrophobic surfaces with hierarchical structure through a solution-immersion process on copper and galvanized iron substrates. *Langmuir*, 2008. **24**(19): p. 10895-10900.

142. H. Liu, S. Szunerits, W. Xu, and R. Boukherroub, Preparation of superhydrophobic coatings on zinc as effective corrosion barriers. *ACS Appl Mater Interfaces*, 2009. **1**(6): p. 1150-3.

143. R. L. Twite and G. P. Bierwagen, Review of alternatives to chromate for corrosion protection of aluminum aerospace alloys. *Progress in Organic Coatings*, 1998. **33**(2): p. 91-100.

144. M. L. Zheludkevich, D. G. Shchukin, K. A. Yasakau, H. Mohwald, and M. G. S. Ferreira, Anticorrosion coatings with self-healing effect based on nanocontainers impregnated with corrosion inhibitor. *Chemistry of Materials*, 2007. **19**(3): p. 402-411.

145. V. Palanivel, D. Zhu, and W. J. van Ooij, Nanoparticle-filled silane films as chromate replacements for aluminum alloys. *Progress in Organic Coatings*, 2003. **47**(3-4): p. 384-392.

146. A. J. Lopez, A. Urena, M. D. Lopez, and J. Rams, Protection against corrosion of aluminium-SiC composites by sol-gel silica coatings. *Surface & Coatings Technology*, 2008. **202**(16): p. 3755-3763.

147. E. Albert, *et al*., Mesoporous silica coatings with improved corrosion protection properties. *Microporous and Mesoporous Materials*, 2015. **206**: p. 102-113.

148. S. Dalbin, G. Maurin, R. P. Nogueira, J. Persello, and N. Pommier, Silica-based coating for corrosion protection of electrogalvanized steel. *Surface & Coatings Technology*, 2005. **194**(2-3): p. 363-371.

149. A. Colas, Silicones: Preparation, properties and performance. *Dow Corning, Life Sciences*, 2005.

150. Y. H. Lin, S. W. Kang, and T. Y. Wu, Fabrication of polydimethylsiloxane (PDMS) pulsating heat pipe. *Applied Thermal Engineering*, 2009. **29**(2-3): p. 573-580.

151. H. Schmid and B. Michel, Siloxane polymers for high-resolution, high-accuracy soft lithography. *Macromolecules*, 2000. **33**(8): p. 3042-3049.

152. J. N. Lee, C. Park, and G. M. Whitesides, Solvent compatibility of poly(dimethylsiloxane)-based microfluidic devices. *Analytical Chemistry*, 2003. **75**(23): p. 6544-6554.

153. J. W. Zhou, A. V. Ellis, and N. H. Voelcker, Recent developments in PDMS surface modification for microfluidic devices. *Electrophoresis*, 2010. **31**(1): p. 2-16.

154. G. Slaughter and B. Stevens, A cost-effective two-step method for enhancing the hydrophilicity of PDMS surfaces. *Biochip Journal*, 2014. **8**(1): p. 28-34.

155. P. Taylor, C. Xu, P. D. I. Fletcher, and V. N. Paunov, A novel technique for preparation of monodisperse giant liposomes. *Chemical Communications*, 2003(14): p. 1732-1733.

156. J. D. Smith, *et al*., Droplet mobility on lubricant-impregnated surfaces. *Soft Matter*, 2013. **9**(6): p. 1772-1780.

CHAPTER 2

MATERIALS AND METHODS

2.1 Materials

2.1.1 Solvents

Water used throughout this work was deionised water obtained from Milli-Q reverse osmosis unit (Millipore). The water pH was 6.7, and the surface tension of the water as measured with the drop shape analysis instrument (DSA 10, Kruss) was 72.5 ± 0.3 mN/m and with measured resistivity less than 18 m.Ω/cm. The water was used for cleaning and as a probe liquid in wetting tests.

Absolute ethanol (analytical grade) was supplied by Fisher Scientific. Ethanol was used for the preparation of silica suspensions/emulsion. It was also used for the termination of liquid phase hydrophobisation reactions, and was a major solvent for surface cleaning.

Hexane (95.0%, anhydrous) was purchased from Sigma-Aldrich. It was used for the preparation of different concentrations of oils used for impregnation of porous silica coatings.

Anhydrous toluene (99.85%, extra dry over molecular sieve, Acros Organics) was purchased from Fisher Scientific. It was used for the preparation of solutions of different concentrations of dichlorodimethylsilane, DCDMS used for liquid phase hydrophobisation process.

Alcoholic potassium hydroxide was prepared using potassium hydroxide (Analytical grade) Fisher Scientific) and ethanol, and was used for the cleaning of the glassware and Teflon tubes. Detailed preparation will be discussed in subsequent section.

Other organic solvents used included chloroform (99.0%), isopropanol (99.0%) and acetone (≥ 99.5%) all analytical grade, supplied by Fisher Scientific and used mainly as surface cleaning solvent.

2.1.2 **Silansing agents**

Different silansing agents were used for the hydrophobisation of solid surfaces, including dichlorodimethylsilane, DCDMS (99.5%, Sigma-Aldrich); *1,1,1,3,3,3*-hexamethyldisilazane, HMDS (99.9%, Sigma-Aldrich); 1H, 1H, 2H, 2H – perfluorodecyltrichlorosilane, PFDTS (97%, Sigma-Aldrich)

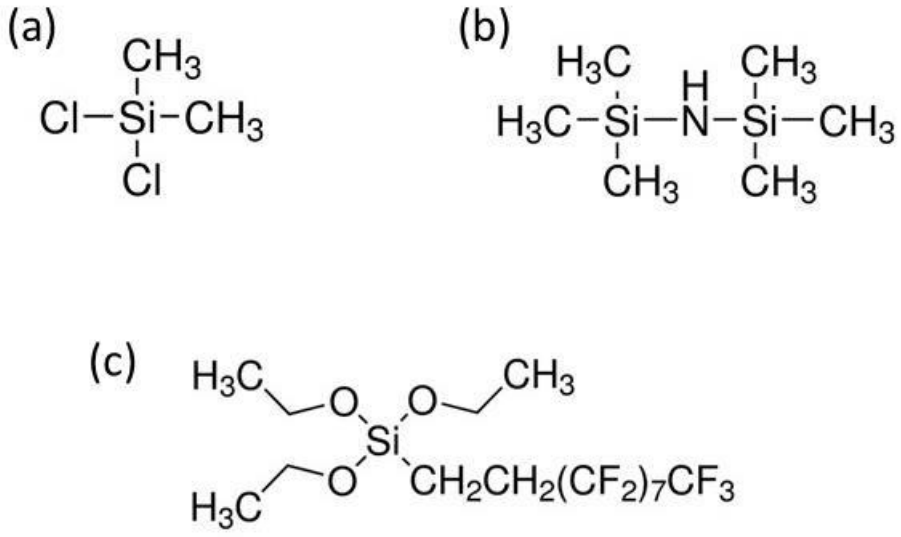

Figure 2.1 Molecular structure of chemicals used the modification of solid materials from hydrophilic to hydrophobic (a) DCDMS. (b) HMDS (c) PFDTS.

2.1.3 **Liquids used for the impregnation of porous coatings**

Squalane (99%, Sigma-Aldrich) was one of the oils used for the impregnation of porous silica coatings due to its lack of volatility. The oil was purified three times by passing it through basic alumina column (pore size: 58 A, pH: 9.5 ± 0.5 in water). Different concentrations of the oil were prepared in hexane prior use.

Silicone oil with viscosity of 20 cSt (25 °C) was obtained from Sigma-Aldrich and also used for the impregnation of the porous silica coatings and preparation of silica dispersions. It was purified in basic alumina before used.

Sylgard 184 is a colourless viscous (5000 cSt) silicone elastomeric poly (dimethyl siloxane), PDMS which come in two parts: A and B. Part A is a pre polymer base and part B is a crosslinking curing agent. The pre-polymer base and curable (mixture of parts A + B) were separately used for the impregnations and wettability studies. It was also used for the hydrophobisation of different structured solid materials.

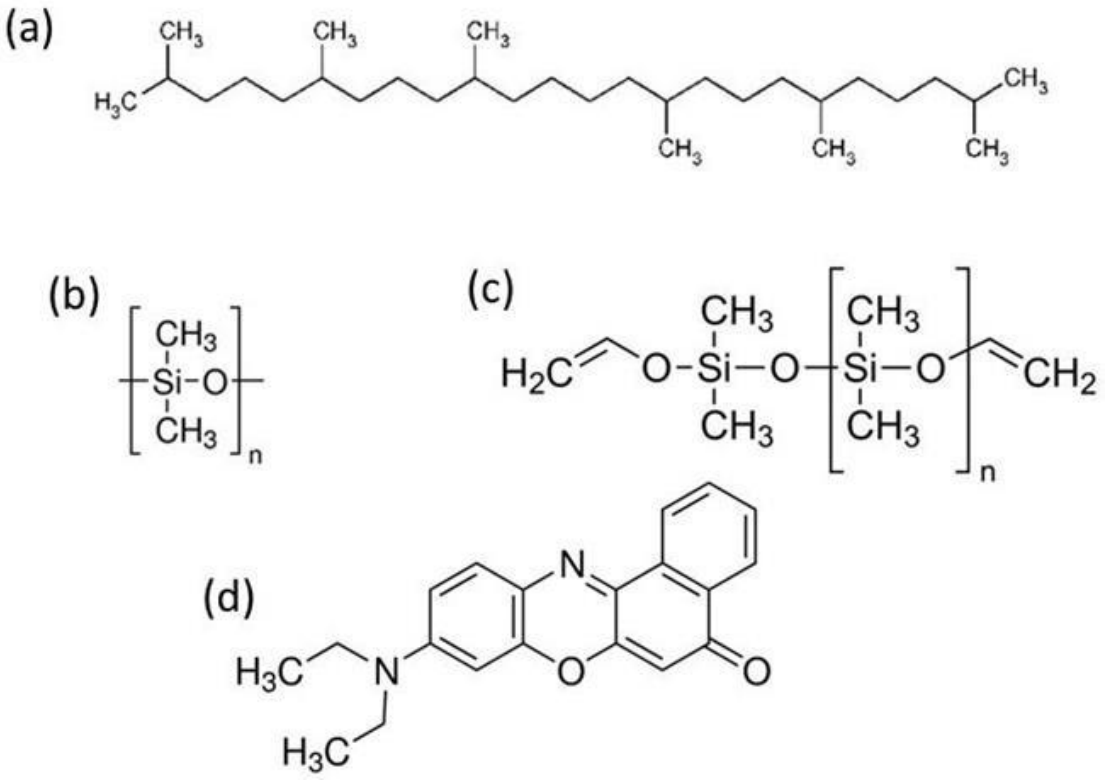

Figure 2.2 Molecular structures of different oils used for the impregnation of the porous substrate. (a) Squalane, $C_{30}H_{62}$. (b) Silicone oil. (c) Sylgard 184. (d) Molecular structure of Nile red, $C_{20}H_{18}N_2O_2$.

2.1.4 **Materials used for fluorescence microscopy**

Nile red was obtained from Sigma-Aldrich (Figure 2.2). It was used to dope the squalane phase as a fluorescent tracer which helps to co-localise the squalane phase in the impregnated coatings and trace the distribution and relative amount of the impregnated oil on the surface. Table 2.1 tabulates some of the other chemicals used in our experiments.

Table 2.1 Summary of other reagents used and the suppliers

Material	Purity/Description	Supplier
Water	Milli-Q	Millipore
Ethanol	Analytical grade	Fisher Scientific
Chloroform	99.0%, laboratory grade	Fisher Scientific
Isopropanol	99.0%, laboratory grade	Fisher Scientific
Acetone	99.5, analytical grade, Acros Organic	Fisher Scientific
Toluene,	99.9, anhydrous, Acros Organic	Fisher Scientific
Hexane	95.0%, anhydrous	Sigma-Aldrich
HDMS	99.9%	Sigma-Aldrich
DCDMS	99.5%	Sigma-Aldrich
PFDTS	97%	Sigma-Aldrich
Hexadecane	99.0%	Sigma-Aldrich
Squalane	99%	Sigma-Aldrich
Silicon oil	20 cSt (25 °C)	Sigma-Aldrich
Sylgard 184	5000 cSt (25 °C)	Dow Corning
Hydrochloric acid	37 %, d = 1.18	Fisher Scientific
Hydrofluoric acid	60 %, general purpose	Fisher Scientific
Nitric acid	70%, laboratory grade	Fisher Scientific
Iron (III) chloride	97%, reagent grade	Sigma-Aldrich

2.1.5 **Solid materials used for wetting studies**

2.1.5.1 Glass slides (smooth and textured)

Microscope glass slides used were premium pathology grades and were purchased as smooth hydrophilic slides from Heathrow Scientific. They were cut to 25 by 25 square millimetre. Apart from smooth glasses, the surfaces of some of these glasses were roughened prior to use. All glass slides (smooth and roughened) were washed successively with ethanol, isopropanol, chloroform and water in an ultrasonic bath for 10 minutes each and then dried in natural air.

2.1.5.2 Sintered glass disc (porous)

Commercially available porous glass (sintered glass disc) with manufacturer porosity grade: G5, and pore size of 1 – 16 μm was produced by Duran Group, Germany and supplied by Schott UK Ltd. The composition of the glass was 81% by weight SiO_2, 13% by weight B_2O_3, 4% by weight Na_2O/K_2O, 2% by weight Al_2O_3. The glass was activated at 110 ℃ and cooled in a desiccator to room temperature before use. The SEM images of the glass are shown in Figure 2.3

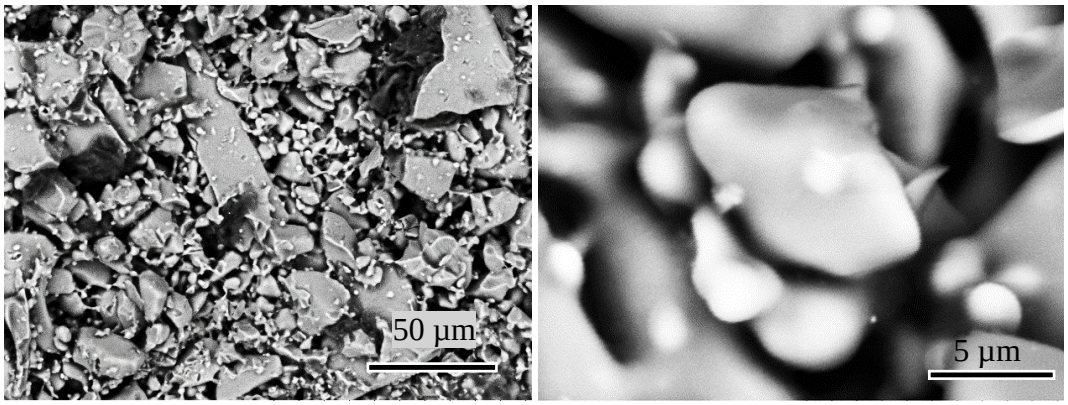

Figure 2.3 SEM image of sintered glass at low and high magnifications. Bars are 50 µm and 5 µm, respectively.

2.1.5.3 Thin layer chromatographic (TLC) plates

Hydrophilic TLC plates (silica gel 60 F_{254}) were obtained from Merck. The plates, with original size of 20 × 20 cm (on aluminium) were cut to 25 mm × 25 mm. Prior to use, dried by heating it in an oven at 110 ℃ for 1 hour, and then stored in a vacuum oven and used within six hours. Figure 2.4 shows typical SEM images of the microscopic structure of the thin layer chromatographic plate.

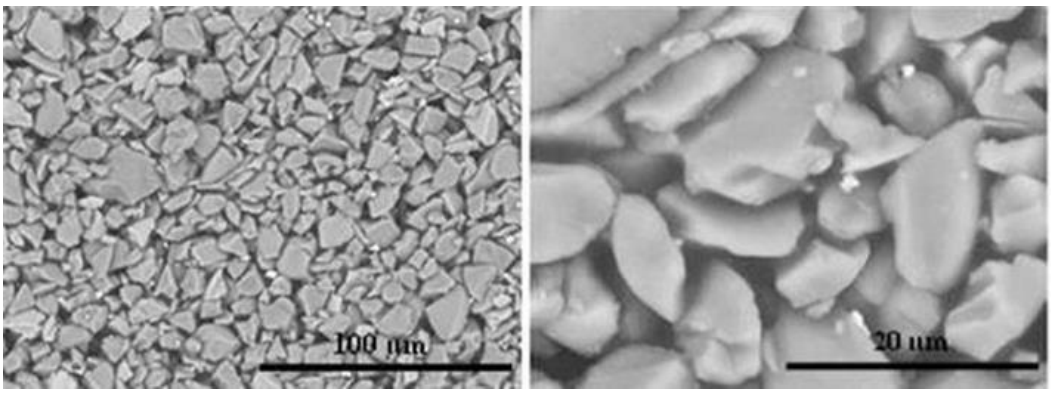

Figure 2.4 SEM image of thin layer chromatographic plate at low and high magnifications.

2.1.5.4 Metal plates

Aluminium (EN AW 1050A H14 – 99.50%, thickness: 1 mm), mild steel (EN3B - 98% thickness: 1 mm), copper (C103, 99.95%, thickness: 1 mm) and brass (CZ106 - 70% cu, 29% Zn, thickness: 1.2 mm) were all obtained from Smiths Metal Centre Ltd, UK. The plates were cut to 25 × 25 mm square. Some of the metal plates were roughened as required prior to use (see 2.2.1). All metal coupons were cleaned ultrasonically with ethanol and acetone for 10 minutes prior to use.

2.1.5.5 Paper Substrates

The paper material used was Sartorius filter paper discs (quantitative grade 292, Fisher Scientific) with 0.18 mm thickness and retention of particle sizes from 5 to 8 µm.

2.1.5.6 Monodisperse silica

Powders of different size of monodisperse hydrophilic silica particles were obtained from Fiber Optic Center Inc. The particles were first cleaned ultrasonically by dispersing 5 g of the particles in 25 mL of ethanol and then agitated for 10 minutes using Grant Ultrasonic bath, MXB6. The samples were then centrifuged for 15 minutes using a benchtop centrifuge (Sorvall Thermo Scientific). The centrifugation was carried out three times with the replacement of the supernatant of the centrifuged sample with fresh ethanol in each successive case. The final settled silica was dried in a vacuum oven at room temperature overnight.

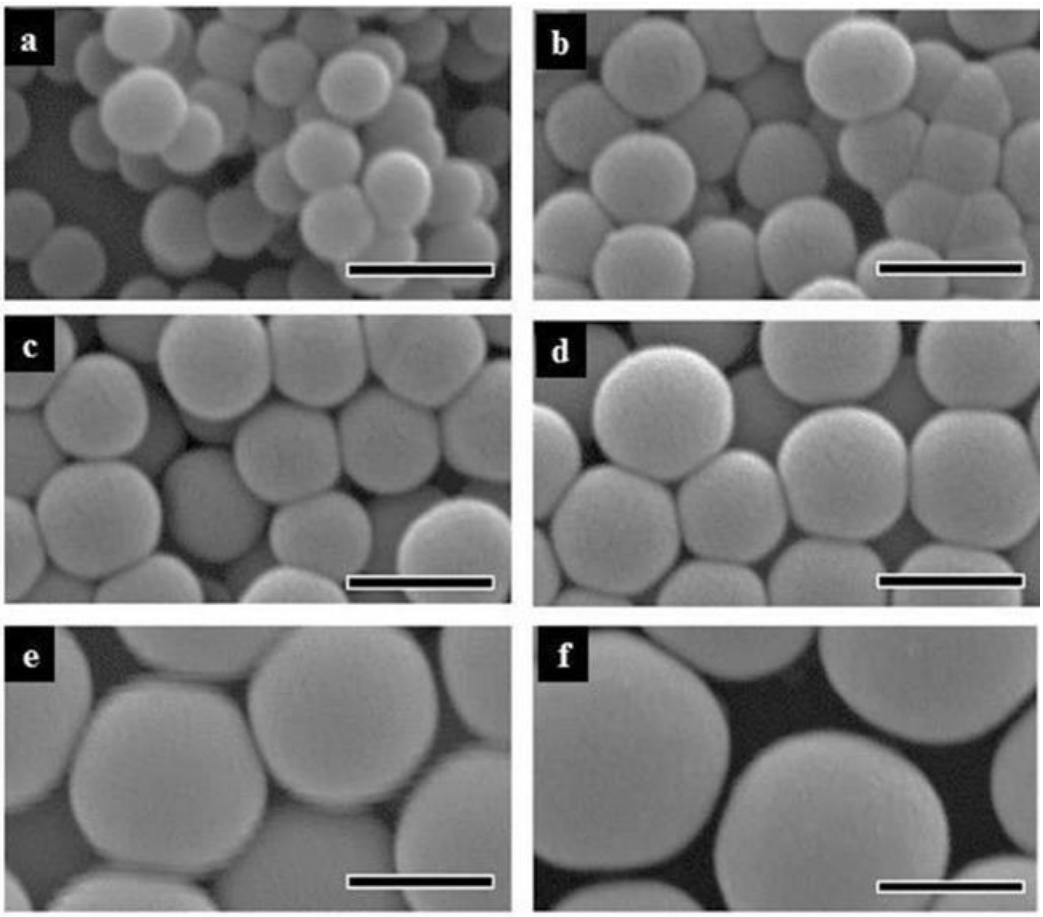

Figure 2.5 SEM images of different monodisperse particles used. 0.2 µm (a), 0.3 µm (b), 0.4 µm (c), 0.5 µm (d), 0.6 µm (e) and 0.7 (f). Bar is 500 nm.

2.1.5.7 Fumed silica and fumed aluminium oxide

The fumed silica particles were the key materials used for the preparation of silica porous substrates and they included hydrophilic and hydrophobic particles. The hydrophilic silica used was Aerosil R200 with specific surface area of 200 m^2/g produced by Evonik Degussa GmbH. According to the material safety data sheet provided by the manufacturer, other properties of R200 included pH: 4.2 ± 0.5, density: 2.2 g/cm^3 and tapped density: 50 g/l. Hydrophobic fumed silica powder, Aerosil R202 was obtained from Evonik Industry and supplied by Lawrence Industry, UK. The

properties as provided by the company included SiO_2 content: 99.8%, specific surface area: 100 ± 20 m^2/g, tapped density: 60 g/L). Aluminium oxide with surface area of 100 m^2/g, and 3.2 g/cm^3 the specific density of the hydrophilic fumed silica and aluminium oxide was made by reacting silicon tetrachloride, $SiCl_4$ or aluminium chloride in an oxy-hydrogen flame. The reaction produces silica or aluminium oxide nanoparticles that are linked together by a combination of fusion and hydrogen bonding to form aggregates with high surface area [1, 2]. According to the manufacturer, Aerosil the R202 was produced by subjecting hydrophilic fumed silica to hydrophobisation with polydimethylsiloxane. No further hydrophobisation of the sample was carried out. Transmission electron microscope (TEM) image of the hydrophobic fumed silica used is shown in Figure 2.6.

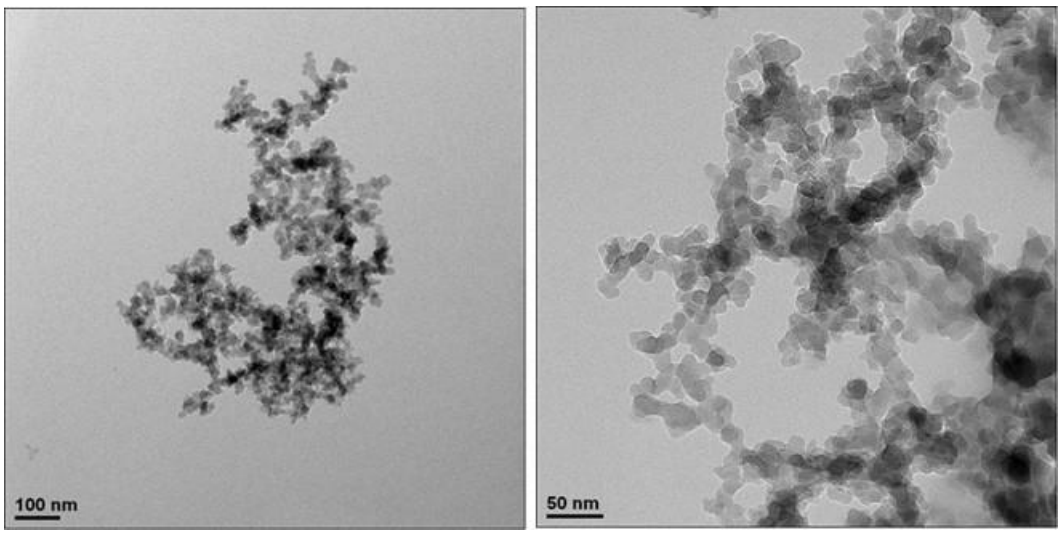

Figure 2.6 Transmission electron microscope (TEM) image of the hydrophobic fumed silica used at different magnifications

2.2 Methods

2.2.1 Etching of solid surfaces

Smooth surfaces, such microscope as glass slides and aluminium were subjected to controlled-etching to obtain rough or structured surfaces. Glass slides were etched by sandblasting smooth microscope slides with F320 alumina sandblasting the grit, with an average grain size of 29 ± 2 μm. The process was carried out using a cabinet sandblasting machine (Guyson). The glass was then cleaned with alcoholic potassium hydroxide (2.1.1) for 30 min in ultrasonic bath. The cleaning was repeated twice with plenty amount of water for 10 min each and then dry naturally in open air before storage in desiccator.

Surfaces of the metal plates, aluminium, mild steel, copper and brass were first polished with fine metallographic abrasive paper (600 grit size) to reduce the surface oxidation layer and other impurities. The plates were then cleaned ultrasonically with ethanol and acetone for 10 minutes in each solvent. The cleaned plates were then subjected to wet chemical etching in appropriate reagents. Aluminium plate were etched for 30 s in acidic echant prepared by mixing 40 mL hydrochloric acid (HCl), 12.5 mL of water (Milli-Q) and 2.5 mL of hydrofluoric acid (HF). Qian and Shen [3]. Iron (mild steel) plates were etched by immersion in 70% nitric acid, HNO_3 in water [4]. Copper and brass plates were etched in aqueous solution of iron (III) chloride, $FeCl_3$ (5 wt.%) containing 100 μL hydrochloric acid, HCl at room temperature for 18 h [5]. In each case, the plates were finally washed in ethanol and water in sequence.

2.2.2 **Hydrophobisation of glass slides and silica particles**

In liquid phase, the hydrophobisation was carried out by preparing solutions of DCDMS in anhydrous toluene at different concentrations using volumetric flasks pre-treated overnight with 0.5 mL DCDMS and washed with chloroform and ethanol to remove excess DCDMS and dried before use. The sample (0.50 g of the purified silica particles or a cleaned glass slide) and magnetic stirrer bar were introduced into a cleaned and dried 40 cm^3 sample tube - Teflon centrifuge tubes (Oak Ridge), pre-labelled with the concentrations of the prepared DCDMS. 35 cm^3 of the prepared DCDMS solutions were then poured into the corresponding Teflon tubes and put in an air-tight box, fitted with gas inlet and outlet. The box was placed on multipoint stirrers (Thermo Electron) and saturated with dry nitrogen gas. The set-up was monitored for one hour with intermittent flushing with nitrogen gas (15 minutes interval) to ensure a negligible humidity rise. At the end of the set time, the reactions were terminated by adding 0.5 mL of ethanol to each vessel. The stirring was allowed to continue for 5 minute before the samples were removed.

The hydrophobised slides were then carefully removed from the reaction vessels with the help of the clips into clean vials already filled with chloroform. They were washed in an ultrasonic bath for 10 minutes and the cleaning repeated with ethanol before they were dried naturally for 2 hour and then stored in desiccators.

The hydrophobised silica particles left in the Teflon tubes after hydrophobisation were recovered by centrifuging the suspension with fresh toluene at 3000 rpm for 15 minutes. The supernatant of the suspension was replaced successively with chloroform and ethanol and centrifugation repeated in each case. The settled silica particles were dried in a vacuum oven at 60 ℃ for 24 h before use.

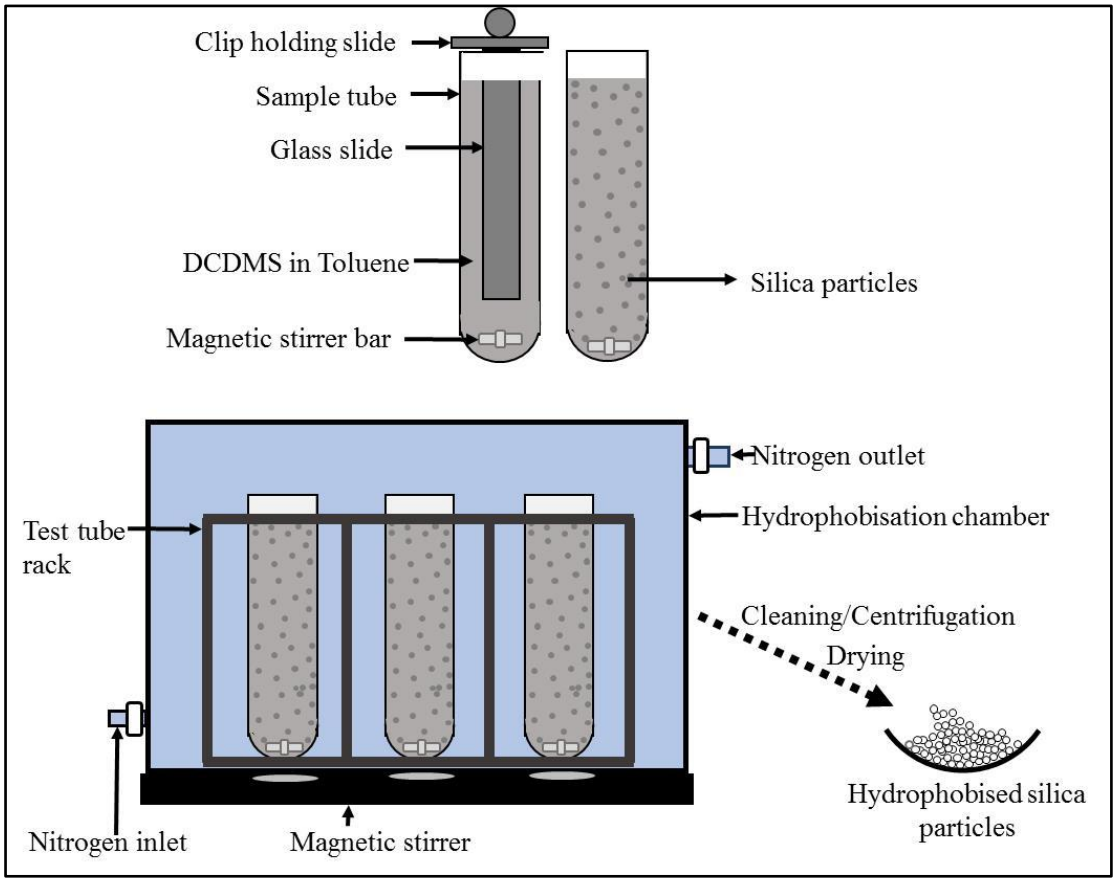

Figure 2.7 Schematic of liquid phase hydrophobisation of glass and silica particles. On top are sample tubes which contain substrates (glass slide or silica particles) and silansing liquid. Illustration of hydrophobisation of silica particles in the chamber placed on multiple positioned magnetic stirrer (RHS). Below is the vessel of hydrophobised silica particles obtained after centrifugal cleaning with solvents followed by drying in the vacuum oven.

2.2.3 **Vapour phase hydrophobisation of glass slides, sintered glasses and TLC plates**

Liquid phase hydrophobisation was mostly used for the modification of uncoated silica particles. Other solid surfaces like glass slides, sintered glass dics, or TLC plates were speedily modified in a vessel saturated with silane vapour. Prior to the hydrophobisation

process, the porous materials (e.g. TLC plates and sintered glasses) were degassed at 100 ℃ for 1 h and placed in a vacuum desiccator to return to room temperature. The hydrophobisation was done by fixing 6 slides on a Teflon holder and placed in an air tight vessel fitted with gas inlet and outlet (Fig. 8). The vessel was flushed with nitrogen for 3 min then 300 µL of dichlorodimethylsilane (or *1,1,1,3,3,3*-hexamethyldisilazane for TLC plates) was immediately introduced into the vessel. The set up was left for at least 1 h in a fume cupboard. In the end the samples were removed and ventilated for 1 h before used.

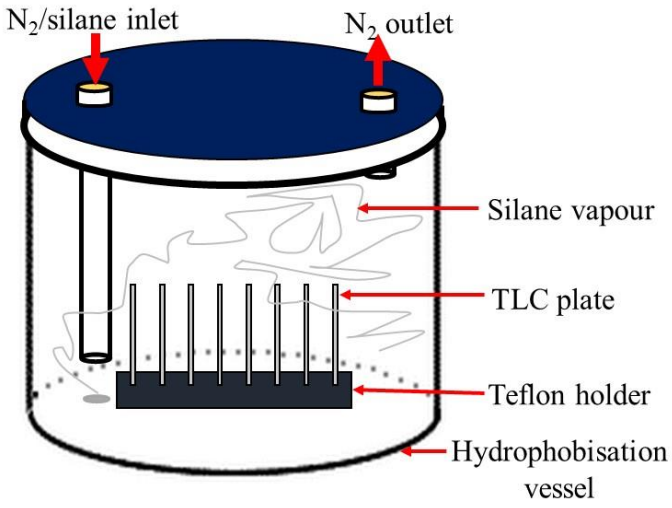

Figure 2.8 Schematics of the experimental set up for the hydrophobisation of solid substrates in vapour phase. Before sealing, the airtight hydrophobisation vessel was first flushed with nitrogen gas and then drops of silansing agent through the inlet. Glass slides are modified by the vapour generated by the silane.

2.2.4 **Hydrophobisation of aluminium metal plates**

Etched and non-etched aluminium plates were hydrophobised by immersion in 2% (volume ratio) ethanol solution of *1H, 1H, 2H, 2H* – perfluorodecyltrichlorosilane in

vessels placed on a magnetic stirring plate at room temperature and left overnight. The plates were recovered and heated in an oven at 120 °C for 1 h and stored in a desiccator.

2.2.5 Preparations of silica dispersion and fabrication of porous silica coatings by a spin coating process

Silica dispersions were prepared by adding dry hydrophobic fumed silica in absolute ethanol to form 5 wt.% dispersion (20 wt.% for monodispersed silica). The mixture was placed in an ice-water bath and ultrasonically dispersed for 10 min using Branson digital sonifier (model 450) set at 50% of the maximum power. About 500 µL of the prepared suspension was deposited on 25 × 25 square millimetre, hydrophobised microscope slide placed on the sample table (vacuum chuck) of the spin coater (model P6700). The suspension drop was spread and coated onto the slide at a maximum spin rate of 2500 rpm for 40 s. (1000 rpm for monodispersed suspensions). The resulting porous coated slides were dried in an oven at 100 °C for 1 h before storage in a vacuum desiccator.

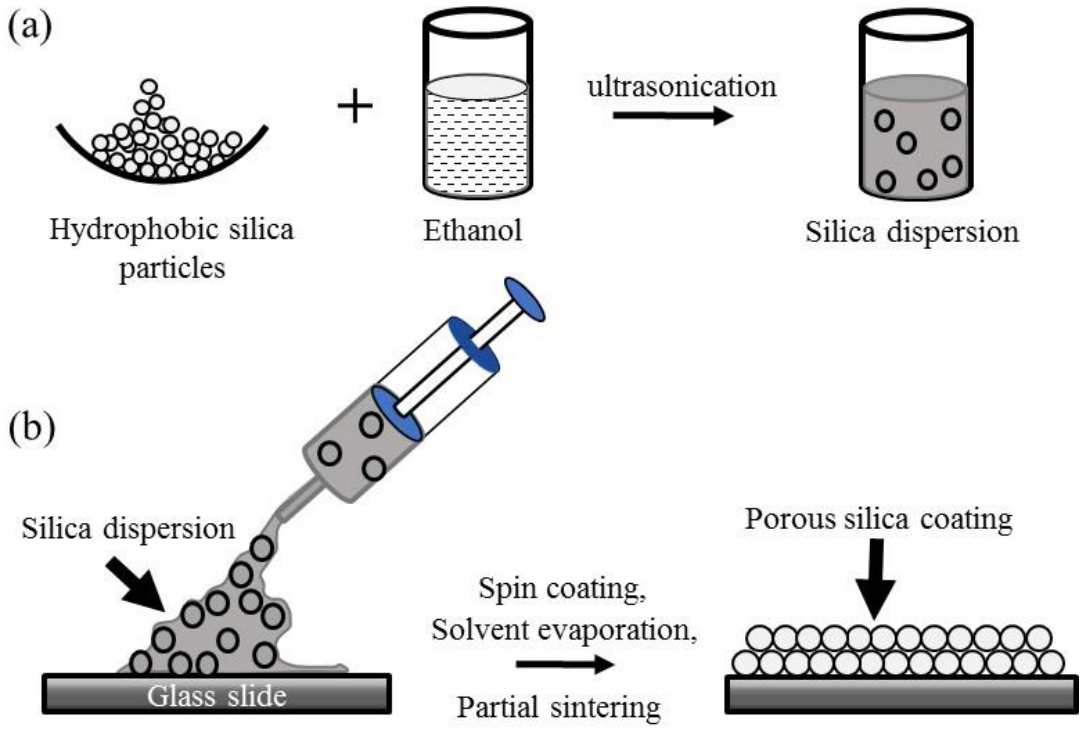

Figure 2.9 (a) Schematics showing the preparation of silica suspension used for the fabrication of porous silica coating by spin coating process (b).

2.2.6 **Fabrication of porous silica substrates by dip-coating method**

In the dip-coating method, the substrate is wetted by dipping into the dispersion and then withdrawn at a constant speed. As the substrate was being withdrawn, the liquid dispersion adhered onto it and some of the adhered dispersion was drained by gravity to produce a thin coated film on the substrate. This is followed by evaporation of the solvent by drying of the coated film. [6, 7]. A syringe pump (NE-1000 obtained from New Era Pump Systems Inc.) was used for the dip-coating. To achieve this, a line with a clip was attached to the pusher block of the pump and suspended vertically downward through a metal support. Two cleaned hydrophobised glass slides were sandwiched and

fixed to the clip. A vessel containing fumed silica dispersion was placed directly below the suspended glass slides (See Figure 2.10). Turning on the pumping and withdrawal button of the machine lowered and pulled out the slides from the coating bath through a perpendicular distance at a set speed. The slides were allowed to remain in the suspension for 1 min before being withdrawn at a constant speed of 5 cm/min. The process was carried out at different suspension concentrations and withdrawal speeds.

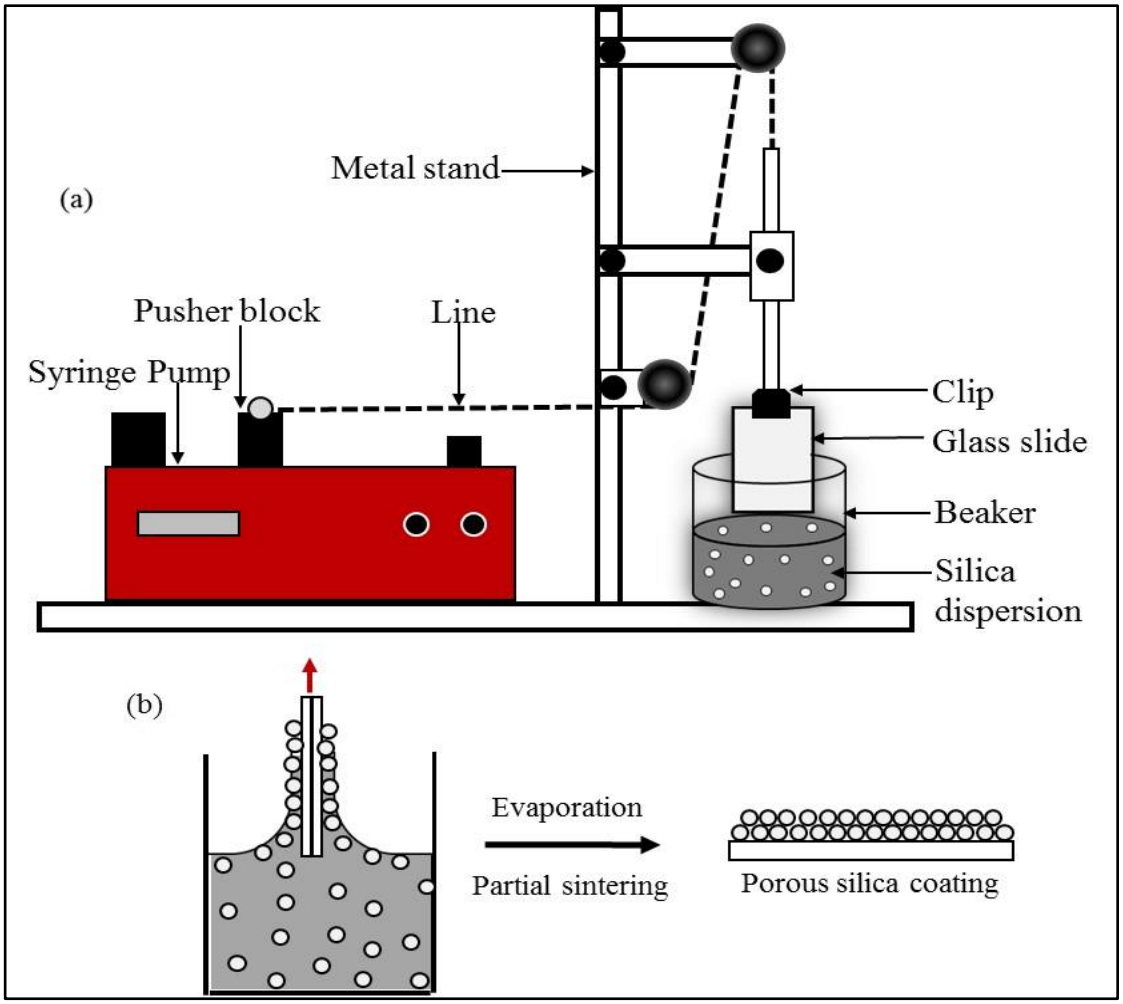

Figure 2.10 Schematic of the dip-coating method: (a) A self-constructed dip-coater using a syringe pump; (b) Illustration of coating mechanism of the process. During the withdrawal of the substrates (shown by the red arrow), the suspension adhered to the substrate and a film of non-volatile species (particles) was coated on the substrate surface after solvent evaporation.

However, the syringe pump is programmed to measure flow rate of a liquid through a cylindrical syringe. Conversion from flow rate (mL/min) to velocity (cm/min) was calculated for the experiment as shown below.

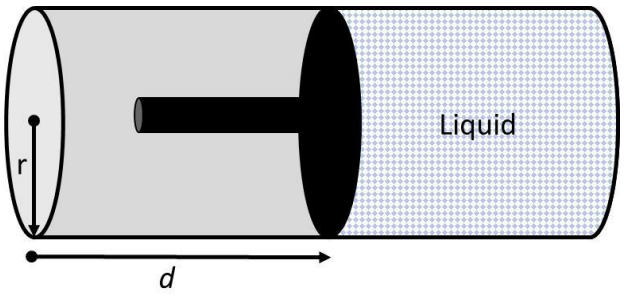

Figure 2.11 Schematics showing liquid flow in a syringe pump and dimensions for the calculation and conversion of flow rate of the syringe pump to dip coating speed. *r* is the inner radius of the syringe, *d* is the distance of liquid flow.

$$Flow\ rate\ = \frac{Volume}{time} = \frac{Area \times distance}{time} = Area\ \times\ Velocity \qquad \textbf{2.1}$$

$$v = \frac{FR}{A} = \frac{FR}{\pi r^2} \qquad \textbf{2.2}$$

where v is the velocity, FR is the flow rate, r is the inner radius syringe used.

2.2.7 **Partial (gradual) impregnations of porous silica coatings using non-volatile oils.**

Non-volatile oil and elastomer (e.g. squalane, silicone oil and Sylgard 184) were prepared and used for the impregnation of the porous or texture materials. Squalane

solution, for instance, was prepared by mixing known portions of squalane in hexane to obtained a specific concentration of the impregnating liquid (vol.%). Other oil solutions were prepared in hexane in the same way. About 100 μL of the oil solution was deposited on the porous coated slides placed on the sample table of a spin coater and spun at 2500 rpm to obtain the impregnated coating (Fig.12). The impregnated surface was transferred to a vacuum desiccator for an hour to ensure the complete evaporation of hexane. Different concentrations of the non-volatile oil solutions in hexane were prepared and impregnated onto the porous coatings.

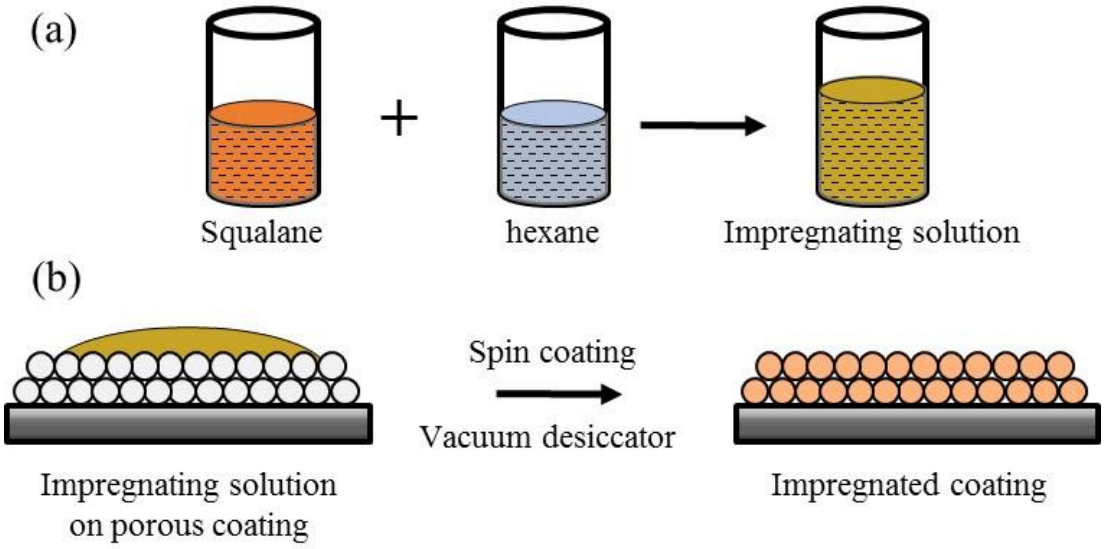

Figure 2.12 Scheme for the preparation of oil used for the impregnation of the porous coating (a) and the impregnation process, (b).

Sylgard 184 elastomer comes in two parts: pre-polymer (part A) and curing agent (part B). Partial impregnations using Sylgard 184 were carried out in two stages involving:

i. The use of pre-polymer base Sylgard (parts A only).

ii. The use of curable Sylgard (mixture of parts A + B).

In each case, different concentrations (wt.%) of the Sylgard solutions were prepared in hexane. In the use of pre-polymer, the impregnations were carried out using the same steps employed for the impregnation of squalane as described above and at the end of the fabrication, the impregnating Sylgard remained liquid on the surface of the porous silica coatings because they were not cured. Curable Sylgard was prepared at a ratio of 10:1 for part A and B, respectively. Unlike the use of pre-polymer, the substrates were further heated at 150 ℃ in an oven to transform (cure) the impregnated film from liquid form to solid state.

2.2.8 **One-step deposition/impregnation of silica coatings**

This technique involves a merger of the fabrication of porous substrate with the impregnation process. A known proportion of the oil (e.g. squalane) in ethanol (fixed vol. %) was prepared and hydrophobic fumed silica was added to this mixture. The dispersion was agitated with an ultrasonic probe and coated onto slides by spin coating, dip-coating, spray coating and brushing.

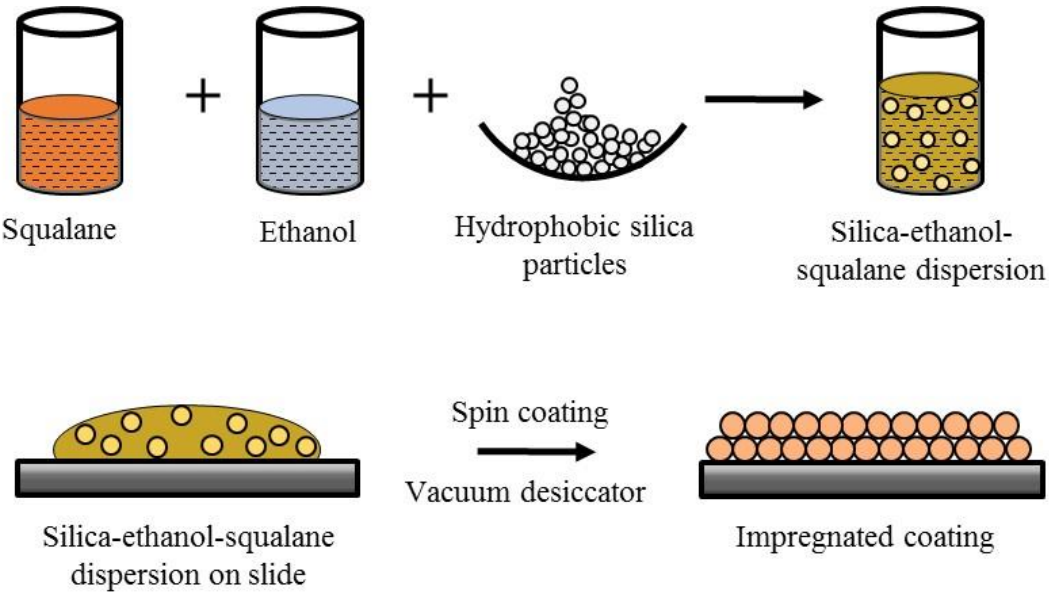

Figure 2.13 Scheme for the preparation of the precursor (a) used for the in situ fabrication/impregnation of silica coating, (b).

2.2.9 **Miscibility of squalane in ethanol**

Ethanol and squalane were mixed in different weight ratios, agitated with a magnetic stirrer for 72 hours and were left to settle until there were clear separation between ethanol and squalane. After the solutions were settled, ethanol and squalane were carefully separated to different glass vessels and their weights taken. Ethanol was then evaporated by placing the vessels in an oven set to 100 ℃ for at least 48 hours. The weight of the non-volatile squalane was measured at the end of 48 h and 6 h later to ensure that it is constant. The average percentage of the measured squalane in the clear solution before evaporation was calculated. The amount of ethanol evaporated was calculated by measuring the weight of the solution in the glass vessel. The weight of the solution was measured first after 24 hour mark, and then for every 2 hours till the 48

hour mark. The dissolution of squalane in ethanol was calculated by the expression below.

$$Squalane\ miscibility = \frac{weight\ of\ squalane}{weight\ of\ mixture} \times 100 \qquad \textbf{2.3}$$

2.2.10 Retentions of oil in different porous silica coatings

Porous coating were fully impregnated with squalane (100%), degassed in a vacuum desiccator and spin coated to uniformLy spread the oil as described in Section 2.2.6. The weights of the impregnated coatings were measured and the coatings were position vertically in a Teflon holder for possible drainage. The weights of the coatings were measured after 24 h successively for 120 h to assess the loss of the impregnated liquid.

2.2.11 Doping of squalane with Nile red and fluorescence microscopy to trace impregnated oil

A solution of 1×10^{-5} M Nile red in squalane was prepared in 50 mL volumetric flask. To ensure complete dissolution of the dye, the Nile red sample (159 µg) was first dissolved in 2 mL of acetone and then added to squalane dropwise with vigorous shaking. The resulting solution was shielded from light and kept open overnight in a desiccator to allow complete evaporation of the acetone.

Fluorescence microscopy was carried out to trace the relative amount and distribution of impregnated oil on the coated surfaces. Here, squalane doped with the Nile red was impregnated onto coatings as previously described in Section 2.2.7. Bright field and fluorescent imaging of the impregnated surfaces were carried out using an optical

microscope. Intensities of images at different concentration of oil impregnation were recorded and analysed using Image-Pro Plus software (6.0 version).

2.2.12 **Determination of coating thickness and porosity**

2.2.12.1 Capillary-driven impregnation

Film thickness and porosity were determined by subjecting the prepared coated surface to capillary-driven impregnation. The coated slide was vertically suspended over impregnating liquid (squalane) and carefully lowered to slightly immersed in squalane at the bottom. Capillary rise of the oil through the silica porous film was monitored until the coated portion was fully soaked with the oil. The mass of the dry coating, (mass of silica) and the mass of the impregnated oil (being the capacity of the voids or pores) were determined gravimetrically and porosity/thickness analysed using the masses and densities of silica and squalane.

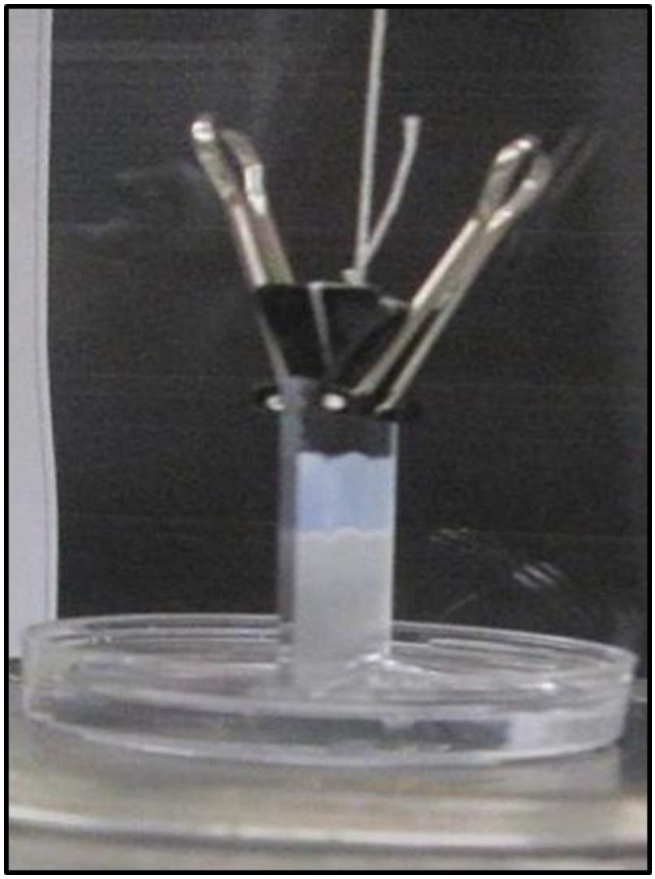

Figure 2.14 Photograph of the experimental set for capillary driven impregnation. The coated slide was suspended to slightly touch the impregnating oil in a Petri dish. The coating was gradually soaked with the oil from the bottom by capillary rise of squalane through the porous coated surface. The capillary front which divide the slide into impregnated and non-impregnated regions kept on moving upward until the coating was fully impregnated.

2.2.13 **Calculation of coating porosity and thickness from capillary impregnation**

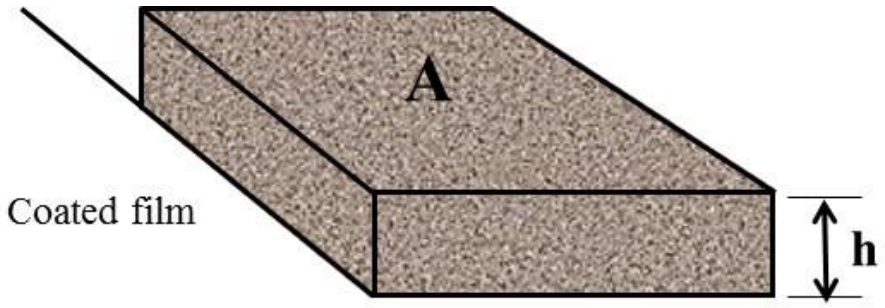

Figure 2.15 Schematic of the coated slide showing the dimensions of the film.

The porosity, ϕ of the coated film in this case is the fraction of the total film volume, V that is not occupied by the solid matter (silica) but with oil, if impregnated. A coated film with thickness h and area A is illustrated in in Figure 2.15. The total volume of film is given by

$$V = A \times h \qquad 2.4$$

This also means that the sum of both the volume of the solid (silica particles), V_S and the pore volume, V_P gives the total volume of the film, V.

$$V = V_S + V_P = A \times h \qquad 2.5$$

Thus,
$$h = (V_S + V_P)/A \qquad 2.6$$

In terms of the material mass and density,

$$V_S = M_S/\rho_S \quad (2.7)$$

$$V_P = M_{oil}/\rho_{oil} \quad (2.8)$$

Hence, the porosity of the coating, ϕ can be given by the equation below.

$$\phi = V_P/(V_S + V_P) \quad (2.9)$$

M_S is the mass of the solid (silica), ρ_S is the density of solid (silica: 2.20 g/cm^3) [2, 8], M_{oil} is the mass of oil (squalane), and ρ_{oil} is the density of oil (squalane: 0.81 g/cm^3) [8-10].

2.2.13.1 Determination of coating thickness using Dektak XT stylus profiler

The Dektak XT stylus surface profiler is an advanced thin and thick film step height measurement tool which takes measurements electromechanically by moving the tip of the diamond stylus over the sample surface in line with programmed scan length, speed, and stylus force. The stylus is linked to a Linear Variable Differential Transformer (LDVT), which produces and processes electrical signals that correspond to surface variations of the sample. To measure the thickness of fumed silica coatings on glass slides, scanning was run through an area between the top surface of the coated film and the pre-determine reference uncoated (scratched) portions of the film. The thickness of the film, *h* was determined as the vertical difference between the top surface and the bottom of the scratch mark (Figure 2.16). The measurement was taken at three different portions of the each coating, and an average reading was calculated on 3 replicated coatings.

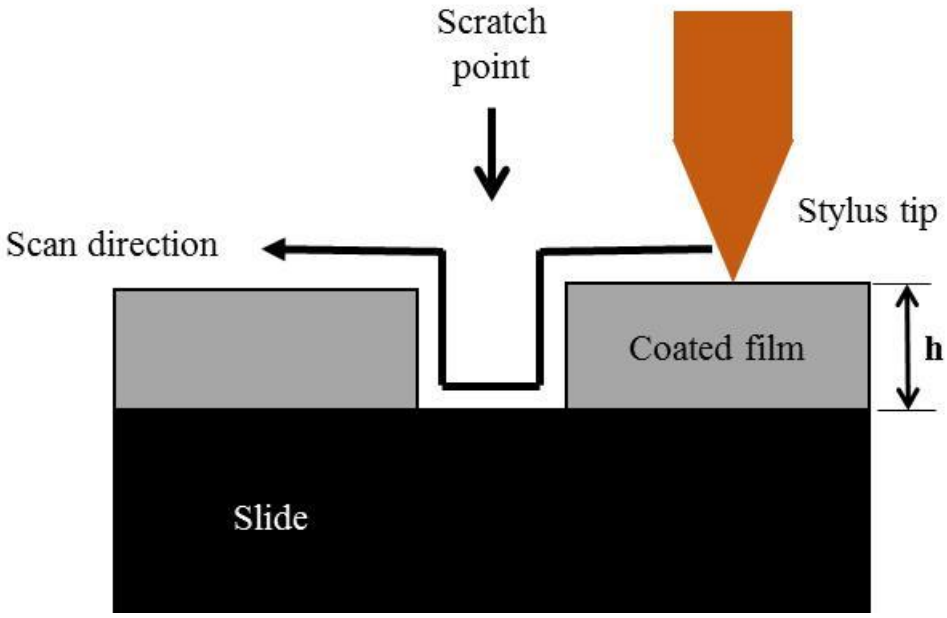

Figure 2.16 Stylus tip (from Dektak XT) scanning through the top surface and bottom (scratch point) of the coating. The thickness of the coating is the vertical distance between the topmost layer and the bottom, and is denoted as h.

2.2.13.2 Determining total mass of impregnated oil, oil inside the pores and over-coated oil layer of the fabricated porous coatings

The amount of the impregnated oil on various surfaces were determined by measuring the mass of the microscope slides used (M_O), mass of the slides coated with silica (M_C), mass of the impregnated coated slides (M_I). To obtain the mass of the oil in the pores only, the excess oil on surfaces of the impregnated coated slides was soaked using filter papers before measuring the slides as M_{IS}. The mass of over-coated layer of oil (M_{OC}) was determined by calculating the difference in the mass the impregnated coating before and after soaking the excess oil with filter paper. In each case, the masses were expressed in grammme per unit area of coverage (g/cm^2).

Impregnated oil (M_{total}) = $M_I - M_C$ 2.10

Oil in the pores only (M_{pore}) = $M_{IS} - M_C$ 2.11

Over-coated oil(M_{excess}) = $(M_I - M_C) - (M_{IS} - M_C) = M_I - M_{IS}$ 2.12

2.2.14 Determining the stability of uncured and cured Sylgard impregnated coatings

This experiment was used to assess the adhesion of the coated surfaces to the substrate. It involves drawing a 50 g load with a metallographic paper base across the coated surfaces. The substrates were placed in a groove separated by a microscope slides which has the same thickness as the slide used for the preparation of the preparation of the coatings. Similar methods have been reported on soft shearing materials [11, 12]. In addition, the weight (load) in this current experiment was uniformLy pulled at 5 cm/min using a syringe pump. An optical microscope was used to access the extent of damage created by the process to various samples surfaces.

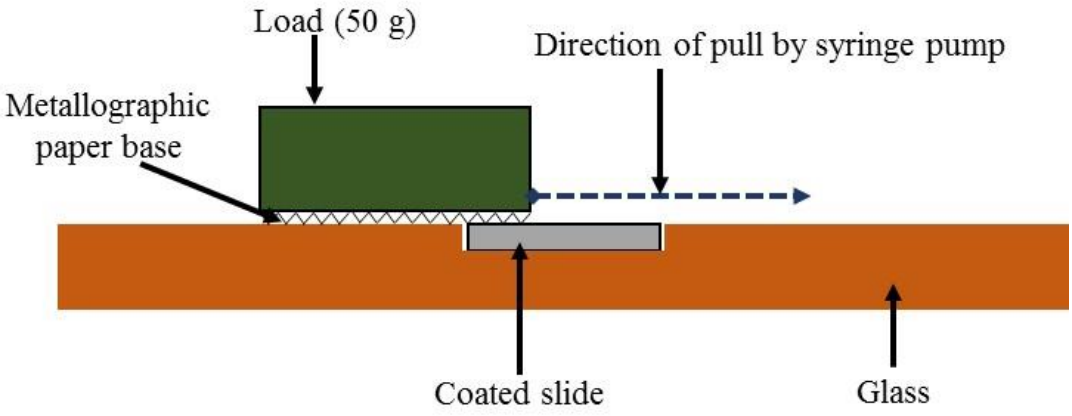

Figure 2.17 Scheme of the experimental set-up used for scratch tests to examine the stability of the coated film**.**

2.2.15 **Surface examinations**

2.2.15.1 Bright field and fluorescence microscopy

Optical microscopy was employed for many purposes. Samples were viewed using Olympus microscope (BX-51) fitted with DP70 digital camera. Transmitted visible light was used to view the prepared slides placed on the microscope stage, images of well-focused samples were then taken. The nature of silica dispersions (emulsion or suspension) was examined by carefully taking a drop of the liquid into a dimpled slide and protected with cover slips before examinations.

Fluorescent microscopy of porous coatings impregnated by squalane doped with Nile red fluorophore was carried out using FITC filter to the Olympus microscope (BX-51). Both bright field fluorescent images were examined. Analysis of fluorescent images (intensity data) were perform using Image-Pro Plus software (6.0 version) and calculated in Excel. The intensities of different impregnated coatings, I were measured with reference to that 0% impregnated coatings, I_0.

Image-Pro Plus software was also useful for the analysis and counting of objects (e.g. adhered cells on slides), automatic repetition of live images or movies at desired intervals.

2.2.15.2 Scanning Electron Microscopy (SEM)

Structural details of micro/nano surfaces were captured for investigation using Hitachi TM-1000 table-top scanning electron microscope and Carl Zeiss Evo 60 scanning electron microscopy. To enhance the surface electro-conductivity and avoid charging

effect, the samples were pre-coated with either a thin film of carbon or gold prior to SEM imaging.

2.2.16 Measuring contact angles of water drops on solid surfaces

Wetting properties of the fabricated surfaces were investigated by measuring advancing and receding contact angles of sessile water drops on the prepared surfaces using drop shape analysis instrument, (DSA 10, Kruss). Water drops were dispensed and withdrawn from the surfaces of the sample placed on the sample stage of the instrument using a syringe pump (New Era) fitted with PTFE tubing and needle. To prevent excessive evaporation of the test liquid, the thermostated trough which surrounds the sample platform, was filled with water and the chamber closed. The stage was illuminated from the side and the camera which is positioned on the opposite side, was used to capture the image of the drop (Figure 2.18a). Contact angles were measured with the dispensed needle embedded in the sessile drop. A small sessile drop of about 3 µL was initially dispensed on the substrate and the droplet was inflated by gradual pumping of more liquid at the rate of 0.2 µL/s. Increasing the drop volume resulted in the contact line advancing outward, consecutive contact angles of the drop during the advancement were recorded till a maximum of 15 µL drop was achieved (Figure 2.18bi). After a stable drop was formed, the syringe pump was reversed and liquid was withdrawn from the inflated drop at the same rate to obtained series of receding contact angles (Figure 18bii). However, on super-hydrophobic and highly slippery surfaces where the drop could easily slide off or stick to the needle, drops were dispensed on the substrates and measurements were taken after a careful withdrawal of the dispense needle to avoid distortion of the drops (Figure 2.18biii). In both methods, each reported

measurement was an average reading of at least 2 different drops made on 3 replicated samples.

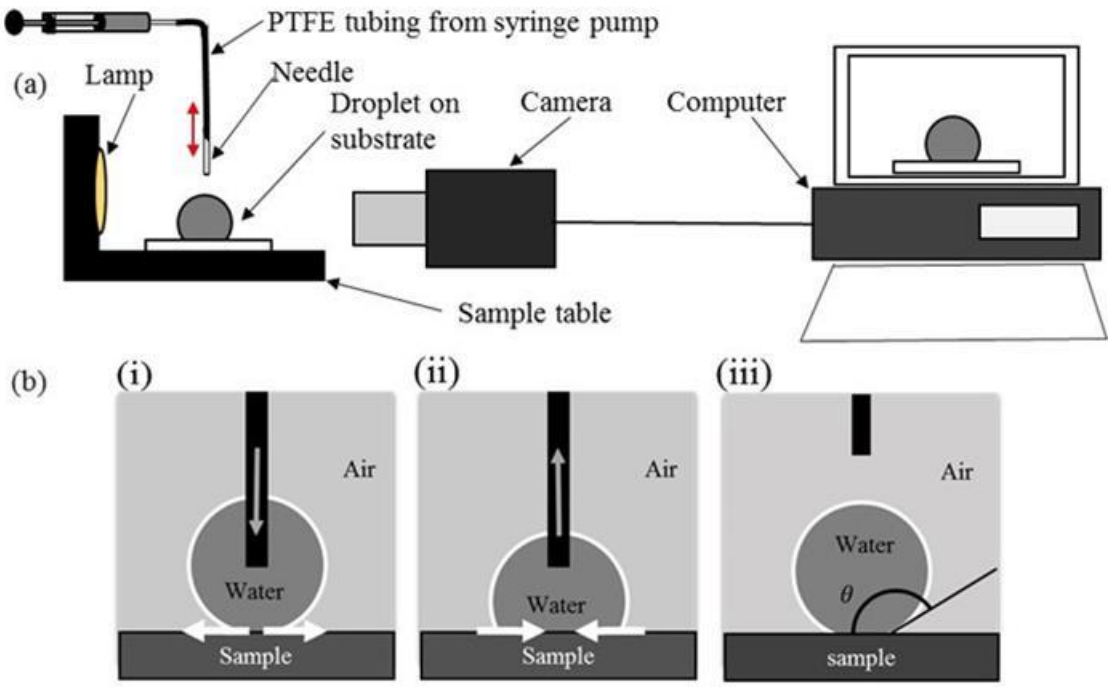

Figure 2.18 A sketch of the experimental set-up for measuring contact angle and studying dynamic wetting properties of solid surfaces by drop shape analysis instrument (DSA 10). (a) Sessile water drop deposited by a syringe pump through a perpendicularly positioned needle on substrate placed horizontally on DSA stage and subsequent capturing and analysis of the drop configuration and contact angle by DSA optical and computing system. (b) Different method of contact angle measurement during advancing, receding with needle inside the drop and the measurement taken after withdrawal of the needle.

2.2.17 **Measuring sliding angles and the determining sliding force of water droplets on samples**

Sliding angles of water droplets on the fabricated coated slides were determined by a tilt experiment. A drop of water was made on a substrate placed horizontally on an in-house made flat Teflon platform (Figure 2.19a). The Teflon groove in the middle of the material allowed an L-shaped needle suspended from the needle support of DSA to fit in and go under the sample (Figure 2.19b). The sample was tilted when the needle support was vertically raised Figure 2.19c, d). A DSA live video was used for monitoring and recording of the minimum angle of inclination or sliding angle created by the initial movement of the drop during the tilt. Sliding forces of the droplets were analysed using the force diagram shown in Figure 18e and reported elsewhere [13, 14].

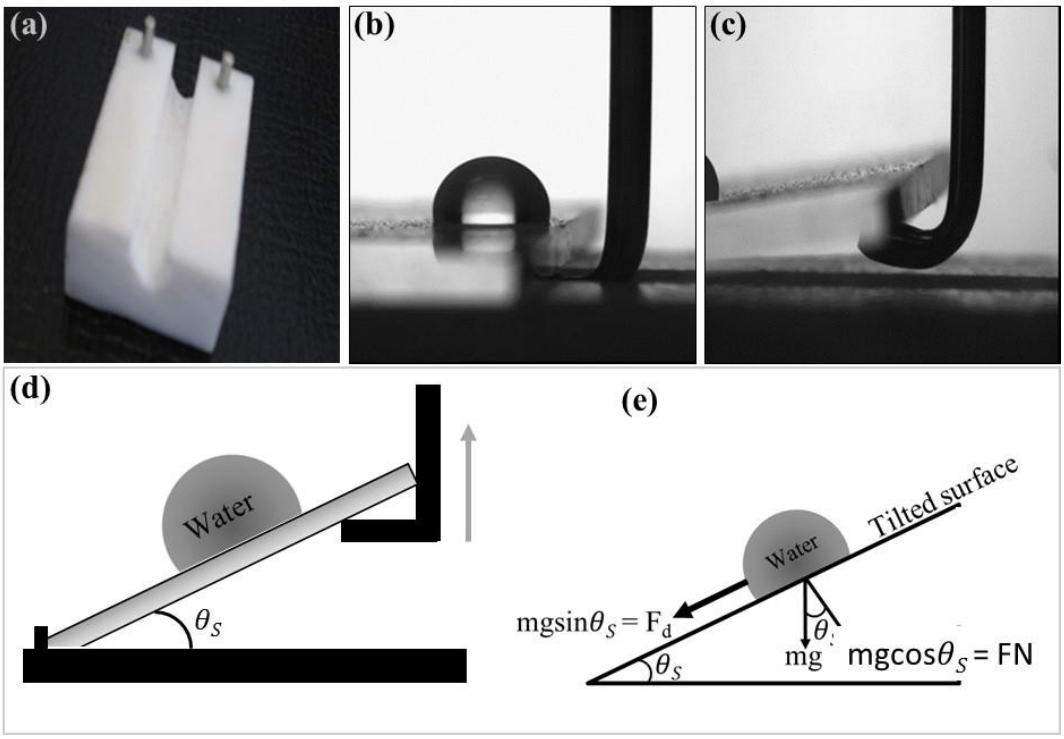

Figure 2.19 Scheme of the experimental set-up for measuring sliding angle and sliding force of the sliding droplet (a) Photograph of PTFE sample base used. Two metal hooks are fixed at the extreme of the Teflon base to wedge the sample slide during tilting. The groove in the middle of the material allows insertion of the L-shaped needle beneath the slide. (b) Typical set up showing image of droplet placed on the slide with the L-shaped needle placed in positions waiting tilting. (c) DSA image showing tilting and the movement of the droplet away from the initial position. (d) Illustrations showing the process in (c) and the sliding angle, θ_S created during the sliding process. (e) Force diagram for the determination of the sliding force of the droplet.

2.2.18 Measuring surface and interfacial tensions of liquid interfaces

DSA 10 instrument was used for the measurement of surface and interfacial tensions using a pendant drop method. Also used were disposable syringes/needle with diameter of 1.65 ± 0.01 mm and a 3 × 3 × 2.5 cm cuvette. A large pendant drop was produced from the tip of needle; DSA magnification and the focus were adjusted for a central and sharp drop formed at the tip of a needle. The surface or interfacial tension was automatically calculated from the shape of the pendant drop using the Laplace equation for capillarity programmed into DSA.

2.2.19 Measuring turbidity of the dispersion and transmittance of the coatings

Turbidity of the suspensions and the transparency of the coatings were investigated using UV-Vis spectrophotometer (Lamda 25, PerkinElmer). 2.5 mL of sonicated suspensions (undiluted) were taken into a cuvette (1 cm path length) and placed in the sample holder of the instrument and the absorbance of light at wavelength 650 nm was measured. The coated slides were also vertically placed across the light path and the absorbance of light, A measured. Transmittance, T was calculated from $A = 2 - \log_{10}\%T$.

2.2.20 Adhesion of algae cells on the fabricated surfaces

The culture media as prepared and reported by Al-Awady *et al*. [15] was received and used for the investigation. The stock solution (culture media) of the cell sample was diluted to obtain an average cell concentration within the range of $(7 \pm 1) \times 10^6$ cell/mL using cellometer (Nexcelom Bioscience). The squalene-impregnated coatings (multiple

step, see 2.2.7) were placed in glass Petri-dishes and 40 mL of the algae media added to fully cover the slides. The slides were kept submerged for the specified periods of the experiment. At the set times, the slides were removed and vertically dipped into a beaker of milli-Q water to remove the excess of non-adhering algal media from the surface. A cover slip was placed on the surface of each slide to prevent drought in the course of further investigations. At least five (5) different spots on each slide were focussed and the number of adhered algae cells counted using optical microscope. An average of the counts was calculated for 3 replicated slides and reported in cell per square millilitre (cell/mm^2). The experimental steps for the cell adhesion is summarised into 3 major steps as shown in Figure 2.20.

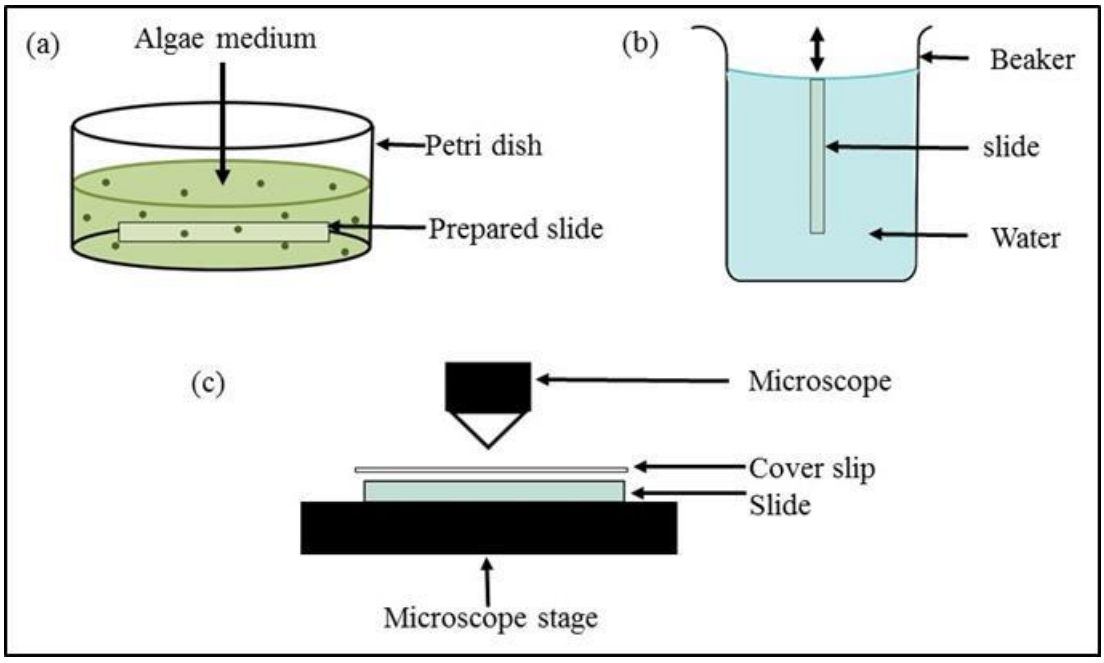

Figure 2.20 Scheme showing experimental steps for the adhesion of algae cells on prepared samples (a) Exposure of the surface to the algae medium, slide in a petri dish totally covered by the culture medium (b) Immersion of the slide into water to wash off of the excess culture medium and loosely attached cells from the slide. (3) Protection of the sample with coverslip and microscope imaging/counting of adhered cells at different points.

2.2.21 Hydrophobisation of different structured solid substrates by partial impregnation using Sylgard solutions.

Hydrophobisation of different structured solid materials such as etched microscope slide, TLC plate, sintered glass disc, aluminium oxide coatings, etched metal substrates (aluminium, mild steel, copper, brass) and filter paper were carried out by first preparing curable Sylgard solution in hexane as described in Section 2.2.7. To obtain a super-hydrophobic surface material on substrates of high surface roughness, the substrates were impregnated with low concentration of the Sylgard solution, preferably 1 wt.% (or less). The impregnated surfaces were then cured for 15 minutes in the oven at 150 ℃. The impregnations were carried out using spin-coating and dip-coating techniques. Nano-porous hydrophilic fumed aluminium oxide coatings were also modified to become super-superhydrophobic by incorporating a low volume fraction of curable Sylgard into fumed aluminium oxide dispersions in ethanol (i.e. by using one-step preparation method - Section 2.2.8) before coating and drying. The wettability of the structured surfaces was tuned by simply varying the concentrations of Sylgard in dispersions between 0.1-1.0 wt.%.

2.3 References

1. S. E. Pratsinis, Flame aerosol synthesis of ceramic powders. *Progress in Energy and Combustion Science*, 1998. **24**(3): p. 197-219.

2. R. Bode, H. Ferch, and H. Fratzscher, Basic characteristics of AEROSIL fumed silica. *Tech Bull-Fine Part*, 2006. **11**: p. 1-70.

3. B. T. Qian and Z. Q. Shen, Fabrication of superhydrophobic surfaces by dislocation-selective chemical etching on aluminum, copper, and zinc substrates. *Langmuir*, 2005. **21**(20): p. 9007-9009.

4. M. N. Qu, *et al*., Fabrication of superbydrophobic surfaces on engineering materials by a solution-immersion process. *Advanced Functional Materials*, 2007. **17**(4): p. 593-596.

5. H. Jie, Q. J. Xu, L. Wei, and Y. L. Min, Etching and heating treatment combined approach for superhydrophobic surface on brass substrates and the consequent corrosion resistance. *Corrosion Science*, 2016. **102**: p. 251-258.

6. H. W. Fang, *et al*., Dip coating assisted polylactic acid deposition on steel surface: Film thickness affected by drag force and gravity. *Materials Letters*, 2008. **62**(21-22): p. 3739-3741.

7. R. Ashiri, A. Nemati, and M. S. Ghamsari, Crack-free nanostructured BaTiO3 thin films prepared by sol-gel dip-coating technique. *Ceramics International*, 2014. **40**(6): p. 8613-8619.

8. T. Aubry, B. Largenton, and M. Moan, Study of aggregate density in fumed silica suspensions. *Journal of Colloid and Interface Science*, 1998. **202**(2): p. 551-553.

9. N. Tripathi, Densities, viscosities, and refractive indices of mixtures of hexane with cyclohexane, decane, hexadecane, and squalane at 298.15 K. *International journal of thermophysics*, 2005. **26**(3): p. 693-703.

10. A. Kumagai and S. Takahashi, Viscosity and Density of Liquid-Mixtures of N-Alkanes with Squalane. *International Journal of Thermophysics*, 1995. **16**(3): p. 773-779.

11. Q. P. Ke, *et al*., Fabrication of mechanically robust superhydrophobic surfaces based on silica micro-nanoparticles and polydimethylsiloxane. *Surface & Coatings Technology*, 2011. **205**(21-22): p. 4910-4914.

12. Y. H. Xiu, Y. Liu, D. W. Hess, and C. P. Wong, Mechanically robust superhydrophobicity on hierarchically structured Si surfaces. *Nanotechnology*, 2010. **21**(15).

13. J. Yang, H. Song, H. Ji, and B. Chen, Slippery lubricant-infused textured aluminum surfaces. *Journal of Adhesion Science and Technology*, 2014. **28**(19): p. 1949-1957.

14. W. Y. L. Ling, T. W. Ng, A. Neild, and Q. S. Zheng, Sliding variability of droplets on a hydrophobic incline due to surface entrained air bubbles. *Journal of Colloid and Interface Science*, 2011. **354**(2): p. 832-842.

15. M. J. Al-Awady, G. M. Greenway, and V. N. Paunov, Nanotoxicity of polyelectrolyte-functionalized titania nanoparticles towards microalgae and yeast: role of the particle concentration, size and surface charge. *Rsc Advances*, 2015. **5**(46): p. 37044-37059.

CHAPTER 3

STRUCTURAL STUDIES OF SOLID SURFACES AND FABRICATION OF NANO-POROUS SILICA COATINGS WITH VARIABLE WETTABILITY

3.1 Introduction

Wetting properties of solid materials are very important for many practical applications. The nature of the material surface therefore plays a vital role in determining the degree of wettability. In a situation where the inherent properties of the solids cannot withstand the impact of the prevalent wetting media, coating of the solid surface with protective or adaptive layers that can resist such a condition is usually adopted as measures to either, preserve, or enhance, applications of the material [1].

The dependence of wettability on surface chemistry and structure of solid materials was discussed in detail in Chapter 1. The direct measurement of surface energy of solid materials is difficult but could be assessed by wetting investigations [2] by measuring the contact angle of liquid droplets on solid surfaces [3]. Materials with high surfaces energy in air are hydrophilic and water drops spread over their surface in air giving contact angles below 90^o. Materials with low a surface energy are hydrophobic and water drops give contact angles bigger than 90^o when placed on their surface in air. Hence, low surface energy materials are usually employed in the modification of hydrophilic solid surfaces into hydrophobic ones. So far, the contact angles of water drops on a ‘smooth’ surface with the lowest achievable surface energy have not exceeded 120° - further contact angle increase is possible only on rough surfaces with special morphology [4].

Following investigations in this area, useful models and mathematical equations provided by Young [5], Wenzel [6] and Cassie and Baxter [7] are fundamentals in understanding solid wettability. The achievements of Cassie-Baxter and Wenzel models in providing descriptive insight into wetting of real surfaces, and subsequent emergence and successes of roughness enhanced surfaces (superhydrophilic and superhydrophobic) in a variety of applications are quite remarkable [8-11]. A fascinating application of superhydrophobic surfaces with micro-/nano-roughness is their use as base materials in another biomimicry phenomenon known as slippery liquid infused porous surfaces (SLIPS). SLIPS as described earlier involve the replacement of the air pocket on a structured surface with oil; such that a thin over-coated layer of the oil is held in place by capillarity and used in wetting control (Chapter 1.6). The work presented in this chapter goes beyond mimicking the bio-inspired lotus (superhydrophobic) or pitcher plant (slippery) surfaces. In this project, gradual transformation of superhydrophobic base material to slippery state is carefully followed by a step-wise impregnation of the material with a non-volatile oil to explore the hidden properties of the surface and various untapped possibilities.

The literature review in Chapter 1 revealed a wide range of different methods for fabrication of structured surfaces at the micro- and nano-scale and the use of various low surface energy chemicals for the modification of solid surfaces. Particle deposition on a solid substrate is one of the methods that can generate structured surface as earlier described (section 1.5.2.1). Such depositions are usually carried out to primarily transfer the roughness at the scale of particles size to the solid interface [12, 13]. Additional property offered by the particle coating on the solid substrate is the creation of porosity to the surface of the material [13]. In this chapter, and indeed the greater part of work in the thesis, silica particles are employed for the fabrications of porous silica coatings as

base materials for further modification with oil, and wettability studies. Silica has been selected because it is readily available on the market in hydrophilic and hydrophobic form in a range of different micro/nanoscale sizes, can be easily modified by chemical treatment and has excellent thermal and mechanical stability. Other attractive properties of silica have been described in Section 1.4.4. Instead of going through rigorous method of fabrication, the particles have been coated onto solid substrates by spin or dip coating methods, both known for their simplicity and proven uniform deposition of thin layer of coatings [14-16]. The aims of the work presented in this chapter are:

i. To study and compare the wetting properties of smooth and rough solid materials.
ii. To investigate the optimum experimental conditions for the fabrication of stable air/oil filled porous silica coatings by spin coating and dip coating methods.
iii. To partially impregnate porous silica coatings with non-volatile oils and investigate the effect of the impregnation on wetting properties of the coatings.

3.2 Experimental

The main part of the work is preceded by a series of experiments to investigate wetting properties of smooth and rough surfaces for a clear understanding of solid wetting. These are carried out by measuring the contact angle of water drops in air on smooth/roughened hydrophilic solid surfaces in comparison to the same surfaces hydrophobised with appropriate low surface energy chemicals. Details on the preparation and roughening of these solid surfaces were described in section 2.1.5. Effects of hydrophobisation and scales of roughness on wettability of solid surfaces have been studied. Materials used in this investigation include smooth and roughened

(sand blasted) glass slides. Fabrications of porous coatings of hydrophobised monodispersed silica particles of various sizes on microscope glass slides by spin coating have also been carried out as described in Section 2.2.5 and their wetting properties investigated. The effect of size of particles in the coating on the contact angle of water drops on the coated surfaces in air and the retention of oil within the liquid impregnated porous coatings have been investigated.

Fabrications of nanoporous fumed silica coatings on microscope glass slides by spin coating and dip coating have been carried out as described in Sections 2.2.5 and 2.2.6, respectively. Effects of various factors, such as the concentration of suspension, spin rate (spin coating) and withdrawal speed (dip coating) are studied in order to find the optimum experimental conditions for even, crack-free coatings. Very significant work in this Chapter is on the partial impregnation of dry fumed silica nanoporous coatings with different amounts of non-volatile oil (squalane). Detailed description of the partial impregnation process was presented in section 2.2.7. Effects of the oil loading in the coatings on the contact angle and sliding angles of water drops are carefully investigated as descried in Sections 2.2.16 and 2.2.17. Detailed characterisation of the coatings, including the thickness and porosity of the coating, fluorescence microscopy to trace the distribution and relative amount of the impregnated squalane have been conducted as described in the relevant sections of Chapter 2.

3.3 Results and discussion

3.3.1 Wettability of smooth and rough glass slides

Hydrophilic microscope glass slides have been hydrophobised using a broad range of concentrations of dichlorodimethylsilane (DCDMS) solutions in dry toluene (section

2.2.2) and the dynamic contact angles of sessile water drops in air on the slides measured as described in section 2.16. The average contact angles obtained at each DCDMS concentration are plotted in Figures 3.1 and 3.2 for smooth and rough hydrophobised slides, respectively. The values of the advancing (θ_A) and receding (θ_R) contact angles, and contact angle hysteresis (CAH = θ_A - θ_R) obtained for smooth and rough surfaces are summarised in Table 3.1.

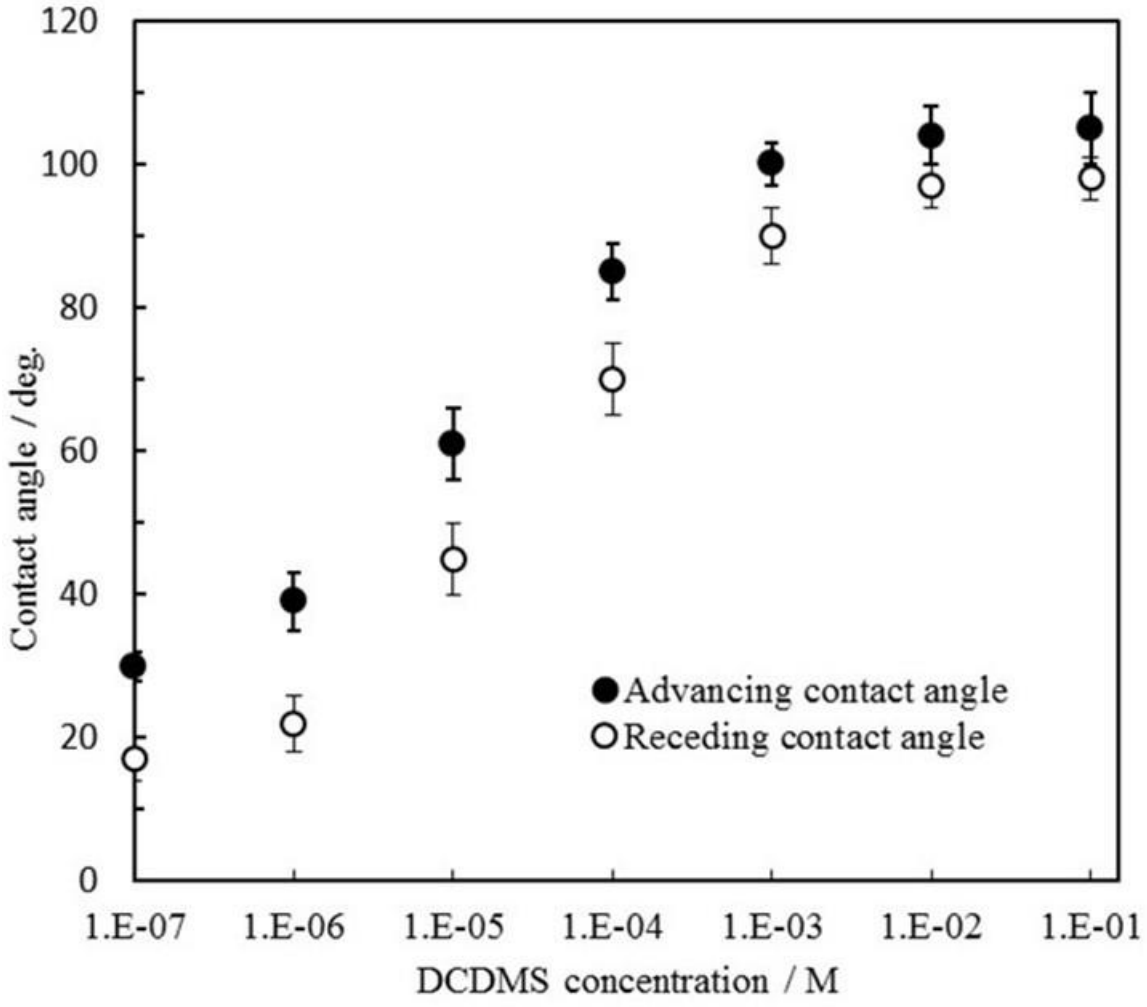

Figure 3.1 Advancing and receding contact angles of water drops on smooth glass slides in air versus concentration of DCDMS solutions used for the glass hydrophobisation.

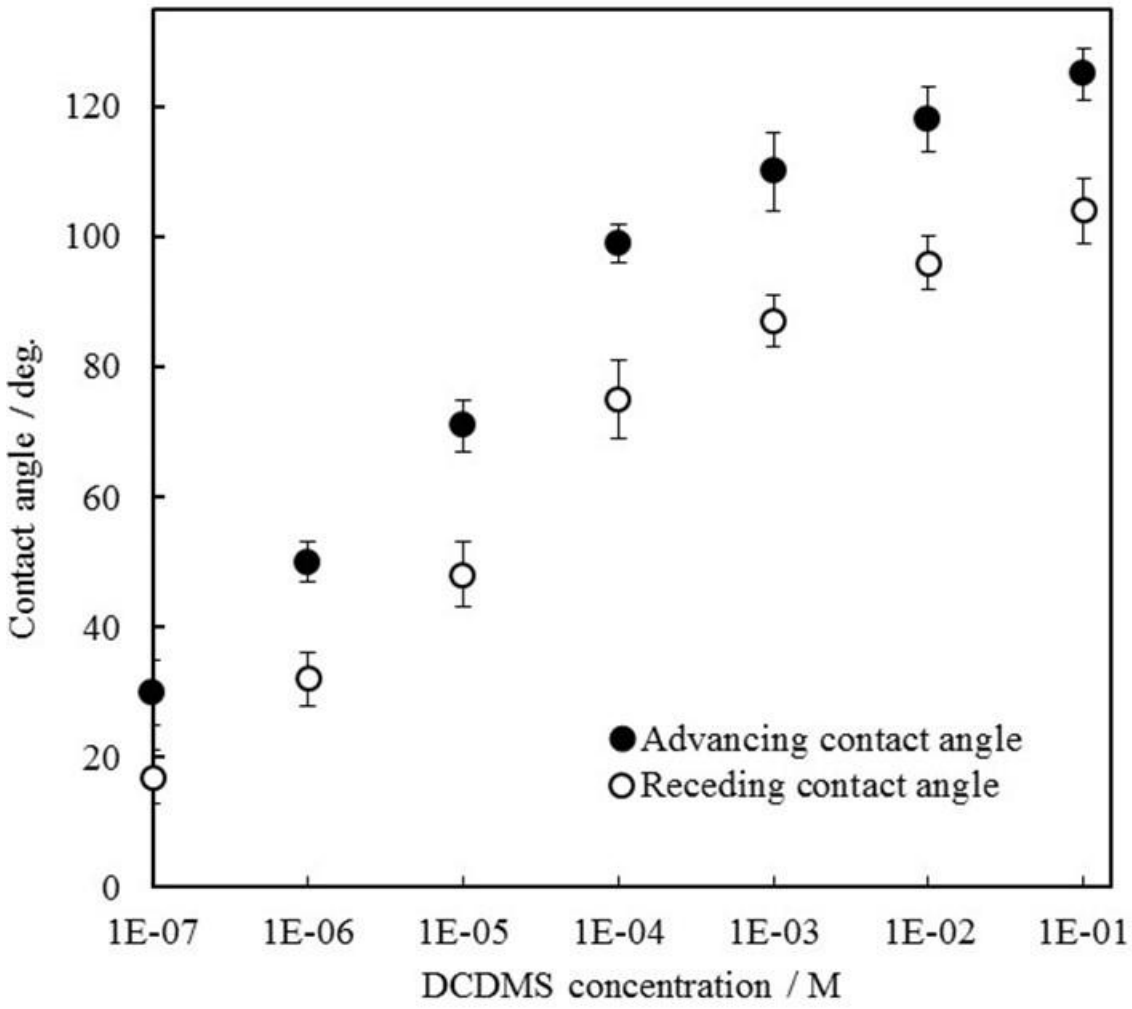

Figure 3.2 Advancing and receding contact angles of water drops on rough (sand blasted) glass slides in air versus concentration of DCDMS solutions used for the glass hydrophobisation.

Table 3.1 Advancing (θ_A) and receding (θ_R) contact angles, and contact angle hysteresis (CAH = θ_A - θ_R) of water drops on smooth and roughened glass slides in air at 22 ± 2 ℃ hydrophobised using different concentrations of DCDMS in toluene.

[DCDMS] / M	Smooth glass			Rough glass		
	θ_A / deg.	Θ_R / deg.	CAH / deg.	θ_A / deg.	θ_R / deg.	CAH / deg.
0×10^{0}	22 ± 2	12 ± 3	10 ± 5	< 5	~ 0	~ 5
1×10^{-7}	30 ± 2	17 ± 3	13 ± 5	32 ± 5	17 ± 4	15 ± 9
1×10^{-6}	39 ± 4	22 ± 4	17 ± 8	50 ± 3	32 ± 4	18 ± 7
1×10^{-5}	61 ± 5	45 ± 5	16 ± 10	71 ± 4	48 ± 5	23 ± 9
1×10^{-4}	85 ± 4	70 ± 5	15 ± 9	99 ± 3	75 ± 6	24 ± 9
1×10^{-3}	100 ± 3	90 ± 4	10 ± 7	110 ± 6	87 ± 4	23 ± 9
1×10^{-2}	104 ± 4	97 ± 3	8 ± 7	118 ± 5	96 ± 4	22 ± 9
1×10^{-1}	105 ± 5	98 ± 3	6 ± 8	125 ± 4	104 ± 5	21 ± 8

It is observed that dichlorodimethylsilane was able to hydrophobise both smooth and rough glass slides from a hydrophilic state to various levels of hydrophobicity in all the concentrations used. From the plots (Figure 3.1 and 3.2), increase in the concentration of DCDMS increases the contact angles of water drops on both smooth and rough slides, indicating increased hydrophobicity of the surface. However, the increase becomes smaller at the higher DCDMS concentrations indicating that there is a limit of hydrophobisation at the experimental conditions. The hydrophobicity of the glass surface is certainly due to the reactivity of dichlorodimethylsilane which involves the replacement of silanol groups (-OH) on the surface of a glass with non-polar methyl groups (Figure 3.3). The amount of OH groups replaced, and therefore the hydrophobicity, increases with the DCDMS concentration. However, some amount of OH groups remains unreacted even at very high DCDMS concentrations due to stearic hindrance by the neighbouring methyl groups already grafted at the glass surface, thus limiting the hydrophobicity and the contact angle value.

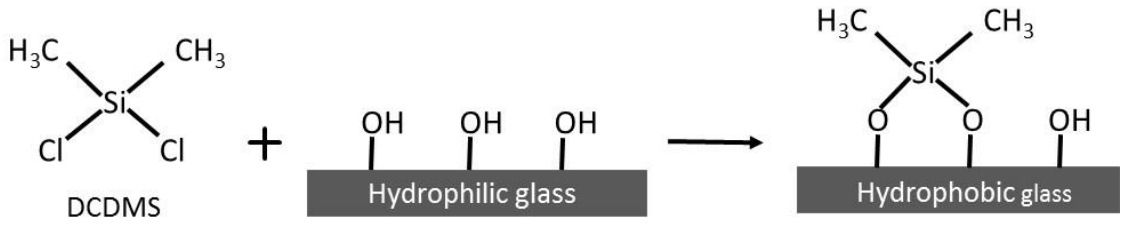

Figure 3.3 Schematic illustration of hydrophobisation reactions of DCDMS with the glass surface.

There are significant differences in the wetting properties of the smooth and rough glass (Table 3.1). The untreated (0 M DCDMS) rough glass slides are more hydrophilic than the smooth ones evident from the much smaller contact angle of water drops on the rough surface. This is in agreement with the Wenzel model prediction that the surface roughness 'magnifies' the wettability, thus a rough hydrophilic surface shows better wettability (smaller contact angle) than a smooth one of the same material. The rough hydrophobised slides show bigger contact angle hysteresis than the smooth ones hydrophobised at the same DCDMS concentration. This suggests that the water drops on rough hydrophobised slides are also in a Wenzel state of wetting i.e. the water follows the solid profile thus increasing the water-solid contact area and the three phase contact line is easily pinned due to roughness. At high DCDMC concentrations, the advancing contact angles on rough surfaces are bigger than those on the smooth hydrophobic glass slides with contact angles bigger than 90^{o} (see the last three rows in Table 3.1) as expected for Wenzel regime of wetting. However, the rough slides show bigger contact angles than the smooth ones even when the latter are hydrophilic. This contradicts to the Wenzel model prediction for the effect of roughness on wetting assuming the both surfaces have the same chemical composition but different roughness. The observed contradiction suggests that the chemical composition of the

smooth and rough slides hydrophobised at the same DCDMS concentration differ. It seems plausible to assume that the roughness has increased the surface density and reactivity of the OH groups, therefore more methyl groups have been grafted on the rough surface than on the smooth one for the same time of DCDMS treatment (1 hour, see section 2.2.1).

3.3.2 Porous coatings made of hydrophobised silica particles with different sizes

As earlier stated, particle deposition on a solid substrate is one of the techniques employed to control surface wettability. The surface properties of the resulting materials are usually dependent on the size of the particles and their wetting properties. The surfaces of such materials often exhibit unique physical and chemical properties compared to the bulk in terms of roughness. Similarly, porous coatings created by particles exhibit different characteristics based on their porosity which are also known to be controlled by the size of particles used [17, 18].

Literature data [17, 18] suggest that the particle size of the coating is an important factor that determines surface morphology and applications of materials. Surface morphology of nano/micro-structures is also related to important physical properties, including the retention and stability of gases or liquids inside the porous coating. Considering the outstanding role of the interface, clearer information on particles that make up the surface of the material and their distribution should definitely be good guiding steps to fabricating stable particulate based materials with controlled wettability. The properties of nanomaterials employed in controlling surface wettability are usually size-dependent. However, it has been reported that the size-dependent properties of silica particles are

not well investigated [19]. In this section, the effect of particle size on wettability of silica particle coatings are studied in order to select suitable coatings for making superhydrophobic and slippery surfaces.

3.3.2.1 Morphology and wetting properties of porous coatings made of hydrophobised silica particles with different sizes

Figure 3.4 provides SEM images of silica coatings of different particle sizes on glass slides. As expected, increasing size of the particles can clearly be observed from the top to the bottom. Another interesting trend gathered from the SEM image is the gradual aggregation of the primary particles when their diameter is progressively decreased from 700 nm to 10 nm. In the bottom images, larger particles can be clearly distinguished as a separate entity in full diameter. As the particle size reduces, aggregation of particles sets in and gradually builds up; this increases upward to a reasonable state at 300 and 200 nm particles. In the case of fumed silica, in addition to the nanoscale dimension of its coating, the degree of aggregations makes it very difficult to identify primary particles with diameter 10 nm. Another useful feature in the images is the gradual increase in roughness of the coatings which tend to follow the size and aggregation of the particles from bottom (larger particles) to the top (smaller particles). The roughness of the coatings changes from being dependent on the size of the particles at the bottom to a combination of the primary particles and aggregates as the particle size gets smaller, thus forming multiscale of roughness.

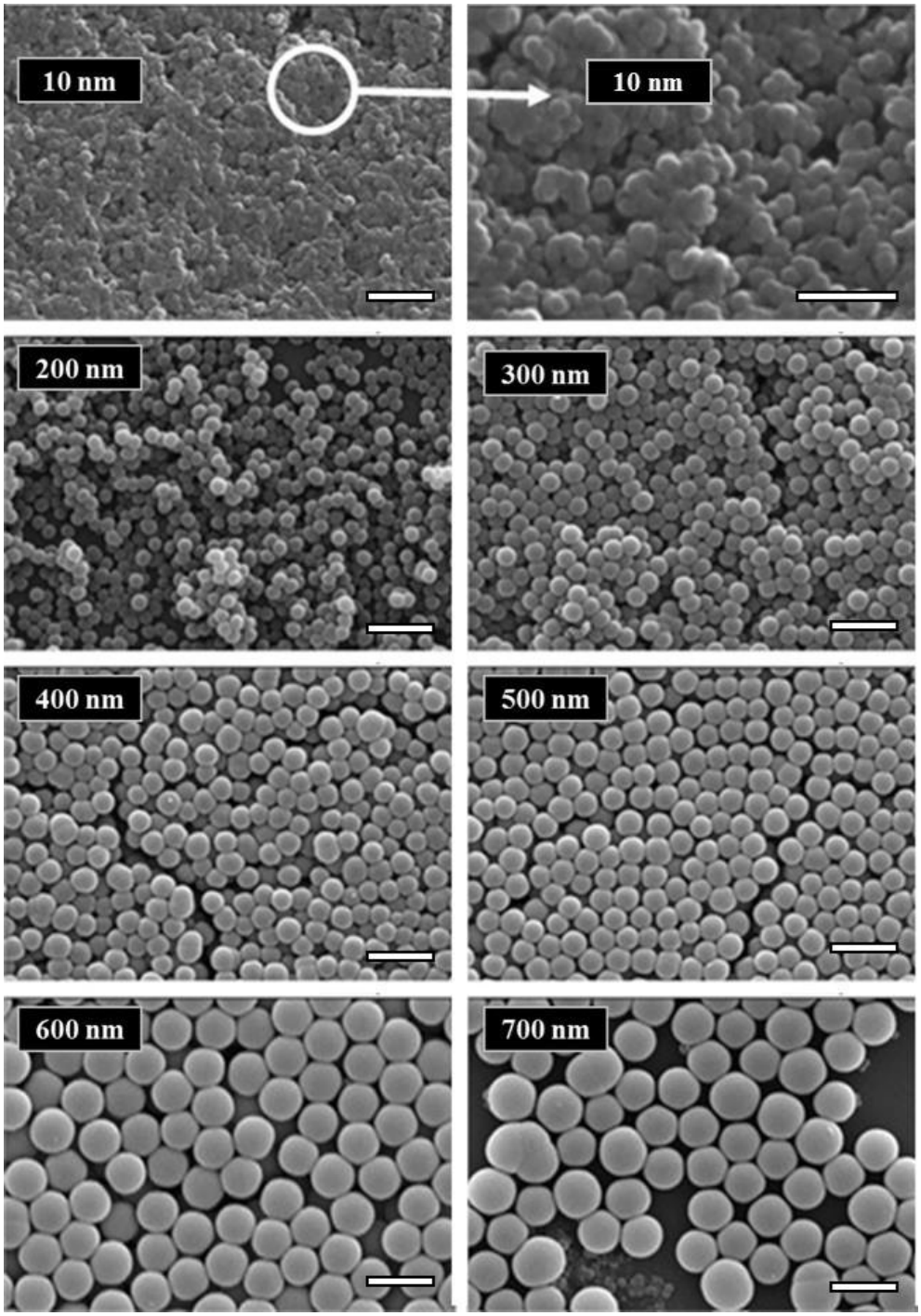

Figure 3.4 SEM images of porous coatings prepared by depositing silica particles of different sizes (shown) on glass slides by spin coating. The particles were hydrophobised in 1×10^{-1} M DCDMS in toluene under magnetic stirring bars for 24 h. The top right image shows the coating of 10 nm particles at higher magnification (bar = 500 nm). All other scale bars = 100 nm each.

Wettability of the coated surfaces were investigated, the advancing and receding contact angle of water drops on different coatings in air as well as the contact angle hysteresis of the porous coatings, are presented in Table 3.2. A plot showing the effect of particle diameter on wettability of the coated surfaces is presented in Figure 3.5. As can be observed, the contact angle of water drops on the coated surfaces varies inversely with the particle size, and proportionally to the degree of surface aggregation or hierarchical formation on morphology. Dual-sized or hierarchical roughness of micro/nano-structures is known for its significant roles in wettability [20-22]. This trend is expected because, in addition to the hydrophobic states of the particles, another influencing factor on wettability is the surface roughness which is higher on smaller particle sizes. Comparison of the wettability data in Table 3.2 and Figure 5 shows that contact angle hysteresis is negligible on silica coating with 10 nm diameter (fumed silica). The hysteresis then increases sharply from the fumed silica coatings (with smallest particle size) to the largest 700 nm coated surface. This is because nano/microstructured surfaces with multiscale roughness have the tendency to provide robust wetting stability due to stable air pockets on structures [22]; stable air pockets on structured surfaces are typical of the Cassie-Baxter state of wetting. It has been reported that the Cassie-Baxter mode of wetting can decrease with increasing the size of surface particles [23]. This is likely the reason for the much lower hysteresis on surfaces coated with smaller particles (10 and 200 nm in diameter) in comparison to those coated with bigger particles. These results show that the particles suitable for the fabrication of superhydrophobic coatings are those with diameters smaller than ~200 nm.

Table 3.2 Advancing and receding contact angles and contact angle hysteresis obtained using water drops on hydrophobised silica particles coating with different particle diameters in air.

Particle diameter/nm	10	200	300	400	500	600	700
Advancing Contact angle / deg.	160 ± 5	148 ± 2	145 ± 1	143 ± 3	143 ± 2	139 ± 2	138 ± 2
Receding contact angle / deg.	160 ± 5	145 ± 3	126 ± 3	120 ± 3	119 ± 3	116 ± 3	116 ± 3
Contact angle hysteresis / deg.	0 ± 0	5 ± 5	20 ± 4	23 ± 6	24 ± 5	23 ± 5	22 ± 5

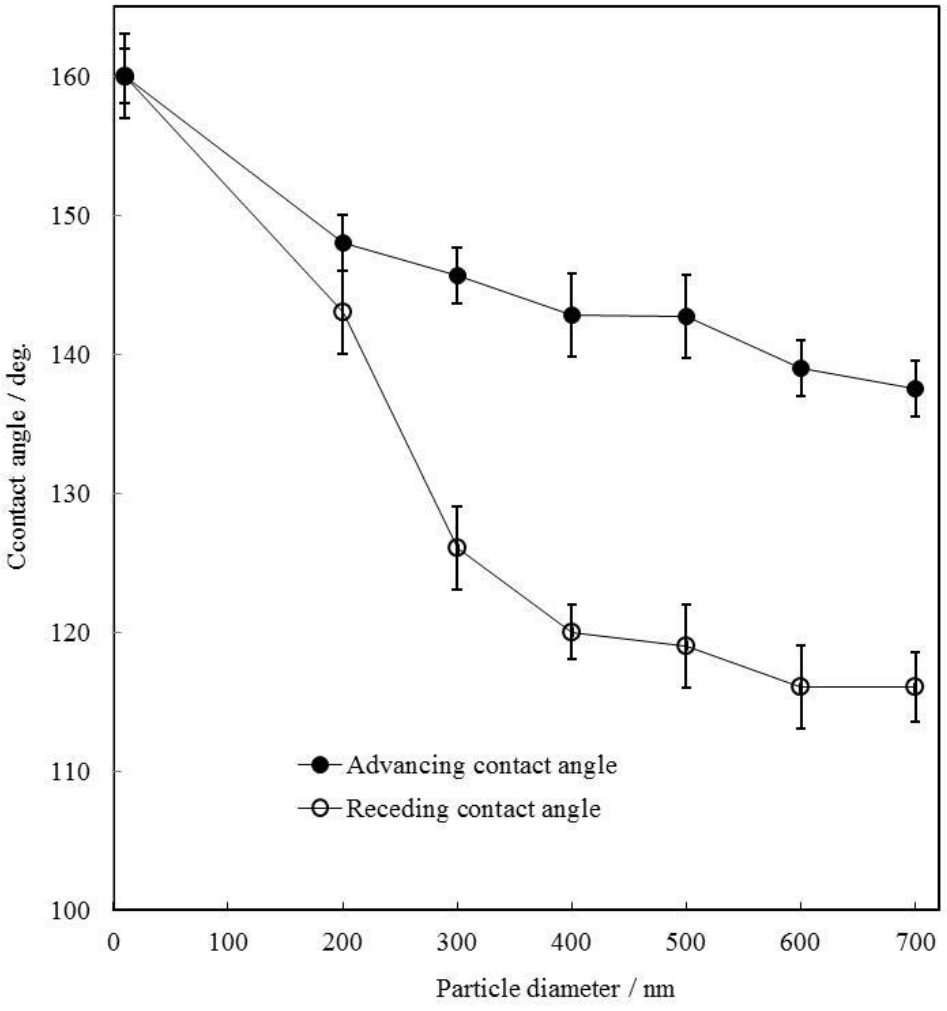

Figure 3.5 Variation of advancing and receding contact angles of water drops on hydrophobised silica coatings with different particle diameters in air.

3.3.2.2 Oil retention in porous silica coatings

It is known that the oil drainage out of the slippery liquid infused porous surfaces (SLIPS) could be detrimental to their performance and practical applications [24]. Therefore, we have investigated the oil drainage from porous particle coatings in order to select the optimum coatings for oil impregnation and preparation of stable SLIPS. Porous substrates made with different particle sizes (shown above) were fully impregnated with squalane, degassed in a vacuum desiccator and spun to uniformLy spread the oil over the coating as described in Section 2.2.7. The impregnated coatings were positioned vertically and left for days for the oil to drain out as described in section 2.2.10. The percentage of oil drainage calculated from the mass loss measured over time is shown in Figure 3.6a and b.

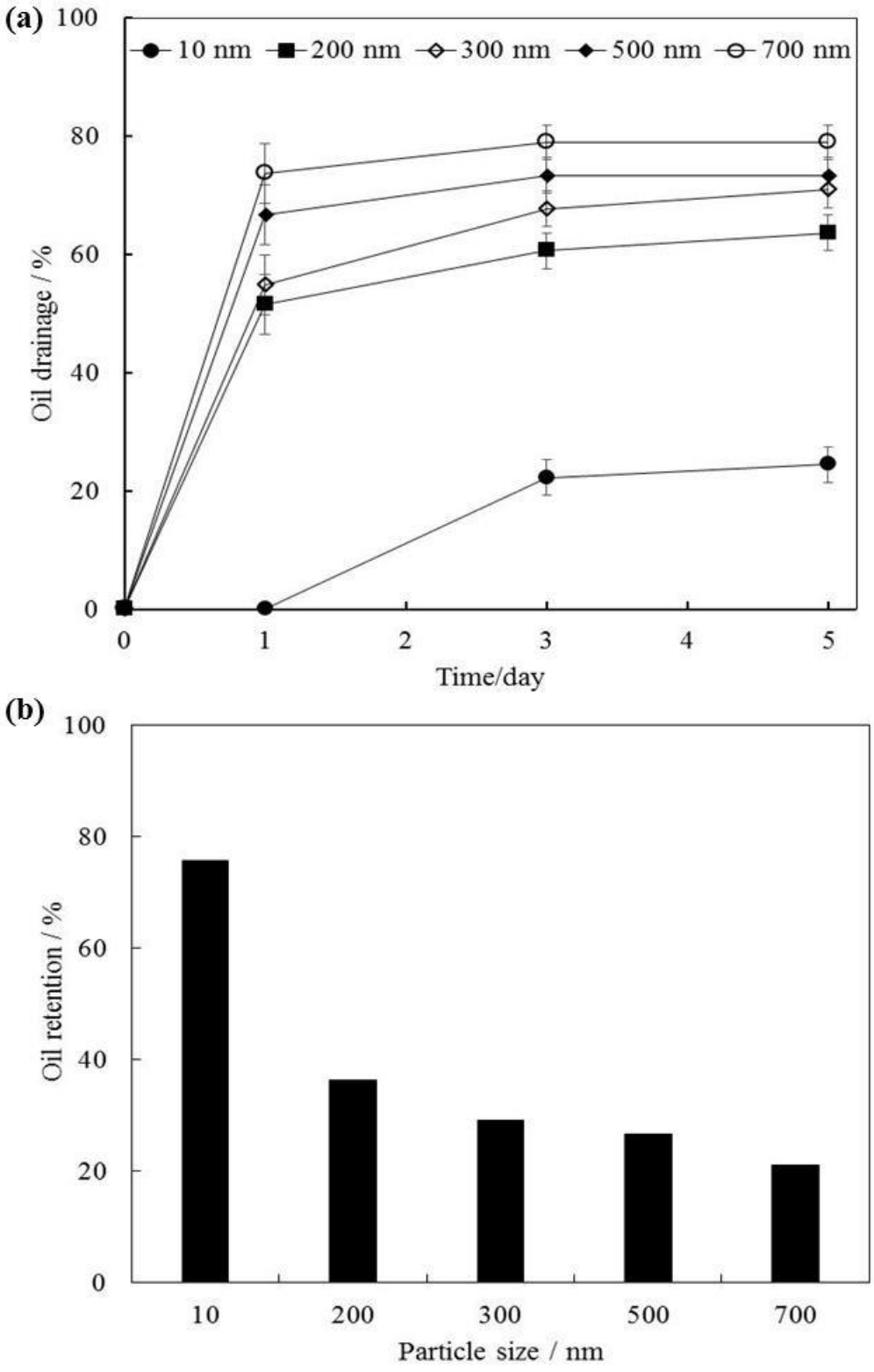

Figure 3.6 Plots showing drainage of impregnated oil (squalane) from porous silica coatings of different particle size versus time, (a). Oil retention in porous coatings after 5 days versus particle size, (b).

Oil drainage is observed to increase with time in all impregnated substrates. The drainage is also proportional to the size of silica particles with maximum and fastest drainage observed on 700 nm coatings and minimum and slowest on 10 nm coatings. The drainage decreases from 700 nm particles serially to 200 nm particles on the first day but with negligible loss of oil from fumed silica coatings (10 nm). However, at the end of the day 3, drainage was observed. Analysis of the process also indicate that fumed silica coatings with smallest particle diameter showed the highest retention of 76% of the total impregnated oil at the end of 5 days while only 21% of the oil was retained in 700 nm monodispersed silica particles (Figure 3.6b).

Surface arrangement of different particles shown by the SEM images in Figure 5 can simply be modelled into three broad categories, namely: loosely-packed particle aggregates, closely packed particles, and multi-layered aggregated particles (Figure 3.7).

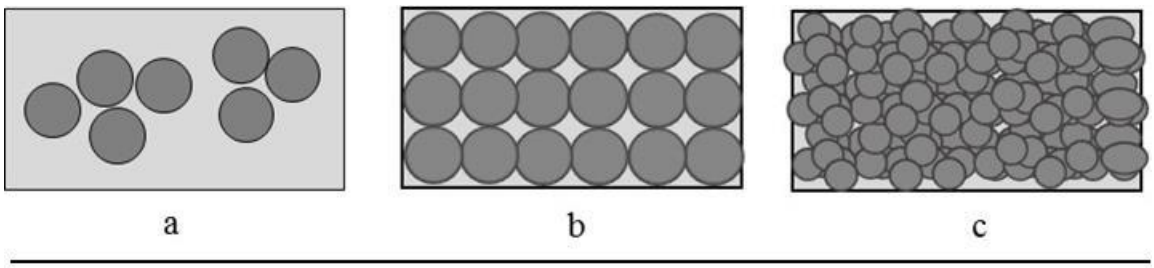

Figure 3.7 Illustration categorising the distributions of silica particles in the coatings, (a) a monolayer of loosely-packed particle aggregates, (b) a monolayer of closely-packed particles, and (c) a multi-layer of aggregated particles.

Using these illustrations, 700 nm silica coatings can fit into category (a) considering its coarser and wider spacing (i.e. large scale structural roughness). This class can easily allow free flow of fluid with less obstruction within the porous network. The same

reason will cause this effect to reduce going through the coatings with intermediate particle diameter in category (b) where particles are closely packed, and drastically reduced in category (c) similar to coatings of fumed silica where particles attain highest compaction compare to others. These results are in line with other findings, which have revealed that an aggregated particle porous material enhances aeration, infiltration and storage of liquid [25]. The retention (or reduced drainage) has also been reported to be mainly linked to liquid bridges between the finer aggregated particles, and that on coarser particulate layers, the drainage is remarkably promoted [26, 27].

The results presented above suggest that fumed silica coating is most suitable for the fabrication of stable superhydydrophobic and slippery surfaces. Further investigation on fumed silica shows that its dispersions are very stable over many weeks. Coatings formed from hydrophobic fumed silica as earlier reported are superhydrophobic and the observed stability of oil within in the coatings makes it a better candidate for fabrication of slippery surfaces – oil impregnated porous substrate. It was also observed that if the coatings are not in a vertical position, the oil can remain for many weeks without being displaced. In subsequent sections of this chapter investigations will be centred on the fabrication of fumed silica coatings, further characterisation of the coatings, oil impregnation and wettability studies.

3.3.3 Porous coatings of hydrophobised fumed silica particles fabricated by the dip-coating and spin-coating methods

The process of depositing layers of micro or nanoparticles on solid surfaces play important roles in determining the surface morphology which in turn controls the wettability and other properties of the material. As earlier described in Section 2.2.5, the

dip-coating process is a simple and cost effective method involving lowering of the substrate to be coated into the dispersion containing particles, followed by the withdrawal of the substrate at a constant speed. As the substrate is being withdrawn, the liquid dispersion adhere onto the solid substrate and coat it. Among other factors, the process is usually controlled by the concentration of the dispersion bath [28-30] and the speed of withdrawing the substrates from the dispersion [31-33].

Spin-coating is another simple method for making coatings with very good results. The process involves deposition of dispersion on the centre of the substrate; the surface is then spun at required speeds to spread and thin the coating materials, which then dries with continued spinning. Similar to dip coating, the morphology and thickness of spin coated materials can be controlled mainly by the concentration of the dispersion and the applied spin coating speed [34-36]. In order to obtain suitable coatings, the controlling factors affecting the two coating methods were investigated and the results are presented below.

3.3.3.1 Effects of silica concentration on dip-coated surfaces

Figure 3.8 (a-c) shows images of fumed silica surfaces prepared by the dip coating process at different concentrations of fumed silica suspension and withdrawn at a constant speed of 5 cm/min. It was found that 1.5 wt.% silica concentration in suspension produced sparingly coated surfaces. Uniform coating was obtained at 3% concentration of silica, whereas at a higher concentration of 5 wt.%, less uniform coatings, with some cracks were observed. From these results, it is clear that the morphology can be manipulated by changing the concentration of the suspension. The poor results at lower concentration of 1.5% can be attributed to insufficient silica particles in the suspension leading to a limited continuous film formation resulting in

some uncoated portions on the surface [37]. High concentration of 5 wt.% delivered too many particles on the surface. As can be observed in the SEM image of the coating.(Figure 3.9) this high loading is known for thicker coatings which are prone to crack due to stresses induced by the drying [37, 38]. This is likely the cause of some cracks on surfaces coated with 5 wt.% silica. At 3 wt.%, the particles are uniformLy deposited due to moderation in the amount of silica in the suspension, and a combination of this concentration of silica suspension with withdrawal at a speed of 5 cm/min certainly falls within optimum condition to achieve critical thickness/morphology of the coating that must not be exceeded to limit crack formations or lower to limit particle discontinuity on morphology [39].

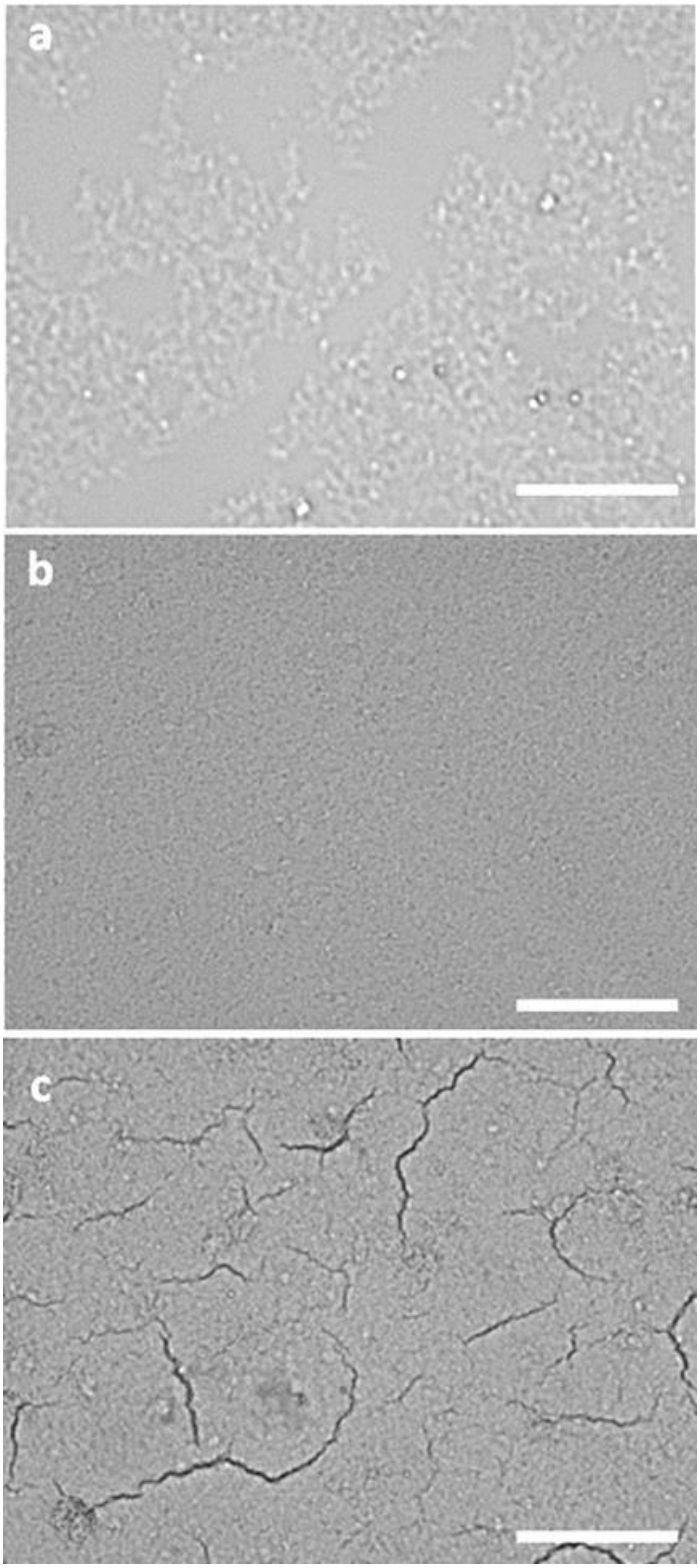

Figure 3.8 Optical images of coatings produced from hydrophobised fumed silica particles dispersed in ethanol at different concentration: a - 1.5%, b - 3% and c - 5% by dip-coating at a constant withdrawal velocity of 5 cm/min. All bars represent 100 μm.

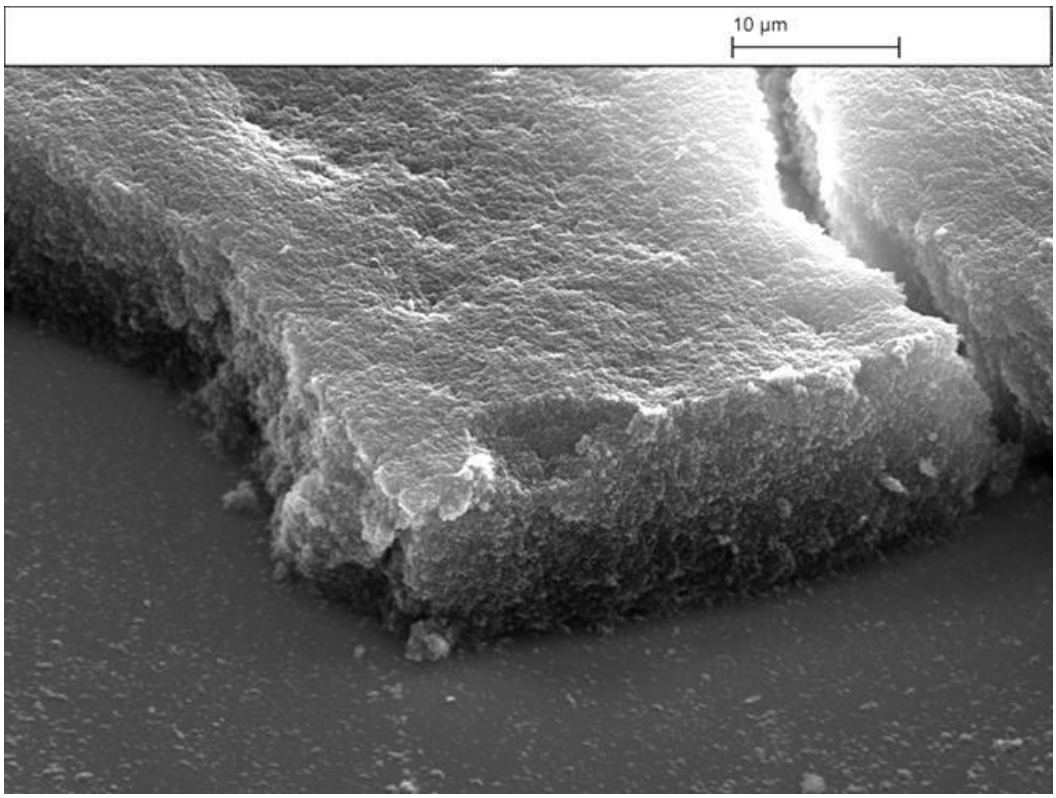

Figure 3.9 SEM images of dip-coated hydrophobic fumed silica coatings on glass slide produced from 5 wt% particle suspension in ethanol at 5 cm/min withdrawal speed. Image tilted to 50°. The thickness of the coating is ~9 -10 µm.

3.3.3.2 Effect of withdrawal speed on dip-coated surfaces

Figure 3.10 shows different surfaces made at different withdrawal velocity at silica concentration of 5 wt.%. It can be observed that although the surface obtained with the lowest withdrawal speed of 1.5 cm/min was less affected, the three different surfaces made at this concentration are cracked. However, further lowering of the withdrawal speed did not produce better results.

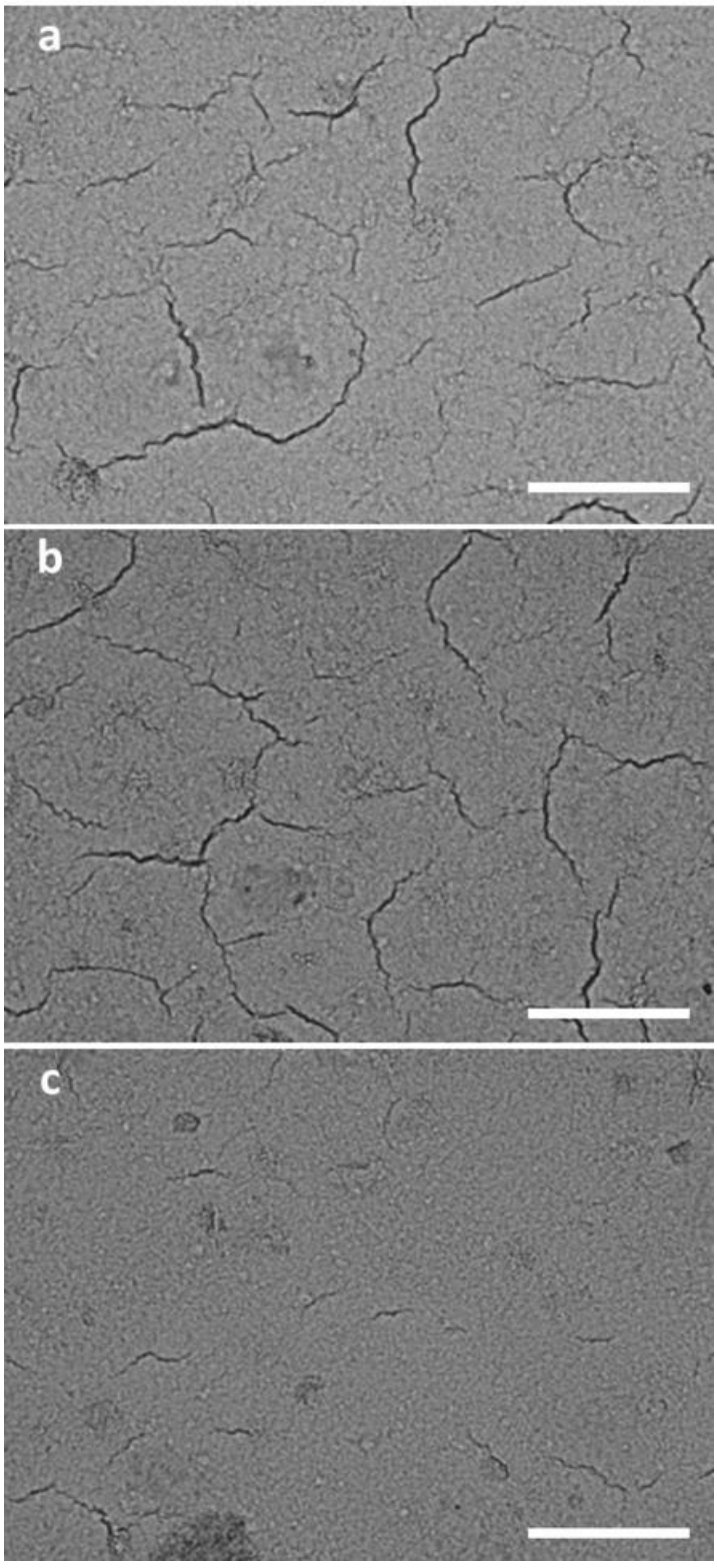

Figure 3.10 Optical microscope images of coatingsproduced from 5% fumed silica suspension by dip-coating at different withdrawal speeds: (a) 5 cm/min (b) 3 cm/min (c) 1.5 cm/min. Scale bars represent 100 μm.

To achieve better results, the concentration of the dispersion was lowered to 4% silica concentration and the substrate withdrawn at the speed of 1-5 cm/min. Images of the coatings are shown in Figure 3.11. The cracks on the coated surfaces tend to reduce with decreasing the withdrawal speed from 5 cm/min to 4 and 3 cm/min where smooth coatings were observed. Further reduction in the speed to 2 cm/min led to discontinuity of the deposited particles on the surface with the presence of uncoated spots. At lower withdrawal speed, there is enough time for the gravitational drainage of the dispersion leading to accumulation of fewer particles to produce thinner and less cracked surfaces recorded at the speed of 3 and 4 cm/min. However, at even lower speeds, the drainage may become so pronounced that some portions of the substrate could be totally drained off as is probably the case for surfaces withdrawn at 2 cm/min.

Interesting result came up at a very low speed of 0.1 cm/min where intermittent break observed in coating produced at a speed of 2 cm/min tend to align parallel to the coated areas to produce a decorative coating shown in Figure 11f. The occurrence is termed ‘coffee ring effect’ and usually arises at very low speed. Because of delays, dispersion which adhered to the substrate become dry due to evaporation of the solvent and gets pinned at the edge. The pinning induces outward capillary flow of the coating solution to replace the fluid. This movement of the solution toward the line create concentrated layers of silica particles and render it thickly coated. At a point the withdrawal movement of the substrate still pulls the substrate upward to break away from the sticking point. This creates a discontinuity, and yet another pinning at a new contact point with a distance equal to the uncoated portion of the substrate [31, 40, 41]. It is therefore worth to note that while lowering the withdrawal speed may be useful to obtain smooth coatings, care should be taken to avoid excessive drainage by gravity or the coffee ring effect caused by excessive evaporation of the dispersion solvent.

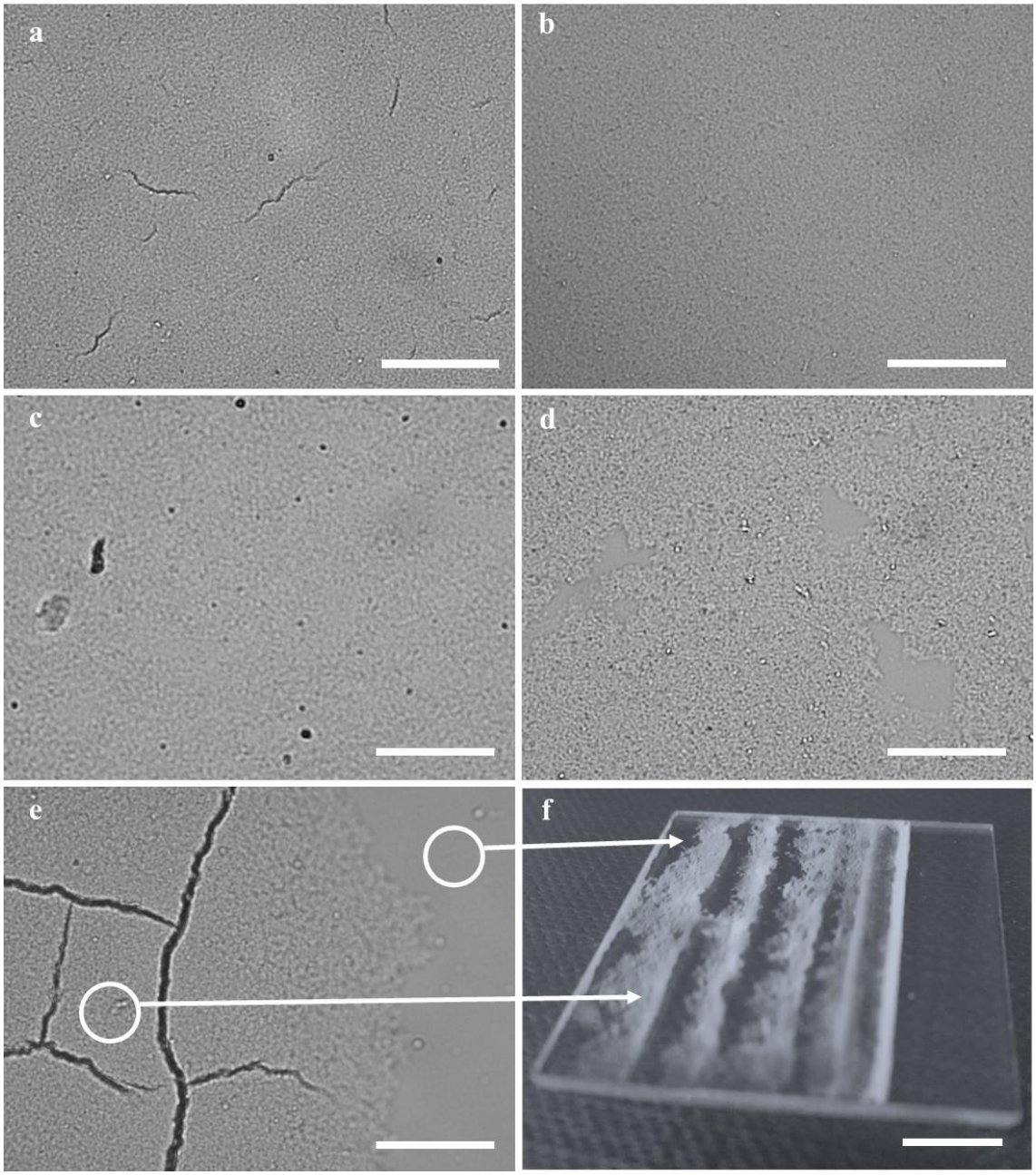

Figure 3.11 Optical microscope images of the fumed silica coated surfaces produced from 4% silica dispersion and withdrawn at different speeds (a) 5 cm/min, (b) 4 cm/min (c) 3 cm/min (d) 2 cm/min, (e) 0.1 cm/min, (f) a low magnification image of (e) revealing the patterned coating formed at a very low withdrawal speed. Scale bars: (a-e) represent 100 μm and (f) represent 5 mm.

3.3.3.3 Effect of particle concentration on spin-coated surfaces

The effect of concentration on the coated slides was somewhat similar to the one reported for dip coated surfaces in the previous section. The concentration of 1.5 wt.% of silica was found to be too low for homogeneous coating at 2500 rpm. Unlike dip-coated slides, 3-5 wt.% silica suspensions are observed to produce uniform coatings. Figure 3.12 shows optical images of fumed silica coatings prepared with different concentration of silica suspension at a constant spin rate of 2500 rpm.

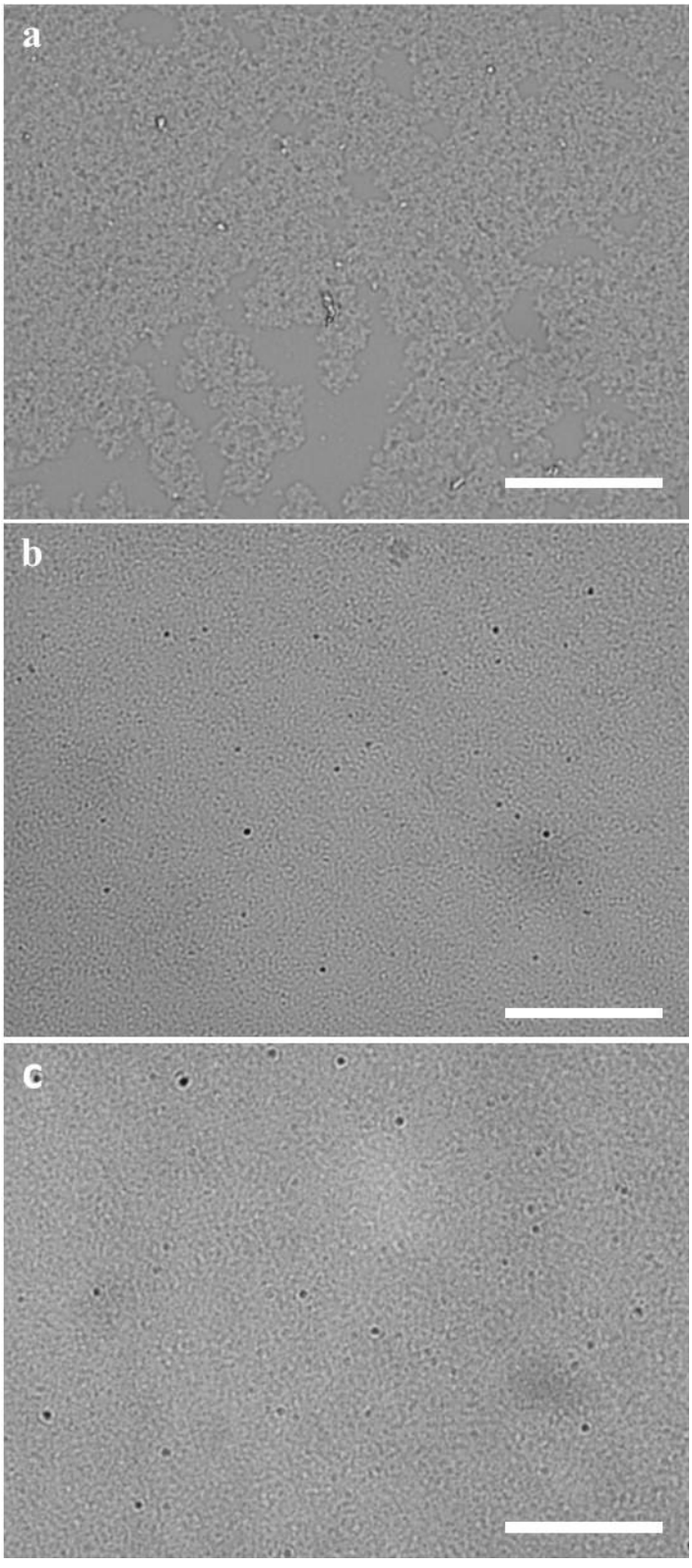

Figure 3.12 Optical images of fumed silica coatings prepared by spin-coating at a constant spin rate of 2500 rpm using silica suspensions with different concentrations : (a) 1.5 wt.%, (b) 3 wt.% and (c) 5 wt.%. All scale bars represent 100 μm.

3.3.3.4 Effect of spin rate on spin-coated silica surfaces

The rotational speed at which the sample is spun on a spin coater (called spin rate, measured in revolution per minute, rpm) was varied at fixed particle concentration of the suspension. The effect of the spin rate on the coating morphology and thickness of the coated samples at 5 wt.% silica suspension in ethanol is shown in Figure 3.13. Uniformity of the coatings gradually sets in from the lowest spin rate of 500 rpm, where cracks are prevalent to 2000 rpm, and continues up to coatings produced at 8000 rpm without noticeable cracks. From lower to higher spin rates, the coating becomes smoother, thinner and visually more transparent. As can be observed from the images, thickness of the coating decreases with increasing the spin rate. The cracks observed in the thicker coatings are typical for drying particular layers due to associated mechanical stresses. The thickness of the coatings measured from SEM images is plotted against the spin rate in Figure 3.14. Increasing the rate of spinning initially leads to sharp decrease in the thickness of the coating. The effect later levels off at higher spin rate.

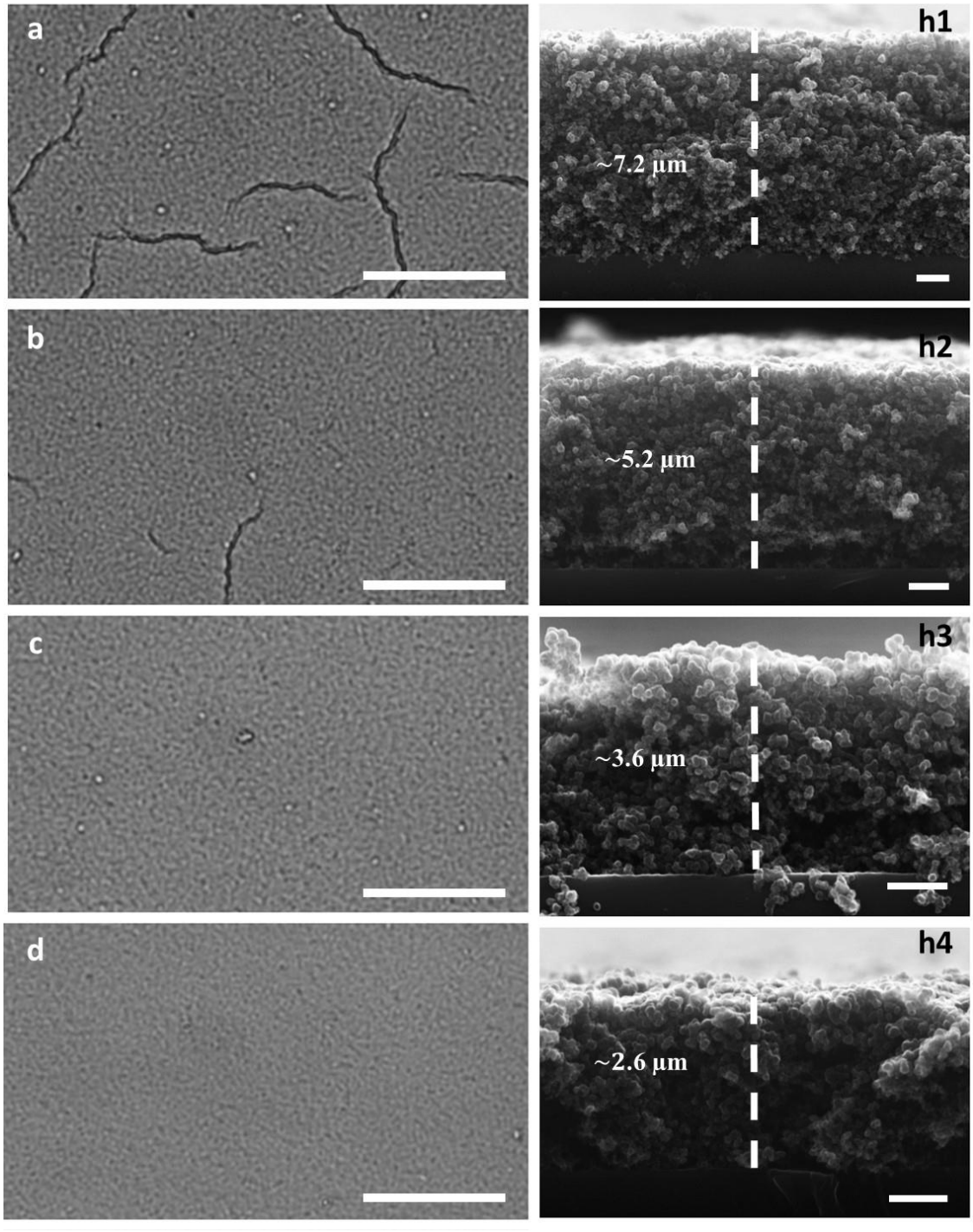

Figure 3.13 Optical microscopy images (left) of the spin-coated hydrophobic fumed silica coatings on glass slides produced from 5 wt.% particle dispersion in ethanol at different spin rates: (a) 500 rpm, (b) 1000 rpm, (c) 2000 rpm, (d) 8000 rpm. The thickness of the coatings (dashed lines) at the respective spin rates are shown by the dashed lines drawn on the side view SEM images. Scale bars are: (a-d) represent 100 µm, (h1- h4) represent 1 µm.

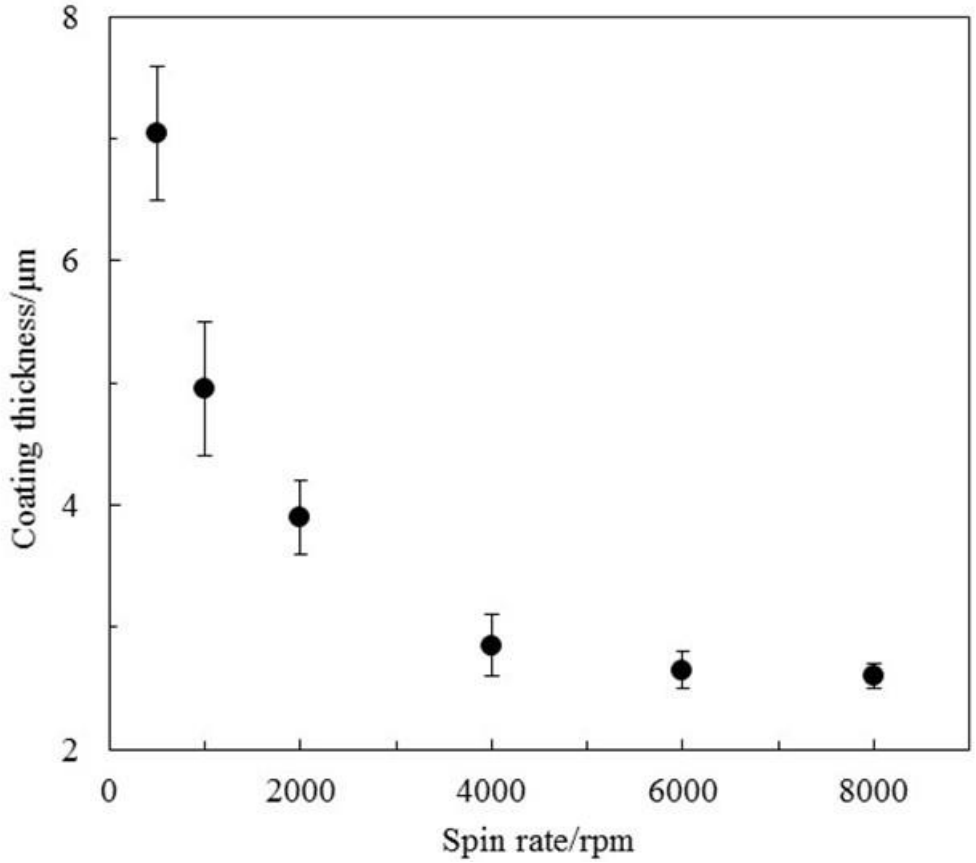

Figure 3.14 Thickness of the fumed silica coatings produced from 5 wt.% silica suspension in ethanol versus the spin rate of the spin coater.

3.3.4 **Wettability of dip-coated and spin-coated surfaces**

Contact angles measurements of water drops in air on dip coated and spin coated surfaces showed that the fully coated surfaces were superhydrophobic. The poorly coated slides produced by spin-coating at low concentration of the silica suspension (1.5%) and the dip-coated surfaces with stripe structure gave varying contact angle ranging from hydrophobic to superhydrophobic, depending on where the drops settle on the surfaces (coated or bare slide). Wetting properties of the uniform coatings are discussed in details in subsequent sections.

3.3.5 **Morphology of fumed silica coatings made by spin-coating**

Scanning electron microscope (SEM) image of a fumed silica coated film is shown in Figure 3.15. Visually, the fumed silica coatings are transparent and smooth but under the SEM most hidden structure of the coatings not visible under optical microscope are revealed. As can be seen, the coatings are porous with hierarchical random roughness at the nanometre and micrometre scales created by aggregates and the primary particles due to the polydispersity and structure of the fumed silica used (section 2.1.5.7). The primary fumed silica particles (~ 10 nm) do not exist in isolation but are fused together to form open branched particle (~ 100 nm). Although the ultrasonification was used to breakdown most of these aggregates, their total destruction was not attainable [42-44].

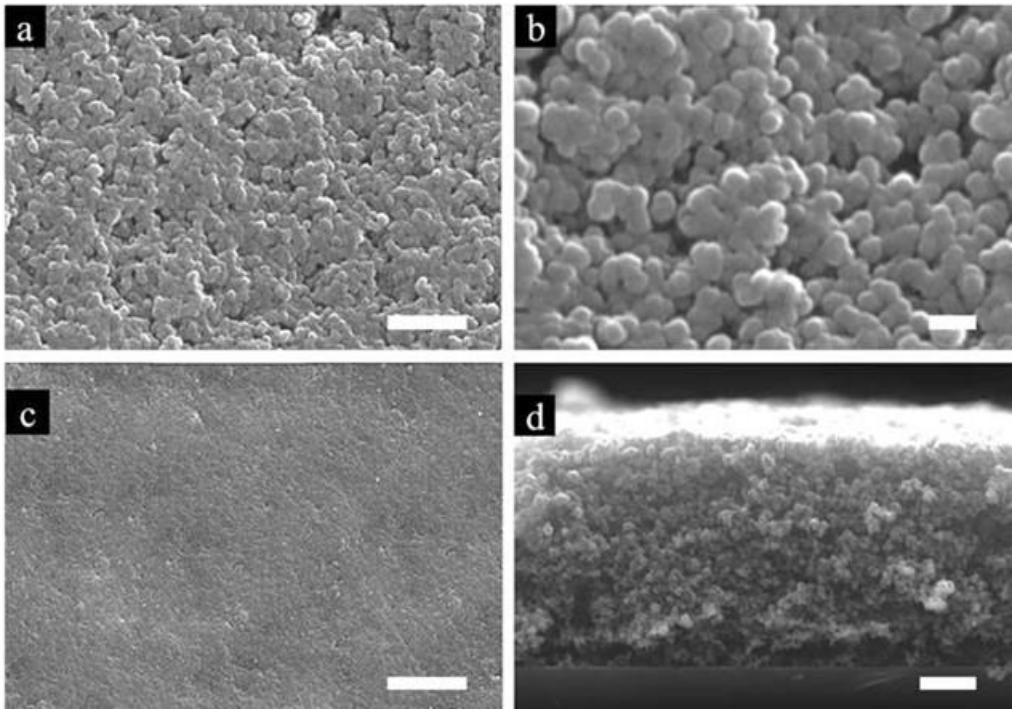

Figure 3.15 SEM images of spin-coated silica film prepared using 5 wt.% hydrophobic fumed silica particles in ethanol. Images are taken at different magnifications and tilted angles of 10° (a-c), and 90° (d). Porosity and thickness of the coating are 86 ± 2% and 3.7 ± 0.6 µm, respectively. Scale bars are represent 1 µm (a, d), 200 nm (b) and 10 µm (c).

3.3.6 **Partial impregnation of fumed silica coated surfaces with squalane**

Conventional method of fabricating a slippery surface, or the so called SLIPS involves immediate infiltration and flooding of porous substrate with oil to create an over-coated layer of oil film [24, 45, 46]. In partial impregnation introduced here, the porous substrates are not fully filled with oil, but the oil is partially or gradually impregnated onto the porous substrate to the required level. In this work the partial impregnation was carried on gradually until the substrate were over-coated with oil layer in a similar way as the conventional slippery surfaces. The actual impregnations were carried out as described in experimental sections (2.2.7). During the impregnation process, the solution of squalane (in hexane) initially flooded the porous substrate but on evaporation of hexane, only squalane was left on the substrate. Different concentrations of squalane solutions were used for the impregnations to achieved different amount of squalane left behind.

Upon impregnation of the dry coating with oil, the coatings gradually undergo changes. The roughness on the impregnated films was observed to gradually decrease with increasing the concentration of squalane solution used (Figure 3.16). The observed progressive smoothness of the substrates is believed to be due to the increasing amount of oil which infiltrates the pores and bridges the particle gaps on the surface.

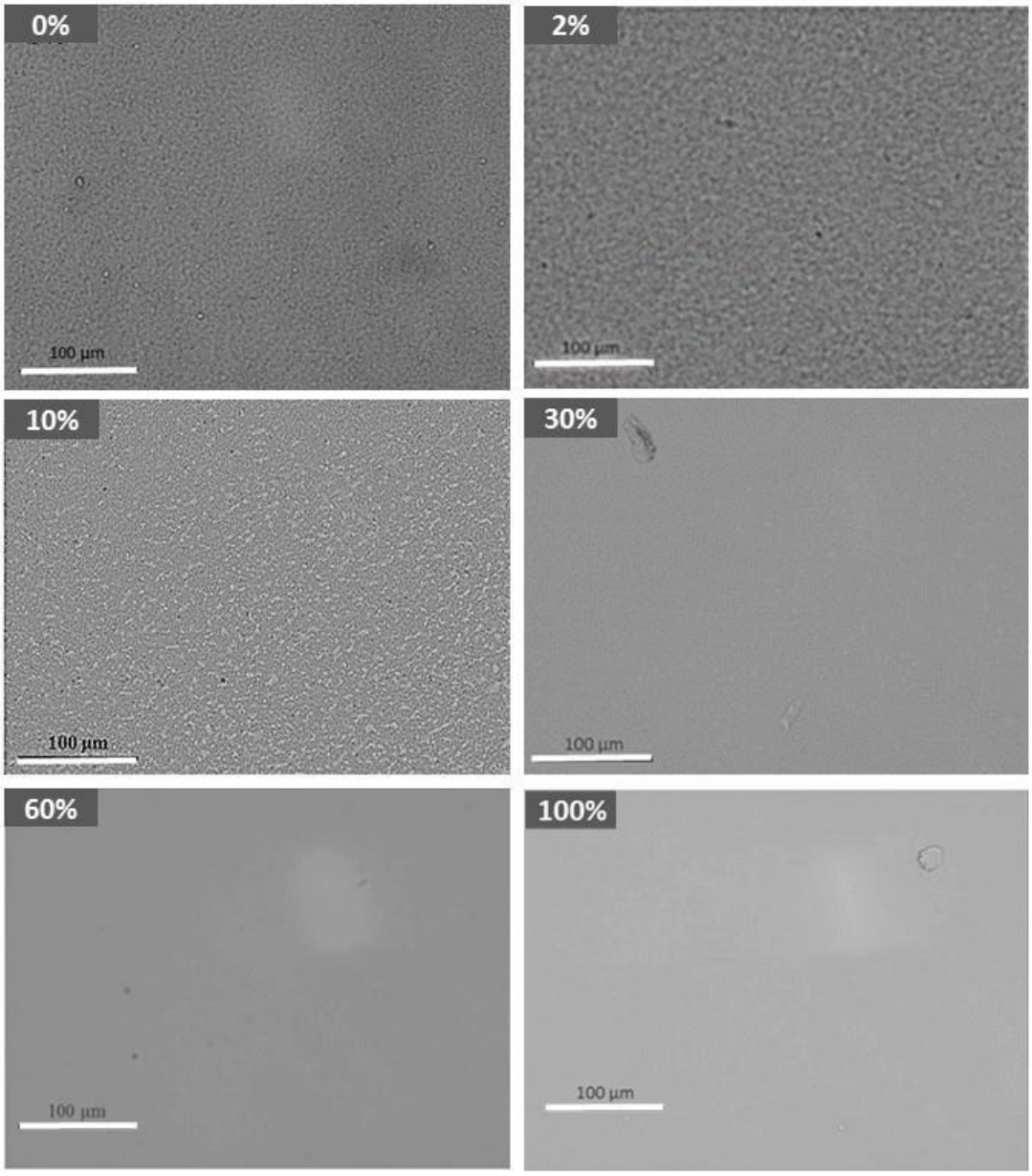

Figure 3.16 Optical microscopy images of fumed silica coatings made on microscope slide using spin coater and impregnated with different concentrations of squalane solutions. Each coating is labelled with the concentration of squalane solution used for its impregnation. 0% coating is a dry coating impregnated with only pure hexane without squalane. The smoothness of the coated surfaces increases with the increasing amount of the impregnated oil, Scale bars represent 100 µm.

3.3.7 Fluorescent microscopy of porous coatings impregnated by squalane doped with Nile red fluorophore

Nile red has been used as a probe for the investigation and detection of hydrocarbon [47], lipids and hydrophobic proteins [48]. Here, we use Nile red as a dopant in squalane and fluorescence microscopy aiming to quantify the amount of squalane on the impregnated porous coatings and visualise its distributions on the surfaces.

Upon impregnation of different coated surfaces with Nile red doped oil, various degrees of fluorescence intensities have been observed under microscope and recorded. Figures 3.17 and 3.18 show the bright field and fluorescent images of different surfaces impregnated at various percentages of squalane solution. Fluorescent images show gradual departure from black coloration of the surface impregnated with 0% (no fluorescence) to reddish-black on surfaces impregnated 2% of squalane and from this surface the reddishness of the surface increases through surfaces impregnated with more concentrated squalane solutions to intense red coloration on surfaces fully impregnated with squalane (100%). Because the red coloration depicts the presence of squalane, this is an indication that the process of gradual impregnation of the porous silica coatings with squalane has been successfully achieved. The oil seems to be spread evenly over the solid surface on visual examinations of the fluorescence results.

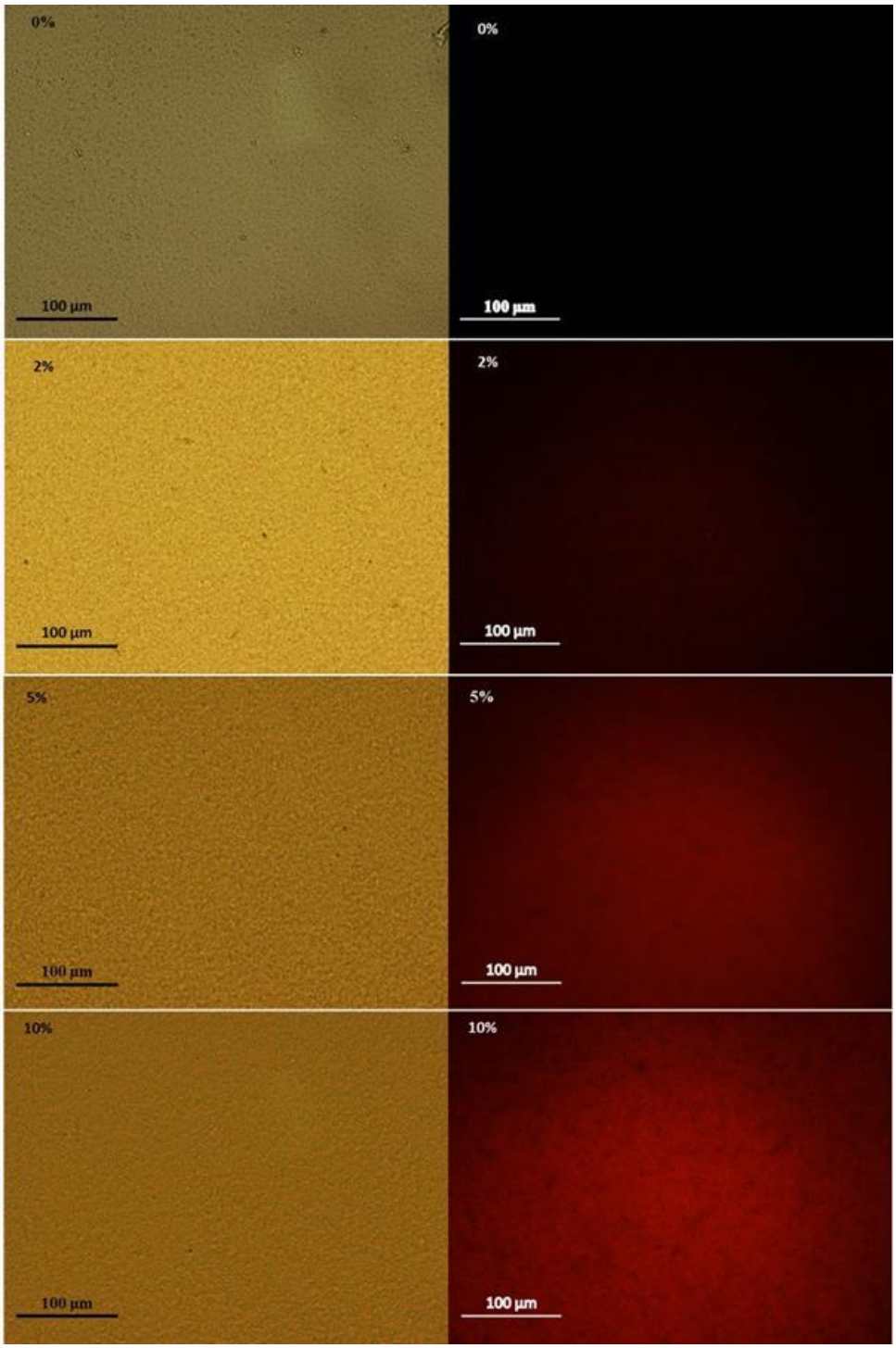

Figure 3.17 Bright field (left column) and fluorescent (right column) images of silica coated slides impregnated with 0 – 10 vol.% squalane (shown) doped with proportional amount of Nile red. 0% represents a coating impregnated using only hexane without squalane or Nile red present. The red colourations reveal the degree of squalane on the surfaces.

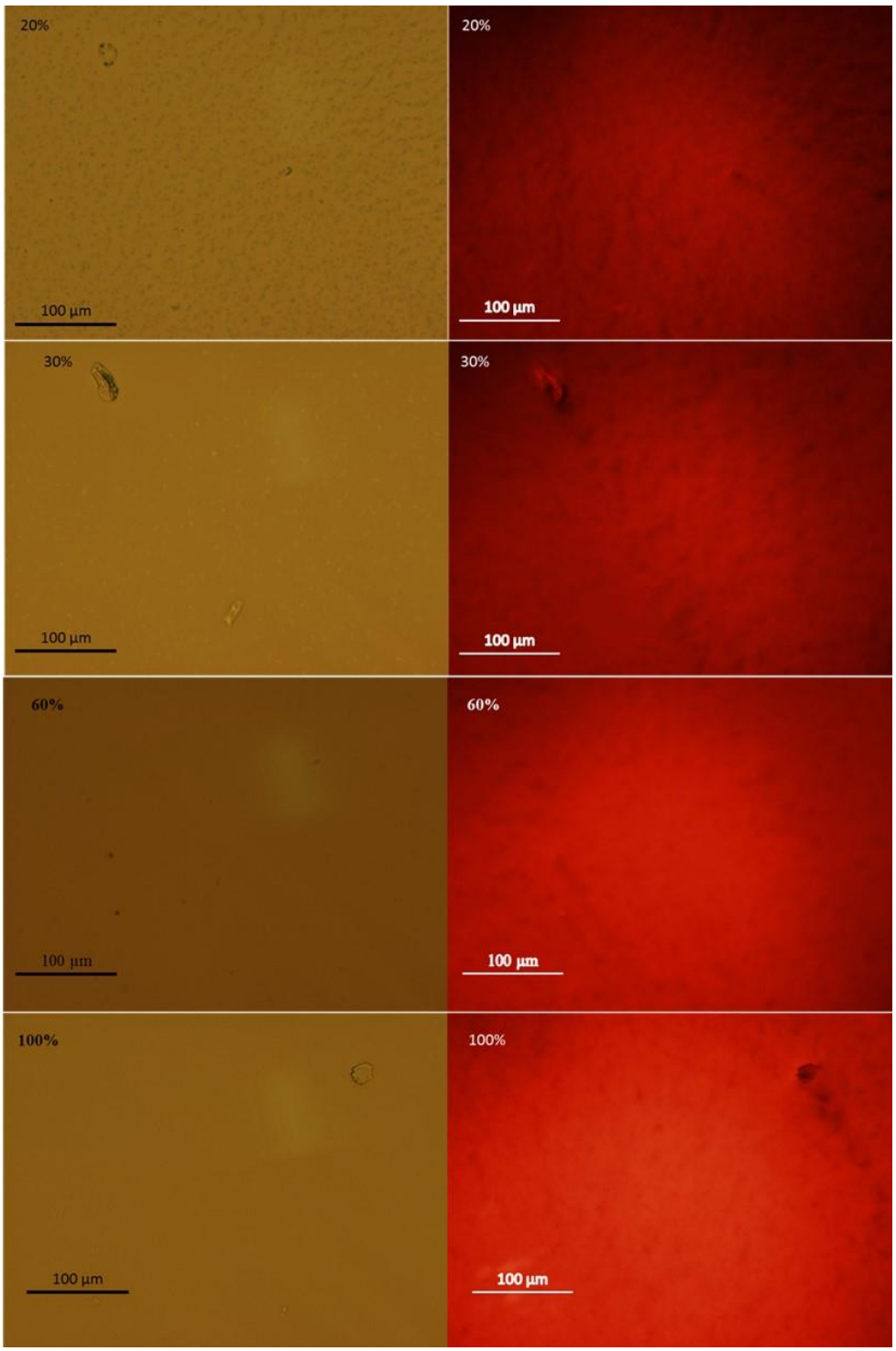

Figure 3.18 Bright field (left column) and fluorescent (right column) images of silica coated slides impregnated with 20 – 100 vol.% squalane (shown) doped with proportional amount of Nile red.

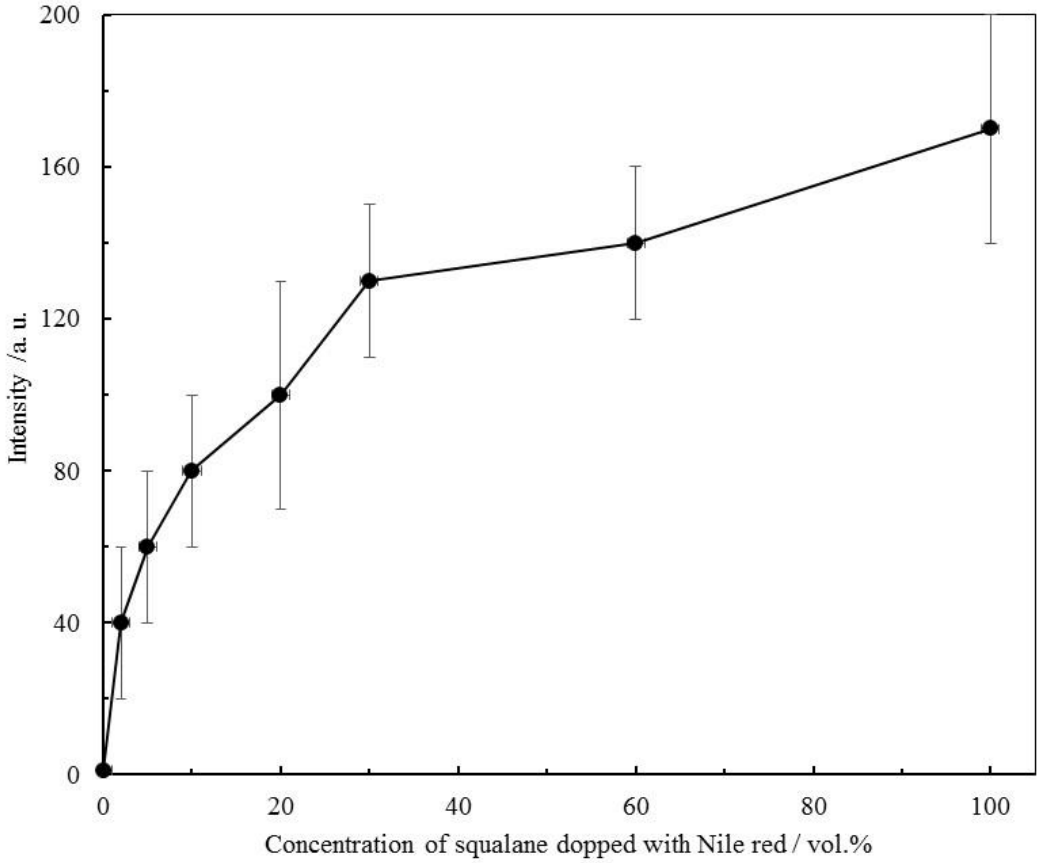

Figure 3.19 Fluorescent intensity of impregnated silica coated-surfaces at different concentrations of squalane doped with Nile-red. The solutions have been made by mixing neat hexane with different amounts of squalane doped with Nile red at concentration 1×10^{-8} mol/mL. The plot shows increasing intensities (vis-à-vis oil concentration of squalane) with progression of impregnation.

The fluorescence intensities emitted from the coatings impregnated using different concentrations of squalane are shown in Figure 3.19. The intensity rapidly increases with the squalane concentration in the impregnating solution up to 30 vol.% and continues gradually to build up further up to 100 vol.% (i.e. pure squalane). In order to extract quantitative information for the amount of squalane deposited on the coating after the solvent (hexane) evaporation, we consider the dependence of the fluorescent intensity on the concentration of fluorophore (Nile red). At low concentrations of

fluorophore, the fluorescence intensity, *I*, is proportional to the fluorophore molar concentration, *c*, as shown in Eq. (3.1) [49].

$$I = klc \tag{3.1}$$

where *k* is a constant proportional to the excitation light intensity and takes into account the quantum yield, and *l* is the thickness of the solution layer. Assuming that the fluorophore is uniformLy distributed in a layer with thickness *l* and area *A*, the fluorophore concentration is given by

$$c = \frac{n}{Al} \tag{3.2}$$

where *n* is the total amount of fluorophore in moles. Combining eqs (1) and (2), we obtain

$$I = k\frac{n}{A} \tag{3.3}$$

Hence, the fluorescence intensity is proportional to the total amount of fluorophore over area *A*. In the considered case, the fluorophore comes from the volume of deposited squalane, V_{sq}, with Nile red concentration c_{NR}. Hence

$$\frac{n}{A} = \frac{V_{sq}}{A} c_{NR} \tag{3.4}$$

Using Eqs (3.3) and (3.4), we obtain

$$\mathcal{v}_{sq} = k_1 I \tag{3.5}$$

where $\mathcal{v}_{sq} = V_{sq}/A$ is the volume of squalane deposited on unit area and $k_1 = 1/kc_{NR}$ is a new constant. Equation 3.5 can be used to calculate the volume of squalane

deposited per unit area of the coating from the measured fluorescence intensity if k_1 is known. To determine k_1, we have measured the mass of squalane on the fumed silica coating deposited by spin-coating of neat squalane (100%) doped with Nile red at concentration 1×10^{-8} mol/mL has been measured. The mass of deposited squalane was found to be 780 ± 80 μg/cm^2. Then, Eq. (3.5) was used to calculate k_1, knowing the squalane density (0.81 g/mL) and the fluorescence intensity (170 ± 30 a.u.). It was found that k_1 = 0.0056 ± 0.0011 μL/(cm^2 a.u.). This value of k_1 was used to calculate the volume of deposited squalane per unit area from the measured fluorescence intensity using Eq. (3.5). Results are shown in Figure 3.20 and Table 3.6.

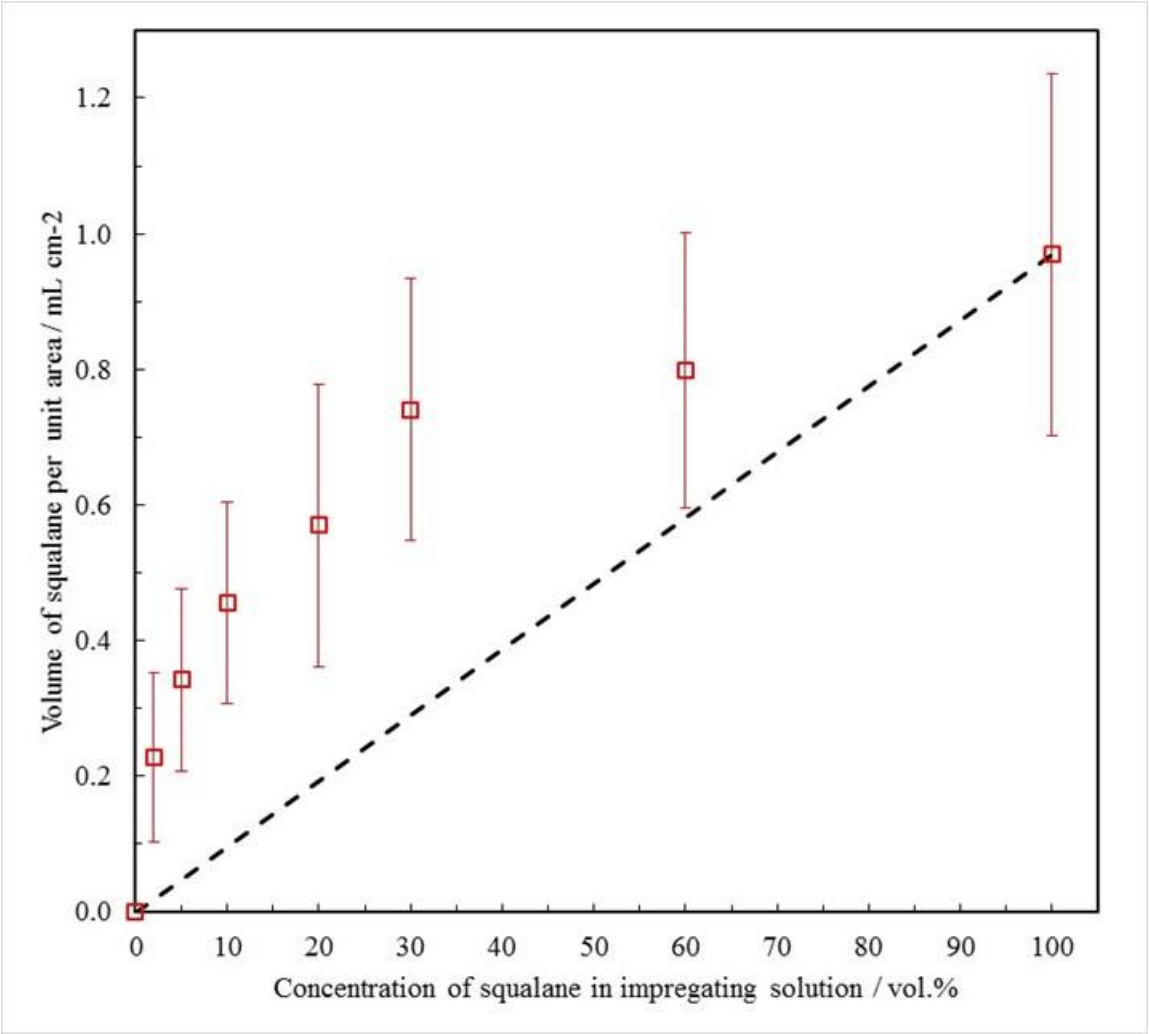

Figure 3.20 Volume of squalane deposited per unit area of the coating versus squalane concentration in impregnating hexane solution. Symbols correspond to values calculated by Eq. (5) with k_1 = 0.0056 ± 0.0011 μL/(cm^2 a.u.) (squares). The dashed line shows the linear dependence of deposited squalane volume expected if the impregnated solution with volume 0.969 μL/cm^2 has been deposited and the hexane (the solvent) evaporated.

Table 3.3 Volume and mass of squalane deposited on unit area of coating calculated from fluorescence intensities (Table 6) and eq. (5) with k_1 = 0.0056 ± 0.0011 μL/(cm^2 a.u.) and a squalane density of 0.81 g/mL.

Squalane in impregnating solution (vol.%)	Squalane volume deposited (μL cm^{-2})	Squalane mass deposited (μg cm^{-2})
0	0	0
2	0.228 ± 0.124	185 ± 100
5	0.342 ± 0.135	277 ± 109
10	0.456 ± 0.149	369 ± 121
20	0.570 ± 0.209	462 ± 169
30	0.741 ± 0.193	600 ± 156
60	0.798 ± 0.203	646 ± 164
100	0.969 ± 0.266	785 ± 215

The dashed line in Figure 3.20 corresponds to a hypothetical process in which squalane solutions with volume 0.969 μL/cm^2 (equal to that of 100 vol.% squalane) have been deposited on unit area of the coating, then the solvent (hexane) has been evaporated, therefore the volume of squalane left is linearly proportional to its concentration in the impregnating solution. One can see that the squalane deposited in the real process of spin-coating (squares) is larger than expected and positive deviations are observed for all squalane concentrations (except at 0 and 100 vol.%). These deviations could be explained taking into account that (i) the volume of squalane solution placed on the coating before the start of the spin-coating process (100 μL) is in excess to that left (deposited) at the end of the process and (ii) the solvent evaporation occurs throughout the whole spin-coating process (40 s). As a result, the concentration of squalane (and the amount of Nile red) increases during spin-coating, thus exceeding the original

concentration in the impregnating solution (shown on the x-axis of Figure 3.19 and 3.20) and giving porous coatings loaded with more squalane than anticipated. Nevertheless, these results show that the amount of squalane deposited on the coatings can be progressively varied from 0 to ~1 μL/cm^2 and in addition to dry or fully impregnated with squalane porous coatings, a broad range of partially impregnated coatings could be achieved.

3.3.8 Mass of squalane deposited on coatings determined by gravimetry

To understand the role of over-coated layer of oil on slippery surface, further characterisation of the impregnated coatings to determination of the actual mass of squalane inside the pores of the substrate and the mass of the over-coated layer of squalane was investigated. The masses were measured gravimetrically as described in section 2.2.13.2 and the results are presented in Figure 3.21 and Table 3.6. The total mass of deposited squalane calculated from the fluorescence intensity (see Section 3.3.7) is also plotted in Figure 3.21 (squares) for comparison. The mass of squalane inside the pores of the coatings was also determined gravimetrically and shown in Figure 3.21 (circles). It is seen that results for the total mass of squalane deposited on 1 cm^2 determined gravimetrically (triangles) are in very good agreement with those obtained by fluorescence experiments. The gravimetrical data have smaller uncertainty and are used in our analysis presented below.

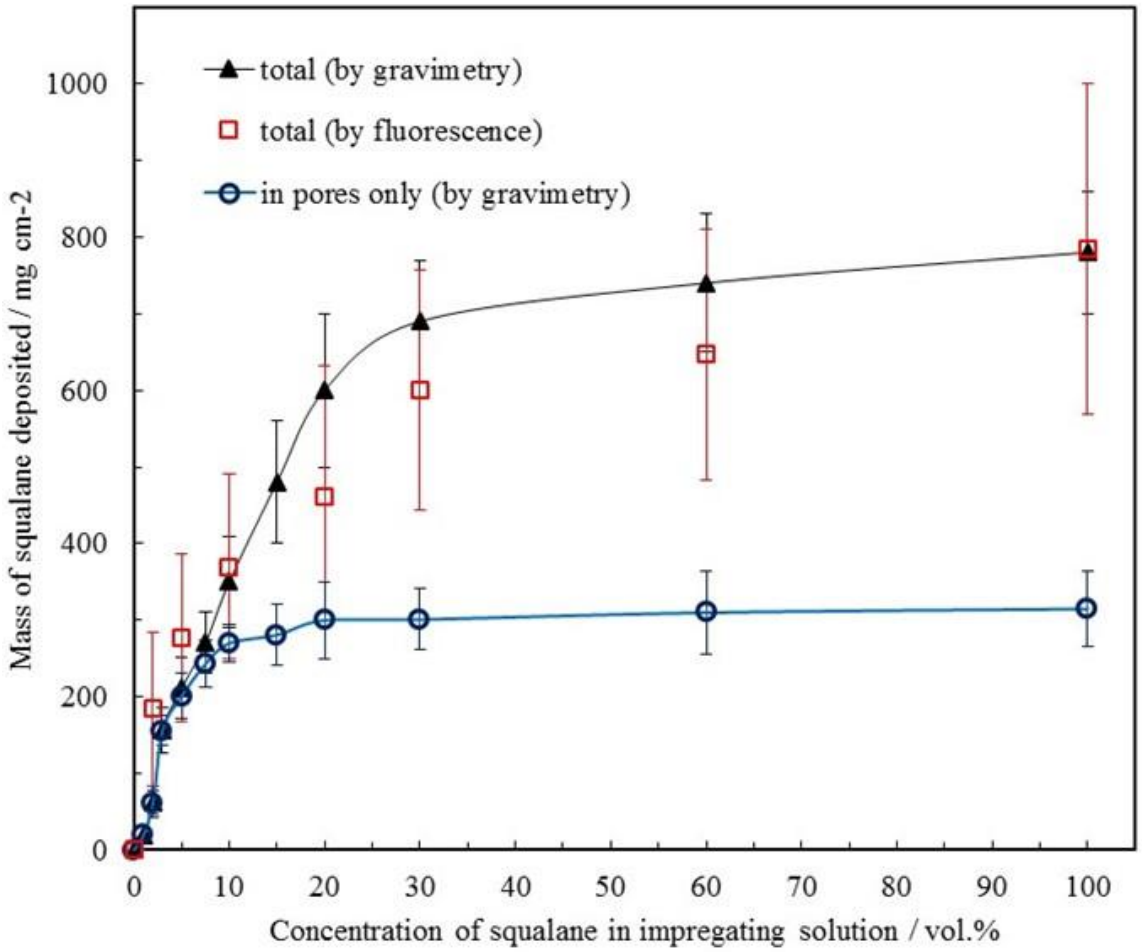

Figure 3.21 Masses of total squalane (triangles and squares) and that in the pores (circles) deposited per 1 cm^2 of the coatings determined by gravimetry (triangles and circles) or fluorescence (squares, see section 3.3.7) after evaporation of the hexane from the impregnating solution versus concentration of squalane in the impregnating solutions.

Using the plots, at the initial stages of the impregnations (0-5 vol.%), it can be observed that the difference between the amount of the total impregnated oil and the amount of oil inside the pores of coatings (both per unit area) within this concentration range is negligible (Figure. 3.21), thus indicating that the pores of the coating are not completely filled with squalane. Beyond this point, the amount of oil inside the pores increases

slowly and levels off when the concentration of squalane in the impregnating solution has exceeded 20 vol.%. The total mass of deposited squalane per unit area, however, increases to bigger values and is significantly larger than that in the pores for concentrations higher than 15 vol.%. This suggests that an over-layer of squalane is present on the top of the oil flooded coating. The average thickness of the over-layer, h_{OL}, has been calculated from the excess oil volume per unit area, V_{excess}

$$V_{excess} = \frac{m_{total} - m_{pore}}{\rho_{sq}} \qquad 3.6$$

where m_{total}, m_{pores} and ρ_{sq} are the total mass, the mass inside pores (both per unit area) and the density of squalane, respectively). The values of h_{OL} are summarised in Table 3.6 and plotted against squalane concentration in the impregnating solution in Figure 3.22. The data show that the layer of excess squalane on the top of the porous coating impregnated with neat squalane (100 vol.%) has a thickness of ~ 6 μm. At lower squalane concentrations down to 30 vol.%, h_{OL} decreases slightly, but is still in the range ~5-6 μm. This is followed by a rapid decrease from ~5 μm to a virtually zero thickness (within the experimental error) at squalane concentrations of 7.5 vol.% or less. These results support our previous conclusion that the adopted procedure of impregnation gives porous coatings loaded with oil in a broad range spanning from coatings with empty (0 vol.% solution) or partially filled with squalane pores (1 – 5 vol.% solutions) to coatings having fully filled by squalane pores and a well-developed over-layer of excess squalane with thickness ~2-6 μm on the top (15 – 100 vol.%). The coatings obtained by impregnation with 7.5 and 10 vol.% squalane solutions fit in between those with partially filled pores and the flooded with squalane coatings. It seems reasonable to assume that the pores in those coatings are completely filled with squalane but the over-layer, if present, has a small or negligible thickness.

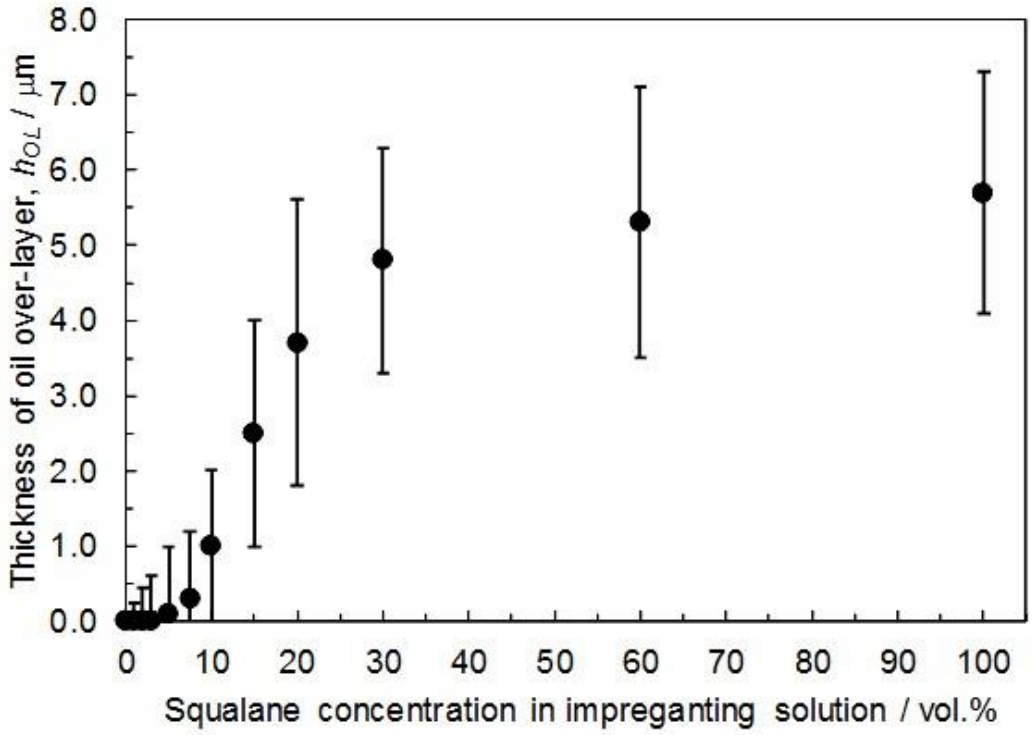

Figure 3.22 Average thickness of squalane over-layer, h_{OL}, versus squalane concentration in impregnating solution (see also Table 3.6).

Table 3.4 Mass of Analysed masses of impregnated squalane on different fabricated coatings showing the proportionate of masses of squalane within the coatings and the thin over-coated layer of oil.

Squalane in impregnating solution (vol.%)	m_{total} (μg cm^{-2})	m_{pores} (μg cm^{-2})	V_{excess} (μL cm^{-2})	h_{OL} (μm)
0	0	0	0	0
1	20 ± 10	20 ± 10	0.00 ± 0.02	0.0 ± 0.2
2	63 ± 20	62 ± 15	0.00 ± 0.04	0.0 ± 0.4
3	157 ± 30	156 ± 20	0.00 ± 0.06	0.0 ± 0.6
5	211 ± 40	201 ± 30	0.01 ± 0.09	0.1 ± 0.9
7.5	270 ± 40	243 ± 30	0.03 ± 0.09	0.3 ± 0.9
10	350 ± 60	270 ± 25	0.10 ± 0.10	1.0 ± 1.0
15	480 ± 80	281 ± 40	0.25 ± 0.15	2.5 ± 1.5
20	600 ± 100	300 ± 50	0.37 ± 0.19	3.7 ± 1.9
30	690 ± 80	301 ± 40	0.48 ± 0.15	4.8 ± 1.5
60	740 ± 90	310 ± 55	0.53 ± 0.18	5.3 ± 1.8
100	780 ± 80	315 ± 50	0.57 ± 0.16	5.7 ± 1.6

3.3.9 **Wettability of partially impregnated surfaces**

Wettability of the fabricated surfaces was evaluated by measuring the contact angles and sliding angles of static water drops on the surfaces in air. The dry fumed silica coatings (0% squalane) showed remarkable water repellence. Water drops have easily rolled away from those coatings without tilting of the surface, a clear indication of its superhydrophobic nature (Figure 3.23a: i-iii). As a result, the contact angle measurements were problematic. Occasionally, some water droplets remained still on the superhydrophobic coating, perhaps stabilised by tiny local defects or cracks and their contact angle was found to be 160 ± 5º. This value should be considered as a lower estimate for the contact angle of water drops on these surfaces in air. Impregnations of squalane onto the coatings have resulted in gradual decrease in the contact angles of the drops, depending on the concentration of the oil (Figure 3.23b, c and d).

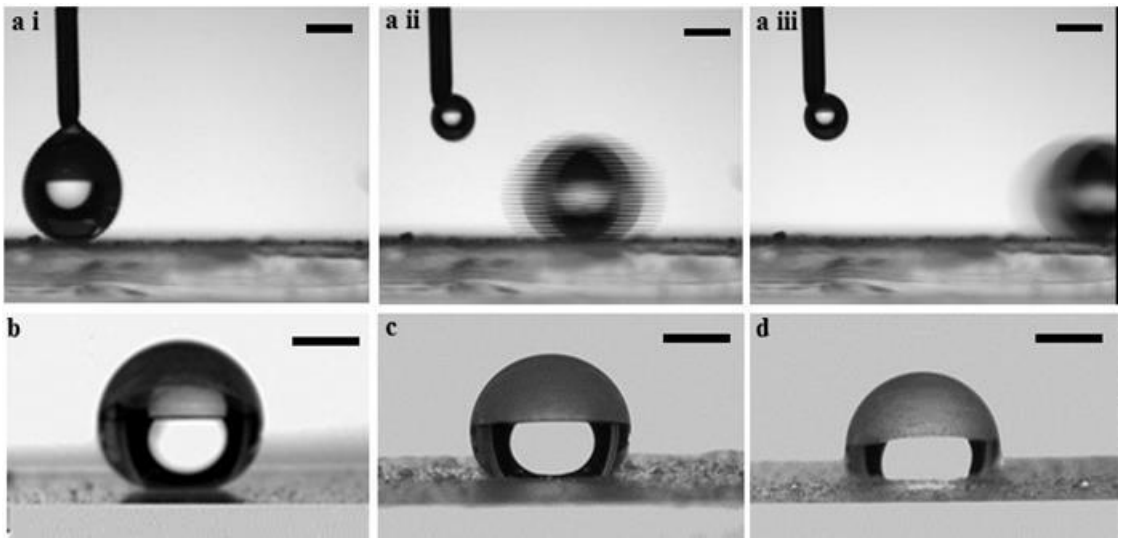

Figure 3.23 Behaviours and configurations of water drops in air placed on hydrophobic fumed silica coatings (spin-coated, see 2.2.5) impregnated at with different concentrations squalane solutions in hexane. TOP (a: i-iii) are consecutive still images from a movie showing rolling water drop (in air) on dry coating (i.e. impregnated with only hexane). BOTTOM (b, c, d) are representative configurations of water drops on coatings impregnated with 2, 10 and 30 vol.% solutions of squalane in hexane. All bars represent 1 mm.

Advancing and receding contact angles, and the contact angle hysteresis measured on coated slides impregnated with different concentrations of squalane are shown Figure 3.24. Fumed silica-coated surfaces impregnated with less amount of squalane (e.g. 2%) show a decrease in contact angles of water drops but still exhibit superhydrophobic behaviour. Progressive increase of the concentration of squalane in the impregnating solutions from 0 to about 30 vol.% results in corresponding decrease in contact angles of water drops from ~160^{o} (0%) to ~105^{o} (30%). Further increase of the squalane concentration does not affect the contact angle which levels off at ~ 105^{o}. Unlike the advancing and receding contact angles, the contact angle hysteresis (CAH) shows non-monotonic behaviour with the increase of squalane concentration. Initially, it increases

from zero, on the dry superhydrophobic surface, to a maximum value of ~14° on surfaces impregnated with 10% of squalane solution. Then the CAH decreases to starting point of the plateau observed on surfaces impregnated with 30% of squalane solution. From 30% constant low hysteresis was observed up to 100% impregnation.

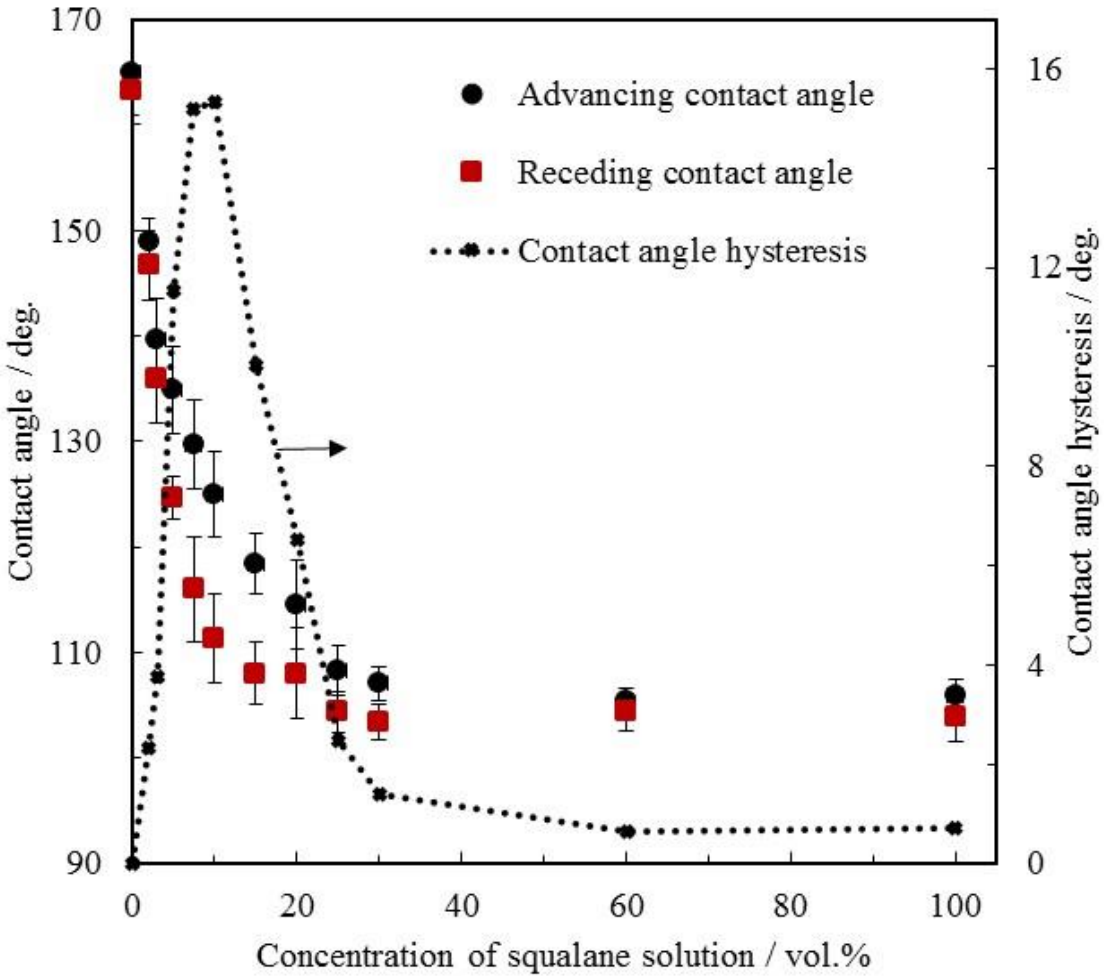

Figure 3.24 Advancing and receding contact angles of 15 µL water drops in air (left axis), and contact angle hysteresis (right axis) on porous fumed silica coatings partially impregnated with different amount of squalane versus concentration of squalane in hexane solution used for impregnation.

Apart from contact angle measurements, sliding angles of water drops on the prepared coating were investigated to understand the extent of water adhesion on the coated surfaces. From the sliding angles, sliding forces, Fd of water drops were derived (Chapter 2.2.17). As can be seen in Figure 3.25, sliding force strictly follows contact angle hysteresis, and increase initially with concentration of the impregnated oil on the surfaces, from 0% to 10%. Surfaces impregnated with 7.5 and 10% squalane solutions exhibited very high adhesion with no sliding when tilted even at 90 º. From 10% to 30%, applications of more squalane on the coatings results in considerable reduction in sliding force. Surfaces impregnated within the range of 30-100% concentration of the squalane were slippery and water droplets could slide off on tilted surfaces as low as 6 ° and the corresponding sliding forces obtained for droplets at this range are as well low Results of the wettability investigations for all the fabricated surfaces are summarised in Table 3.7.

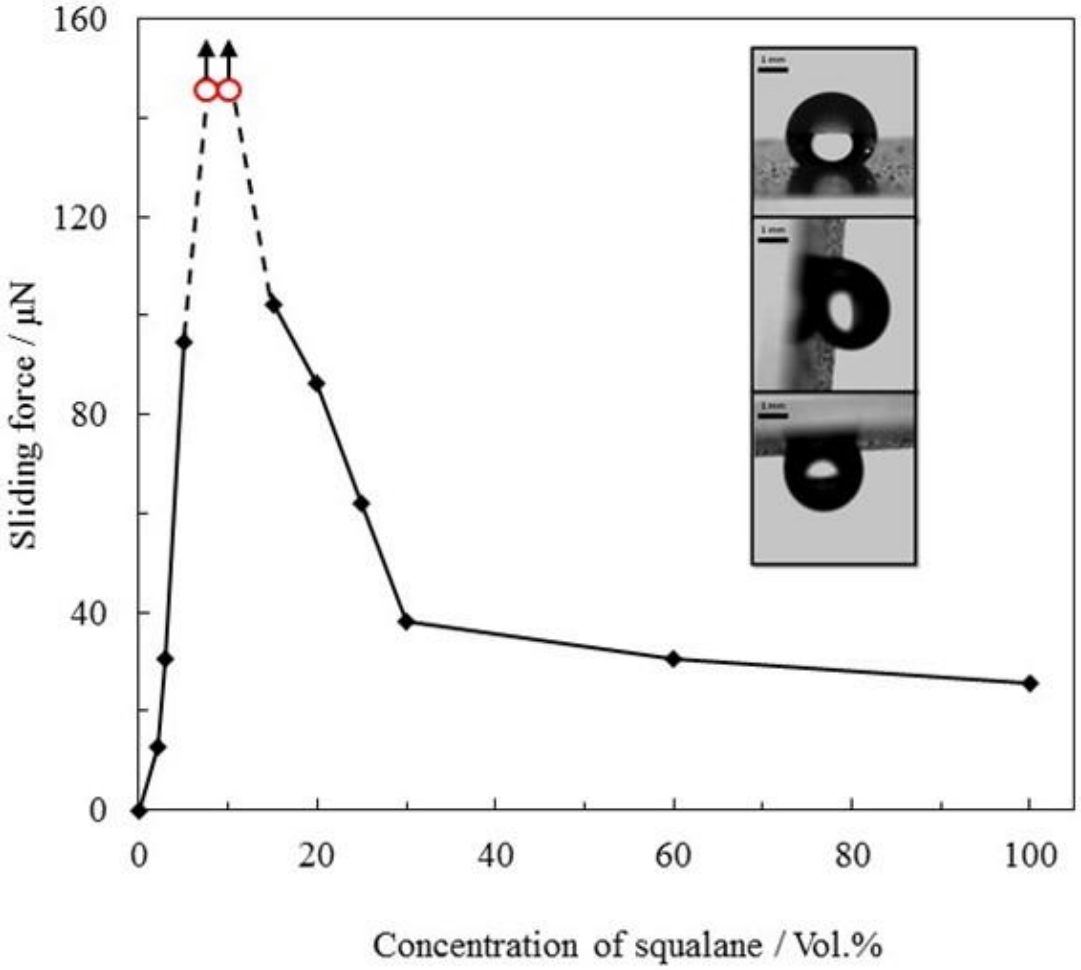

Figure 3.25 *S*liding force of 15 µL water drops on porous fumed silica coatings partially impregnated with different amount of squalane versus concentration of squalane in hexane solution used for impregnation. On surfaces impregnated with 7.5 and 10% squalane solutions (circles), no sliding of the droplet was observed and the sliding force should be bigger than 147 µN**.** Insets are images of water droplet on 10% impregnated surface in air at tilt angles 0^o (left), 90^o (middle) and 180^o (right). Dashed lines show the location of solid surface. Scale bars = 1 mm.

Table 3.5 Summary of wettability investigations on porous fumed silica coatings partially impregnated with different amount of squalane using 15 µL of water drops in air, including advancing and receding contact angles, contact angle hysteresis, sliding angles, sliding force, drop surface interactions.

[Squalane] / Vol.%	θ_A / deg.	θ_R / deg.	CAH / deg.	θ_S / deg.	Fd / µN	Drop surface Interaction
0	165 ± 5	165 ± 5	0 ± 0	0 ± 0	0 ± 0	Superhydrophobic, non-sticky
2	149 ± 2	147 ± 3	2 ± 5	5 ± 2	13 ± 5	Superhydrophobic, non-sticky
3	140 ± 4	136 ± 4	4 ± 8	12 ± 3	31 ± 8	sticky
5	135 ± 4	125 ± 2	10 ± 6	40 ± 5	90 ± 10	sticky
7.5	130 ± 4	116 ± 5	14 ± 9	N/A	< 147	Very sticky
10	127 ± 4	113 ± 4	14 ± 8	N/A	< 147	Very sticky
15	118 ± 3	108 ± 3	10 ± 6	44 ± 4	100 ± 10	sticky
20	115 ± 4	108 ± 4	7 ± 8	36 ± 3	86 ± 7	sticky
25	108 ± 2	104 ± 2	4 ± 4	25 ± 4	60 ± 10	slippery
30	107 ± 2	103 ± 2	4 ± 4	15 ± 5	40 ± 10	slippery
60	105 ± 1	104 ± 2	1 ± 3	9 ± 3	30 ± 10	Very slippery
100	106 ± 1	105 ± 2	1 ± 3	10 ± 4	30 ± 10	Very slippery

Gradual impregnation of the silica nano-porous substrate leads to progressive displacement of air in the pores by squalane. Apart from changes in the surface texture of the coatings (rough to smooth), the process is certainly associated with changes from the surface chemistry of the original material (coatings) to that of squalane, including its slippery nature and surfaces energy. The observed changes in physical appearances and behaviours of various impregnated coatings are direct consequences of the impregnated squalane. However, because different amount of squalane were impregnated, the coatings tend to exhibit different characteristics on these bases.

The high contact angle of water drops with rolling tendency observed on dry fumed silica coated surfaces is a clear indication that the dry hydrophobic fumed coated surfaces are superhydrophobic. As noted in the preceding section, the nano-sized roughened surface of the porous fumed silica coatings harbours some air pockets and the combined effects of these hydrophobic particles and the air pockets is significantly

responsible for the non-wetting characteristic of the surfaces. Silica-air composite surface is most likely exhibiting Cassie-Baxter mode of wetting and is the reason for high contact angle, low hysteresis, and excellent self-cleaning characteristic [50].

In the other extreme case of surfaces impregnated within the range of 30-100 vol.% solution of squalane, they show negligible change in contact angle and have a small contact angle hysteresis and sliding force. It is thought that the pores within this range were sealed with squalane and that the amount of squalane was enough to bridge between particles and aggregates, eliminate the surface roughness and a thin over-coated layer of squalane was formed such that the resulted surface becomes smoother homogeneous squalane based surface and water drop sits on the oil (Figure 3.26). The slippery characteristic, or low drag forces observed on the resulting surface within this range is associated with the slimy tendency of squalane, non-polar or immiscible nature of squalane towards water and the surface tension of squalane.

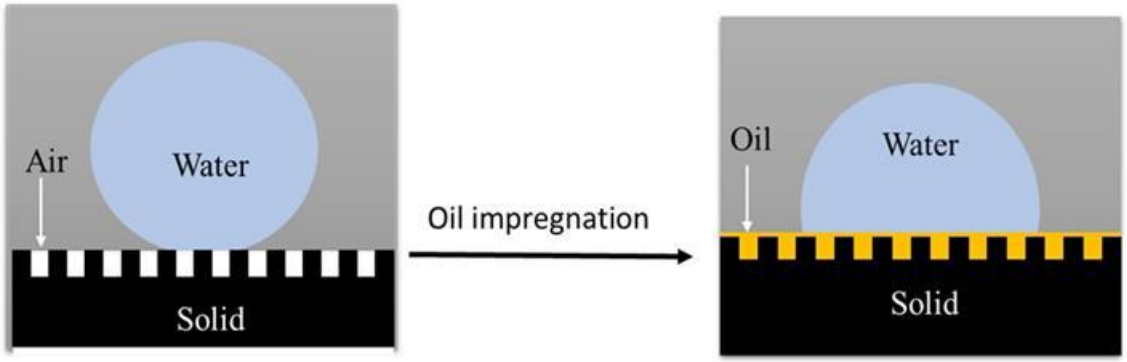

Figure 3.26 (a) is an illustration showing dry porous silica coating where water sits on silica-air composite surface. (b) is the coating obtained after impregnation and full replacement of the surface air pockets of (a) with oil to create over-coated layer of oil. In (b) water sits on homogeneous surface consisting only oil.

In this case of wetting of smooth homogeneous surface, the Young equation (Eq. 1.2) should hold as illustrated by the diagram in Figure 3.27. Here we assume that the water droplet sits on a thin flat film of oil and is not in contact with the solid beneath. The low values of the contact angle hysteresis, sliding angle and sliding force are in support of this assumption.

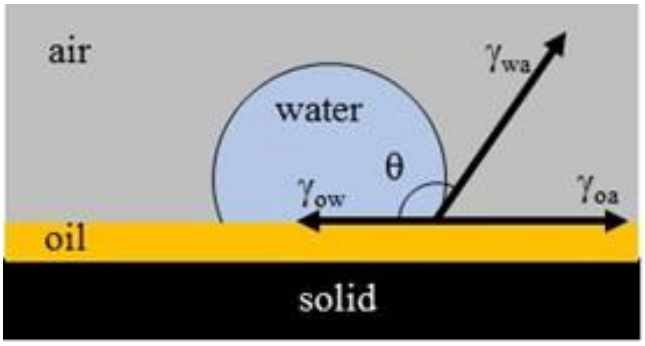

Figure 3.27 Interfacial tension force diagram for a water drop sitting on a very thin layer of immiscible oil (squalane) in air.

In the case above, the contact angle of water on the surface can be given by

$$cos\theta = \frac{\gamma_{oa} - \gamma_{ow}}{\gamma_{wa}} \qquad 3.7$$

where γ_{oa} is the oil-air surface tension, γ_{ow} oil-water interfacial tension and γ_{wa} is water-air surface tension. In order to test the experimental results obtained with this model, surface tension of water, that of squalane and interfacial tension of squalane-water were measured by the pendant drop method as described in Chapter 2, section 2.2.18 (see Table 3.9).

Table 3.6 Surface tension of squalane-air, water-air and interfacial tension of squalane-water interfaces measured by the pendant drop method at 21 ± 1 ℃. Each reported value is an average of 3 measurements.

Liquid	Surface tension / mN/m
Squalane-air	28.2 ± 0.5
Water-air	72.5 ± 0.3
Squalane-water	52.2 ± 0.2

Using the experimental values from Table 3.8 and Eq. 3.7, the contact angle of water was calculated to be 109 ± 2°. This value is in very good agreement with average of advancing and receding contact angle $\theta_{av} = (\theta_A + \theta_R)/2$ = 105 ± 3° obtained on the coatings impregnated with 30 – 100 vol.% squalane solutions (see Table 3.7).

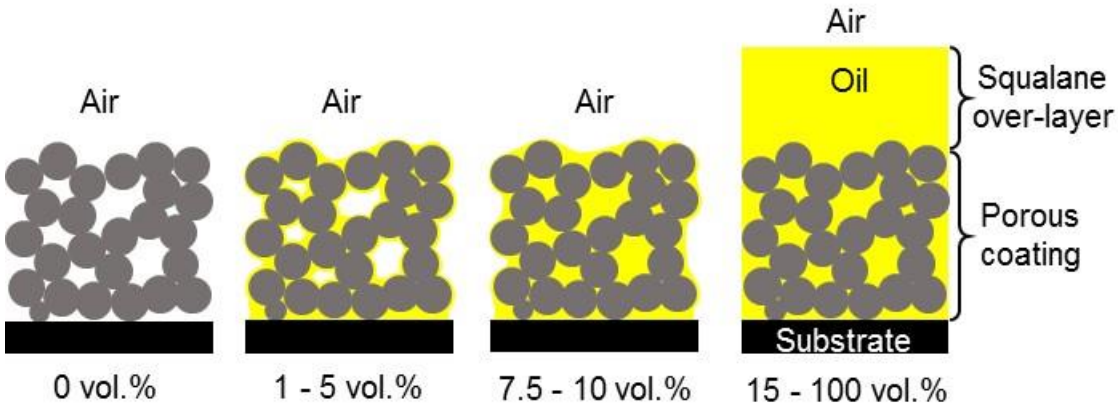

Figure 3.28 Schematic diagrams of squalane distribution in porous coatings impregnated with squalane solutions at concentrations shown after evaporation of the solvent (hexane).

The wetting behaviour of porous fumed silica coatings partially impregnated with squalane is more difficult to quantify because the surfaces are rough and heterogeneous. As mentioned before, squalane gradually fills in the gaps between the particles (Figure 3.21). One can expect that, at low concentrations of impregnating solution, the fumed silica particles are covered with a very thin layer of squalane because they are hydrophobic, hence, well wet by oil. When the amount of deposited squalane increases, the small pores will be filled first due to capillary action. Then the larger pores will be filled until the air is completely displaced from the coating (7.5 – 10 vol.%). When a water drop is placed on partially impregnated surfaces, it will be in contact with (i) the tops of solid particles, (ii) air trapped in the large pores at the surface and (iii) squalane filled in the smaller pores. When the amount of squalane is progressively increased, the area of contact between water and air (a very hydrophobic material with contact angle 180º) is reduced at the expense of the area of contact with less hydrophobic oil surface with contact angle of ~109º. The three phase contact lines on such very heterogeneous surfaces can be strongly pinned resulting in significant contact angle hysteresis, large sliding angle and sliding force.

3.4 Conclusions

Hydrophilic and hydrophobic glass surfaces can be fabricated by etching to create roughness on the surface of the glass. Better hydrophilic and hydrophobic states can be achieved when the scale of roughness is very small in order of micro-nanoscale. Such roughness enhanced surfaces were obtained in this work by depositing 10-700 nm silica particles on solid substrates. In addition to induced wetting control, porous surfaces controlled by different sizes of the silica particles were created. Such porous surfaces are of high importance in wettability as they can trap air or retain liquids like oil that

can further be used to control the interactions of other liquids. To obtain coatings with high air/oil stability, oil retention capabilities of the coatings were investigated. Fumed silica particles with 76% oil retention for 5 days was selected and fabricated for wetting studies against larger size silica particle with low retention of oil.

Uniform depositions of the silica particles were achieved by the application of dip and spin coating processes. Smooth coatings can be obtained with dip coating when 4 wt.% silica dispersion in ethanol is used and the slides withdrawn at 3-4 cm/min, or 3 wt.% and the slide withdrawn at 5 cm/min. In the case of spin coating 3-5 wt.% silica dispersion spun at the spin rate of 2000 rpm and above was the best condition to obtain smooth coatings. The thickness of the fabricated coatings were found to vary inversely with the spin rate of the spin coater and directly with the withdrawal speed in dip coatings

The partial impregnation of the coatings with different amounts of oil (squalane) allows us to gradually tune its wetting behaviour of the nano-porous silica coatings for many applications, including self-cleaning superhydrophobic surfaces, drag-free slippery surfaces and adhesive surfaces. The superhydrophobic surfaces are believed to be caused by the synergy from the air pockets and the hydrophobic nano-porous silica particles while the slippery coatings are as a result of the full replacement of the silica-air composite surface by slimy oil (squalane). The wetting behaviour of porous fumed silica coatings partially impregnated with squalane is more difficult to quantify because the surfaces are rough and heterogeneous, and water drops placed on the surfaces have the tendencies to establish contact with the tops of solid particles; non-displaced air trapped in the surface pores and squalane partially filled in the pores.

3.5 References

1. L. Gunther and W. Peukert, Control of coating properties by tailored particle interactions: relation between suspension rheology and film structure. *Colloids and Surfaces a-Physicochemical and Engineering Aspects*, 2003. **225**(1-3): p. 49-61.

2. I. Stalder and J. H. Bilgram, The measurement of the solid-liquid surface free energy of xenon. *Journal of Chemical Physics*, 2003. **118**(17): p. 7981-7984.

3. E. L. Decker, B. Frank, Y. Suo, and S. Garoff, Physics of contact angle measurement. *Colloids and Surfaces a-Physicochemical and Engineering Aspects*, 1999. **156**(1-3): p. 177-189.

4. P. Siffalovic, *et al.*, Towards new multifunctional coatings for organic photovoltaics. *Solar Energy Materials and Solar Cells*, 2014. **125**: p. 127-132.

5. T. Young, An Essay on the Cohesion of Fluids. *Phil. Trans. R. Soc. Lond.*, 1805: p. 65-87.

6. R. N. Wenzel, Resistance of solid surfaces to wetting by water. *Industrial and Engineering Chemistry*, 1936. **28**: p. 988-994.

7. A. B. D. Cassie and S. Baxter, Wettability of porous surfaces. *Transactions of the Faraday Society*, 1944. **40**: p. 546.

8. T. Ning, W. G. Xu, and S. X. Lu, Fabrication of superhydrophobic surfaces on zinc substrates and their application as effective corrosion barriers. *Applied Surface Science*, 2011. **258**(4): p. 1359-1365.

9. W. Jiang, *et al*., Preparation and Antiscaling Application of Superhydrophobic Anodized CuO Nanowire Surfaces. *Industrial & Engineering Chemistry Research*, 2015. **54**(27): p. 6874-6883.

10. J. T. Wang, *et al*., Double biomimetic fabrication of robustly superhydrophobic cotton fiber and its application in oil spill cleanup. *Industrial Crops and Products*, 2015. **77**: p. 36-43.

11. Y. L. Shi, W. Yang, and X. J. Feng, Fabrication of Superhydrophobic-superoleophilic Cotton Fabric and Its Application in Water-oil Separation. *Chemical Journal of Chinese Universities-Chinese*, 2015. **36**(9): p. 1724-1729.

12. F. Li, *et al*., Fabrication of fluorinated raspberry particles and their use as building blocks for the construction of superhydrophobic films to mimic the wettabilities from lotus leaves to rose petals. *Polymer Chemistry*, 2015. **6**(37): p. 6746-6760.

13. W. Ming, D. Wu, R. van Benthem, and G. de With, Superhydrophobic films from raspberry-like particles. *Nano Letters*, 2005. **5**(11): p. 2298-2301.

14. T. Ogi, L. B. Modesto-Lopez, F. Iskandar, and K. Okuyama, Fabrication of a large area monolayer of silica particles on a sapphire substrate by a spin coating method. *Colloids and Surfaces A: Physicochemical and Engineering Aspects*, 2007. **297**(1): p. 71-78.

15. P. Jiang and M. J. McFarland, Large-scale fabrication of wafer-size colloidal crystals, macroporous polymers and nanocomposites by spin-coating. *Journal of the American Chemical Society*, 2004. **126**(42): p. 13778-13786.

16. F. Iskandar, M. Abdullah, H. Yoden, and K. Okuyama, Silica films containing ordered pores prepared by dip coating of silica nanoparticles and polystyrene beads colloidal mixture. *Journal of sol-gel science and technology*, 2004. **29**(1): p. 41-47.

17. F. Iskandar, Mikrajuddin, and K. Okuyama, Controllability of pore size and porosity on self-organized porous silica particles. *Nano Letters*, 2002. **2**(4): p. 389-392.

18. W. J. Iley, Effect of Particle-Size and Porosity on Particle Film Coatings. *Powder Technology*, 1991. **65**(1-3): p. 441-445.

19. I. Ab Rahman and V. Padavettan, Synthesis of Silica Nanoparticles by Sol-Gel: Size-Dependent Properties, Surface Modification, and Applications in Silica-Polymer Nanocomposites-A Review. *Journal of Nanomaterials*, 2012.

20. X. Fan, L. Niu, Y. H. Wu, J. Cheng, and Z. R. Yang, Assembly route toward raspberry-like composite particles and their controlled surface wettability through varied dual-size binary roughness. *Applied Surface Science*, 2015. **332**: p. 393-402.

21. X. M. Chen, J. A. Weibel, and S. V. Garimella, Exploiting Microscale Roughness on Hierarchical Superhydrophobic Copper Surfaces for Enhanced Dropwise Condensation. *Advanced Materials Interfaces*, 2015. **2**(3).

22. P. F. Hao, C. J. Lv, F. L. Niu, and Y. Yu, Water droplet impact on superhydrophobic surfaces with microstructures and hierarchical roughness. *Science China-Physics Mechanics & Astronomy*, 2014. **57**(7): p. 1376-1381.

23. C. Dorrer and J. Ruhe, Some thoughts on superhydrophobic wetting. *Soft Matter*, 2009. **5**(1): p. 51-61.

24. J. D. Smith, *et al*., Droplet mobility on lubricant-impregnated surfaces. *Soft Matter*, 2013. **9**(6): p. 1772-1780.

25. A. Carminati, A. Kaestner, P. Lehmann, and H. Fluhler, Unsaturated water flow across soil aggregate contacts. *Advances in Water Resources*, 2008. **31**(9): p. 1221-1232.

26. K. Saleh, D. Steinmetz, and A. Hemati, Experimental study and modeling of fluidized bed coating and agglomeration. *Powder Technology*, 2003. **130**(1-3): p. 116-123.

27. S. Radice and S. Mischler, Effect of electrochemical and mechanical parameters on the lubrication behaviour of Al2O3 nanoparticles in aqueous suspensions. *Wear*, 2006. **261**(9): p. 1032-1041.

28. G. Ilgu, Y. Caglar, S. Ilican, M. Caglar, and S. Ruzgar, The Effect of Sol Concentration on the Structural and Electrical Parameters of Nanostructure ZnO Films by Sol Gel Dip Coating. *Journal of Nanoelectronics and Optoelectronics*, 2014. **9**(5): p. 618-623.

29. G. Nam, *et al*., Effect of Co Doping Concentration on Structural Properties and Optical Parameters of Co-Doped ZnO Thin Films by Sol-Gel Dip-Coating Method. *Journal of Nanoscience and Nanotechnology*, 2014. **14**(11): p. 8544-8548.

30. T. Sato, Effect of turnover rate on the change of concentration of an unstable compound in a dip coating bath. *Journal of Coatings Technology*, 2000. **72**(906): p. 81-83.

31. H. Uchiyama, M. Hayashi, and H. Kozuka, Spontaneous pattern formation on silica and titania dip-coating films prepared at extremely low substrate withdrawal speeds. *Rsc Advances*, 2012. **2**(2): p. 467-473.

32. K. Yasuda, T. Koshiba, and N. Mori, Effects of rheological property of coating liquid and withdrawal velocity on dip coating process in manufacturing of capsules. *Nihon Reoroji Gakkaishi*, 2004. **32**(2): p. 85-90.

33. E. V. Rebrov and J. C. Schouten, Limiting withdrawal rate and maximum film thickness during dip-coating of titania sols onto a Si substrate. *Chemical Engineering and Processing*, 2011. **50**(10): p. 1063-1068.

34. D. W. Schubert and T. Dunkel, Spin coating from a molecular point of view: its concentration regimes, influence of molar mass and distribution. *Materials Research Innovations*, 2003. **7**(5): p. 314-321.

35. M. Z. Musa, *et al*., Effects Of Spin Coating Speed On Nanostructured Titanium Dioxide (TiO(2)) Thin Films Properties. *Enabling Science and Nanotechnology*, 2011. **1341**: p. 33-36.

36. R. T. Ginting, C. C. Yap, M. Yahaya, V. Fauzia, and M. M. Salleh, Active Layer Spin Coating Speed Dependence of Inverted Organic Solar Cell Based on Eosin-Y-Coated ZnO Nanorod Arrays. *3rd Isesco International Workshop and Conference on Nanotechnology 2012 (Iwcn2012)*, 2013. **431**.

37. B. Hatton, L. Mishchenko, S. Davis, K. H. Sandhage, and J. Aizenberg, Assembly of large-area, highly ordered, crack-free inverse opal films.

Proceedings of the National Academy of Sciences of the United States of America, 2010. **107**(23): p. 10354-10359.

38. A. Torabi, T. H. Etsell, and P. Sarkar, Dip coating fabrication process for micro-tubular SOFCs. *Solid State Ionics*, 2011. **192**(1): p. 372-375.

39. C. J. Brinker and A. J. Hurd, Fundamentals of Sol-Gel Dip-Coating. *Journal De Physique Iii*, 1994. **4**(7): p. 1231-1242.

40. J. X. Huang, R. Fan, S. Connor, and P. D. Yang, One-step patterning of aligned nanowire arrays by programmed dip coating. *Angewandte Chemie-International Edition*, 2007. **46**(14): p. 2414-2417.

41. P. J. Yunker, T. Still, M. A. Lohr, and A. G. Yodh, Suppression of the coffee-ring effect by shape-dependent capillary interactions. *Nature*, 2011. **476**(7360): p. 308-311.

42. M. L. Eggersdorfer and S. E. Pratsinis, The Structure of Agglomerates Consisting of Polydisperse Particles. *Aerosol Science and Technology*, 2012. **46**(3): p. 347-353.

43. R. Wengeler, F. Wolf, N. Dingenouts, and H. Nirschl, Characterizing dispersion and fragmentation of fractal, pyrogenic silica nanoagglomerates by small-angle x-ray scattering. *Langmuir*, 2007. **23**(8): p. 4148-4154.

44. W. E. Smith and C. E. Zukoski, Aggregation and gelation kinetics of fumed silica-ethanol suspensions. *Journal of Colloid and Interface Science*, 2006. **304**(2): p. 359-369.

45. P. Kim, *et al*., Liquid-Infused Nanostructured Surfaces with Extreme Anti-Ice and Anti-Frost Performance. *Acs Nano*, 2012. **6**(8): p. 6569-6577.

46. T. S. Wong, *et al*., Bioinspired self-repairing slippery surfaces with pressure-stable omniphobicity. *Nature*, 2011. **477**(7365): p. 443-7.

47. N. M. Pinzon, K. G. Aukema, J. A. Gralnick, and L. P. Wackett, Nile Red Detection of Bacterial Hydrocarbons and Ketones in a High-Throughput Format. *Mbio*, 2011. **2**(4).

48. P. Greenspan and S. D. Fowler, Spectrofluorometric Studies of the Lipid Probe, Nile Red. *Journal of Lipid Research*, 1985. **26**(7): p. 781-789.

49. B. Valeur and M. N. Berberan-Santos, *Molecular fluorescence: principles and applications*. 2012: John Wiley & Sons.

50. C. Neinhuis and W. Barthlott, Characterization and distribution of water-repellent, self-cleaning plant surfaces. *Annals of Botany*, 1997. **79**(6): p. 667-677.

CHAPTER 4

PREPARATION OF OIL-IMPREGNATED POROUS COATINGS ON SOLID SUBSTRATES BY A ONE-STEP DEPOSITION PROCESS

4.1 Introduction

In our previous studies (Chapter 3), porous fumed silica coatings were first fabricated on solid substrates (glass slides), then, the dry coatings were impregnated with squalane solutions which produced partially or fully squalane impregnated coatings after evaporation of the solvent (hexane). Superhydrophobic, sticky and slippery surfaces with respect to water wetting were fabricated in a multi-step process including:

i. Preparation of fumed silica suspension in ethanol;
ii. Coating of the suspension on glass slides using a spin coater;
iii. Preparation of a non-volatile oil (squalane) solution in volatile solvent (hexane);
iv. Impregnation of the dry porous coatings with squalane solutions and evaporation of the volatile solvent.

For practical purpose, the above listed processes seem a long way to fabricate the impregnated coatings despite the fact that it is simpler than many other methods used for the fabrications of superhydrophobic and slippery surfaces. Here, we aim to develop a simpler one-step fabrication technique to achieve coatings similar to the ones produced by multiple steps but with less time and cost of fabrication.

4.2 Experimental

In the preparation of the coating precursor, silica, non-volatile oil (squalane or silicone oil) and ethanol as a solvent are incorporated into one system to form a dispersion which is then coated onto slides or other solid materials directly by spin coating, dip coating, spraying onto surfaces or deposited on solid surfaces by brushing. Detailed procedure for the preparation of the dispersion is described in Chapter 2.2.7. In this case, steps (i) and (ii) mentioned above (section 4.1) are merged, and so are step (iii) and (iv); hexane is eliminated to serve cost.

To understand the nature of the dispersion formed by the mixture, a miscibility study of the squalane in ethanol was performed (2.2.9) and the dispersions were examined under microscope as described in Section 2.2.15. To assess the turbidity of the dispersions, their apparent absorbance was measured using a UV-Vis spectrophotometer (Sect. 2.2.19). The transparency of the coated films were also assessed by UV-Vis spectrophotometer measurements (Sect. 2.2.19). The wettability of different impregnated coatings was evaluated by measuring the contact angles of water drops on the coatings in air. The flexibility and viability of the technique were tested by comparing coatings produced by different techniques (e.g. spin coating and spray coating) and composition of the dispersion (e.g. change in silica concentration or impregnating oil).

4.3 Results and discussions

4.3.1 Characterisation of liquid dispersions used in the coating process

4.3.1.1 Physical appearance of the dispersions

In the previous Section (Chapter 3) fumed silica dispersions were prepared using only one liquid (ethanol) but in this Chapter the dispersions are made using both the solvent (ethanol) and the oil (squalane). However, not all liquids can mix together to form a uniform solution. The miscibility of squalane oil in ethanol carried out as described in Section 2.2.9 was found to be 3.9 ± 0.3%. As is well known, squalane is non polar and normally, non-polar compounds are usually not miscible with polar ones, but ethanol being bipolar or amphipathic (i.e. possessing both polar and non-polar properties), is able to undergo partial miscibility with the oils. However, mixing a higher proportion of squalane in ethanol resulted in separation of both liquids as shown in Figure 4.1a. Addition of fumed silica particles to these systems and final preparations of the dispersions resulted in increasing milk whiteness of the dispersion as the concentration of the oil increases. Figure 4.1b shows physical appearances of the dispersions prepared using squalane in ethanol. Also observed was the gradual decrease in the flow (viscosity) of the dispersion with the increasing concentration of squalane.

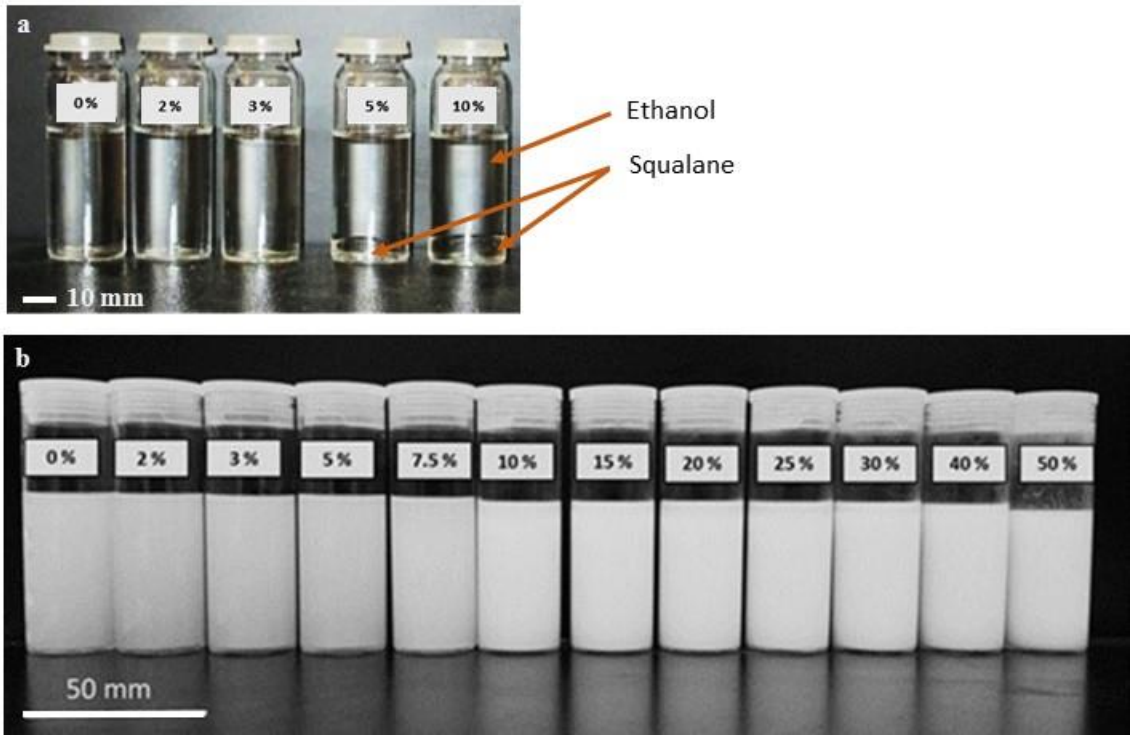

Figure 4.1 Digital images showing (a): the mixture of squalane in ethanol from 0 - 10%. Between 0-3% homogeneous solutions are observed. At higher concentration of 5% and above, squalane becomes immiscible and form droplets shown by the arrows. (b) Dispersions obtained after the addition fumed silica particles (5 wt.%) squalane-ethanol mixture. The whiteness of the dispersion increases with immiscibility from 0-50%.

4.3.1.2 Structure of dispersions assessed by optical microscopy

Microscopic examinations of the dispersions revealed that increase in squalane ratio gradually change the colloidal suspension of silica to emulsions with the formation of noticeable droplets at squalane concentrations of 3 wt.% (Figure 4.2). At a lower concentration of squalane (e.g. 2 wt.%) as can be seen in miscibility images in Figure 1a, the dispersions are without liquid-liquid interfaces so the particles were freely dispersed in the medium. As the concentration of squalane increases, liquid-liquid interfaces are formed; particles are trapped at the interfaces and in the process the oil droplets are stabilised in the dispersion [1-4]. At initial stage of the droplet formation

(e.g. 5% squalane concentration), a few tiny droplets widely spaced apart are observed. This is certainly due to the small amount of oil present in the dispersions. As the concentration increases, the droplets grow bigger in size and number and hence become closer to one another as it is the case with 15% silica dispersion in Figure 4.2. Further increase in oil fraction up to 30% leads to a dispersion with a very congested droplets. It is observed that the viscosity behaviours of the dispersions depend on the liquid fraction of the dispersed phase (squalane). At low volume fraction, the droplets are Brownian and the dispersions is Newtonian with viscosity close to that of the continuous phase. Increase in volume fraction of the dispersed phase brings the droplets in close contact and this tends to inhibit particles motion. Increase in concentration in the dispersed phase is the major cause of increased viscosity at higher concentration of squalane [5-7].

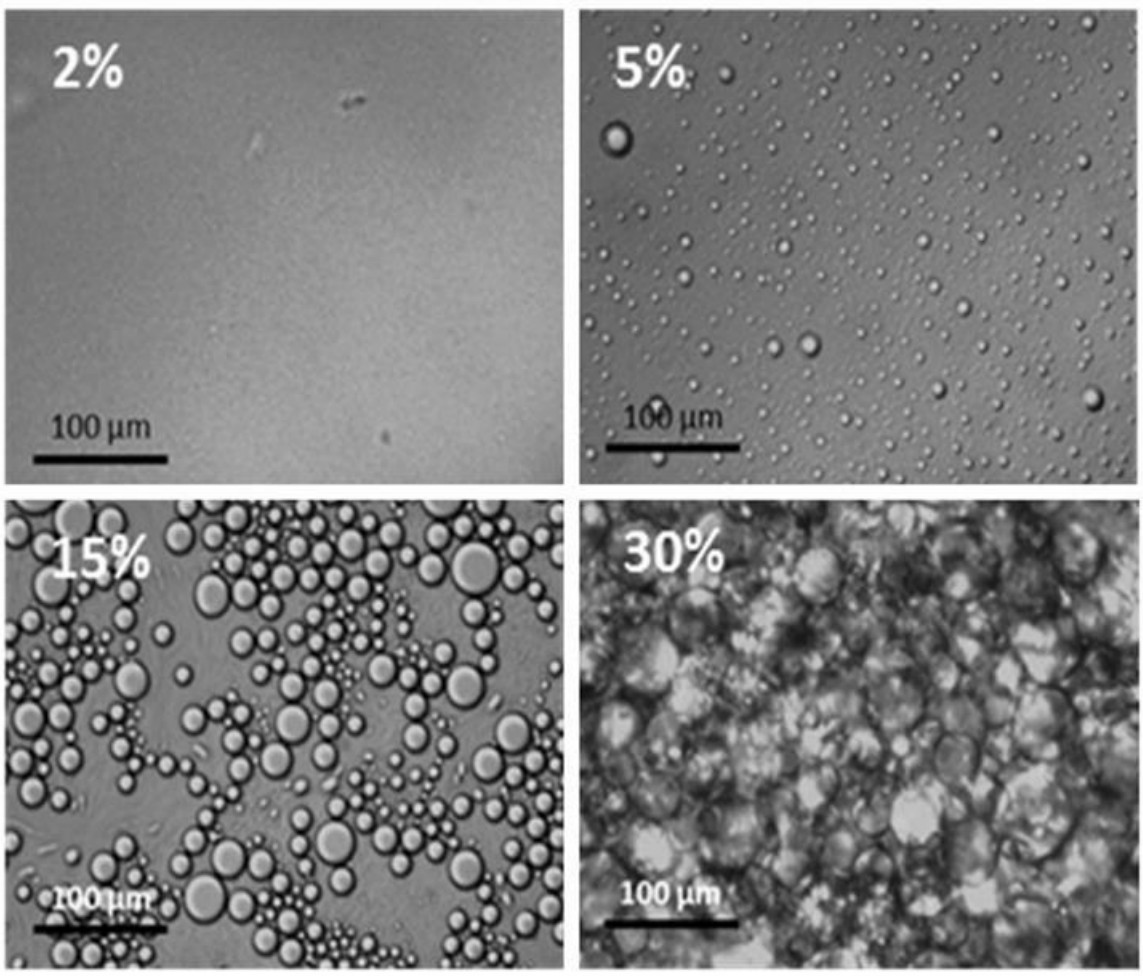

Figure 4.2 Optical microscope images of silica dispersions in ethanol-squalane system at different concentration of squalane. Dispersions formed with squalene concentration in the dispersion lower than 3 wt.% show negligible droplets but emulsions are clearly observed from 5 wt.% concentration of squalane and upward.

4.3.1.3 Turbidity of the dispersions

Turbidity of the dispersions was assessed by investigating their apparent absorbance at 650 nm relative to 0% squalane dispersion using UV/Vis spectrophotometer. The reduction of the transmitted light intensity in this case is mainly due to losses due to scattering from the particles and oil droplets in the dispersion. The results of the investigations are shown in Figure 4.3.

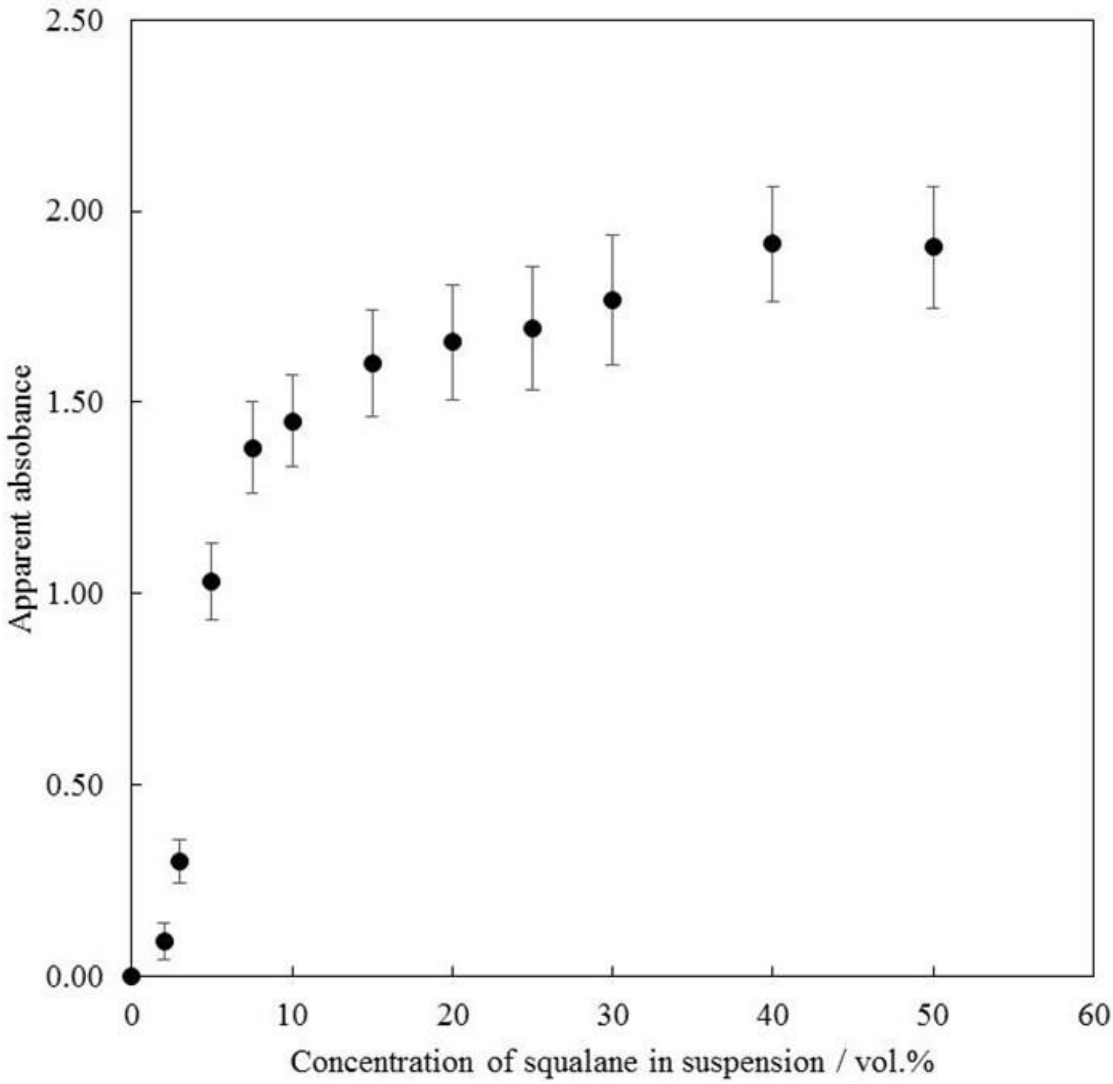

Figure 4.3 Apparent absorbance of the different dispersions versus squalane concentration measured by a UV/Vis spectrophotometer at 650 nm using 0% (without squalane) fumed silica dispersion in ethanol as a reference .Cuvette path length = 1 cm.

Apparent absorbance (and therefore turbidity) of the dispersions increases with the increase in squalane concentration. In this case, the presence of droplets in the dispersions certainly interferes with the lights which make the incident light beam to experience incoherent scattering and reflections. The added contribution of all these reflections in every droplet results in the white appearance of the dispersion to the eyes [8]. Thus, the increasing number of droplets in higher volume fraction of squalane causes light rays to be more scattered, reflected or (to smaller extent) absorbed rather than transmitted through the samples [8-10].

4.3.2 Morphology of coated films on solid substrates

Figure 4.4 shows the optical images of squalane impregnated silica coatings fabricated using fumed silica dispersions in ethanol containing different concentrations of squalane. The coatings are found to be gradually wetted by squalane in a similar manner as the impregnated coatings produced in multiple-step process in Chapter 3. The underlying mechanism of the coating process remain similar, involving the evaporation of the volatile liquid solvent (during the coating and drying processes) and retention of the non-volatile squalane which, upon drying, redistributes and penetrates in the pores between silica particles depending on its concentration in the dispersion. As can be seen from the images, coatings obtained from dispersion with less and higher concentration of squalane can clearly be focussed when either silica or squalane dominates the surfaces (e.g. 2 or 40%). Coatings produced with moderate amount of squalane show complex texture due to oil interference between the oil and solid particles.

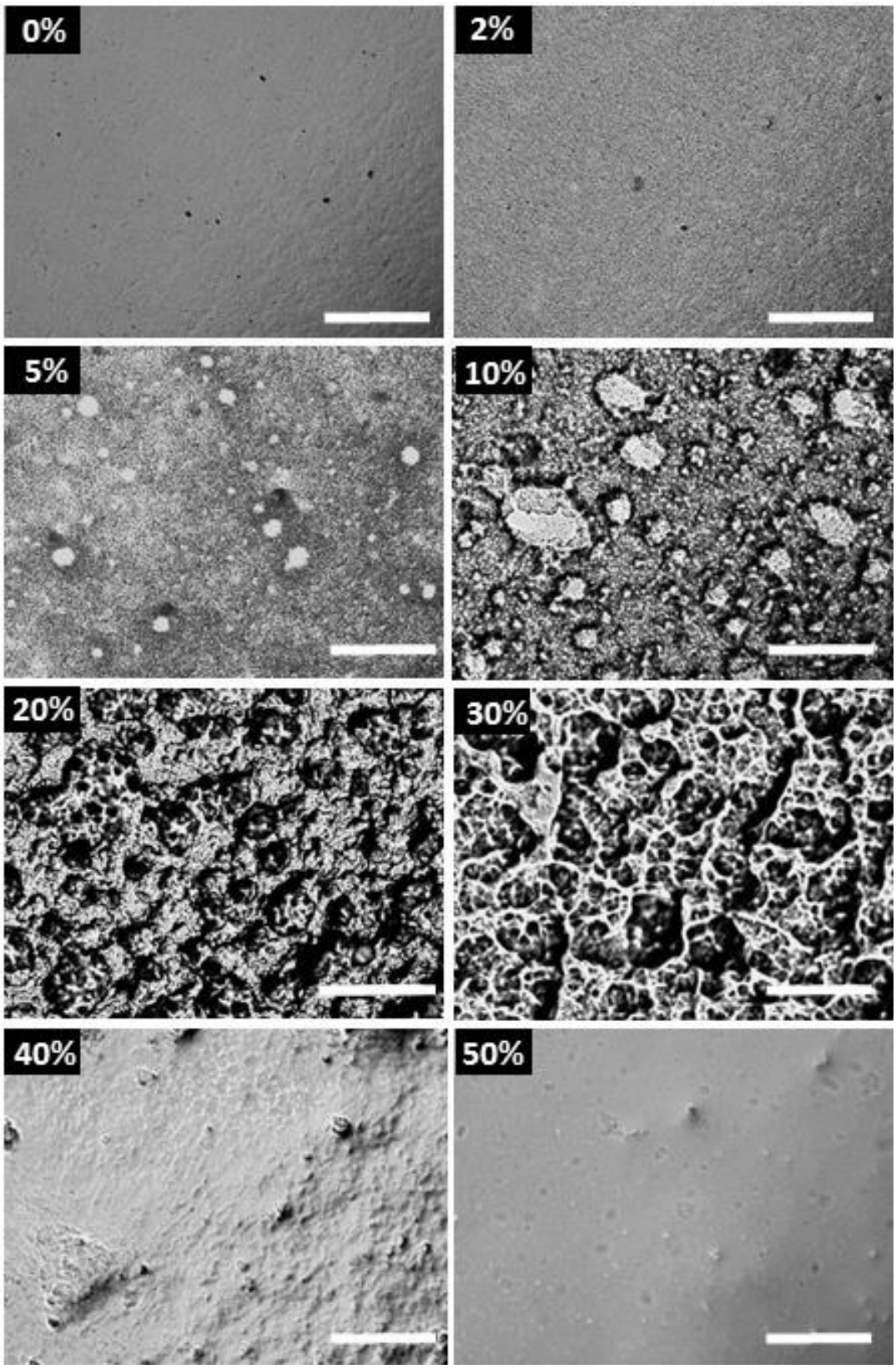

Figure 4.4 Microscopic images of the different coatings fabricated using 5% silica ethanol dispersion at different concentrations of squalane in the dispersions. The concentrations of the dispersion are displayed on respective coatings. Bar = 100 µm

4.3.3 Optical transmittance of the coatings

Low magnification digital camera images showing physical appearances of the impregnated coatings were also taken and are presented in Figure 4.5. Consecutive increment in the squalane concentration the dispersions is found to impart a systematic characteristic colour change to the resulted coatings. Dry coatings (without squalane) and coatings loaded with higher amount of squalane are similar in appearance and transparent to light. As can be observed from the images, the black colour background in which the coatings are being placed can be clearly seen through the surface of these coatings whereas other coatings in middle zone (2-40%) tend to exhibit different degree of opacity looking whitish to the eyes. Coating produced from 5% squalane dispersion is observed to attain the highest opacity. For better understanding, the overall transparency of the coatings were studied by investigating light transmittance through the fabricated surfaces using UV/Vis spectrophotometer and the results are shown in Figure 4.6.

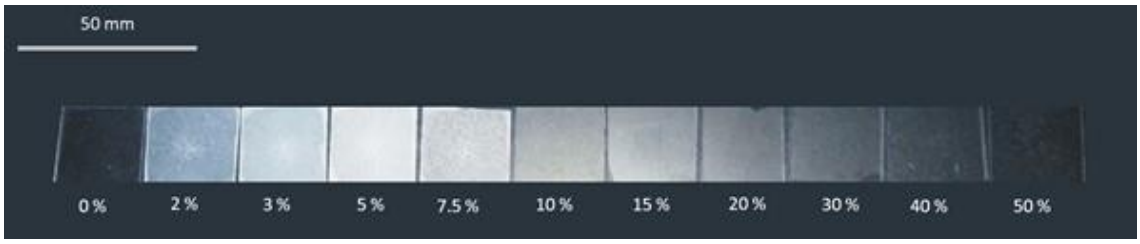

Figure 4.5 Digital photographs showing physical appearances of the different impregnated coatings fabricated with different concentrations of squalane in 5% fumed silica dispersion in ethanol. The coated slides are placed on a table with black background. The coatings obtained at both 0 and 50% squalane concentration are highly transparent as the colour of the table can be seen through the slides whereas the rest show different degree of opacity with a maximum at 5% squalane concentration.

A typical spectral profile of the transmitted light through the different impregnated silica coatings is shown in Figure 4.6. It is observed that fumed silica coatings without squalane impregnation are most transparent with and average light transmittance of 93 ± 3%. The transmittance decreases from the dry coatings, (0%) to the coated surface produced from 5% squalane dispersion where the highest opacity with the least transmittance of 7 ± 0 is recorded, and then increases steadily to transparent surfaces loaded with highest amount of squalane (using 50% dispersions).

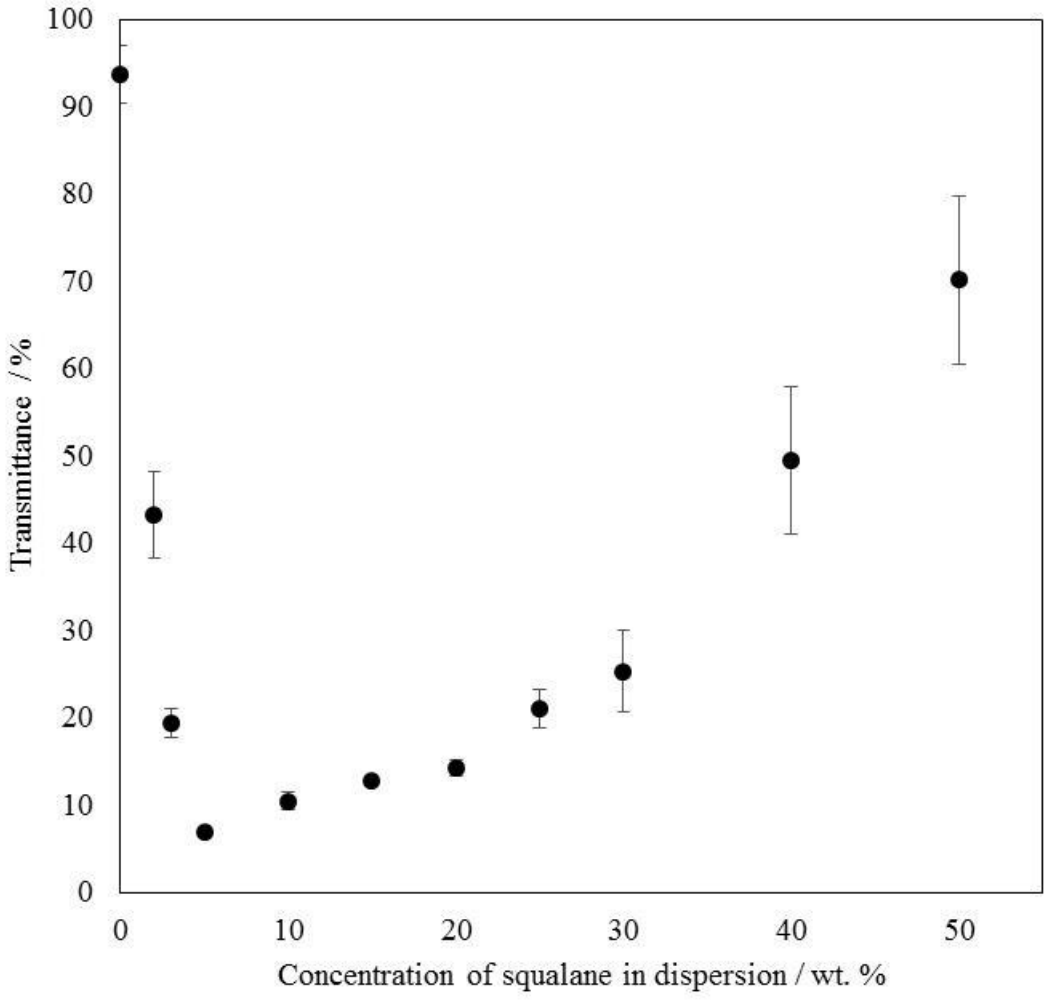

Figure 4.6 Transmittance of the different impregnated coatings at 650 nm in air measured by a UV/Vis spectrophotometer.

It is interesting that the opacity of the coating shows a similar trend to the sliding angle or adhesion force studied in Chapter 3. On the most opaque surfaces, the opacity of the coatings just like the sliding force decreases toward coatings with low and high squalane loadings, respectively. This supports our hypothesis that the partially impregnated with oil porous coatings are highly heterogeneous in nature and simultaneously contain empty and (partially) filled with oil pores. Such structures should have significant light scattering ability, hence lower transparency.

Although this work is not focussing on optical properties of the surfaces, it is worthy to note that partial impregnation technique employed here is capable of tuning the optical properties of fumed silica coating which may find applications other fields other than wetting [11-13]. Transparent films with reduced reflection like the fumed silica coating are useful in solar cell applications, displayed windows and lenses to reduced reflection and improve device performance since less light is lost [11, 12].

4.3.4 **Wettability of the coated surfaces**

Wettability of the fabricated surfaces was assessed using advancing contact angles of water drops on the surfaces in air. The results of the wettability of the surfaces are shown in Figure 4.7. Water drops on the dry fumed silica coating and other impregnated surfaces varies in a similar fashion to those obtained on surfaces produced with multiple steps in Chapter 3. However, unlike the previous studies, where a plateau was obtained in the wettability curve from surfaces coated with 30 vol.% squalane solution, a little shift in the wettability of the surfaces such that relatively constant contact angles are obtained from surfaces coated with dispersions of squalane concentrations 40% or higher. This observation reveals that the *in situ* technique tends to conserve more oil than external deposition of the oil onto the coatings.

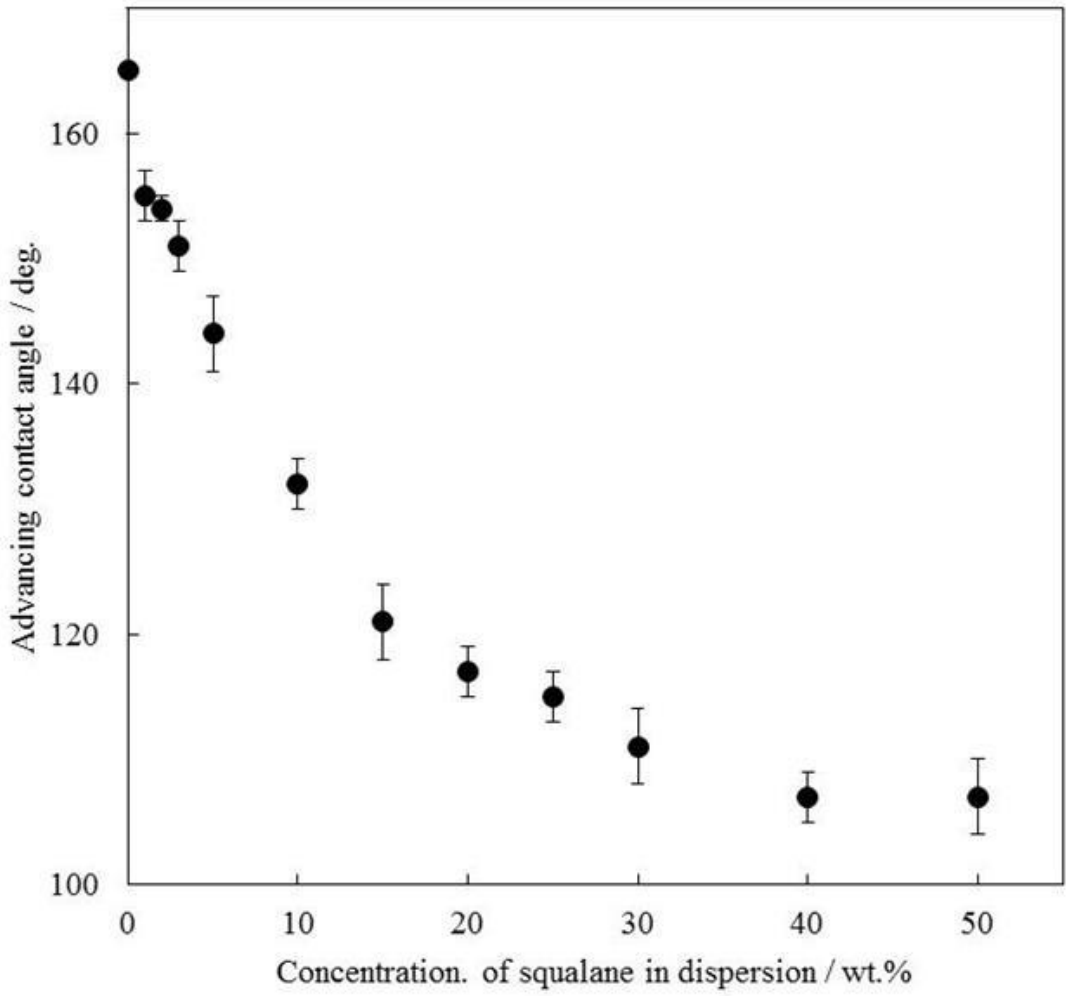

Figure 4.7 Advancing contact angles of water drops on coatings in air versus concentration of squalane in the dispersions used in the coating process.

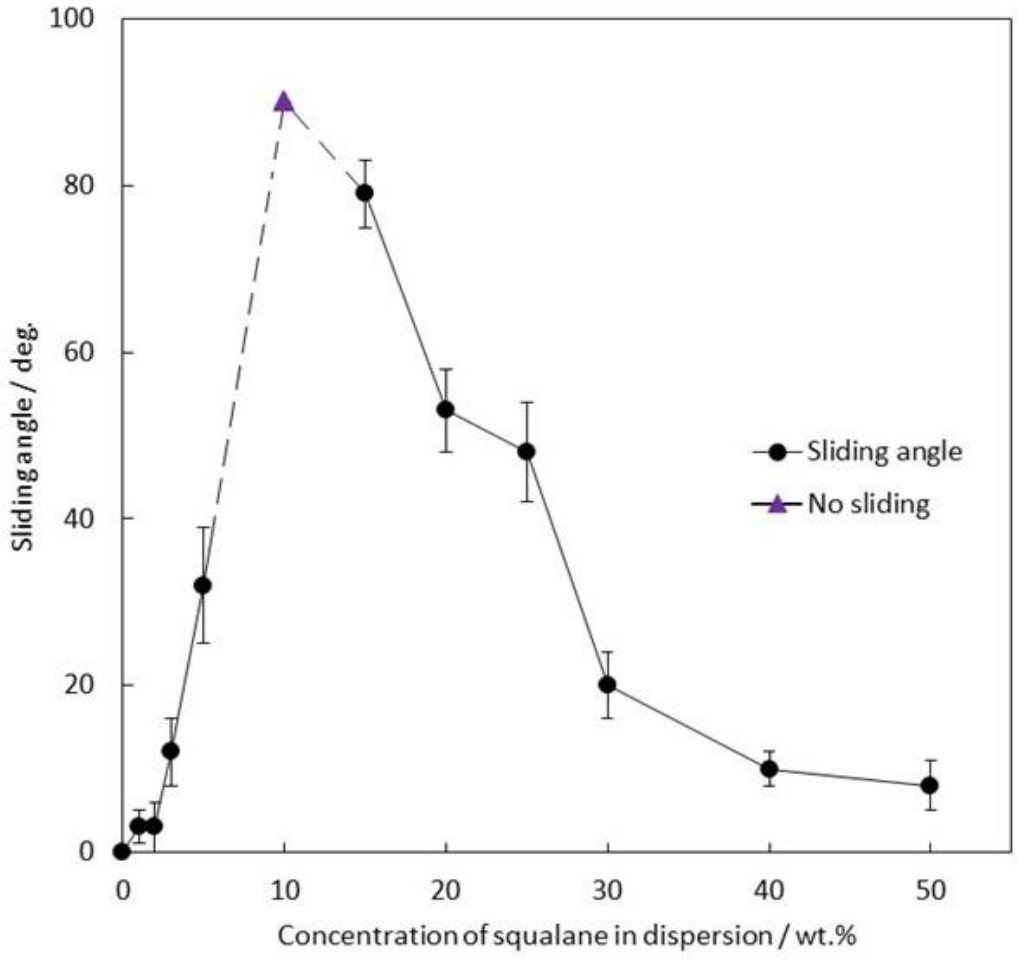

Figure 4.8 Sliding angles of water drops (12 ± 2 µL) on coatings in air versus concentration of squalane in the dispersions used in the coating process. No sliding of water drops on the coating at 10% squalane (triangle) was observed.

The sliding angles of water drops on the surfaces are shown in Figure 8. As can be seen that the variation of the sliding angle follows a similar trend as that obtained for coatings prepared by a multiple step method (see Chapter 3), with low water adhesion on superhydrophobic surfaces (0-3%), and different degrees of adhesion observed on surfaces coated with 5-30% dispersions, with the greatest stickiness on surfaces coated with 10% dispersion. Surfaces coated with 40-50% squalane dispersions are slippery with very low water adhesion.

General comparison of the wettability of coatings produced by one-step deposition process and those by the multiple step method (Chapter 3) shows a very strong similarity (Figure 4.9). Contact angles of water drops are observed to vary in a similar manner on impregnated coating produced by the two methods. They gradually decrease with increasing the load of squalane on the coating until a low constant value is reached on the squalane flooded coatings. Adhesion of water droplets on the different impregnated coatings in the present technique is also observed to follow the same trend as shown by the multiple step method.

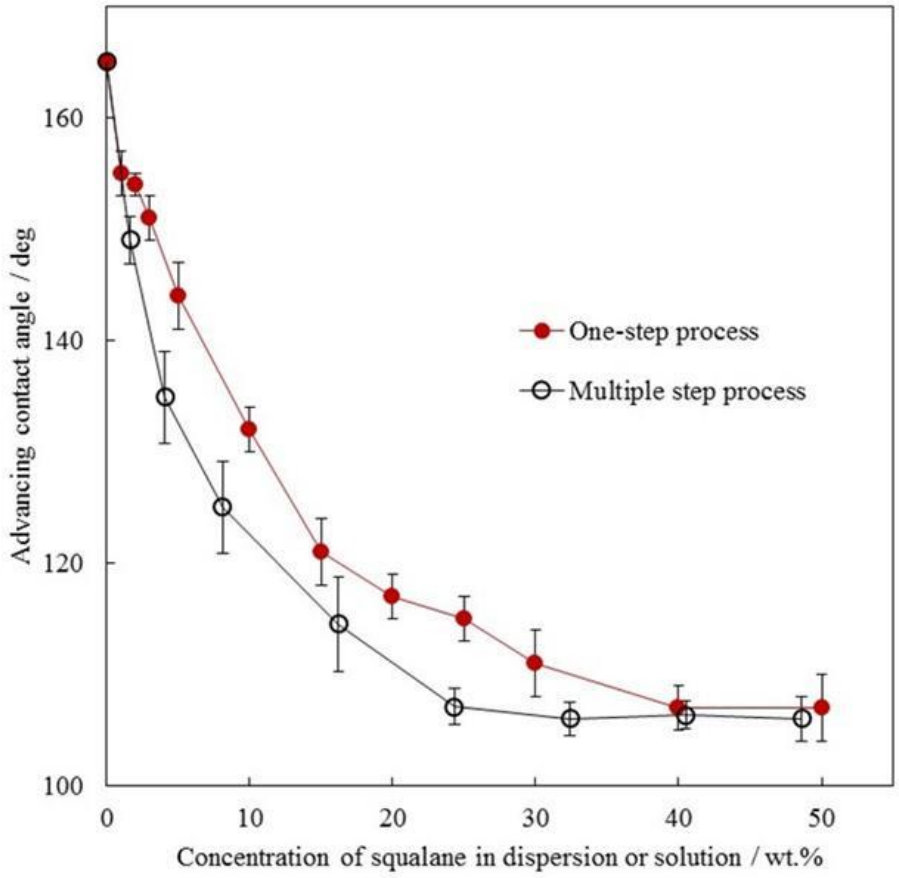

Figure 4.9 Advancing contact angles of water drops on squalane impregnated coatings fabricated using the multiple step process (Chapter 3) and one-step deposition technique vesrsus squalane concentration. Note that squalane concentrations used in the multiple step process shown here have been converted to wt.% using the squalane density (0.81 g/mL).

4.3.5 **Effect of different factors on the production of coatings by one-step deposition process**

4.3.5.1 Replacement of the impregnation oil

Further investigations were carried out by replacing squalane in the dispersions with silicone oil. The coated surfaces obtained by the one-step deposition technique using silicone oil (section 2.1.3) instead of squalane are shown in Figure 4.10.

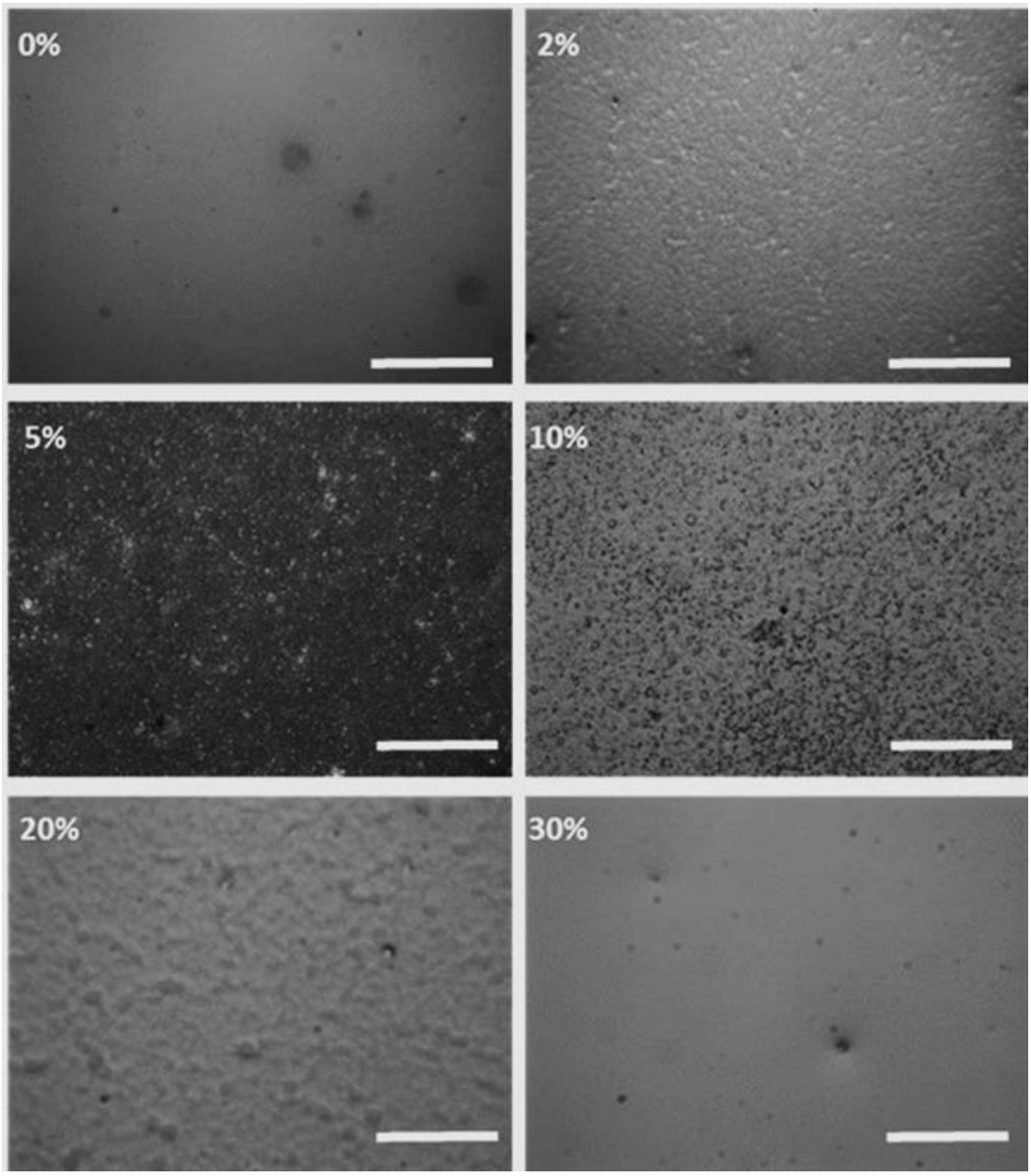

Figure 4.10 Microscopic images of the different coatings fabricated using 5% silica ethanol dispersion at different concentrations of silicone oil in the dispersions. Smooth oil flooded surface is shown on coating obtained from 30% dispersion. The concentrations of the dispersion are displayed on respective coatings. Scale bars represent 100 µm.

Similar to squalane, silicone oil impregnated coatings vary in morphology from a clear dry coating through translucent/opaque surfaces (e.g. 5%) to transparent oil impregnated

surfaces. Slightly different from squalane impregnated coatings, a smooth coated surface with a relatively constant contact angle with higher impregnated surfaces were obtained on coating produced from 30% silicone oil dispersion (Figure 4.11). This indicates that different oils can lubricate the surface more or less easily than squalane. The result obtained with the replacement of squalane with silicone oil is evidence that different non-volatile oils or lubricants can be used for impregnating structured porous surfaces depending on the intended applications of the materials.

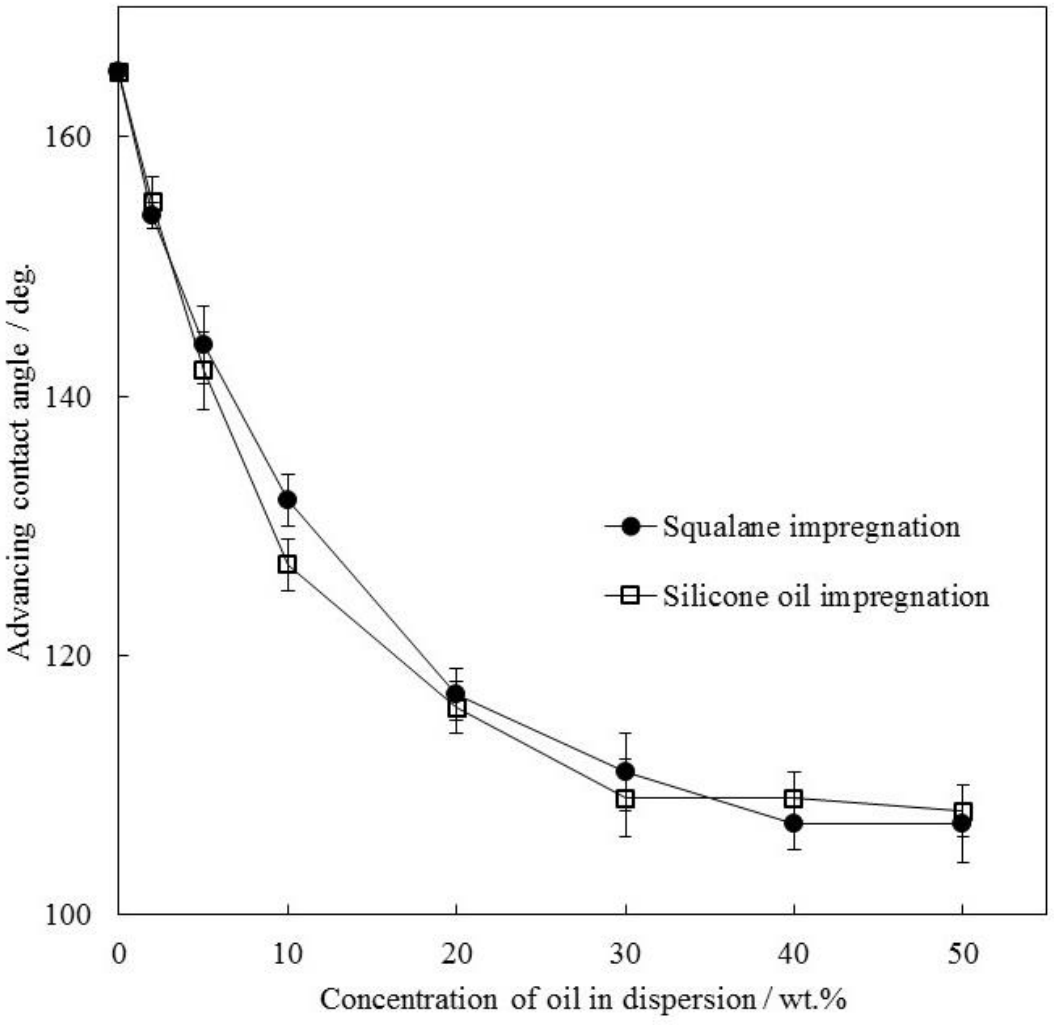

Figure 4.11 Comparison of advancing contact angle of water drops (in air) on coatings impregnated at different concentrations of squalane or silicone oil.

4.3.5.2 Effect of fumed silica concentration in the coating dispersion

Another adjustment for the control over the wettability of the fabricated coating was investigated by reducing the concentration of silica particle content of the dispersions from 5 to 3 wt.%. This change led to more squalane becoming available for the lubrication of a less amount of fumed silica particles compared to dispersions with 5 wt.% silica content. Based on this adjustment, coatings produced using 10% squalane dispersion was found to be slippery; high degree of stickiness shifted to lower concentration of the oil compared with the earlier investigations. Plots showing the effect of change in the concentration of fumed silica in the dispersions are presented in Figures 4.12 and 4.13, respectively.

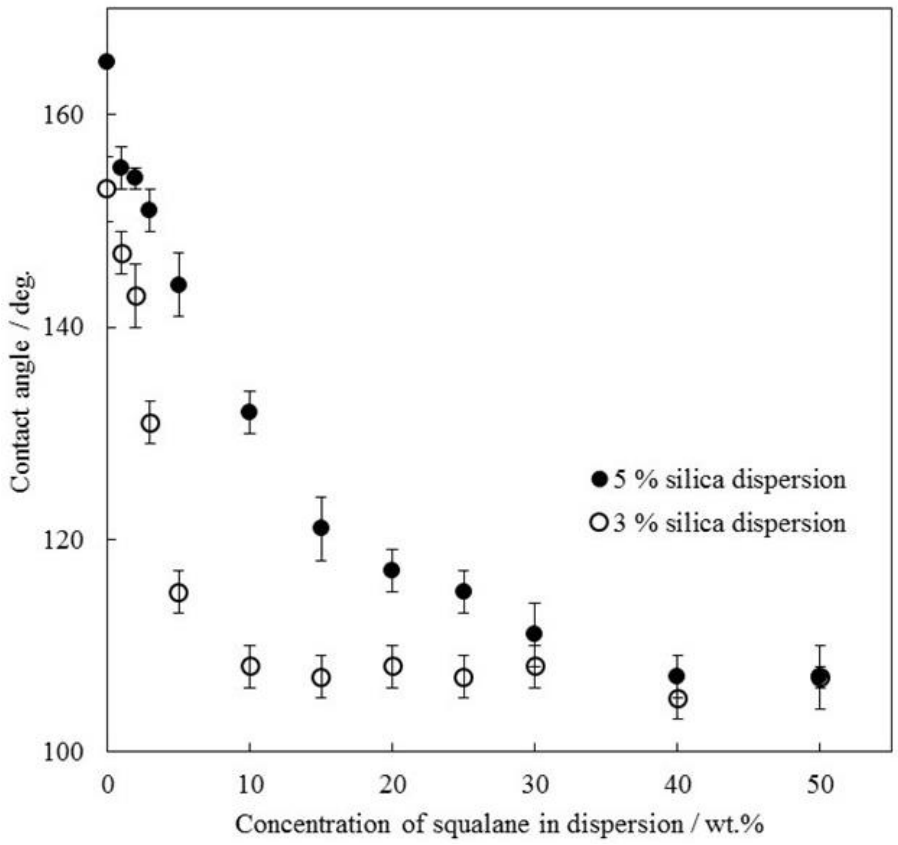

Figure 4.12 Effect of change in fumed silica contents of the dispersion (5 to 3 wt.%) on advancing contact angles of water drops on the resulted impregnated coatings in air at different concentrations .of squalane in the dispersions

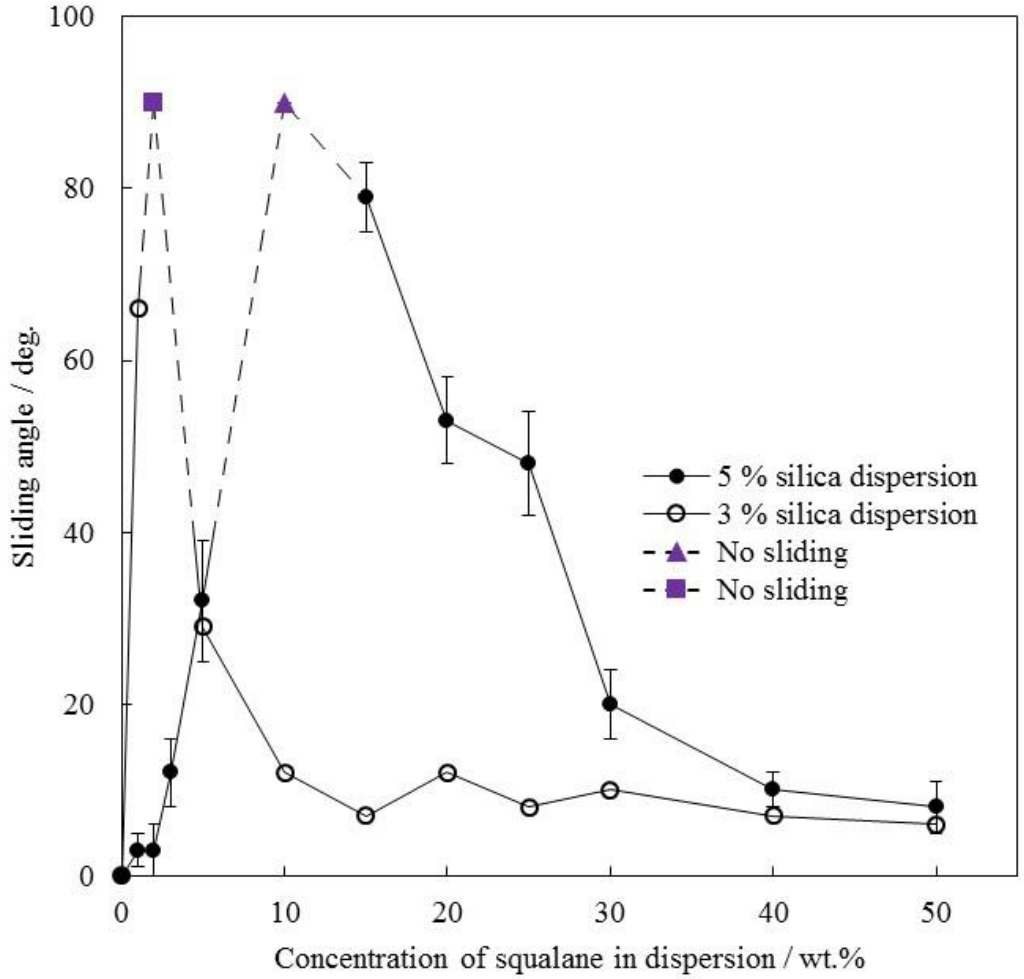

Figure 4.13 Sliding angles of water drops (12 ± 3 µL) in air on surfaces fabricated using 3 and 5 wt.% fumed silica dispersion at different concentrations of squalane in the coating dispersion.

From these results, it is obvious that fabrication with using the one-step method can allow the coatings to be controlled simply by manipulating the variable components of the dispersion used for coating the solid substrate.

4.3.5.3 Method of deposition used in the coating process

Apart from formulation tuneability, flexibility in machine or apparatus used in coating deposition is another attractive characteristic of the one-step method of preparation of oil-impregnated coatings. In addition to the spin and dip coating methods described earlier, the formulated dispersions were also introduced into spray vessels and coated onto solid substrates as described in the experimental section. Comparison of the wettability of the spray-coated surfaces with those produced by spin coating show no remarkable difference. Figure 4.14 shows advancing contact angles of water drops (in air) on coatings fabricated using spin coating and spray coating methods. The findings shows that the spraying dispersions for making coatings with specific wetting characteristics (superhydrophobic, slippery or sticky) can be formulated in advance or even tested on sites.

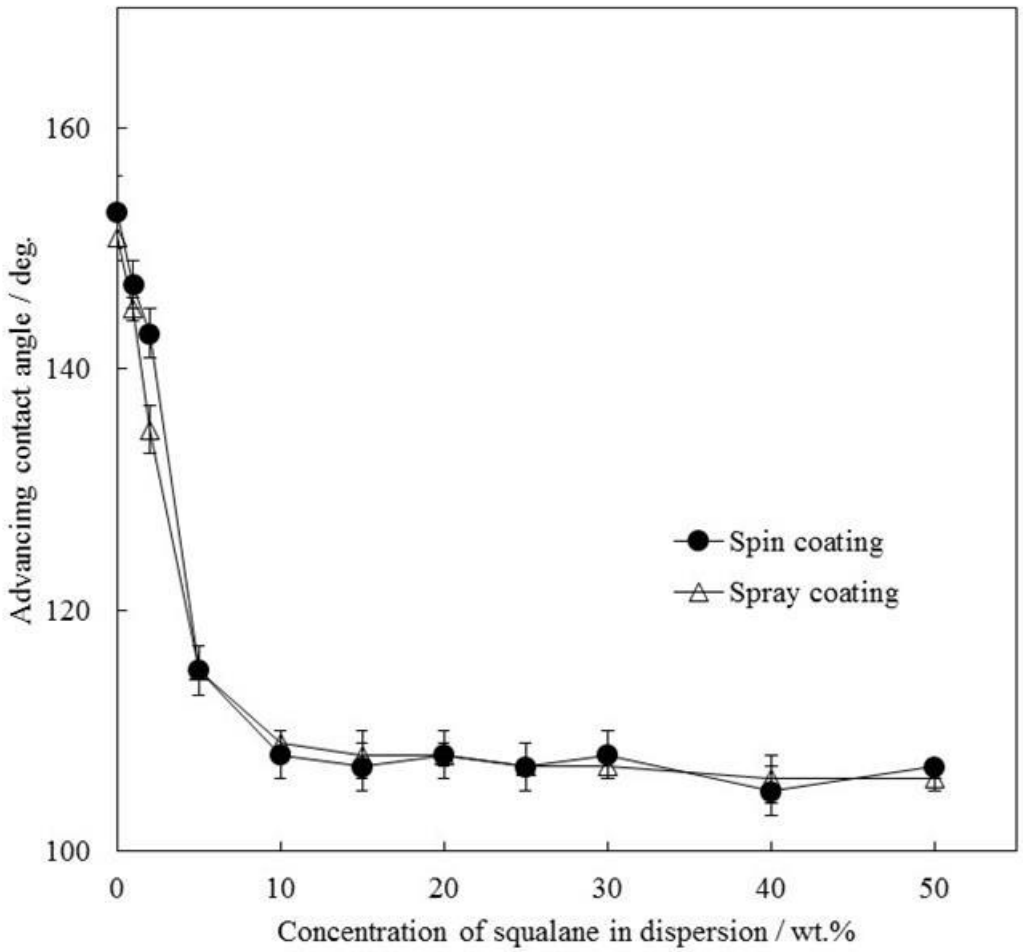

Figure 4.14 Advancing contact angles of water drops on coatings fabricated by spin coating or spraying of 3 wt.% fumed silica dispersions in ethanol loaded with different concentration of squalane.

The ability of using different techniques/apparatus for the fabrication makes the process versatile and very effective. Even with differences in the outputs operational processes, if such differences can be adjusted to achieve the results within reasonable cost, then such process can easily be transferred to the industry. For instance, if one type of equipment is capable of making a large turnover of materials, while another possesses higher precision and quality capabilities to produce the same material, when market demands great variety, the producer will be flexible enough to easily aligned or find alternatives to satisfy the market needs at different rates [14].

4.4 Conclusions

The findings presented here have demonstrated important practical points:

1. Superhydrophobic, sticky and slippery surfaces can be produced in a similar manner as the multiple step method used in Chapter 3 and commonly used in research laboratory by simply depositing appropriate non-volatile oil containing dispersions onto solid surfaces.
2. The preparation of oil-impregnated coatings by one-step deposition in which the coating dispersion is prepared by incorporating solid particles, oil and solvent into one system is not only simple but shows clear flexibility in production routes including, simple experimental adjustment as well as flexibility in the machine/apparatus such as: spin coating, dip coating, spray coating and brushing.
3. The simultaneous coating/impregnation employed by this technique is far simpler than known methods presently used for the fabrication of the newly invented slippery liquid infused porous substrates (SLIPS).
4. The fabrication technique is definitely a simple and good method for large scale production of coated solid layers and dispersions.

4.5 References

1. T. S. Horozov, R. Aveyard, J. H. Clint, and B. Neumann, Particle zips: Vertical emulsion films with particle monolayers at their surfaces. *Langmuir*, 2005. **21**(6): p. 2330-2341.

2. T. S. Horozov, B. P. Binks, and T. Gottschalk-Gaudig, Effect of electrolyte in silicone oil-in-water emulsions stabilised by fumed silica particles. *Physical Chemistry Chemical Physics*, 2007. **9**(48): p. 6398-6404.

3. B. P. Binks and T. S. Horozov, *Colloidal particles at liquid interfaces*. 2006: Cambridge University Press.

4. P. S. Clegg, *et al*., Emulsification of partially miscible liquids using colloidal particles: Nonspherical and extended domain structures. *Langmuir*, 2007. **23**(11): p. 5984-5994.

5. L. Becu, P. Grondin, A. Colin, and S. Manneville, How does a concentrated emulsion flow? Yielding, local rheology, and wall slip. *Colloids and Surfaces a-Physicochemical and Engineering Aspects*, 2005. **263**(1-3): p. 146-152.

6. T. F. Tadros, Correlation of viscoelastic properties of stable and flocculated suspensions with their interparticle interactions. *Advances in Colloid and Interface Science*, 1996. **68**: p. 97-200.

7. R. Chanamai and D. J. McClements, Dependence of creaming and rheology of monodisperse oil-in-water emulsions on droplet size and concentration. *Colloids and Surfaces a-Physicochemical and Engineering Aspects*, 2000. **172**(1-3): p. 79-86.

8. L. Gratton, T. López-Arias, G. Calza, and S. Oss, The whiteness of things and light scattering. *Physics Education*, 2009. **44**(4): p. 411.

9. M. Sadar. *Making sense of turbidity measurements-advantages in establishing traceability between measurements and technology*. in *2004 National Monitoring Conference, Chattanooga, TN, USA*. 2004.

10. K. N. Pearce and J. E. Kinsella, Emulsifying Properties of Proteins - Evaluation of a Turbidimetric Technique. *Journal of Agricultural and Food Chemistry*, 1978. **26**(3): p. 716-723.

11. A. Banerjee and D. Das, Fabrication of Highly Transparent Diamond-like Carbon Anti-Reflecting Coating for Si Solar Cell Application. *Solid State Physics: Proceedings of the 58th Dae Solid State Physics Symposium 2013, Pts a & B*, 2014. **1591**: p. 856-857.

12. S. G. Lee, D. S. Ham, D. Y. Lee, H. Bong, and K. Cho, Transparent superhydrophobic/translucent superamphiphobic coatings based on silica-fluoropolymer hybrid nanoparticles. *Langmuir*, 2013. **29**(48): p. 15051-7.

13. V. Interrante, H. Fuchs, and S. Pizer, Illustrating transparent surfaces with curvature-directed strokes. *Visualization '96, Proceedings*, 1996: p. 211-+.

14. D. Upton, What really makes factories flexible? *Harvard business review*, 1995. **73**(4): p. 74-84.

CHAPTER 5

FABRICATION OF COATINGS WITH TUNABLE WETTABILITY USING CURABLE SYLGARD 184

5.1 Introduction

Materials with tunable wettability are of interest due to vast potential applications. Successful control and applications of such material can only be achieve if the wetting properties the materials are clearly uncovered. In Chapter 3 the effect of gradual impregnation of squalane on porous silica coatings was investigated. Contact angle of water drops in air on these surfaces were found to decrease with increasing impregnation of the oil onto the coatings which was attributed primarily to gradual replacement of the original surface of the coatings by squalane. The superhydrophobic and slippery behaviour of the dry coatings and fully impregnated surfaces seemed less complex, but the reason behind the sticky behaviour of water drops on partially impregnated surfaces could not be well established. The difficulty was attributed to the inability to clearly image the liquid-impregnated surfaces with scanning electron microscope. After several failing efforts to uncover this interesting property of the surface, curable polydimethylsiloxane, PDMS (Sylgard 184, Dow Corning) has been found useful and brought into this present work to advance the investigations.

Generally, the unique properties of PDMS have made the material stand out in many valuable applications. The soft nature of cured PDMS elastomers is highly desirable in structural modifications and mimicry, especially in lithography [1-7]. The hydrophobic properties of the material are highly beneficial in many respects. In addition to being environmentally friendly, PDMS is inexpensive, elastic, self-sealable and transparent. PDMS stability in aqueous system is essential in the control of surface wettability

against water [8]. In order to benefit from the striking properties of PDMS various techniques have been used to transform it from hydrophobic to hydrophilic using different techniques (e.g. oxygen plasma treatment and UV treatments etc. [9]. Other areas of application of PDMS include cosmetics, for head lice on scalp [10], antifoaming agent in cooking oil [11] and as material in regenerative medicine (e.g. regenerative tissue) [12]. The shortcoming of PDMS is its tendency to swell in organic solvents such as hydrocarbons, toluene, and dichloromethane. Although swelling PDMS has found some applications [3], generally, it will render low performance when in use with these organic liquids. However, once such a solvent is evaporated or removed, the wettability of the PDMS is easily reverted to its hydrophobic state [8, 9, 13].

In addition to other properties of PDMS, it is observed that Sylgard 184 is a non-volatile hydrophobic liquid (non-polar) like squalane used in the previous study, and therefore a good replacement for it. Additional, and the most attractive property of the Sylgard 184 to this work, is the easy tendency of transforming it from liquid form to solid state by curing. In this Chapter, porous silica coatings are impregnated with liquid Sylgard 184 using only the polymer base (i.e. without curing agent present); the wettability of the coatings are investigated and compared with the previous findings. The coatings have also been impregnated using mixtures of the polymer base (part A) and the curing agent (part B). In the later impregnations, the impregnated Sylgard coatings have been polymerised to obtain the prototype or duplicates of the liquid impregnated surfaces in solid states. Examination of these cured impregnated surfaces under a scanning electrons microscope have brought clearer insights into the structural changes on partially impregnated nano-porous surfaces. The findings have further uncovered a new and effective method of surface modification using partial impregnation technique. Apart from these findings, silica-Sylgard coatings with greater stability and resistance to mechanical abrasion have been reported. We demonstrate that the wettability of

structured surface can be transform drastically from hydrophilic to superhydrophobic state by appropriate selection of impregnation solution without significant alteration in surface roughness.

5.2 Experimental

Partial impregnation of silica coatings was carried out using Sylgard 184 as impregnating oil. The impregnation with Sylgard was divided into two experimental sections: impregnation with the pre-polymer base and impregnation with a mixture of polymer base and the curing agent (detail descriptions are presented in Section 2.2.7). The wettability of the impregnated coatings was assessed by measuring the contact angle of water drops on the coatings in air as described previously. Changes in surface structures of the cured impregnated coatings were characterised by Scanning Electron Microscopy (SEM). Stability of the Sylgard impregnated coatings was investigated using scratch tests as described in Section 2.2.14. Application of partial impregnation process for the hydrophobisation and tunability of structured surfaces including, glass, thin layer chromatographic plates, fumed aluminium oxide coatings, metal and paper surfaces.

5.3 Results and discussion

5.3.1 Impregnation with pre-polymer base of Sylgard 184

Results for wettability of the surfaces impregnated with the pre-polymer base of Sylgard 184 (without curing agent) at different concentration of Sylgard solutions in hexane are presented in Figure 5.1.

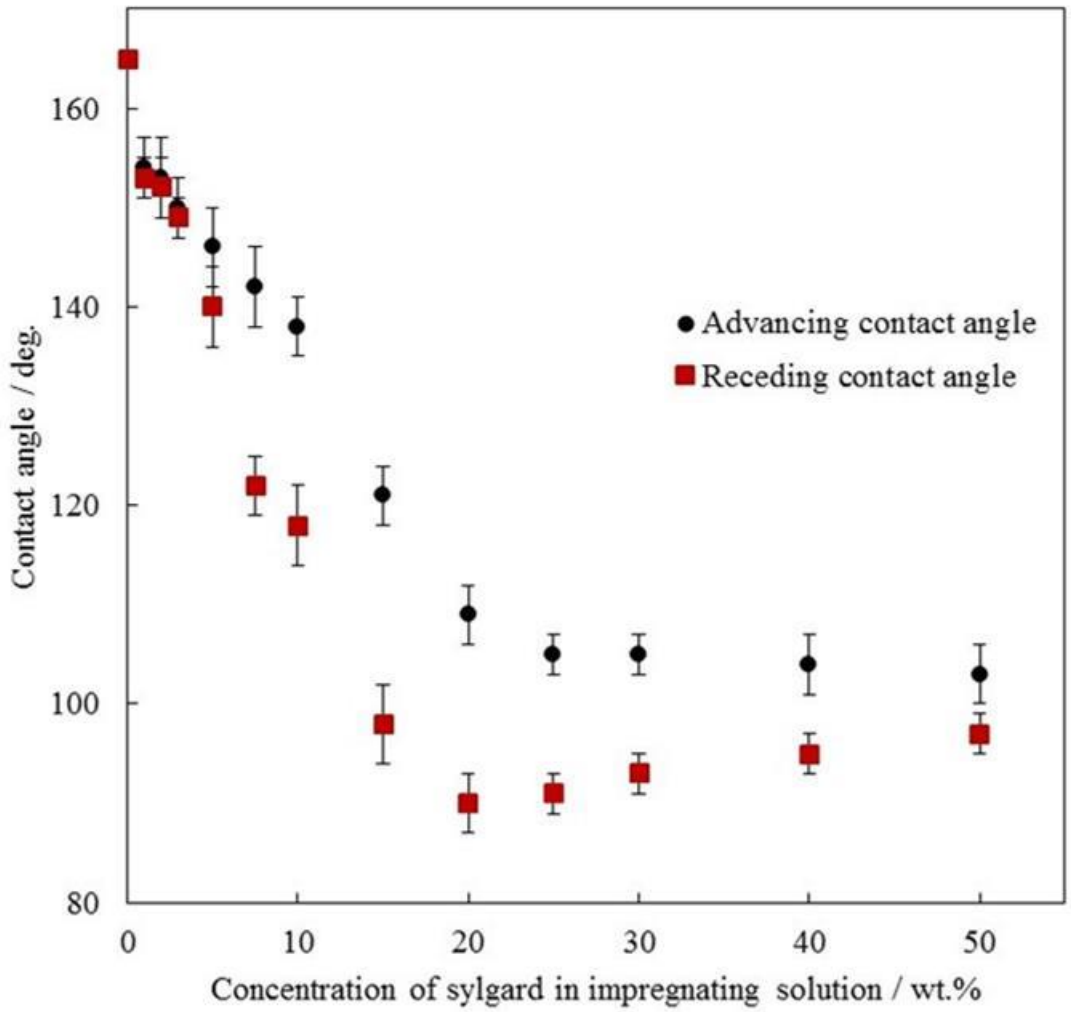

Figure 5.1 Advancing and receding contact angles of water drops on Sylgard-impregnated coatings in air versus the concentration of Sylgard in the impregnated solutions. In the above results, the impregnated Sylgard solutions are without the curing agent and the impregnated Sylgard therefore remained as liquid on the hydrophobic fumed silica coatings after the evaporation of hexane.

As can be observed in Figure 5.1, coated surfaces impregnated with very low concentrations of Sylgard solutions are superhydrophobic with high contact angle of water drops, but the contact angle decreases with increasing concentration of the Sylgard solution. The finding shows similar trend to squalane or silicone oil impregnated surfaces earlier studied Chapters 3 and 4.

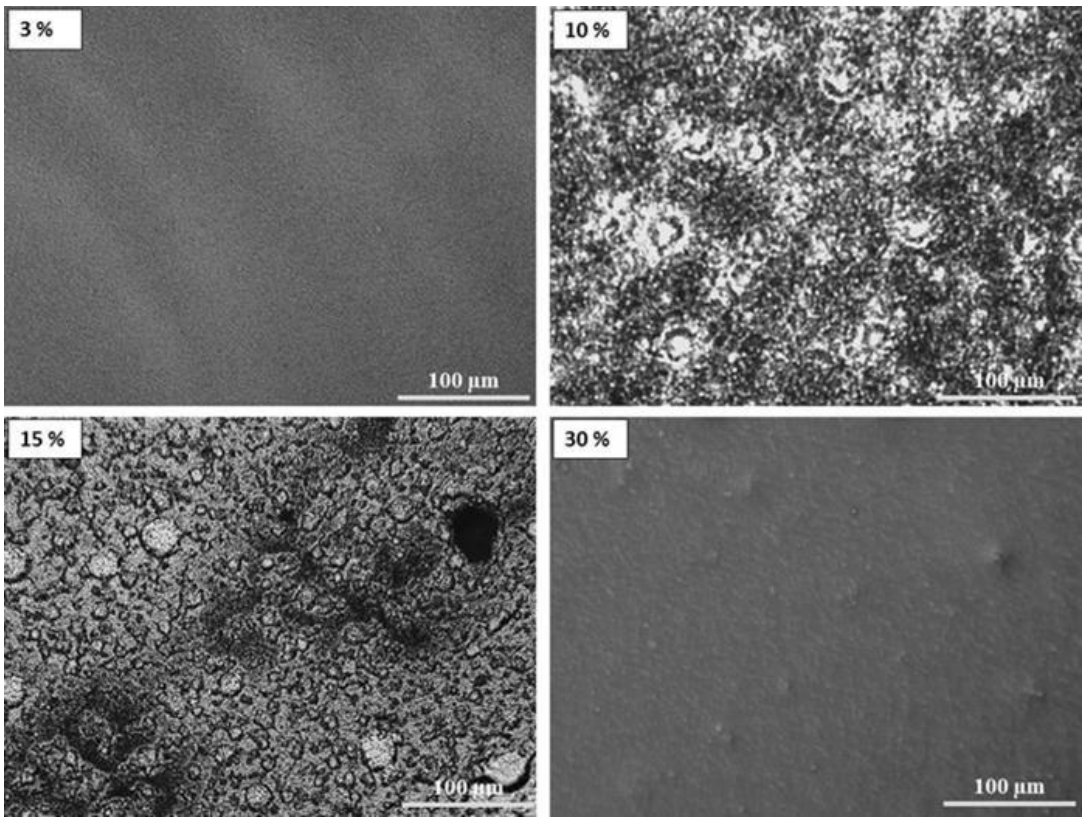

Figure 5.2 Microscope images Sylgard-impregnated silica coatings prepared from 5 wt.% hydrophobic fumed silica dispersion in ethanol and spin-coated onto microscope glass slides, and then the coatings were impregnated with different concentrations of non-curable Sylgard solutions (without the curing agent).

Microscope images of selected Sylgard impregnated coatings are presented in Figure 5.2. These images also show similarity in morphology, coatings impregnated with less amount of oil and over-coated oil are transparent in visible light and are shown with minimal interferences. Surface morphology of coatings impregnated with a limited amount of Sylgard solutions (10-20 wt.%) looks highly textured and cannot be clearly viewed. This is yet another similarity of these surfaces compared with those obtained when squalane and silicone oil solutions were used. Thus in addition to other properties of Sylgard that will be investigated in this current Chapter, the observed similarities of Sylgard on the silica-coated surfaces to those of squalane make it a good replacement candidate to mimic and probe our earlier investigations.

5.3.2 **Preparation and wettability of cured coatings**

In the previous Section, the impregnated liquid Sylgard was not cured. However, using curable Sylgard solutions with both pre-polymer base and curing agent present (10:1 ratio, respectively), allows for the impregnated liquid to be transformed to solid state after curing. Also, proper examination of the surface morphology the resulting impregnated coatings using SEM as will be shown in subsequent sections were achieved. The contact angles of water drops in air placed on these cured Sylgard impregnated coatings are shown in Figure 5.3.

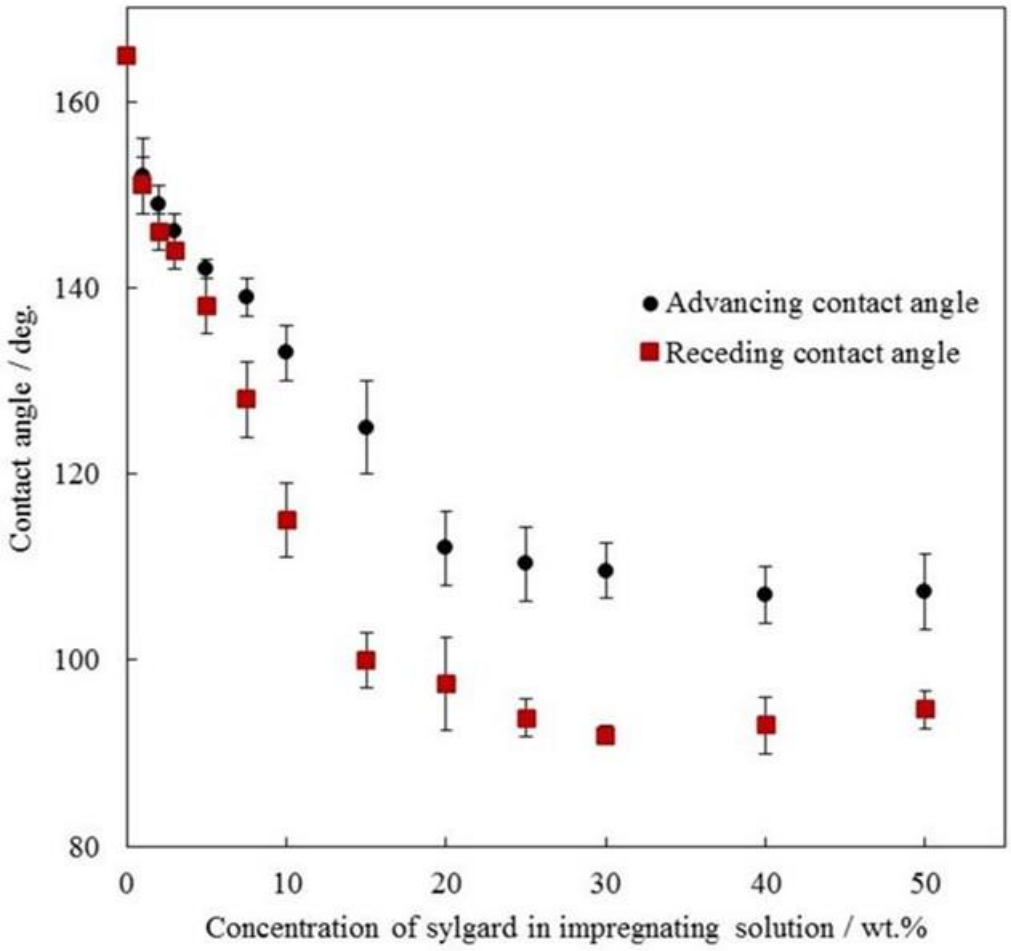

Figure 5.3 Advancing and receding **w**ater drops contact angles in air placed on coatings impregnated with different concentrations of Sylgard solutions and then cured to solid state. The horizontal axis shows the concentration of the Sylgard solution used for the impregnation of the coatings. Here Sylgard remains solid on the surface.

The wettability of the cured surfaces, as can be seen in Figure 5.3, tends to follow that of the liquid impregnated surfaces. Both coatings show high contact angles on surfaces partially filled with oil, however, higher contact angle hysteresis is observed on cured coating especially on those impregnated with higher amounts of oil. The differences are due to the fact that the pinning of the three phase contact line is less pronounced on coatings covered with liquid Sylgard than the ones impregnated with solid Sylgard (cured). Wettability data for both the uncured and cured Sylgard impregnated coatings are summarised in Table 5.1.

Table 5.1 Advancing and receding contact angles, and contact angle hysteresis of water drops in air on liquid and cured Sylgard 184 impregnated coatings at different concentrations of the impregnating Sylgard solutions in hexane**.**

[Sylgard solution] / M	Liquid Sylgard impregnated coatings			Cured Sylgard impregnated coatings		
	Advancing contact angle / deg.	Receding contact angle / deg.	Contact angle hysteresis / deg.	Advancing contact angle / deg.	Receding contact angle / deg.	Contact angle hysteresis / deg.
0	165 ± 5	165 ± 5	0	165 ± 5	165 ± 0	0
1	154 ± 3	153 ± 5	1	152 ± 4	151 ± 3	1
2	153 ± 4	152 ± 3	1	149 ± 2	146 ± 2	3
3	150 ± 3	149 ± 2	1	146 ± 2	144 ± 2	2
5	146 ± 4	140 ± 4	6	142 ± 1	138 ± 3	4
7.5	142 ± 4	122 ± 3	20	139 ± 2	128 ± 4	11
10	138 ± 3	118 ± 4	20	133 ± 3	115 ± 4	18
15	121 ± 3	98 ± 4	23	125 ± 5	100 ± 3	25
20	109 ± 3	90 ± 3	19	112 ± 4	98 ± 5	15
25	105 ± 2	91 ± 2	14	110 ± 4	94 ± 2	17
30	105 ± 3	93 ± 2	12	110 ± 3	92 ± 1	18
40	104 ± 3	95 ± 2	9	107 ± 3	93 ± 3	14
50	103 ± 3	97 ± 2	6	107 ± 2	95 ± 2	13

5.3.3 Surface morphology of cured Sylgard impregnated coatings

Optical images of cured Sylgard impregnated coatings are presented in Figure 5.4. From the images, interferences associated with the oil impregnated surfaces are considerably reduced especially on moderately impregnated surfaces. A careful look at the images shows that they are clearer and the surface structures are more distinctive than liquid oil impregnated surfaces. However, the distribution of the oil on the micro-structured surfaces is not well visualised due to the limited magnification of the optical microscope used.

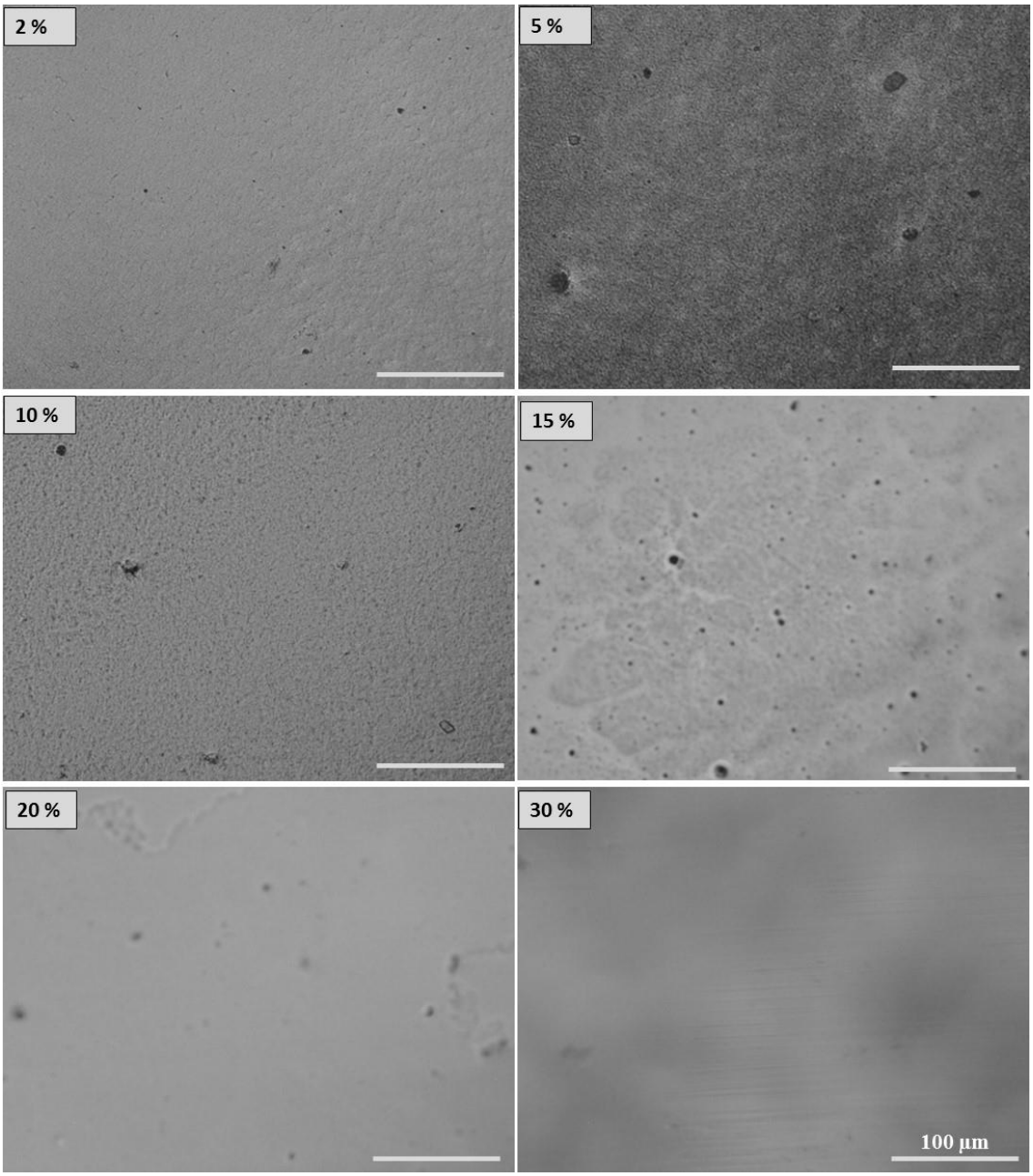

Figure 5.4 Optical images of cured coatings impregnated with different concentrations of Sylgard solutions. Each coating is label with the concentration of the Sylgard solution used for its impregnation. All scale bars represent 100 µm.

Detailed morphologies of the nano-porous coatings shown in Figure 5.4 were recaptured at higher magnification using scanning electron microscope. The SEM

images of the coatings are presented in Figures 5.5 - 5.7. At lower concentrations, the effect of the impregnation was less and the surfaces particles are clearly seen. Closer observation on moderately impregnated surfaces (e.g. 10, 15%) shows that the surface particles on the coatings are thinly coated with the oil. Also on these coatings, inter-particle gap are nearly bridged by the impregnated oil leaving wider spaces between the surface aggregates which are not fully bridged. However, surfaces roughness is still present on the coating. With 20 and 30% solutions, both the individual particles, aggregates and the gaps between them are fully covered, but the thickness of the impregnated liquid on 20% seems to be too thin to fully eliminate the surface roughness. Coatings impregnated with 30 wt.% and beyond are noticeably smoother than other ones with low impregnated with low oil fractions.

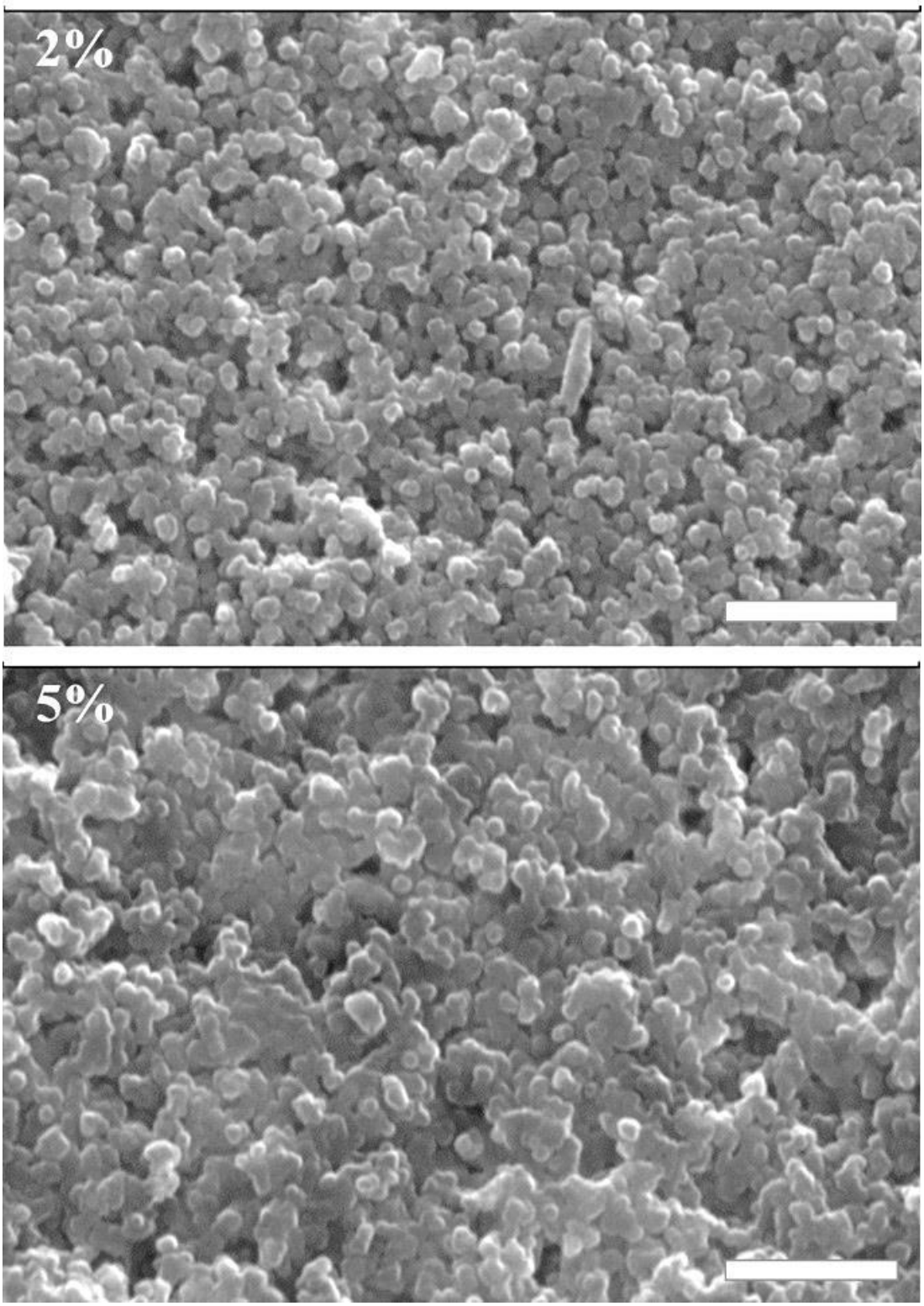

Figure 5.5 SEM images of cured coatings impregnated with 2% and 5% Sylgard solutions. Each coating is labelled with the concentration of the Sylgard solution used for its impregnation. All scale bars represent 1 μm.

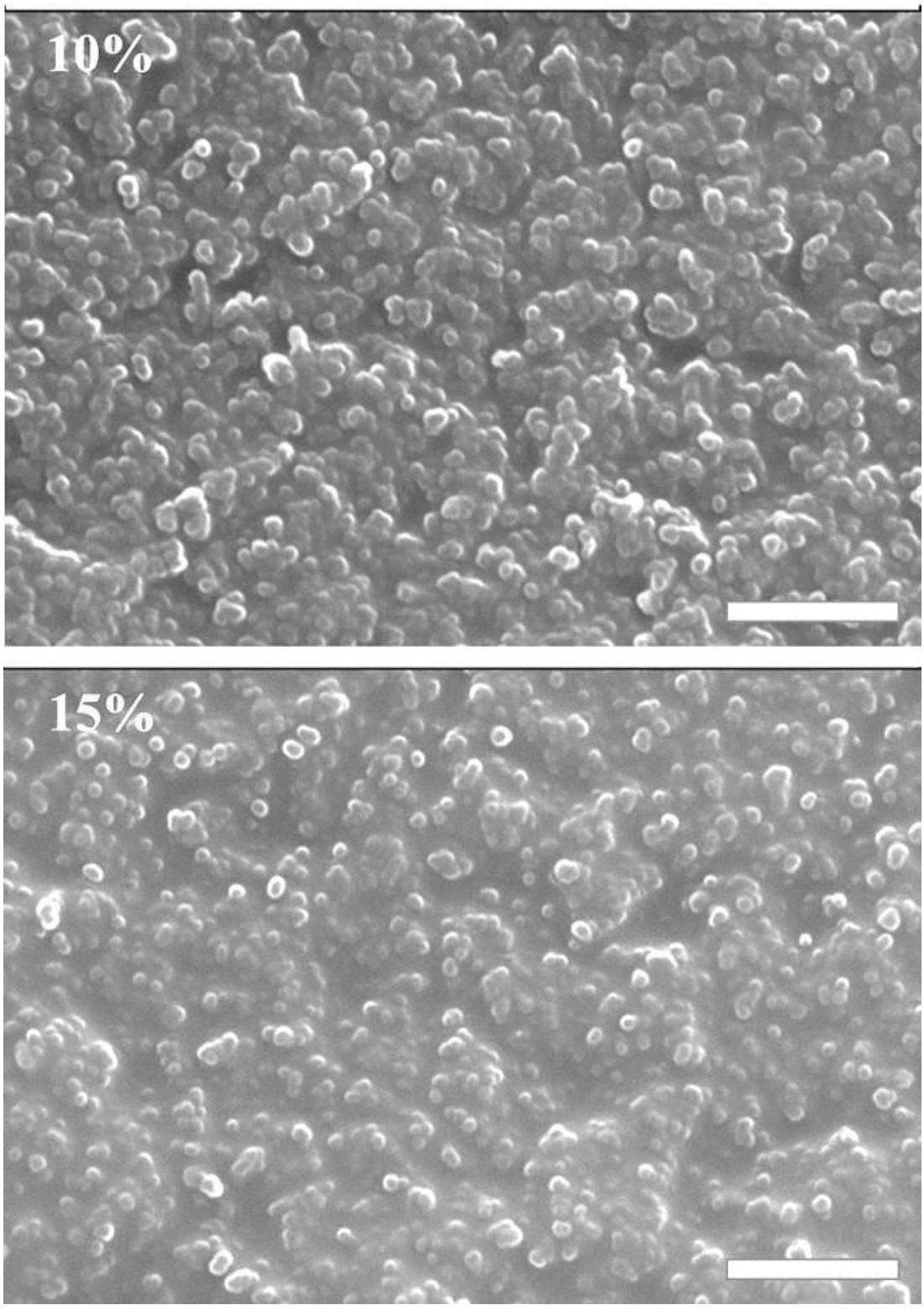

Figure 5.6 SEM images of cured coatings impregnated with 10% and 15% Sylgard solutions. Each coating is labelled with the concentration of the Sylgard solution used for its impregnation. All scale bars represent 1 μm**.**

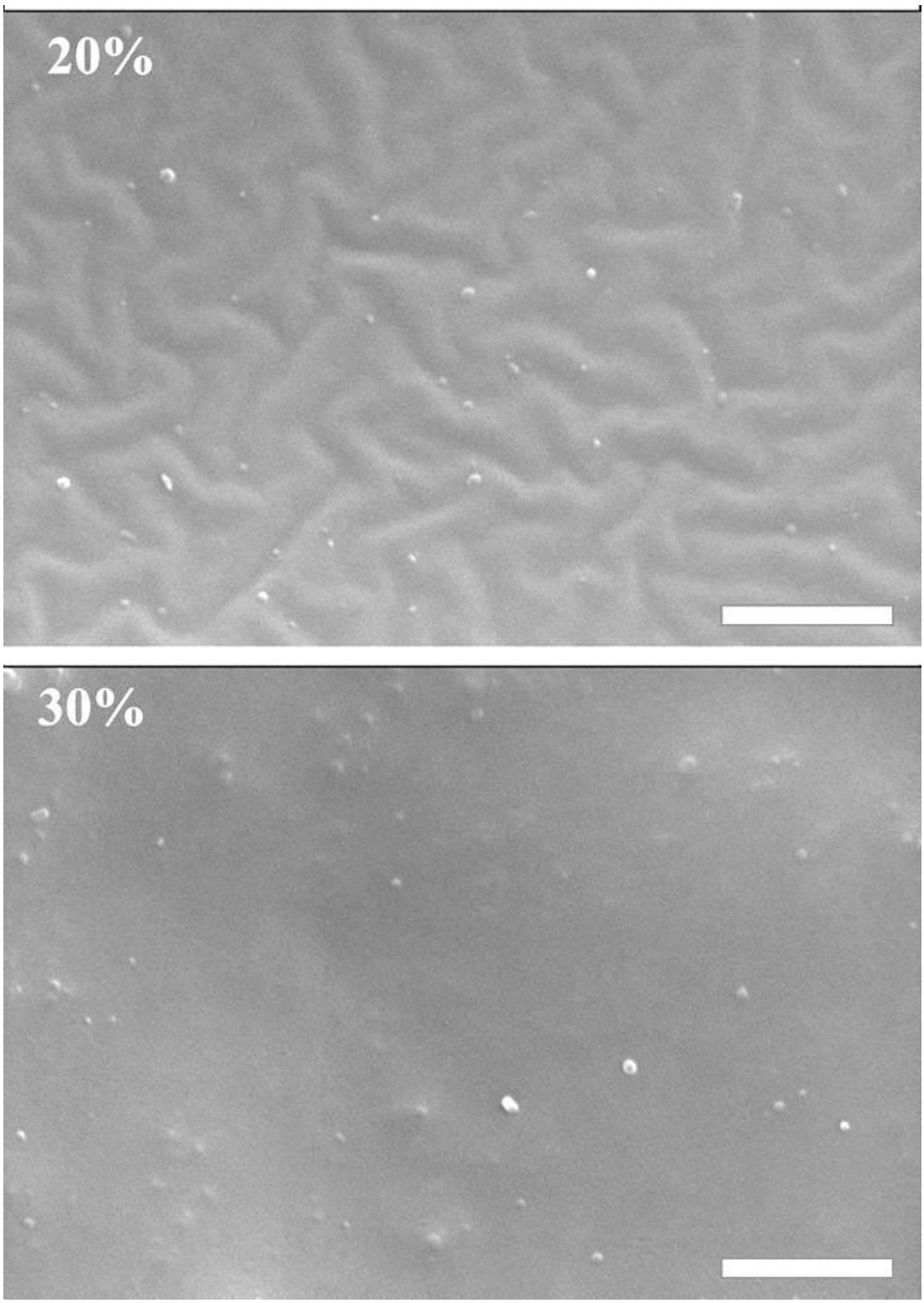

Figure 5.7 SEM images of cured coatings impregnated with 20% and 30% Sylgard solutions. Each coating is labelled with the concentration of the Sylgard solution used for its impregnation. All scale bars represent 1 μm.

5.3.4 **Stability of uncured and cured Sylgard impregnated coatings**

An organic/inorganic hybrid-polymer have greater potential for future coating systems, is known to offer special advantages such as a chemical and mechanical stability and scratch resistance due to the inorganic network and high elasticity of the organic polymer [14]. Studies have shown that PDMS has good adhesion to glass, aluminium, and other solid substrates [14, 15]. In this study the stability of the liquid and cured Sylgard impregnated coatings are investigated as described in the experimental Section and the impact of scratches on the coatings were observed and used to measure the stability of the coated surfaces. The optical images of the coatings taken after the scratch tests are shown in Figure 5.8.

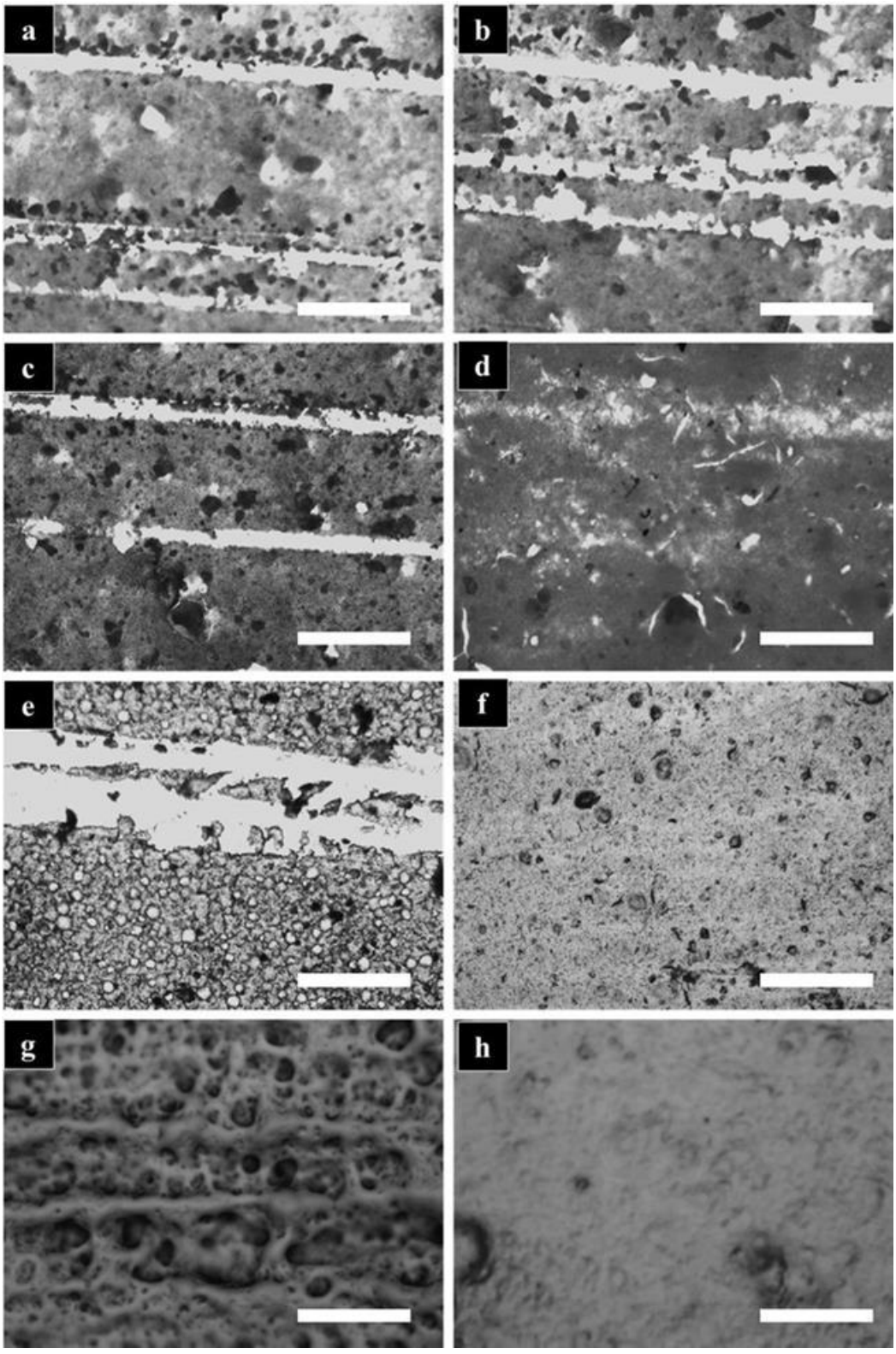

Figure 5.8 Scratch test on cured (right) and uncured (left) porous fumed silica coatings impregnated with different concentrations of pre-polymer base and curable Sylgard 184 solutions in hexane: (a, b) 2%, (c, d) 5%, (e, f) 10%, (g, h) 30%. Each scale bar represents 100 μm.

Images show that at lower Sylgard concentrations, both cured and uncured coated surfaces can be observed to succumb to scratches. The scratches are still observed on uncured surfaces impregnated with 5 and 10 wt.%. In contrast, cured coatings impregnated with 5 wt.% solution offers significant resistance to scratches, and on the one impregnated with 10 wt.%, the scratch marks are very faint and so is the coating impregnated with 30 wt.% solution. The strong resistance to scratches by the cured coatings are certainly due to the adhesive bond between the silica particles, the glass substrates and Sylgard. Figure 5.9 shows cross section of a cured coating that was impregnated with 5 wt.% Sylgard. The SEM image reveals the substructure of the silica particle which are cemented in some portions by a jelly-like film known to be the cured Sylgard and the glass.

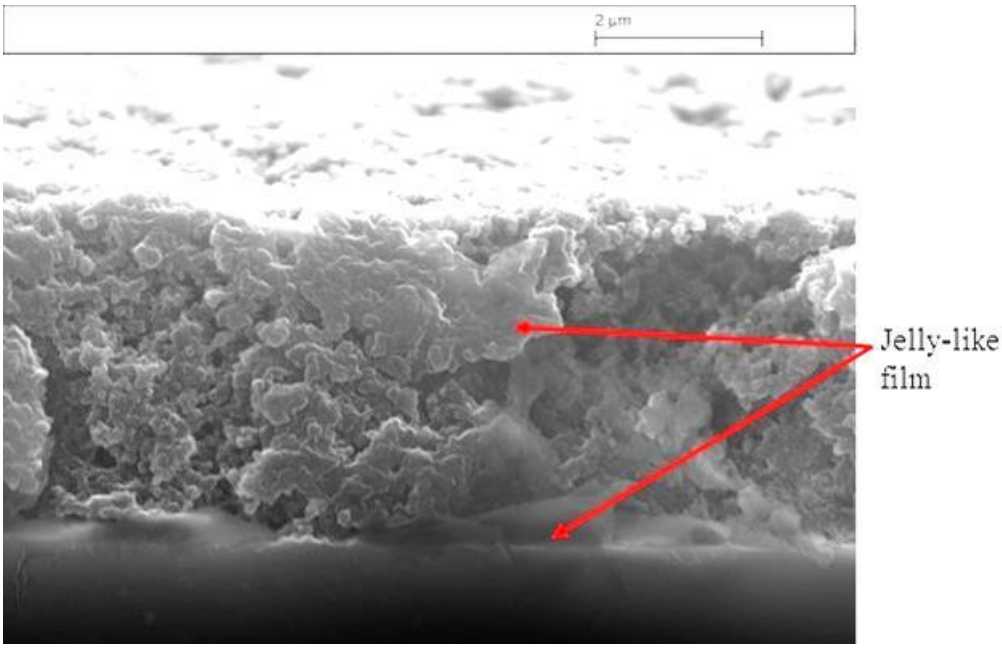

Figure 5.9 SEM image of the cross section of fumed silica coated film that has been impregnated with 5 wt.% Sylgard solution and cured at 150 ℃. The substructure of the film is united in within and to the substrate (glass) by a polymer of cured Sylgard which enhances the film stability.

The scratch test on uncured coatings impregnated with 30 wt.% Sylgard only generate scratch marks that are time dependent. The images of the coating shown in Figure 5.8 were taken within approximately 30 s after the scratching. The timing became necessary due to immediate self-healing on fabricated surfaces loaded with higher amount of liquid Sylgard. The self-healing process of the coating is illustrated in Figure 5.10. The feature which can be attributed to the flow tendency of the liquid oil on the coated surface, is an outstanding positive characteristic of slippery liquid infused porous substrates, SLIPS.

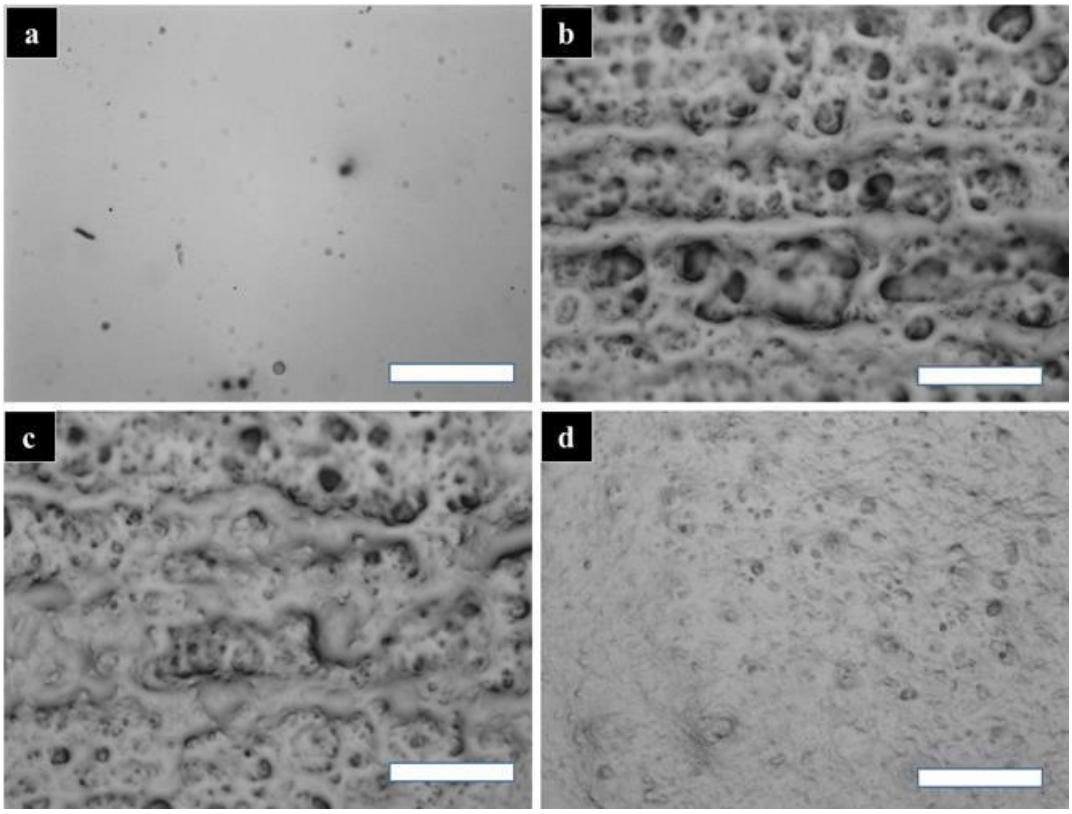

Figure 5.10 Scratch test on the surface impregnated with 30 wt.% Sylgard solution showing progressive changes/self-healing on the surface of the coating: (a) before scratching; (b) 30 s after scratching. (c) 60 s after scratching; (d) 2 h after the scratching. Immediately after scratching, the liquid oil moves into the damage portions of the coating (b), overflow the bank and tend to cement the neighbouring layers (c). After 2 h, the damages on the coatings are remarkably healed (d). All scale bars represent 100 µm.

The observed stronger stability of the cured Sylgard coatings is supported by the earlier investigations [16, 17]. Satyanarayana *et al.* reported a PDMS adhesive bonding process that proved reliable to overcome the disadvantages of the traditional expensive Micro-electromechanical systems (MEMS) wafer bonding processes that have been borrowed from the integrated circuit (IC) industry. According to the authors, the attractive features of the PDMS bonding technique include: low/room temperature, multi-material compatibility, reversibility and biocompatibility, and described the bonding process as an easy and versatile process for bonding PDMS, glass, silicon and silicon nitride surfaces [16]. Similarly, Cayre and Paunov have employed the adhesive bond offered by curable polydimethylsiloxane to pull out trapped hydrophobic silica particles at the surface of the aqueous gel in the so called 'gel trapping' technique [17]. Our results show that a combination of silica-Sylgard on glass can offer robust protective layer depending on the applications.

5.3.5 Re-examinations of wetting properties of fumed silica porous coatings impregnated with non-volatile oil

Understanding and the descriptions of the water wettability on different coated surfaces impregnated with squalane especially on moderately impregnated coatings was hampered by the inability to clearly observe the surface structures of the liquid impregnated coatings. From the results of the investigations presented in the preceding Sections, more detailed information on the surface structures of cured Sylgard impregnated coatings which is serving as the prototype of our earlier investigated coatings have been obtained using the SEM. Earlier, impregnated surfaces were classified into superhydrophobic, sticky and slippery surfaces based on water drop interaction on these surfaces. The possible causes of various behaviours of water drops on the surfaces are re-examined and discussed in the subsections below.

5.3.5.1 Superhydrophobic surfaces

Figure 5.11 shows SEM images of both the top and side views of dry coatings and coatings impregnated with 2 wt.% Sylgard solution. Careful observation of the coatings shows no noticeable change in morphology compared with the images of the dry coating without oil impregnation. Microstructures of the coatings including the tiny fused particles as well as the bigger aggregated particles are clearly shown. The exposed pores are empty, as it can be seen through to several particles underneath. The side view of the coating also indicates individual particles of the coating from the bottom to the highly roughened top surface. Thus, the hierarchical nature of the film is maintained. It is therefore certain that these empty spaces between the particles and aggregates accumulate air which together with the hydrophobic fumed silica particles imparts superhydrophobicity as earlier described in Chapter 3. This means that the extent and effect of impregnating with 2 wt.% oil solution is not enough to seriously interfere with the structure and the original superhydrophobic state of the dry coatings.

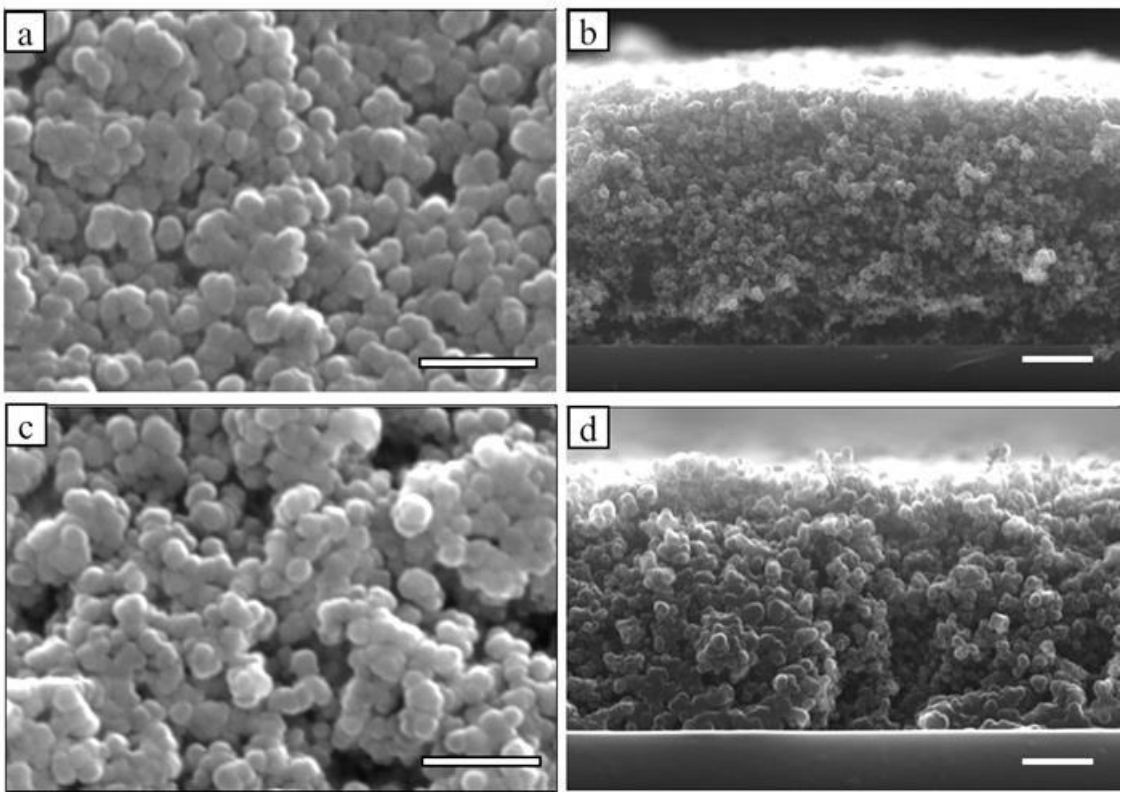

Figure 5.11 Top and side views of superhydrophobic fumed silica coatings impregnated with 0% (a, b) and 2% (c, d) Sylgard solution and cured at 150 ℃, respectively. The surface particles are clearly distinctive and the pores are empty. Individual particles of the coating from the bottom to the highly roughened top surface are also separable without noticeable bridging by the impregnated Sylgard. Scale bars (a, c) represent 500 nm and (b, d) represent 100 nm.

5.3.5.2 Sticky surfaces

In the earlier investigation (Chapter 3), the stickiness of the water drops was found to increase with increase in the oil impregnation. As can be observed in Figures 5.5 – 5.7, the increase in the impregnation of the dry fumed silica coating with the oil leads to gradual closure of the porous networks of the coatings. The extent of oil infiltration into the coatings with 10 wt.% oil solution is shown in Figure 5.12. In Figure 5.12a (top view), individual particles of the film that are distinctive on superhydrophobic film are bridged by the oil or Sylgard layer. In addition to the elimination of the roughness offered by the smaller particles by the oil layer, the exposed pores/gaps between the

bigger aggregates are remarkably filled by the oil and the depths reduced. The elimination of most of the nano-scale of roughness associated with the smaller particles by the oil bridges leads to a new but larger scale (microscopic scale) roughened topography that is mainly linked to oil or Sylgard-cemented aggregates. The implication of this change is the loss of hierarchical nature of film which is synonymous to superhydrophobicity. The image shown in Figure 5.12b (side view) seems that the porous network of the coating is totally filled from the bottom leaving the coating with no or limited pores deep below. Hence, the relatively high contact angle (up to a 130°) observed on coatings impregnated with 10 wt.% oil solution can principally be attributed to the roughness the resulting surface. However, the micro-structures on these surfaces tend to loss of some of the dual scale of nanoscopic-microscopic scales of roughness to a larger microscopic scales compared to the ones on dry coatings (see Figure 5.11). Considering these large scale of roughness, Wenzel mode of wetting, which is associated with stickiness, or high contact hysteresis, is most likely the cause of large hysteresis and adhesion tendencies on these surfaces.[18-21].

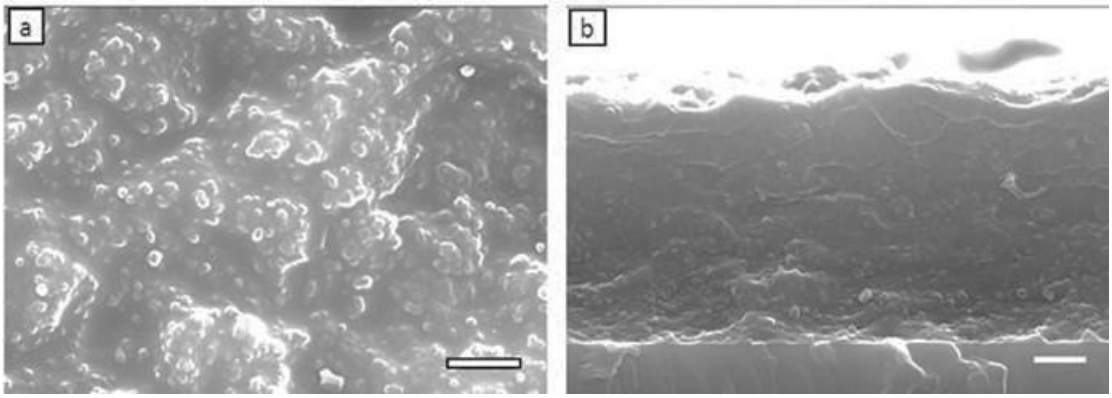

Figure 5.12 Top and side views of sticky fumed silica coating impregnated with 10% Sylgard solution and cured at 150 ℃. The surface nano-scale particles are clearly bridged and the pores are filled by Sylgard. The surface roughness comes mainly from the Sylgard bridged aggregates and the wider gaps between them. The porous network between particles of the coating from the bottom to top surface is remarkably closed and the top surface as shown by (b) is characterised by larger-scale roughness.

The above observation in the SEM images, reminds one of the previous finding in Chapter 4 where the initial increase in the surface impregnation decreases the transparency of the coating from superhydrophobic to sticky surfaces. It has been reported that as the scale of surface roughness is increased, the scattering of light also increases, therefore diminishing the transparency of a material. This is because visible light is in the range 350–750 nm, to maintain complete transparency to visible light; a surface would have to have features less than 100 nm [22].

5.3.5.3 Slippery surfaces

SEM images of the coatings impregnated with 30 wt.% solution of Sylgard confirm our earlier findings that the impregnated coatings which exhibited slippery effect were fully over-coated with the oil. In addition, unlike sticky surfaces, it is worth noting that the surface is over-coated with a significant layer of the oil to fully eliminate the surface roughness. The oil as seen in the images renders the surfaces of the coating very smooth (Figure 5.13a) and relatively flat as seen in the side view of the coating (Figure 5.13b). And because the surface is only covered with the oil, the water drops the surface are likely to display the characteristic contact angle of the impregnating liquid as was confirmed. The slippery nature of the oil makes water drops sliding easy at the slightest inclination.

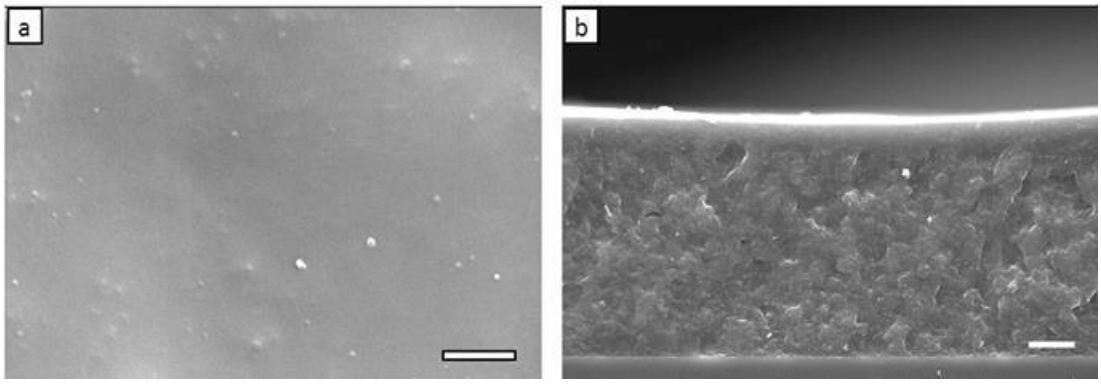

Figure 5.13 Top and side views of slippery fumed silica coating impregnated with 30 wt.% Sylgard solution and cured at 150 ℃. The surface nano-scale particles are completely covered. The surface is relatively smooth (a) and flattened with by the overcoated Sylgard layer (b).

5.3.6 Deposition of an ultra-thin cured PDMS layer on solid surfaces by partial impregnation process

From the SEM investigations, it is clear that the impregnated oils are thinly coated onto the surface structures, and then build up with increasing concentration of the oil to a larger thickness which finally fills the surface pores and then continues to increase. Thus, partial impregnation employed in this work can effectively be used to tune the thickness of coated layers on material surfaces. The thickness of coatings on solid, including ultra-thin coatings, can play very significant roles in material applications [23, 24].

As the impregnated oil thickness increases with oil concentration, it is certain that very thin coated layer of the impregnating liquid will be realised by also using a very low concentration of the liquid. In this work, it was therefore predicted that if the thickness of the coated Sylgard is thin enough to follow the surface roughness without bridging

the surface structures (nano/microscale), then the impregnated liquid can be used to modify the material provided the coated material remains stable on the surface. Considering the case of using squalane or Sylgard with hydrophobic status, a high contact angle of water drop is therefore expected. However, this effect has not been well noticed in the previous investigations. The negligible effect of this likelihood, as will be seen in later part of this Section, is because the surfaces of the coating is already hydrophobic, further deposition of the hydrophobic oil layer on the surface particle resulted in no observable change.

To uncover the prediction, structured hydrophilic silica based materials (e.g. TLC plates, sintered glass disc and roughened glass slide) oxide coatings were subjected to partial impregnation using low concentrations of Sylgard solutions. Initially, commercially available hydrophilic thin layer chromatographic (TLC) plates which are similarly porous as fumed silica coated surfaces were used for the tests. Figure 5.14 shows images and the rate at which the surface of the hydrophilic TLC plate adsorbs water drop in contact with it. It was observed that within a second water spreads and makes a film on the TLC plate surface indicating the superhydrophilic state of the plate.

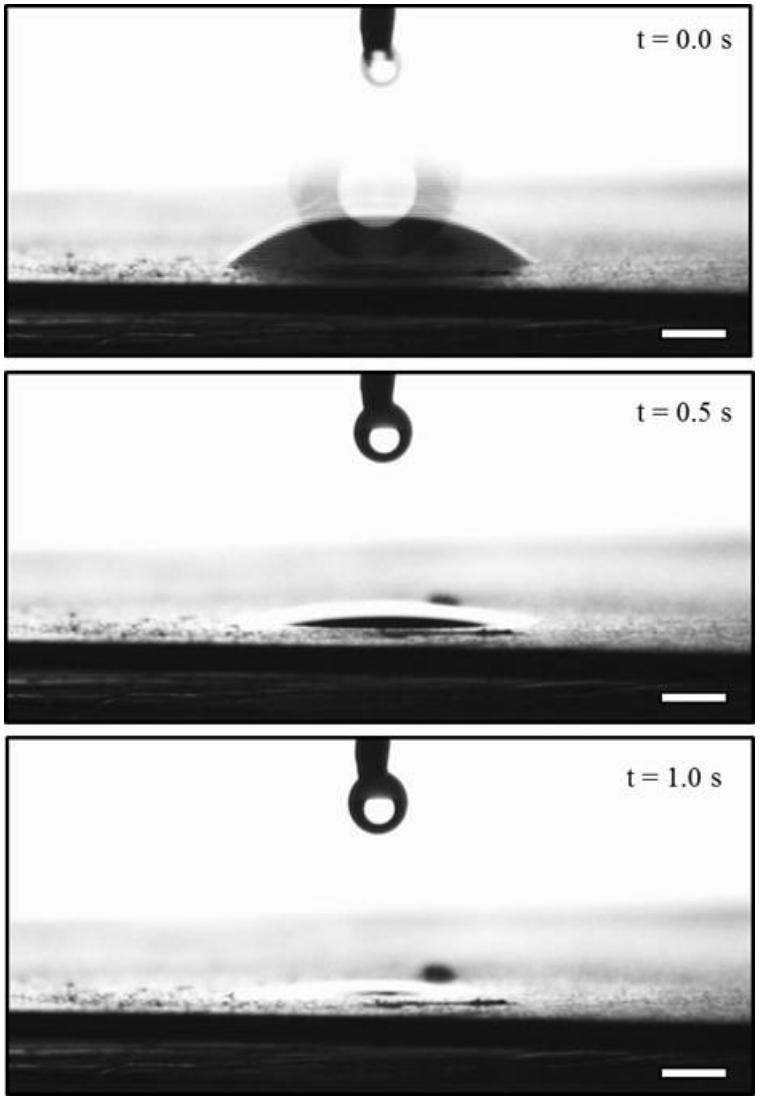

Figure 5.14 Still images from a movie showing wettability of water drop (in air) on hydrophilic thin layer chromatographic plate with time. All bars = 1 mm

Figure 5.15 shows images and behaviour of a water drop gently placed on a TLC plate which has been impregnated with 1 wt.% of pre-polymer base of Sylgard 184.

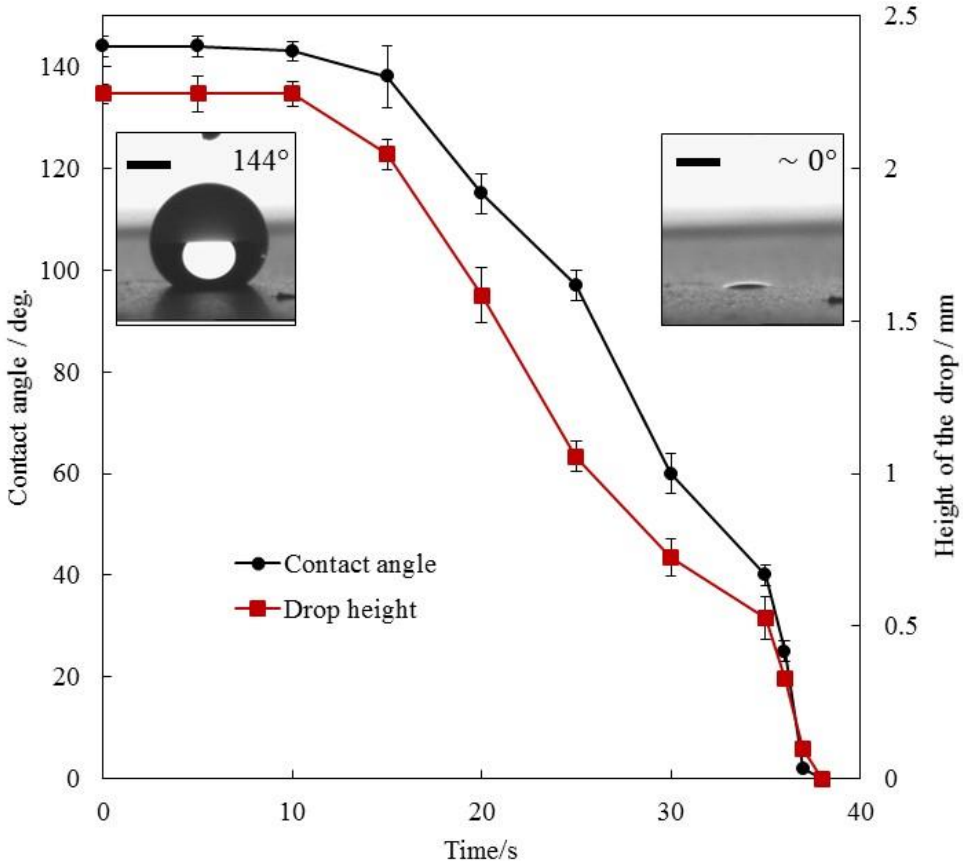

Figure 5.15 Plots showing behaviour of water drop gently placed on TLC surface that has been impregnated with 1 wt.% of pre-polymer base of Sylgard 184. The inserted images show the configuration of water drop immediately and 36 s after it was placed on the surface.

It can be observed that a water drop placed on the Sylgard impregnated TLC surface without curing could hydrophobise the surfaces of the plate and thus raise the contact angle of water drop to ~144^{o}. Initially, the droplet was relatively stable for about 10 s, and then collapsed into the pores of the TLC plate. Unlike the dry TLC plate which absorbs water as soon as it touches the surface, the high contact and the subsequent maintenance of the drop configuration for a certain period can be attributed to the fact that the water drop initially sits on a very thin layer of Sylgard deposited on the surface

of particles in the porous coating. Such a layer makes the particles hydrophobic, thus preventing water penetrating inside the pores and the water drops show high contact angles similar to those observed on dry hydrophobic silica particle coatings. After some time, the thin oil films become unstable and breaks, water comes in contact with the hydrophilic particles beneath and penetrates inside the pores of the TLC plate over time.

Contrary to the above observation with water drops on pre-polymer base impregnated TLC surfaces, water drops placed on cured Sylgard impregnated TLC surface shown in Figure 5.16 remains stable with a constant contact angle and height throughout the investigation time. A water drop is stable on this surface because the coated Sylgard is cured and bonded to the TLC surface making it to act as a barrier to water penetration to the bulk material. This findings therefore means that the porous superhydrophilic TLC plate can be modified by impregnation with 1 wt.% Sylgard solution in hexane.

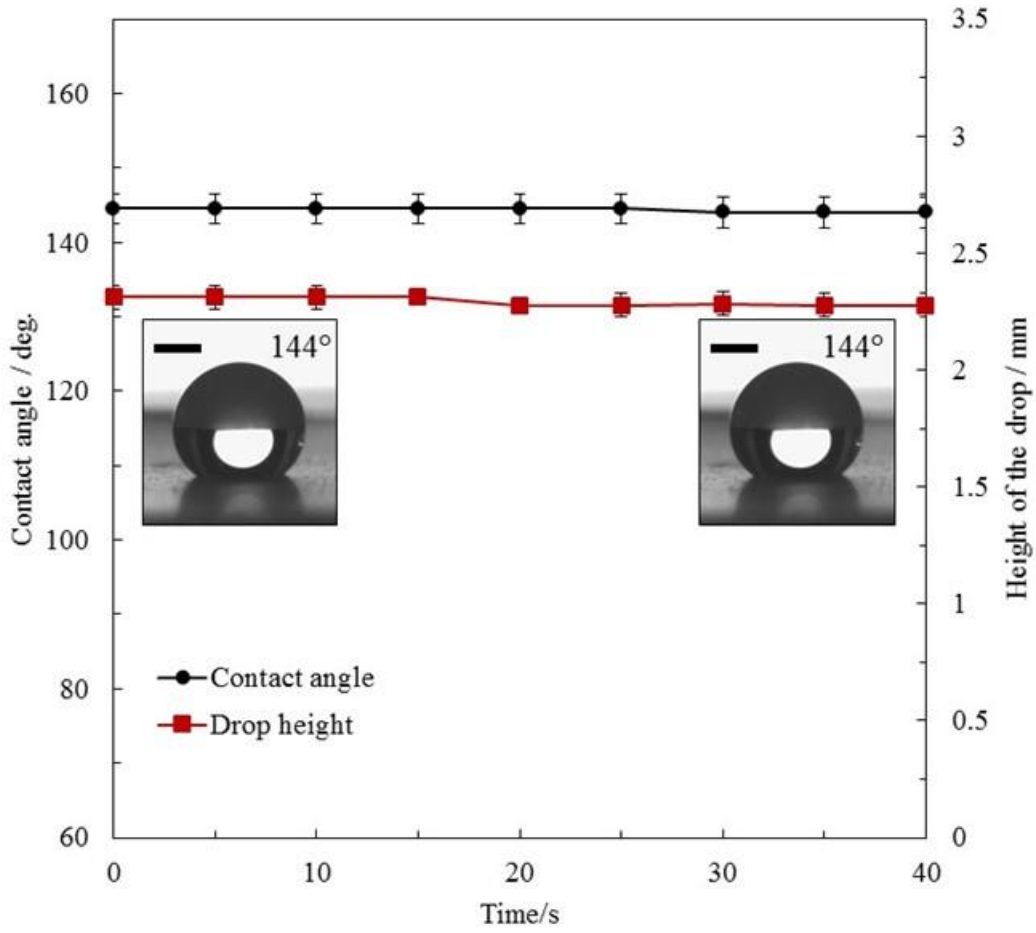

Figure 5.16 Plots showing stability of water drop gently placed on TLC surface that has been impregnated with 1 wt.% Sylgard solution and cured at 150 ℃. The inserted images are the configuration of water drop at initial and 40 s of placement.

The technique was further applied for the impregnation of a rough glass slides and sintered glass discs. Contact angles of water drops on the surfaces were 26 ± 2° for rough glass slide and 134 ± 1° for sintered glass discs (Figure 5.17). Comparison of the Sylgard modified glass slides with those of DCDMS (25 ± 4°) shows a very good agreement, indication that the use of Sylgard can produce a low surfaces energy for the hydrophobisation process similar to more expensive DCDMS.

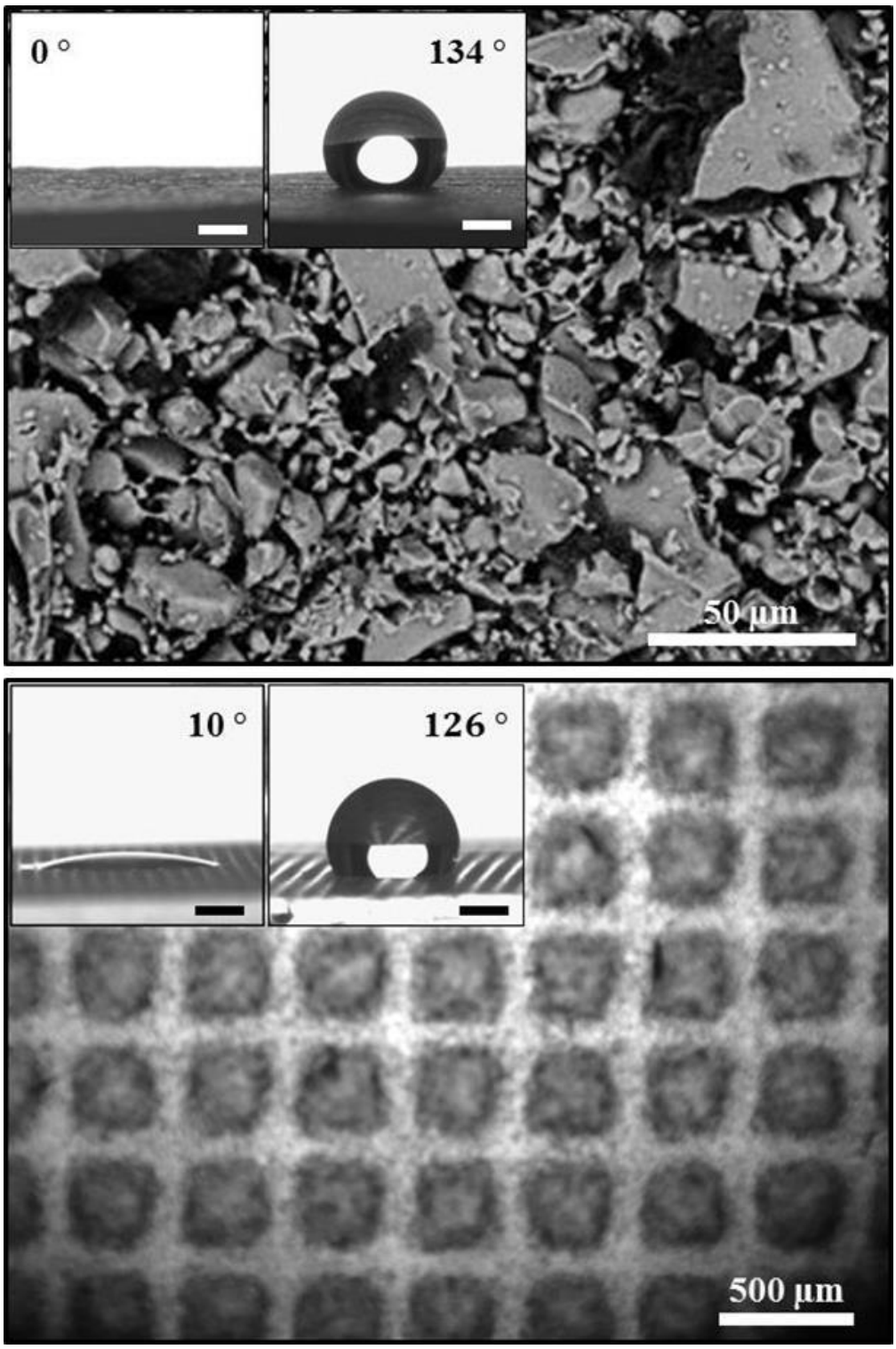

Figure 5.17 Impregnation of sintered glass disc (top) and roughened microscope glass slide (bottom) with curable Sylgard (1 wt.%). Inserted images on each are water contact angles on the respective surfaces before and after the hydrophobisation. Scale bars on sintered glass (a, b) = 50 µm, 500 µm on rough glass slide and 1 mm on all inserted images.

These results confirm one of our earlier hypothesies (Figure 3.28) that the impregnated oil in partial impregnation is thinly coated onto the structured surfaces. This also falls in line with the observations gathered from the SEM analysis. The stability of the impregnated oil depends on the weight of the external impacting factor (such as water drops) and the thickness of the over-coated layer of the oil. A very thin oil layer or heavy water drop, for instance may allow impregnation through the oil to the solid surface and subsequently exhibit higher hysteresis. In the case of cured Sylgard, the impregnated oil is stable to sustain the water droplet. If very thin stable impregnated layers are grown on the micro/nano-structured materials without remarkable bridging of the surface structures, formation of oil-air composite surface on structured material is possible, and the process can be used for surfaces modification of the materials as shown in subsections below.

5.3.6.1 Hydrophilic to superhydrophobic ultra-thin Sylgard-modified aluminium oxide coatings tuned from dispersions

In order to understand the wettability of coatings similar to hydrophobic fumed silica, we have investigated the partial impregnation of fumed aluminium oxide coatings produced from ethanol (or water) dispersions using a dip-coating method. The same procedures used for the preparation of porous fumed silica coating were followed for the preparation of 10 wt.% fumed aluminium oxide coatings (section 2.2.6). Impregnations and curing of the coatings with 1 wt.% Sylgard solution transformed the hydrophilic coatings to superhydrophobic surfaces with average contact angle of 162 ± 2 and 159 ±3 for water and ethanol based coatings, respectively. Stable contact angles of water drops on the coatings before and after modifications with Sylgard solution are presented in Figure 15.8.

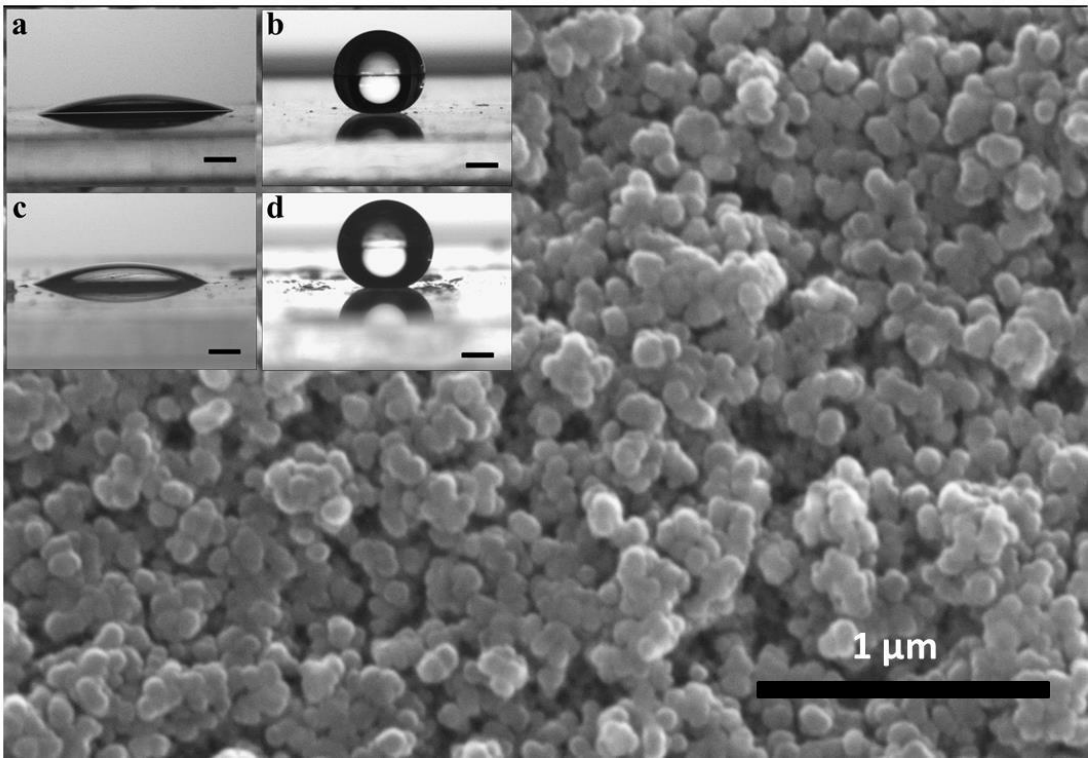

Figure 5.18 SEM image of aluminium oxide coating (dip-coated). Inserted are contact angles of water drops on Sylgard-modified coatings in air before (a, c) and after (b, d) the hydrophobisation coatings prepared from 10 wt.% particles in ethanol (ab), and water (c,d). Bars on inserted images represent 1 mm.

Beside the direct modification to superhydrophobic coatings with Sylgard, the wettability of the fabricated coatings has been tuned by varying the volume fractions of curable Sylgard in dispersions of fumed aluminium oxide particles using Sylgard 184 as the impregnating oil via the one-step method (see section 2.2.8) with the volume fraction of the Sylgard in the dispersion varied between 0.1 - 1.0 wt.%. Based on the confirmation of the mechanism of partial impregnation in the last section, the tunability has been carried out within a range of Sylgard concentration lower than 1 wt.% in the dispersion to avoid bridging of the structures by the higher concentrated of the impregnated Sylgard. Figure 5.19 shows the contact angle of water drops on the tuned coatings in air.

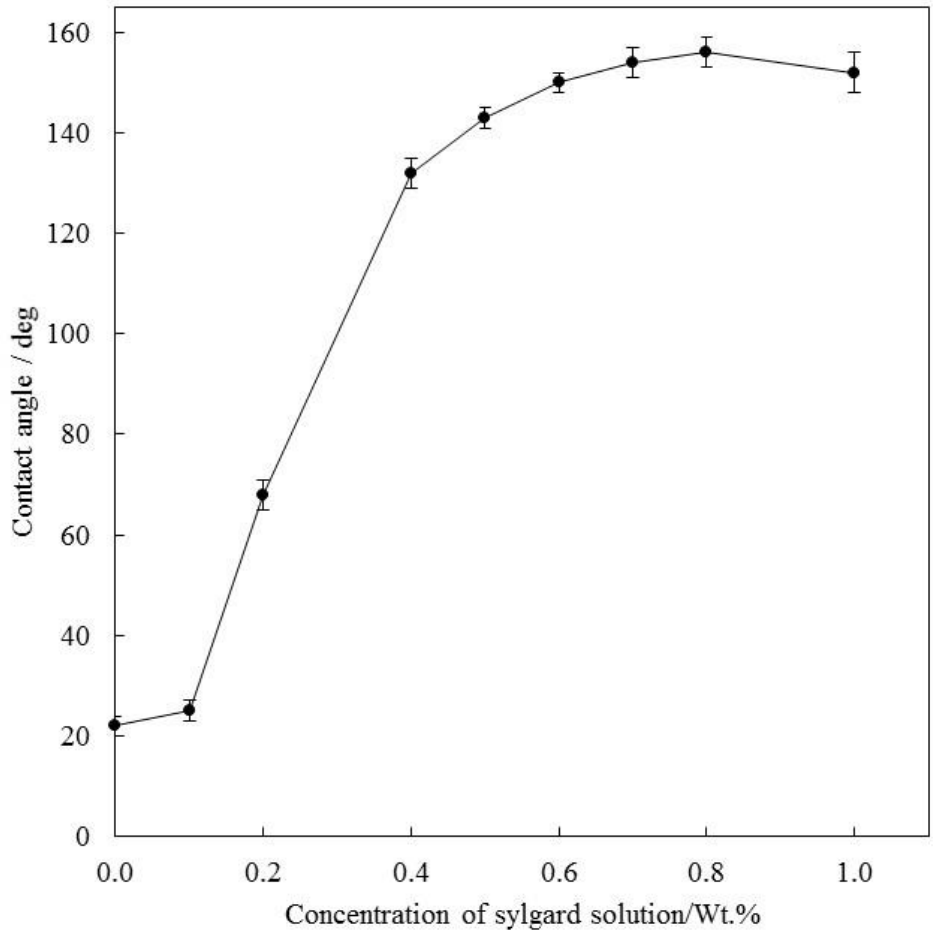

Figure 5.19 Contact angle versus concentration of Sylgard in 10 wt.% ethanol dispersion of fumed aluminium oxide particles dip-coated on glass slides.

As can be seen, gradual impregnations of the aluminium oxide coatings have been used to tune the contact angle of the coated surfaces from hydrophilic to superhydrophobic surfaces. Although as at the time of this report, the dispersions and the coatings were not adequately characterised, the tunability of the coatings wettability from the Sylgard-particle dispersions, will definitely create a wider research opportunities and applications in coating technology in the future.

5.3.7 A novel method for fabrication of superhydrophobic metal surfaces using curable Sylgard.

Metal substrates typically require protection coatings to prevent corrosion which silicone elastomer like Sylgard can successfully provide [25]. These elastomeric protected surfaces are used in variety of electronic, manufacturing and construction applications because they can effectively act as physical barrier coatings. The hydrophobic nature of the materials repels the moisture and further reduced water/corrosive media adsorption on the surface and therefore preventing the underlying metals from corrosion attack. Creating superhydrophobic from hydrophobic surface amplifies the aforementioned inherent properties of silicone elastomers and offers additional interesting characteristic of self-cleaning among others. Practically, a range of superhydrophobic metal surfaces have been reported in literature. In the process of lowering the surface energy of metal surfaces, the overwhelming majority of the reports used expensive chemical reagents (e.g. perfluorosilane) [26]. This high cost of fabrication has been noted as a serious limitation against commercial production of such metal substrates [14].

Silicone elastomers, including Sylgard, have been used as adhesive promoters to bond other sublayers that can be hydrophobised easily to superhydrophobic. Direct coating of ultra-thin PDMS or other polymeric film onto structured substrates using simple methods such as dip or spin coating to obtain superhydrophobic substrates is rarely, if at all reported. Commonly reported are ultra-thin films laid using complex and expensive chemical or physical vapour deposition techniques using gas-phase materials and plasma bombardment. Interestingly, surface coatings derived from the partial impregnating solution employed in this current work can be used to grow thin films of different thicknesses, including ultra-thin films. Taking advantage of the adhesive

property of Sylgard to various solid surfaces, in this work we have specifically roughened different metals substrates, including aluminium, iron, copper and brass by chemical etching in appropriate reagents and then modified the resulting structured surfaces by impregnating them with curable Sylgard 184. At a constant concentration of Sylgard solution, the superhydrophobicity of the metals were observed to depend on the scale of roughness of the metal surface. Average contact angle of water drops on the metal surfaces in air and the respective structured superhydrophobic surfaces are presented in Table 5.2 and Figure 5.20. The superhydrophobic surfaces are possible because of the presence of patterned microstructure as revealed by scanning electron microscopy (SEM) together with the low surface energy of the cured thin films provided by Sylgard.

The contact angle of water drops on the metal surfaces could be tuned by partial impregnation with higher concentrations of Sylgard solutions. Rough aluminium substrates have been tuned this way and it is shown in Figure 5.21.

Table 5.2 Average contact angle of water drops on structured aluminium, iron, copper and brass metal surfaces in air.

Contact angles of metals / deg.			
Metal	Before etching	After etching	Hydrophobised
Aluminium	86 ± 1	69 ± 5	162 ± 3
Iron	85 ± 1	67 ± 2	152 ± 2
Copper	75 ± 1	65 ± 4	148 ± 3
Brass	61 ± 1	57 ± 2	154 ± 2

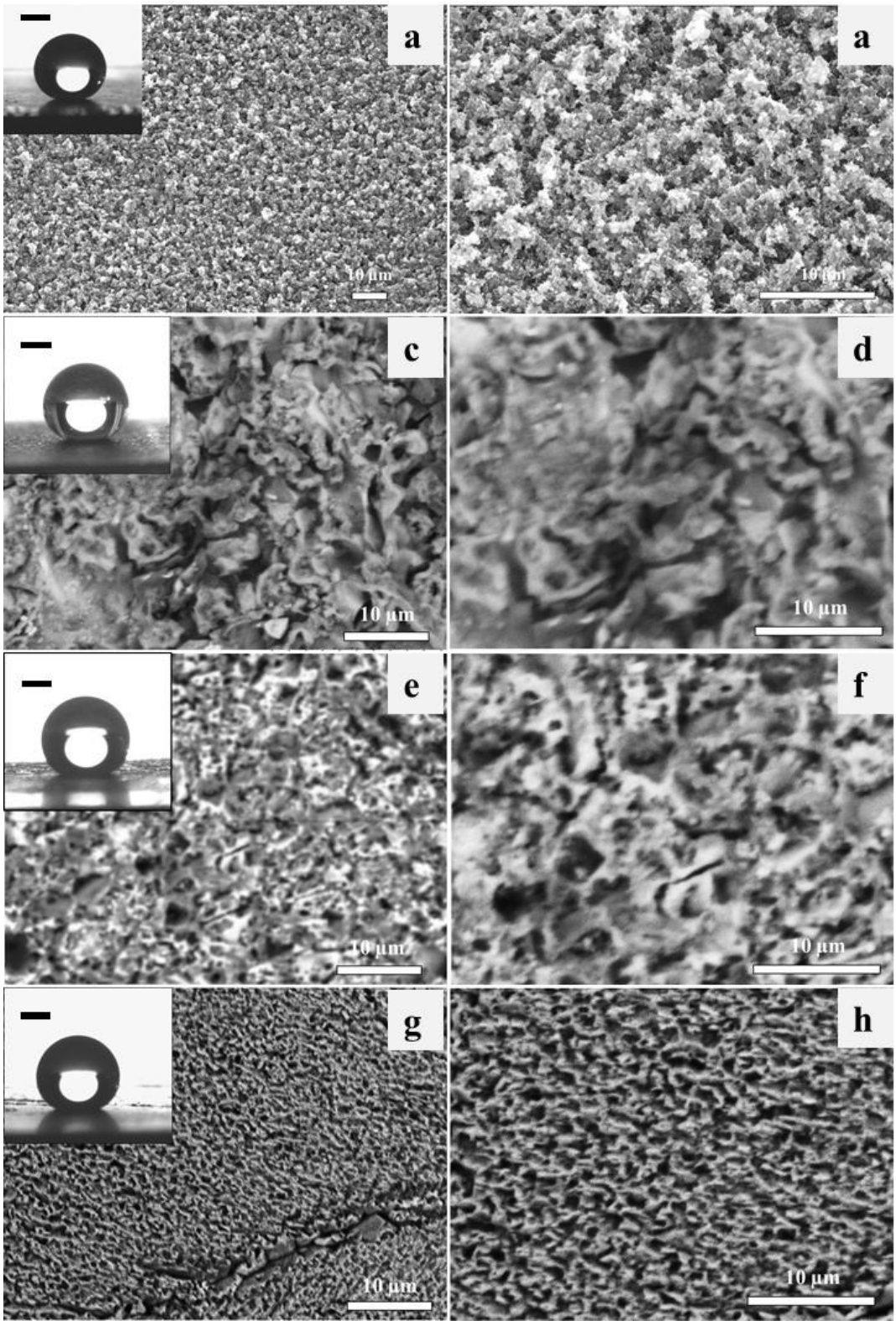

Figure 5.20 SEM images of the different structured metal surfaces impregnated with 1 wt.% Sylgard solution in hexane; (a, b) aluminium (c, d) iron (e, f) copper (g, h) brass. Inserted are contact angles on the respective metal surfaces in air. All bars on roughened metals represent 10 µm, and 1 mm on inserted contact angle images.

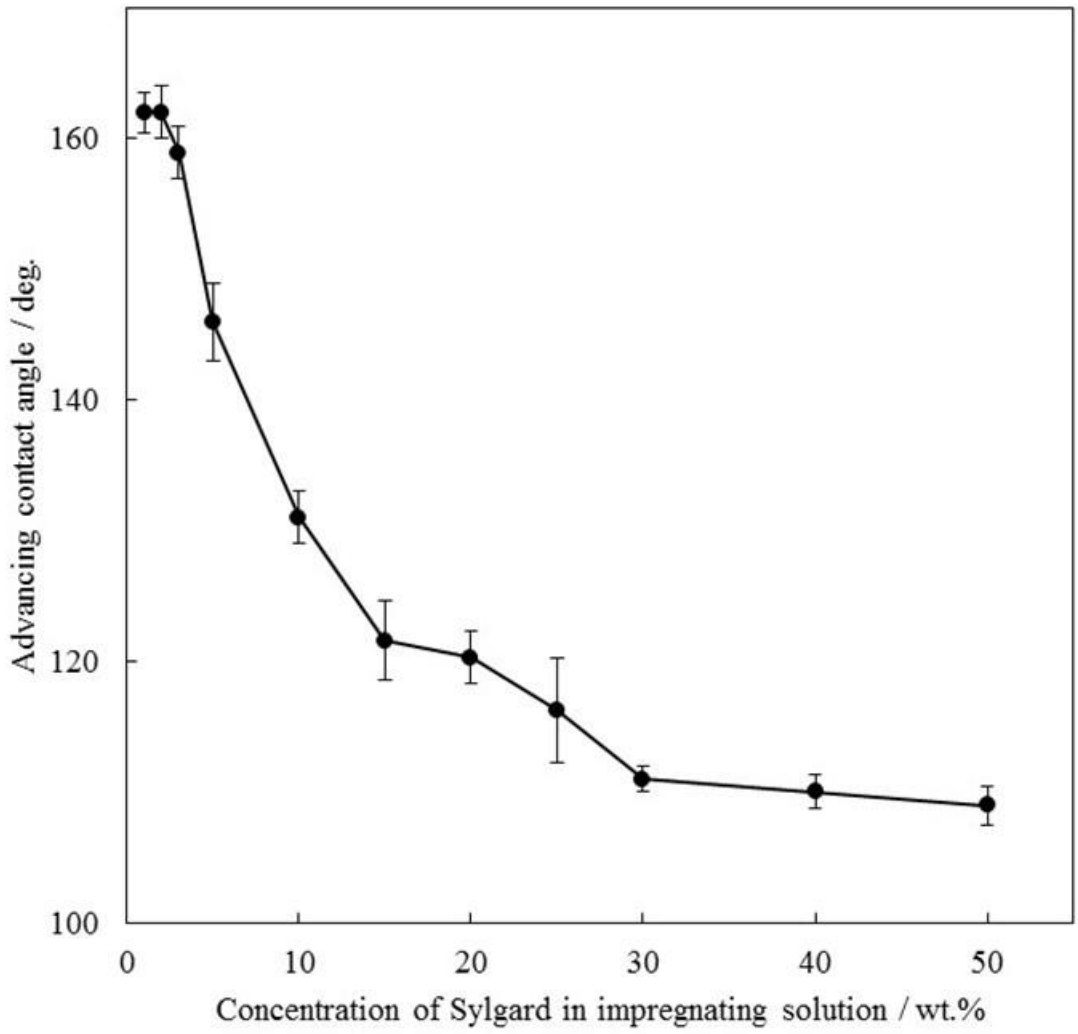

Figure 5.21 Variation of water drop contact angle in air with the concentration of the solution used for the impregnation of etched aluminium surfaces.

5.3.8 Hydrophobisation of paper surface by partial impregnation with Sylgard 184 solutions

Papers are sheets of dry cellulose material generally processed from wood. It is inexpensive and are found virtually everywhere and used for a variety of applications such as printing and writing (e.g. books), cleaning (e.g. tissues), packaging (boxboard) laboratory analysis (e.g. filter/litmus papers), medium of exchange (e.g. money) and

many other paper composite products. Ordinary papers are easily wetted by water and are always hidden from moisture. Although the high wettability of paper is beneficial in some applications (e.g. cleaning, filtration), many other applications especially the valuable paper products and packages require adequate surface protection against unwanted wetting. In addition, modification of paper surface can widen its applications. Filtration process, for instance, is readily used in the clinical, research and industrial laboratories for sample clarification, purifications, sterilisation and concentrations. Commonly used cellulose surfaces or papers will allow the infiltration of both polar and non-polar liquids and are therefore not suitable for the separating a mixture of oil and water due to the amphiphilicity nature of the surfaces [27, 28]. Separation of oil from water is of greater significance, especially for the clean-up of oil spills on sea and routine quantitative and qualitative analysis in laboratories [29]. One of the modification methods employed to control the wettability of paper surfaces, or widen its application, is through hydrophobisation. Apart from surface chemistry of the paper, the wettability of the paper surface is influenced by a combination of the porosity/roughness. The roughness and porosity of paper arises from the spaces between fibres as well as the intrinsic porosity of the fibre walls [30]. Interestingly, in a report by Balu *et al*, the superhydrophobic paper surfaces have been achieved by selective etching by oxygen plasma and then the deposition of a fluorocarbon film [31]. Also, spray coating of alcohol suspension of hydrophobic silica particles on paper surfaces has been reported to produce transparent superhydrophobic paper [32]. In spite of these successes, the former (plasma modification) is expensive and involves sophisticated equipment. On the other hand, the transparent superhydrophobic paper surface offered by silica may be susceptible to quick depletion as the silica cannot be strongly bonded to paper surface at high temperatures.

Having noticed that the porous surface of paper present an enabling platform for easy modification, a robust superhydrophobic paper has been produced simply by dipping filter paper into 1 wt.% Sylgard solution in hexane and removed within a second and then cured at 65 ℃. The fascinating feature of the modification with Sylgard in this present work is the possibility of bonding the elastomer on many solid surfaces including porous paper. Upon hydrophobisation of the filter paper with Sylgard, the surfaces of the paper remained transparent and became superhydrophobic with an average water contact angle of 149 ± 2° (Figure 5.22).

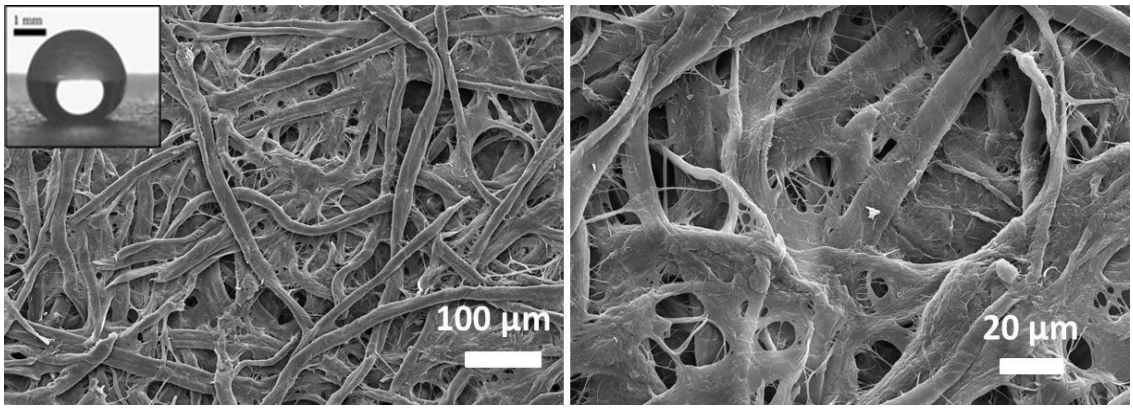

Figure 5.22 SEM images of filter paper used. Inserted is the DSA image of water drop (148 °) on 1 wt.% Sylgard-hydrophobised filter paper in air.

Strong water resistance of the Sylgard coated paper as indicated by the above Figure can serve as a useful measure to protect paper from water induced rupturing or decomposition. It has been reported that the rate of degradation of cellulose containing 4% (w/w) of absorbed moisture is 20 times higher than for cellulose containing 0.5% (w/w) moisture [33]. Furthermore, investigations into microbial deterioration of cultural heritage and works of art, manuscripts and archives in national libraries, public museums and in private art collections have revealed that the presence of water on cellulose surfaces would favour the proliferation and subsequent destructions by biofilms [34, 35]. Hence, direct contact of water with paper, or its exposure to humid

environment, can endanger the durability of unprotected paper materials. Non-wetting characteristic exhibited by the hydrophobised paper as demonstrated in our results can be used for the protection of the paper product against damage by moisture. Better still, the hydrophobised papers exhibit superoleophilic behaviour toward hexadecane drops. The opposing behaviours of the hydrophobised paper towards oil and water could probably make it suitable to be used as separation media for oil-water mixtures.

Generally, the modification of paper surface by partial impregnation using low concentration of Sylgard is quite simple and involves low cost of the materials and instrumentations.

5.4 Conclusions

Polymeric materials have a lot to offer in surface science and the durability of materials. It is difficult to image liquid impregnated surfaces under scanning electron microscope. A simple approach involving the use of silicone elastomer (Sylgard 184) has been developed to overcome this difficulty. Squalane impregnated fumed silica-coated surfaces, previously studied, have clearly been mimicked by impregnating the same surfaces with transparent Sylgard 184 silicone. The coatings are then cured to obtain a solid impregnated layer that can withstand the SEM imaging which is a useful tool for characterising and understanding material surfaces. This has revealed that in the course of gradual impregnations, fumed silica coated surface can be transformed from hierarchical dual scale of roughness (nano/microscales) to larger scales capable of undergoing Wenzel mode of wetting, and in turn high contact angle hysteresis/sticky droplets.

The study about the incorporation of curable Sylgard into the fumed silica coatings has shown evidences of improved stability of the coatings. The Sylgard was observed to act

as an adhesion promoter within the silica particles and between the coated film and the glass substrate. However, over-coated liquid impregnated coatings have also shown exceptional self-healing characteristics due to instant re-distribution and sealing of the surfaces in an event of scratch or damage.

This study has also revealed that in partial impregnation, the impregnated oils are initially thinly coated onto the surface structures, and then build up with increase in the concentration of the oil to a larger thickness which finally fills the surface pores and level up the surface. Thus, partial impregnation employed in this work can effectively be used to tune the thickness of the newly introduced SLIPS, a point which is receiving criticism and has not been properly addressed, yet it is the key factor of the invention. In this work, the wettability of fumed aluminium coatings have been tuned by impregnating the structured coatings with low concentration of Sylgard solutions (0.1-1 wt.%) to obtain variable contact angles on the coatings such that the impregnated layers of oil are thin enough to follow the surface roughness without significantly bridging the micro/nano structures. Because the surface structures are intact in the process, a general simple method of solid surface modification has been developed and superhydrophobic surfaces have been created on different structured solid materials including, metals and papers. The fabricated structured superhydrophobic metals (e.g. aluminium, iron, copper and brass) surfaces seem very promising to withstand harsh environmental conditions including corrosion. Also, transparent superhydrophobic Sylgard-modified paper material could serve as excellent protective coating against deterioration of paper products by water. The finding with Sylgard is a more environmental friendly method and a potential substitute to costly chemical or physical vapour deposition techniques mainly employed for the fabrication of ultra-thin protective polymeric films.

5.5 References

1. S. Bargir and D. M. Allen, Use of a PDMS spring element for ink jet printing applications. *Microsystem Technologies-Micro-and Nanosystems-Information Storage and Processing Systems*, 2010. **16**(7): p. 1239-1242.

2. Y. W. Liu, *et al*., Surface Structures of PDMS Incorporated with Quaternary Ammonium Salts Designed for Antibiofouling and Fouling Release Applications. *Langmuir*, 2013. **29**(9): p. 2897-2905.

3. C. V. Rumens, M. A. Ziai, K. E. Belsey, J. C. Batchelor, and S. J. Holder, Swelling of PDMS networks in solvent vapours; applications for passive RFID wireless sensors. *Journal of Materials Chemistry C*, 2015. **3**(39): p. 10091-10098.

4. A. Kachroudi, S. Basrour, L. Rufer, A. Sylvestre, and F. Jomni, Dielectric properties modelling of cellular structures with PDMS for micro-sensor applications. *Smart Materials and Structures*, 2015. **24**(12).

5. N. S. Tambe and B. Bhushan, Micro/nanotribological characterization of PDMS and PMMA used for BioMEMS/NEMS applications. *Ultramicroscopy*, 2005. **105**(1-4): p. 238-247.

6. J. H. Tong, C. A. Simmons, and Y. Sun, Precision patterning of PDMS membranes and applications. *Journal of Micromechanics and Microengineering*, 2008. **18**(3).

7. H. Yu, G. Zhou, F. S. Chau, and S. K. Sinha, Soft lithography replication based on PDMS partial curing. *Microsystem Technologies*, 2011. **17**(3): p. 443-449.

8. D. Lee and S. Yang, Surface modification of PDMS by atmospheric-pressure plasma-enhanced chemical vapor deposition and analysis of long-lasting surface hydrophilicity. *Sensors and Actuators B-Chemical*, 2012. **162**(1): p. 425-434.

9. J. W. Zhou, A. V. Ellis, and N. H. Voelcker, Recent developments in PDMS surface modification for microfluidic devices. *Electrophoresis*, 2010. **31**(1): p. 2-16.

10. I. F. Burgess, The mode of action of dimeticone 4% lotion against head lice, Pediculus capitis. *BMC Pharmacol*, 2009. **9**: p. 3.

11. <2 McDonald s Food Facts- Ingredients (PDF). McDonald s Restaurants of Canada Limited. 2013-09-08. p. 13..pdf>.

12. E. Engel, A. Michiardi, M. Navarro, D. Lacroix, and J. A. Planell, Nanotechnology in regenerative medicine: the materials side. *Trends Biotechnol*, 2008. **26**(1): p. 39-47.

13. J. N. Lee, C. Park, and G. M. Whitesides, Solvent compatibility of poly(dimethylsiloxane)-based microfluidic devices. *Analytical Chemistry*, 2003. **75**(23): p. 6544-6554.

14. A. S. H. Makhlouf and I. Tiginyanu, *Nanocoatings and ultra-thin films: Technologies and applications*. 2011: Elsevier.

15. L. Kersey, V. Ebacher, V. Bazargan, R. Z. Wang, and B. Stoeber, The effect of adhesion promoter on the adhesion of PDMS to different substrate materials. *Lab on a Chip*, 2009. **9**(7): p. 1002-1004.

16. S. Satyanarayana, R. N. Karnik, and A. Majumdar, Stamp-and-stick room-temperature bonding technique for microdevices. *Journal of Microelectromechanical Systems*, 2005. **14**(2): p. 392-399.

17. O. J. Cayre and V. N. Paunov, Contact angles of colloid silica and gold particles at air-water and oil-water interfaces determined with the gel trapping technique. *Langmuir*, 2004. **20**(22): p. 9594-9599.

18. H. Teisala, *et al.*, Nanostructures increase water droplet adhesion on hierarchically rough superhydrophobic surfaces. *Langmuir*, 2012. **28**(6): p. 3138-45.

19. T. G. Cha, J. W. Yi, M. W. Moon, K. R. Lee, and H. Y. Kim, Nanoscale Patterning of Microtextured Surfaces to Control Superhydrophobic Robustness. *Langmuir*, 2010. **26**(11): p. 8319-8326.

20. B. Cortese, *et al.*, Superhydrophobicity due to the hierarchical scale roughness of PDMS surfaces. *Langmuir*, 2008. **24**(6): p. 2712-2718.

21. M. J. Liu, Y. M. Zheng, J. Zhai, and L. Jiang, Bioinspired Super-antiwetting Interfaces with Special Liquid-Solid Adhesion. *Accounts of Chemical Research*, 2010. **43**(3): p. 368-377.

22. P. Roach, N. J. Shirtcliffe, and M. I. Newton, Progess in superhydrophobic surface development. *Soft Matter*, 2008. **4**(2): p. 224-240.

23. B. Mecheri, L. Piras, L. Ciotti, and G. Caminati, Electrode coating with ultrathin films containing electroactive molecules for biosensor applications. *Ieee Sensors Journal*, 2004. **4**(2): p. 171-179.

24. M. A. Surmeneva, T. M. Mukhametkaliyev, H. Khakbaz, R. A. Surmenev, and M. B. Kannan, Ultrathin film coating of hydroxyapatite (HA) on a magnesium-calcium alloy using RF magnetron sputtering for bioimplant applications. *Materials Letters*, 2015. **152**: p. 280-282.

25. R. G. Jones, W. Ando, and J. Chojnowski, *Silicon-containing polymers: the science and technology of their synthesis and applications*. 2013: Springer Science & Business Media.

26. Z. W. Wang, Q. Li, Z. X. She, F. N. Chen, and L. Q. Li, Low-cost and large-scale fabrication method for an environmentally-friendly superhydrophobic coating on magnesium alloy. *Journal of Materials Chemistry*, 2012. **22**(9): p. 4097-4105.

27. W. G. Glasser, *et al.*, About the structure of cellulose: debating the Lindman hypothesis. *Cellulose*, 2012. **19**(3): p. 589-598.

28. F. Jiang and Y. L. Hsieh, Amphiphilic superabsorbent cellulose nanofibril aerogels. *Journal of Materials Chemistry A*, 2014. **2**(18): p. 6337-6342.

29. Q. Zhu, Q. M. Pan, and F. T. Liu, Facile Removal and Collection of Oils from Water Surfaces through Superhydrophobic and Superoleophilic Sponges. *Journal of Physical Chemistry C*, 2011. **115**(35): p. 17464-17470.

30. R. Pelton, Bioactive paper provides a low-cost platform for diagnostics. *Trac-Trends in Analytical Chemistry*, 2009. **28**(8): p. 925-942.

31. B. Balu, V. Breedveld, and D. W. Hess, Fabrication of "roll-off" and "sticky" superhydrophobic cellulose surfaces via plasma processing. *Langmuir*, 2008. **24**(9): p. 4785-4790.

32. H. Ogihara, J. Xie, J. Okagaki, and T. Saji, Simple Method for Preparing Superhydrophobic Paper: Spray-Deposited Hydrophobic Silica Nanoparticle Coatings Exhibit High Water-Repellency and Transparency. *Langmuir*, 2012. **28**(10): p. 4605-4608.

33. J. Scheirs, G. Camino, and W. Tumiatti, Overview of water evolution during the thermal degradation of cellulose. *European Polymer Journal*, 2001. **37**(5): p. 933-942.

34. K. Sterflinger and G. Pinar, Microbial deterioration of cultural heritage and works of art - tilting at windmills? *Applied Microbiology and Biotechnology*, 2013. **97**(22): p. 9637-9646.

35. A. Michaelsen, G. Pinar, and F. Pinzari, Molecular and Microscopical Investigation of the Microflora Inhabiting a Deteriorated Italian Manuscript Dated from the Thirteenth Century. *Microbial Ecology*, 2010. **60**(1): p. 69-80.

CHAPTER 6

BIO-FOULING OF STRUCTURED SILICA COATINGS

6.1 Introduction

Generally, fouling refers to undesired deposition or accumulation of material on surfaces. Such materials may stem from scaling or precipitation of mineral materials, accumulation of particles, organic matter build up, or accumulation of living organisms. The latter is termed biofouling - adhesion of microorganism to surfaces [1]. These organisms can colonise a solid surface within a few hours of exposing it to medium that is infested by the micro-organisms. If the organism can successively settle on the surface, they secrete sticky extracellular polymeric substance (EPS) onto the surface and become properly attached. The attached cells can then divide rapidly to form colonies that eventually coalesce to form a biofilm, which may grow in thickness up to 500 μm [2, 3]. The preferred form of life for many micro-organisms occurs in biofilms or aggregates [4].

The practical consequences of biofouling are enormous. The magnitude of problems associated with biofouling, which include increased drag, corrosion of metal surfaces, stains/difficulty in cleaning and contaminations were described in Chapter 1 (Sect 1.5). Unfortunately man's efforts to present an effective check to biofouling system have lingered for years. Quite opposing to these effort, biofilms can exist in various extreme conditions including pH range between 0.5-14, temperature from -5 to 120 ℃, etc. and are reported as the most successive form of life [4]. Notwithstanding, many steps have been adopted to address biofouling problems [1, 5]. Ability to effectively design anti-biofouling solid surface which happen to be the initial contact point to biofilms will go a long way to controlling biofilm and prevent harmful effect associated with the use of biocides as well as reduce the

cost of cleaning the material surfaces. The main aim of the work presented in this Chapter is to investigate the adhesions of algae cells on different squalane-impregnated silica coatings described in the previous Chapter 3.

6.2 Experimental

Adhesion of algae cells on various partially (gradual) squalane-impregnated porous silica coatings (section 2.2.7) were carried out by submerging the coatings fully in algae media and kept for different time of the experiment, and then withdrawn and dipped in milli-Q water to remove excess algal media from the surface. The surface of the slides were thereafter protected with cover slips and placed under a microscope for the cells to be counted. Detailed procedures are described in Chapter 2 (Section 2.2.20).

6.3 Results and discussions

6.3.1 Algae cell adhesion on superhydrophobic, sticky and slippery surfaces

Algae cell adhesion results for different impregnated surfaces are summarised in Table 6.1. Figure 6.1 shows optical microscope images of superhydrophobic, sticky and slippery surfaces after 15 min (minimum) and 24 h (maximum) incubation time in cell media.

Table 6.1 Adhesion of algae cells expressed as number of cells/mm^2 on surfaces impregnated with different concentrations of squalane solutions at different time of incubation.

	Concentration of squalane in impregnating solution								
Incubation time/h	0%	2%	5%	10%	15%	20%	30%	60%	100%
0.25	9 ± 3	70 ± 30	300 ± 100	1400 ± 200	300 ± 90	130 ± 30	14 ± 7	7 ± 7	7 ± 3
1	7 ± 7	100 ± 40	400 ± 100	2100± 300	500± 100	130 ± 60	40 ± 10	40 ± 20	21 ± 7
2	8 ± 1	210 ± 40	500 ± 100	2600 ± 200	500 200	270± 70	50 ± 20	40 ± 10	28 ± 8
4	12 ± 2	350 ± 50	700 ± 200	3000 ± 400	700± 300	260± 80	70 ± 10	40 ± 10	21 ± 7
12	12 ± 2	469 ± 40	1600 ± 300	5000 ± 600	1400 ± 400	400 ± 100	80± 30	40± 20	40 ± 10
24	14 ± 6	690 ± 40	2900± 500	6000 ± 700	2800 ± 500	500 ± 60	100± 30	60 ± 20	30 ± 10

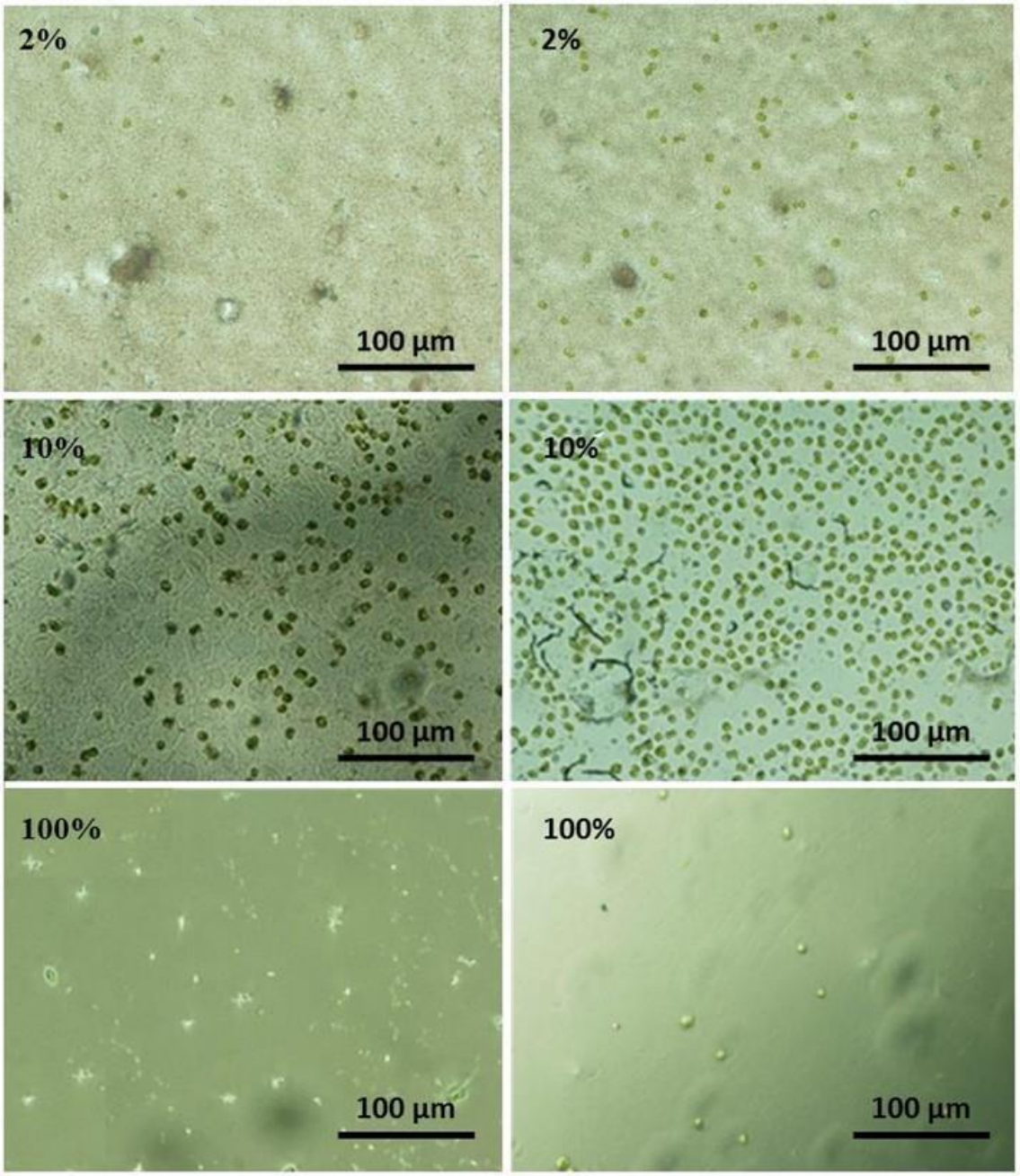

Figure 6.1 Optical images showing adhesion of algae cells on superhydrophobic (2% squalane solution), sticky (10% squalane solution) and slippery (100% squalane) surfaces at incubation time of 15 min (left) and 24 h (right). The concentrations shown correspond to the concentration of squalane solutions used for the impregnation of the hydrophobic fumed silica coatings.

It can be seen in Table 6.1 that the adhesion of the cells on all the coated surfaces increases with time throughout the incubation period. However, both superhydrophobic

and slippery surfaces show less dependence on time. Surface density of algae cell adhesion on superhydrophobic, partially impregnated and slippery surfaces with time is shown in Figure. 6.2.

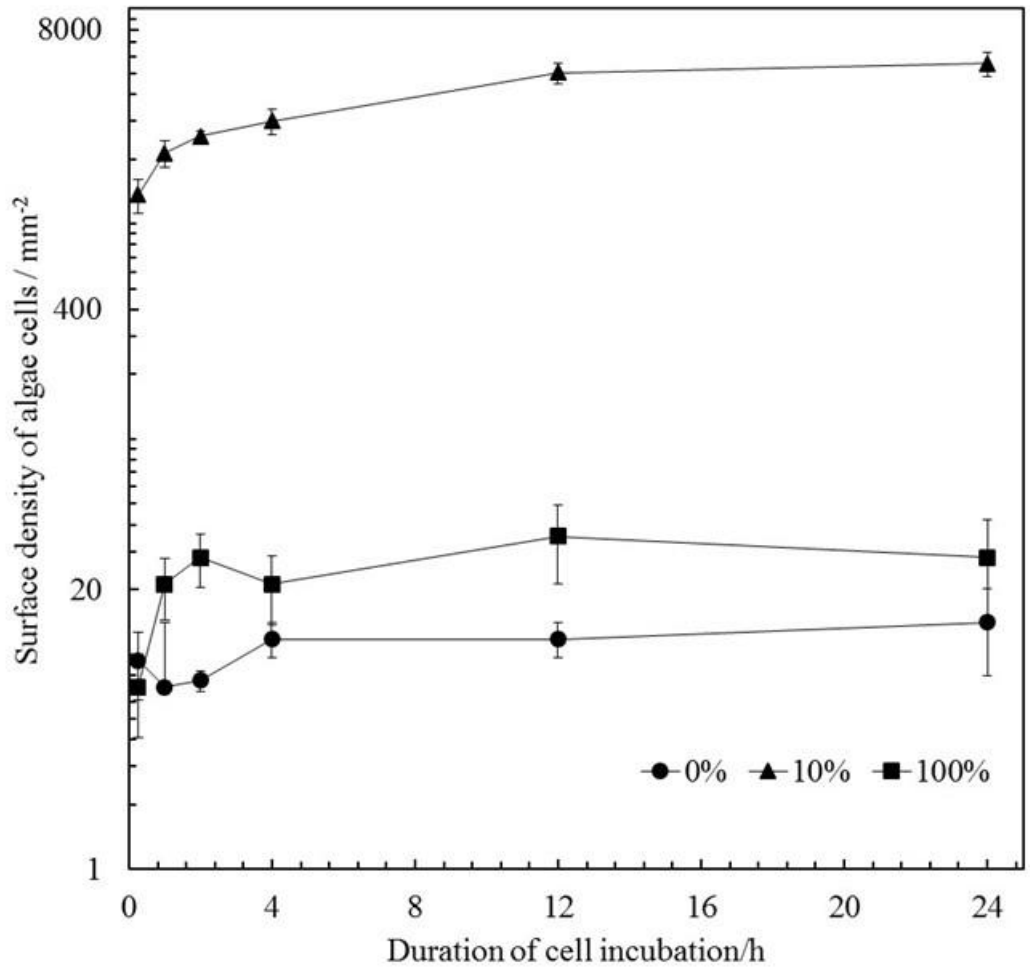

Figure 6.2 Comparison of algae cell adhesion at different time on selected porous fumed silica coatings impregnated with different concentrations of squalane solutions in hexane - superhydrophobic (0% impregnated surfaces), sticky (10% impregnated surfaces) and slippery (100% impregnated surfaces).

Gradual impregnation of the coatings has also been observed to affect the degree of cell adhesion on the coated surfaces. The greatest adhesion of cells on the coatings is recorded on coatings partially impregnated with 10% of squalane solution (sticky

coatings). Unlike these partially impregnated coatings, dry (0% impregnated) superhydrophobic and slippery (100%) coatings exhibit good anti-biofouling characteristics with good resistance to the adhesion of the cells. The effects of oil impregnation on the silica coated surfaces are shown in Figure 6.3.

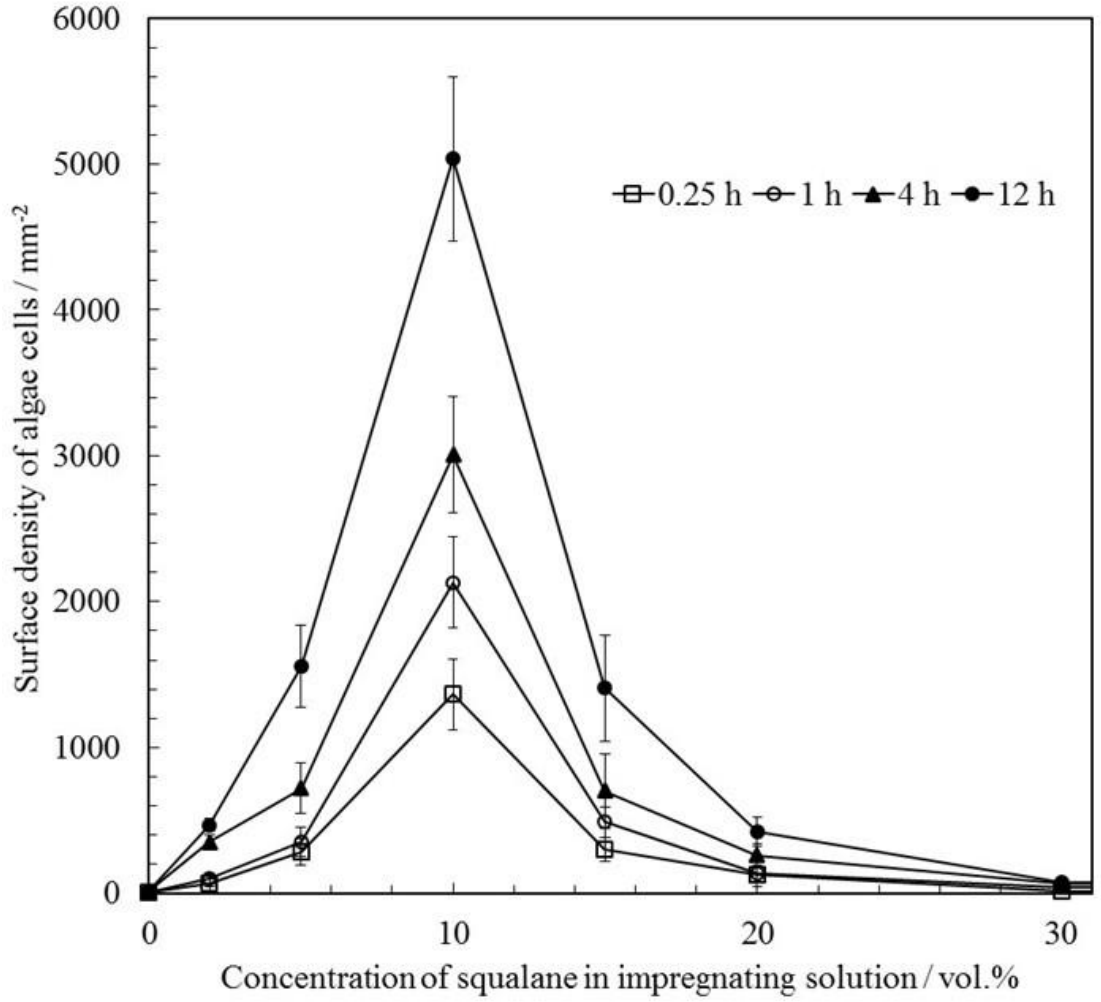

Figure 6.3 Adhesion of algae on selected fumed silica coatings impregnated with different concentrations of squalane solutions at different incubation times.

It is interesting to note the correlation between cell adhesion and the adhesion of water droplets or sliding force previously studied on these surfaces. Variation in celladhesion on the coated surfaces may be attributed to the different structures and properties of the surfaces. The low adhesion of cells on superhydrophobic surfaces is probably due to

failure of the cells to establish reasonable contact with these surfaces due to their physical states (including topography) and chemical compositions. It was noticed that immediately after withdrawal from the algae media, the coated surface appeared crowded with the cells but cells seemed to lose grip on the superhydrophobic surface easily during washing with water. The massive adhesion on sticky surfaces may likely be attributed to larger scale of roughness comparable to the cell size, thus cells could deform slightly to follow the surface topography increasing their contact with the underlying interface that leads to stronger adhesion [6]. On surfaces over-coated with oil, the fluid characteristic of the surfaces minimise friction and mechanical locking of the cell adhesive properties, enhances slippage [7] and the cells can be easily removed during the washing step.

6.3.2 Comparative investigations of algae cells adhesion on smooth hydrophilic and hydrophobic glass slides

The fabricated surfaces were further evaluated by subjecting the fabricated superhydrophobic and slippery surfaces to algae media alongside with hydrophilic and hydrophobic glass slides for 24 hours. The results of cell adhesion on smooth hydrophilic and hydrophobic glass slides are presented in Table 6.2. Figure 6.4 compares the adhesion the cells on different surfaces.

Table 6.2 Cell adhesion on smooth hydrophilic and hydrophobic glass slides at different incubation times.

Incubation time / h	Cells/mm^2	
	Hydrophilic slide	Hydrophobic slide
0.25	$10 \pm 1 \times 10^2$	$4 \pm 0 \times 10^2$
1.00	$20 \pm 2 \times 10^2$	$10 \pm 1 \times 10^2$
2.00	$22 \pm 2 \times 10^2$	$10 \pm 1 \times 10^2$
4.00	$25 \pm 3 \times 10^2$	$18 \pm 1 \times 10^2$
12.00	$45 \pm 5 \times 10^2$	$28 \pm 2 \times 10^2$
24.00	$90 \pm 10 \times 10^2$	$35 \pm 3 \times 10^2$

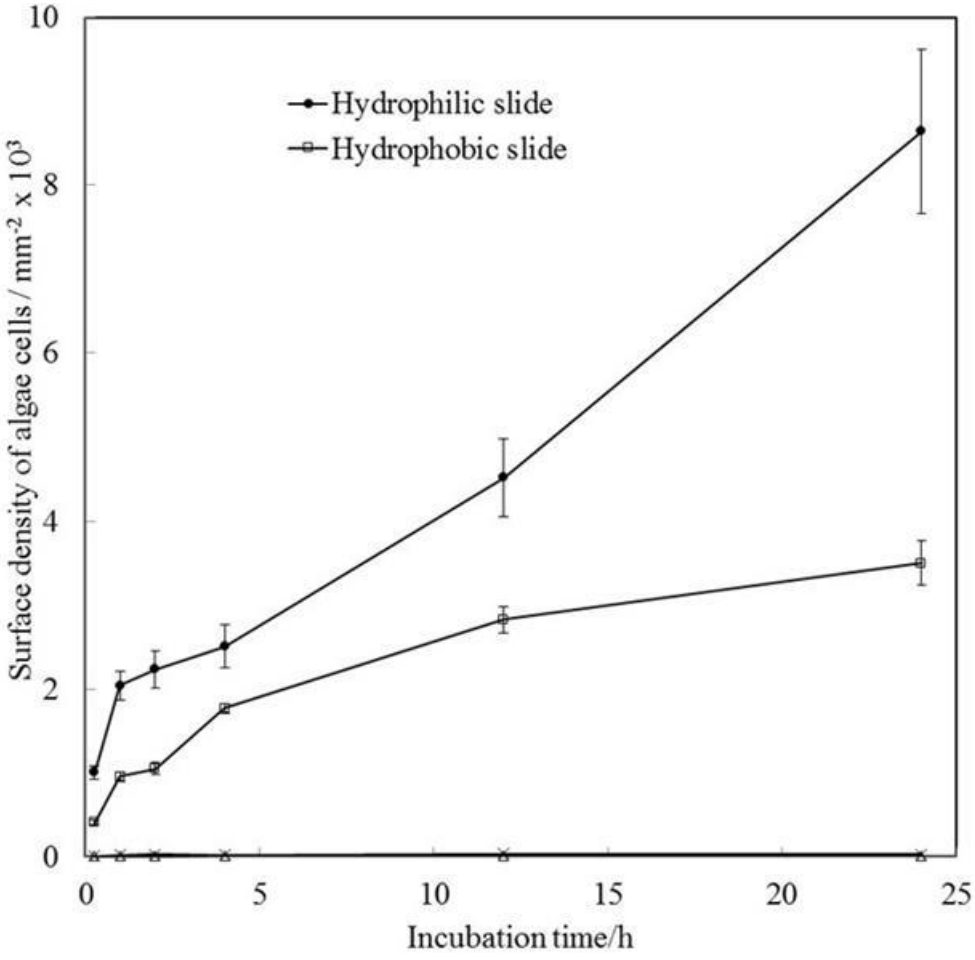

Figure 6.4 Plots comparing adhesion of algae cells on fumed silica coated superhydrophobic surfaces (without oil impregnation), fumed silica coating fully impregnated with squalane, smooth hydrophilic and hydrophobic glass slides.

Hydrophilic glass slide shows the highest number of cells adhered per square millimetre. The cell adhesion on smooth hydrophobic glass slides is smaller but still significant. The adhesion on both smooth slides increases with the incubation time. However, both superhydrophobic and slippery surfaces exhibit high resistance to adhesion of algae cells that is much smaller in comparison to smooth surfaces. Krishnan *et al.* investigated anti-biofouling properties of comb like block copolymer with an amphiphilic side chain and observed lower settlement on glass surface compared to the comb like copolymer and PDMS surfaces. However, exposure of the surfaces to turbulent flow indicated stronger attachment of the *Navicula* (boat-shaped algae) to glass surface with only 69 ± 3% removal from glass surface compared 81 ± 5% from comblike copolymer. The authors cautiously attributed the stronger attachment to glass to hydrogen bonding or electrostatic interaction with the glass surface [8].

On the other hand, Scardino *et al.* studied the role of nano-roughness in antifouling and tested three superhydrophobic coatings differing in their chemical composition and architecture against major fouling species such as *Amphora sp.*, *Ulvarigida*, *Polysiphonia sphaerocarpa, Bugula neritina* and *Amphibalanus amphitrite* in settlement assays. The superhydrophobic surface which had nanoscale roughness alone deterred the settlement of all the tested fouling organisms, compared to selective settlement on the superhydrophobic coatings with nano- and micro-scale architectures. The effective deterrence of settlement and attachment was linked to the length scales at the nanoscale in terms of rough architecture on the surface, and the larger percentage of air incursions at the interface [9].

A related investigation by Zhang *et al.* [10] investigated the fouling behaviour of smooth and roughened superhydrophobic coatings. The effect of nanoscale interfacial roughness on the adhesion of single and mixed cultures of micro-foulant for periods of

up to 6 months using visual and wettability measurements. According to the authors, detailed analysis indicated virtually no micro-organism attached to the superhydrophobic surfaces in the first weeks of immersion compared with smooth substrates, which exhibited fouling within a day. However, the anti-biofouling properties of the superhydrophobic coatings were found to decrease in fouling resistance when exposed longer than 2-month period. The diminishing fouling resistance was attributed to the loss of superhydrophobicity, which can occur due to air dissolving in water over long periods of submersion, leading to the destruction of pores, or the development of a conditioning layer of macromolecules which alter the chemical and physical structures of the surface [9, 10].

In our work presented here, it is too early to speculate the cause of the observed findings as detailed interactions of the algae cells with the glass surfaces or the prepared silica coated surfaces were not investigated. This seems an exciting direction for future research.

6.4 Conclusions

This study demonstrates that interplay with the solid surface architecture and chemistry or/with additional special composite properties (e.g. impregnated oil) can systematically be used to manipulate adhesion of cells on solid materials with negligible toxicity to the environment. Hydrophobic nano-porous fumed silica coatings have been found to offer significant resistance to algae cells adhesion. In addition, when these coatings are impregnated with a non-volatile and non-toxic oil (squalane) to create over-coated oil layer, the coatings were equally observed to exhibit excellent anti-fouling property toward the algae cells. Although detailed investigation to link the algae cells interactions with the surfaces chemistry have not yet been carried, it is evident in this

study that the cells can be washed off these two set of surfaces easily due to nano-scale roughness and the presence of stable slimy over-coated oil layer, respectively. Moderate impregnation of the coatings with the oil was found to reduce the anti-fouling resistance drastically. Previous investigations on similar surfaces (Chapter 5) indicate a change from nanoscale roughness to larger microscale. Furthermore, it is possible that limited oil on the coatings can transform it to become adhesive in nature thereby promoting cell adhesion similar to strong water adhesion or sliding force earlier recorded on this surfaces (Chapter 3).

Although, superhydrophobic and slippery surfaces which show promising anti-biofouling properties may be useful in short term applications, the period of investigation (24 h) seems inadequate to clearly assess the complex interactions of biofilms on solid surfaces. The initial limitations of this investigation had been the stability of the coatings beyond the 24 h, however, improved Sylgard-assisted coatings (silica-Sylgard composite films) have been found to be more robust nano-coated surfaces and will definite remain stable during longer investigations. A greater understanding of gradual impregnated micro/nanoporous substrate to manipulate surface wetting, including biofouling would expose more hidden properties of the structured solid substrates and this will be crucial in the development of environmental friendly anti-biofouling solid materials.

6.5 References

1. H. C. Flemming, Biofouling in water systems - cases, causes and countermeasures. *Applied Microbiology and Biotechnology*, 2002. **59**(6): p. 629-640.

2. M. E. Callow and J. A. Callow, Marine biofouling: a sticky problem. *Biologist*, 2002. **49**(1): p. 1-5.

3. L. Heng, Y. L. Yanling, G. J. Weijia, L. Xing, and G. B. Li, Effect of pretreatment by permanganate/chlorine on algae fouling control for ultrafiltration (UF) membrane system. *Desalination*, 2008. **222**(1-3): p. 74-80.

4. S. Schulte, J. Wingender, and H.-C. Flemming, *Efficacy of biocides against biofilms*, in *Directory of Microbicides for the Protection of Materials*. 2004, Springer. p. 93-120.

5. H. A. Videla, Prevention and control of biocorrosion. *International Biodeterioration & Biodegradation*, 2002. **49**(4): p. 259-270.

6. W. Teughels, N. Van Assche, I. Sliepen, and M. Quirynen, Effect of material characteristics and/or surface topography on biofilm development. *Clinical oral implants research*, 2006. **17**(S2): p. 68-81.

7. A. K. Epstein, T. S. Wong, R. A. Belisle, E. M. Boggs, and J. Aizenberg, Liquid-infused structured surfaces with exceptional anti-biofouling performance. *Proceedings of the National Academy of Sciences of the United States of America*, 2012. **109**(33): p. 13182-13187.

8. S. Krishnan, *et al*., Anti-biofouling properties of comblike block copolymers with amphiphilic side chains. *Langmuir*, 2006. **22**(11): p. 5075-5086.

9. A. J. Scardino, H. Zhang, D. J. Cookson, R. N. Lamb, and R. de Nys, The role of nano-roughness in antifouling. *Biofouling*, 2009. **25**(8): p. 757-767.

10. H. Zhang, R. Lamb, and J. Lewis, Engineering nanoscale roughness on hydrophobic surface - preliminary assessment of fouling behaviour. *Science and Technology of Advanced Materials*, 2005. **6**(3-4): p. 236-239.

CHAPTER 7

SUMMARY OF MAIN FINDINGS, CONCLUSIONS AND FUTURE WORK

7.1 Main findings and conclusions

In this thesis, fundamental principles of wetting of smooth and rough solid surfaces, including Young, Wenzel and Cassie-Baxter modes of wetting, transitions between the different wetting regimes, contact angle hysteresis and consequences of the various wetting conditions have been studied and presented for adequate understanding of the surface wetting phenomena. The overview of the literature has revealed that greater inspirations to control the wettability of liquids on solid materials are drawn from the surfaces of some natural organisms. It is well known that a superhydrophobic surface observed in natural organisms, such as lotus plant, can be achieved when air fills the micro or nanostructures of artificial hydrophobic surfaces. Similarly, the rim of the pitcher plant is another attractive natural available slippery surface model designed with microstructures. The rim of this plant has recently been mimicked by filling surface microstructures with liquid oil to obtain a slippery artificial surface known as SLIPS. However, the link between the air filled structured surfaces and the liquid filled structured surfaces has not been fully established. The overall aim of this research was to carefully investigate the gap between the air-filled structured (superhydrophobic) materials and the oil-filled structured (slippery) surface with intention to fully understand micro/nanostructured surfaces for effective control. This has been pursued by selecting simple and inexpensive but durable materials (e.g. silica particles, squalane, PDMS) and methods (e.g. dip coating, spin coating, chemical etching) to fabricate different structured coatings and materials. Amongst other techniques, we have introduced partial (or gradual) impregnation, which allows liquid to be filled into porous

or structured materials, very little at a time till the substrates is completely filled and over-coated with the impregnating liquid.

In this project, we have demonstrated that the wettability of glass surface and silica coatings can be tuned by the level of exposure to the hydrophobising chemical and the degree of surface roughness. It was also found that the water contact angle and the retention or stability of impregnated oil in the fabricated silica coatings increase inversely with the size of the silica particles with fumed silica the nano-porous fumed silica showing the highest resistance to oil drainage. It has also been shown that uniform depositions of the silica particles coatings can be achieved by interplay with the concentration of the silica suspensions, the withdrawal speed of the dip-coater and the spin rate of a spin coater. In this work, 3-5 wt.% silica dispersion, spun at the spin rate of 2500 rpm (spin-coating) or 3 wt.% dispersions withdrawn at 5 cm/min (dip-coating) were found suitable for various investigations.

The partial impregnation of the coatings with different amounts of oil (squalane) allows us to gradually tune its wetting behaviour of the nano-porous silica coatings for many applications, including self-cleaning superhydrophobic surfaces, drag-free slippery surfaces and adhesive surfaces. The superhydrophobic surfaces are believed to be caused by the synergy from the air pockets and the hydrophobic nano-porous silica particles while the slippery coatings are as a result of the full replacement of the silica-air composite surface by slimy oil (squalane). The wetting behaviour of porous fumed silica coatings partially impregnated with squalane is more difficult to quantify because the surfaces are rough and heterogeneous, and water drops placed on the surfaces have the tendencies to establish contact with the tops of solid particles; non-displaced air trapped in the surface pores and squalane partially filled in the pores.

A simplified one-step fabrication technique that can trigger large scale production of oil-impregnated silica coatings has been introduced. Findings presented in this work have demonstrated that different coatings achieved in multiple-steps process can be reproduced by direct deposition of dispersions prepared by incorporating suitable amount of silica particles, squalane and ethanol into one system. We have also shown that the simplicity and flexibility of the one-step method by merely adjusting the dispersion components (e.g. oil or particle concentration) to obtain desired superhydrophobic, slippery or sticky coatings dispersions which can be applied to the surface using a wide range of simple coating techniques including, spin coating, dip coating, spray coating and certainly brushing. The simultaneous coating/impregnation from a single dispersion presented here is far simpler and time saving than any known methods presently used for the fabrication of slippery or oil-impregnated substrates.

Also, partial impregnations of curable Sylgard onto the fumed silica coatings have shown evidences of improved stable coatings compare to uncured oil-impregnated coatings. The Sylgard has been observed to act as adhesive promoter within the silica particles and between the coated film and the glass substrate.

Partially impregnated Sylgard coatings have been polymerised to obtain the prototype or duplicates of the liquid impregnated surfaces in solid states. Examinations of these cured impregnated surfaces under scanning electrons microscope have brought clearer insights into the structural changes on partially impregnated nano-porous surfaces. Studies with Sylgard has also revealed that in partial impregnations, the impregnated oils are initially thinly coated onto the surface structures, and then build up with increase in the concentration of the oil to a larger thickness which finally fills the surface pores and level up the surface. Based on these findings, we have further uncover a new and effective method of surface modification using partial impregnation

technique to grow ultra-thin protective polymeric films of Sylgard on solid surfaces which seems to be a promising low cost alternative technique to expensive physical or chemical vapour deposition techniques. The Sylgard-modified superhydrophobic aluminium, iron, copper and brass appear very likely to withstand harsh environmental conditions including corrosion. Also, transparent superhydrophobic Sylgard-modified paper material produced by the same method could serve as excellent protective coating for valuable paper materials.

Practical applications of partially impregnated nano-porous silica coatings in algae cells media have shown that the coatings can systematically be used to manipulate adhesion of biofilms on solid materials with negligible toxicity to the environment. Dry hydrophobic nano-porous fumed silica coatings have been found to offer significant resistance to algae cell adhesion within 24 hours. In addition, when these coatings are impregnated with a non-volatile oil (squalane) to create over-coated oil layer, the coatings are equally observed to exhibit excellent anti-biofouling property toward the cells. Although detailed investigations to link the algae cells interactions with the surface chemistry the samples have not yet been carried out, it is evident in this study that the cells can be washed off these two set of surfaces easily due to nano-scale roughness and the presence of stable slimy over-coated oil layer, respectively. Moderate impregnation of the coatings with the oil was found to reduce the anti-biofouling resistance drastically. Furthermore, we have observed algae cells adhesion to follow a similar trend as water drops sliding force on the same coatings. Greater understanding of gradual impregnation of porous substrate to manipulate surface wetting, including biofouling would expose more hidden properties of the structured solid substrates and this will be crucial in the development of environmental friendly anti-biofouling solid materials.

7.2 Future work

It is observed that different thickness of over-coated layer of oil can be achieved on oil-impregnated porous substrates. How this thickness can affect the slipperiness of the surface has not been investigated. Partial impregnation employed in this work can be used to tune the thickness of oil-impregnated surfaces. The thickness of the over-coated oil layer is the key factor of the invention of slippery surfaces. Investigations on how different thicknesses of over-coated layer of oil will affect the wettability of the surfaces will be a very interesting direction for future research.

Our results have demonstrated that nano-porous silica coatings, partially impregnated with squalane can be used to control algae cells bio-fouling. However, we were only able to investigate algae cells adhesion on squalane impregnated coatings within 24 hours due to stability of the coatings in the media. This period of investigation seems inadequate to clearly assess the complex interactions of biofilms on solid surfaces. Application of a more robust Sylgard-impregnated coatings prepared in the later part of this work will definitely remain stable over a longer period for anti-biofouling investigations.

The work with Sylgard 184 presents many opportunities for further investigations. We found that different metals can be modified to superhydrophobic states by partial impregnation with curable Sylgard. However, adequate characterisations of the coated metal surfaces was not carried out. It is rare to use a single low cost reagent (diluted PDMS) to hydrophobise different materials as reported in this work, however, adequate investigation of the stability and other properties of the fabricated materials will enhance the future applications of the materials. Specifically, applications of the superhydrophobic metal surfaces in acidic and alkaline corrosive environments are of significant practical importance and would require further investigation.